AD-A124 579   MODELING ANALYSIS AND OPTIMIZATION ISSUES FOR LARGE   1/3
SPACE STRUCTURES(U) NATIONAL AERONAUTICS AND SPACE
ADMINISTRATION HAMPTON VA LANG.   L D PINSON ET AL.
UNCLASSIFIED   FEB 83 NASA-L-15564 NASA-CP-2258   F/G 22/1   NL
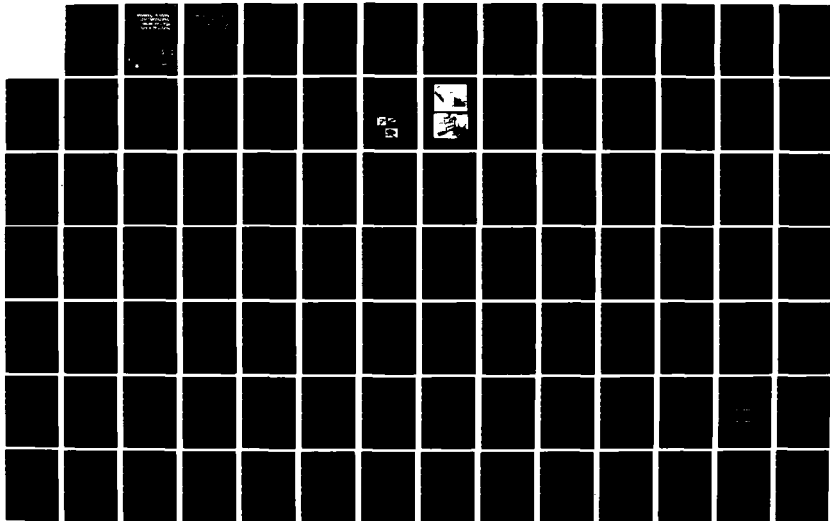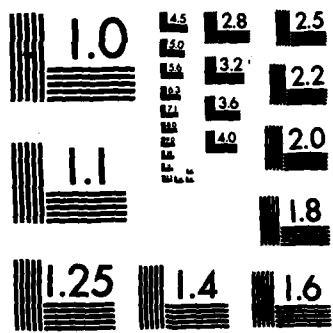
MICROCOPY RESOLUTION TEST CHART

NATIONAL BUREAU OF STANDARDS-1963-A

③

NASA Conference Publication 2258

Modeling, Analysis, and Optimization Issues for Large Space Structures

DTIC
ELECTE
FEB 1 7 1983
E

Proceedings of a workshop held in
Williamsburg, Virginia
May 13-14, 1982

AD A 124579

DTIC FILE COPY

This document has been approved
for public release and sale; its
distribution is unlimited.

NASA

83 02 017 024

Modeling, Analysis, and Optimization Issues for Large Space Structures

Compiled by
Larry D. Pinson
Langley Research Center

Anthony K. Amos
Air Force Office of Scientific Research

, V. B. Venkayya
Air Force Wright Aeronautical Laboratories

NASA

PREFACE

This document contains the proceedings of the Air Force/NASA Workshop on Modeling, Analysis, and Optimization Issues for Large Space Structures held in Williamsburg, Virginia, May 13-14, 1982. The workshop was jointly sponsored by NASA Langley Research Center, the Air Force Office of Scientific Research, and the Air Force Wright Aeronautical Laboratories. The theme of the workshop was modeling, analysis, and optimization of large space structures, including structure-control interaction. Speakers were drawn primarily from industry, with participation from universities and government. The workshop was organized into three sessions: mathematical modeling, analysis methodology, and optimization for controllability. Results of the workshop were discussed in a final session. Summaries of the sessions were presented by session technical secretaries, and general discussion followed. In addition to this fourth session, ample time was allowed within each session for discussions on topics of individual papers. Introductory remarks were made by Dr. Michael J. Salkind, Air Force Office of Scientific Research, and Mr. Robert C. Goetz, NASA Langley Research Center. A list of workshop attendees is included in the front of this document.

The workshop organizers express their appreciation to the session chairmen, speakers, and panelists, whose efforts contributed to the technical excellence of the workshop. Session chairmen were Dr. Larry D. Pinson, NASA Langley Research Center; Mr. M. A. Ostgaard, Air Force Wright Aeronautical Laboratories, and Dr. V. B. Venkayya, Air Force Wright Aeronautical Laboratories. Thanks are also due to session secretaries Dr. J. Housner, Dr. John Gubser, Dr. V. B. Venkayya, and Mr. B. Hanks.

Larry D. Pinson
NASA Langley Research Center

Anthony K. Amos
Air Force Office of Scientific Research

V. B. Venkayya
Air Force Wright Aeronautical Laboratories

Accession For		
NTIS GRA&I		X
DTIC TAB		☐
Unannounced		☐
Justification		
By		
Distribution/		
Availability Codes		
Dist	Avail and/or Special	
A		

CONTENTS

ATTENDEES

Mr. Michael H. Ackroyd
Rensselaer Polytechnic Institute
Dept. of Civil Engineering
Troy, NY 12181

Dr. Howard M. Adelman
MS/243, Loads and Aeroelasticity
    Division
NASA Langley Research Center
Hampton, VA 23665

Dr. K. T. Alfriend
Department of the Navy
Naval Research Laboratory, Code 7920
4555 Overlook Avenue, S. W.
Washington, DC 20375

Mr. Sam Altman
Dept. of Communications
Communications Research Center
Ottawa, Canada

Dr. Anthony K. Amos
AFOSR
Bolling Air Force Base
Washington, DC 20332

Professor Holt Ashley
Stanford University
Dept. of Aeronautics/Astronautics
369 Durand Building
Stanford, CA 94305

Dr. J. N. Aubrun
Lockheed Palo Alto Research Center
D/52-56, B/201
3251 Hanover Street
Palo Alto, CA 94304

Dr. Leon Y. Bahar
Department of Mechanical Engineering
& Mechanics
Drexel University
Philadelphia, PA 19104

Professor Peter M. Bainum
Howard University
Department of Mechanical Engineering
Washington, DC 20059

Mr. Siva S. Banda
Flight Dynamics Laboratory
AFWAL/FIGC
Wright Patterson AFB, OH 45433

Dr. H. T. Banks
Brown University
Division of Applied Math
Providence, RI 02912

Mr. Christopher Beattie
Johns Hopkins Applied Physics
Laboratory, Room 2-244
Johns Hopkins Road
Laurel, MD 20707

Mr. Stavos A. Belbas
University of Maryland
E. E. Department
College Park, MD 20742

Dr. Laurence Bellagamba
HR Textron Inc.
17748 Skypark Boulevard, Suite 150
Irvine, CA 92714

Mr. William H. Bennett
Department of the Navy
Naval Research Laboratory, Code 7926B
4555 Overlook Avenue, S. W.
Washington, DC 20375

Mr. Douglas E. Bernard
Stanford University
Dept. of Aeronautics & Astronautics
778 Moreno Avenue
Palo Alto, CA 94303

Mr. Robert L. Berry
Martin Marietta Denver Aerospace
MS/M0486
P. O. Box 179
Denver, CO 80201

Mr. Charles L. Blackburn
Kentron International
MS/246
NASA Langley Research Center
Hampton, VA 23665

Mr. Carl Bodley
Martin Marietta Denver Aerospace
MS/M0486
P. O. Box 179
Denver, CO 80201

Ms. Mary Bowden
Massachusetts Institute of Technology
33-407
Cambridge, MA 02139

Dr. Taft H. Broome
Civil Engineering
Howard University
2300 - 6th Street, N. W., Room 1026
Washington, DC 20059

Mr. William L. Burkett, Jr.
Hughes Aircraft Company
Bldg. S-12, MS V-362
P. O. Box 92919
Los Angeles, CA 90009

Mr. Charles J. Camarda
MS/243, Loads and Aeroelasticity
Division
NASA Langley Research Center
Hampton, VA 23665

Dr. Michael F. Card
MS/244, Structures & Dynamics Division
NASA Langley Research Center
Hampton, VA 23665

Mr. Douglas Caswell
Department of Communications
Communications Research Center
Ottawa, Canada

Dr. H. M. Chun
C. S. Draper Laboratory
555 Technology Square
Cambridge, MA 02139

Mr. Roy R. Craig, Jr.
The University of Texas at Austin
Department of Aerospace Engineering &
Engineering Mechanics
Austin, TX 78712-1085

Professor Edward Crawley
Aeronautics and Astronautics, 37-361
Massachusetts Institute of Technology
77 Massachusetts Avenue
Cambridge, MA 02139

Mr. Paul Convertito
Perkin/Elmer Corporation
MS/813
100 Wooster Heights Road
Danbury, CT 06810

Mr. A. J. Cwiertny
A3-202-13-3
McDonnell Douglas Astronautics Co.
5301 Bolsa Avenue
Huntington Beach, CA 92647

Mr. John Dahlgren
Code RTE-6
NASA Headquarters
Washington, DC 20546

Mr. Melvin J. Ferebee, Jr.
SSD, Systems and Experiments Branch
MS/364
NASA Langley Research Center
Hampton, VA 23665

Dr. Patti L. Daniel
(ICASE) Math Department
Southern Methodist University
Dept. of Mathematics
Dallas, TX 75275

Dr. Shalom Fisher
Department of the Navy
Naval Research Laboratory, Code 7922
4555 Overlook Avenue, S. W.
Washington, DC 20375

Mr. Ronald Dotson
Lockheed Missiles & Space Company
Dept. 62-61, Bldg. 104
P. O. Box 504
Sunnyvale, CA 94088

Mr. David W. Fox
AFOSR
Bolling Air Force Base
Washington, DC 20332

Professor Earl H. Dowell
Department MAE
D-202 Engineering Quadrangle
Princeton University
Princeton, NJ 08544

Mr. Harold P. Frisch
NASA
Goddard Spaceflight Center
Greenbelt, MD 20771

Dr. Thomas A. Dwyer, III
The Aerospace Corporation
Mail Station M4/971
P. O. Box 92957
Los Angeles, CA 90009

Mr. John Garba
Jet Propulsion Laboratory
MS/157/316
4800 Oak Grove Drive
Pasadena, CA 91109

Dr. Remi C. Engels
Martin Marietta Aerospace
Strategic Systems Division
Aerospace, POB 179, D6072
Denver, CO 80201

Dr. L. Bernard Garrett
SSD, Systems & Experiments Branch
MS/364
NASA Langley Research Center
Hampton, VA 23665

Mr. Bernard Epstein
AFOSR/NM
Bolling Air Force Base
Washington, DC 20332

Capt. David A. Glasgow
AFOSR/NA
Bolling Air Force Base
Washington, DC 20332

Mr. Richard Faison
NASA Langley Research Center
MS/431
Hampton, VA 23665

Dr. R. Gluck
TRW Electronics & Defense Sector
Bldg. R5, Mail Station B-131
One Space Park
Redondo Beach, CA 90278

Mr. Robert C. Goetz
Structures Directorate
MS/118
NASA Langley Research Center
Hampton, VA 23665

Mr. Harold A. Hamer
MS/161, Control Theory & Flight
Management Branch
NASA Langley Research Center
Hampton, VA 23665

Dr. Richard J. Gran
Grumman Aerospace Corporation
Mail Stop A08-35
Bethpage, NY 11714

Mr. Brantley R. Hanks
Structural Dynamics Branch, SDD
MS/230
NASA Langley Research Center
Hampton, VA 23665

Mr. John L. Gubser
McDonnell Douglas Astronautics Co.
Dept. E236, HQS, Bldg. Rm. 478
P. O. Box 516
St. Louis, MO 63166

Mr. Harry Harcrow
Martin Marietta - Denver Aerospace
P. O. Box 179
Denver, CO 80201

Dr. Sol Gully
Alphatech, Inc.
3 New England Executive Park
Burlington, MA 01803

Mr. J. K. Haviland
Mechanics & Aerospace Engineering
University of Virginia
Charlottesville, VA 22901

Professor Raphael T. Haftka
VPI&SU
Dept. of Engineering Science &
Mechanics
Blacksburg, VA 24061

Dr. Donald P. Hearth
Director
MS/106
NASA Langley Research Center
Hampton, VA 23665

Mr. William N. Hall
AF Geophysics Laboratory
Spacecraft Environment Branch
AFGL/PHK
Hanscom AFB, MA 01731

Dr. Garnett C. Horner
MS/230, Structural Dynamics Branch, SDD
NASA Langley Research Center
Hampton, VA 23665

Dr. Jerrold Housner
MS/230, Structural Dynamics Branch, SDD
NASA Langley Research Center
Hampton, VA 23665

Dr. William L. Hallauer, Jr.
Dept. of Aerospace & Ocean Engineering
VPI&SU
Blacksburg, VA 24061

Mr. Frederick Ham
Harris Corporation, GESD, MS 22 2402
P. O. Box 37
Melbourne, FL 32935

Dr. Earle Huckins, III
MS/158, Large Space Antenna Systems
Technology Office
NASA Langley Research Center
Hampton, VA 23665

Mr. Peter C. Hughes
Institute for Aerospace Structures
University of Toronto
4925 Dufferin Street
Toronto, Canada M345T6

Mr. David C. Hyland
Massachusetts Institute of Technology
Lincoln Laboratory, D-382
P. O. Box 73
Lexington, MA 02173

Dr. Samir Ibrahim
Old Dominion University
Dept. of Mechanical Engineering
Norfolk, VA 23508

Dr. Suresh M. Joshi
ODU Research Foundation
MS/161
NASA Langley Research Center
Hampton, VA 23665

Dr. Jer-Nan Juang
MS/230, Structural Dynamics Branch, SDD
NASA Langley Research Center
Hampton, VA 23665

Professor John L. Junkins
ESM Department
VPI&SU
Blacksburg, VA 24061

Mr. M. P. Kamat
VPI&SU
Blacksburg, VA 24061

Dr. Charles Keller
AFWAL/FIBRC
Wright Patterson AFB, OH 45433

Dr. N. S. Khot
AFWAL/FIBRA
Wright Patterson AFB, OH 45433

Dr. W. G. Krauss
Caltech
Pasadena, CA 91125

Mr. Michael Krim
Perkin/Elmer Corporation, MS/813
100 Wooster Heights Road
Danbury, CT 06810

Dr. Robert M. Laurenson
McDonnell Douglas Astronautics Co.
P. O. Box 516
St. Louis, MO 63166

Mr. E. Burton Lightner
MS/158, STFEO
NASA Langley Research Center
Hampton, VA 23665

Mr. Charles Lin
Old Dominion University
Dept. of Mechanical Engineering
Norfolk, VA 23508

Mr. Robert E. Lindberg
Code 7926
Naval Research Laboratory
Washington, DC 20375

Mr. Robert G. Loewy
Rensselaer Polytechnic Institute
110 Eighth Street
Troy, NY 12181

Professor Richard Longman
Dept. of Mechanical Engineering
Columbia University
New York, NY 10027

Dr. Michael Lyons
Integrated Systems Incorporated
151 University Avenue, Suite 400
Palo Alto, CA 94301

Mr. A. N. Madiwale
Massachusetts Institute of Technology
Lincoln Laboratory, Rm. D-435
244 Wood Street
Lexington, MA 02173

Mr. Jack MaHaney
Mechanical Engineering & Mechanics Dept.
Old Dominion University
Norfolk, VA 23508

Mr. Gerard Mayer
University of Virginia
Dept. of Aeronautical & Mechanical
Engineering
Charlottesville, VA 22901

Mr. Samuel McIntosh, Jr.
Nielsen Engineering & Research, Inc.
510 Clyde Avenue
Mountain View, CA 94043

Dr. Leonard Meirovitch
VPI&SU
Dept. of Engineering Science & Mechanics
Blacksburg, VA 24061

Mr. _bert Miserentino
SDD, Structural Dynamics Branch
MS/230
NASA Langley Research Center
Hampton, VA 23665

Dr. George Morosow
Martin Marietta-Denver Aerospace
MS/M0486
P. 0. Box 179
Denver, CO 80201

Dr. V. Mukhopadhyay
George Washington University - JIAFS
MS/243
NASA Langley Research Center
Hampton, VA 23665

Mr. Michael F. Mullette
Mechanical & Aeronautical Engineering
University of Virginia
Charlottesville, VA 22901

Dr. William A. Nash
Department of Civil Engineering
4-16030
University of Massachusetts
Amherst, MA 01003

Dr. Ted Nishimoto
Rockwell International
Mail Code SL-26
12214 Lakewood Blvd.
Downey, CA 90241

Mr. Thomas Noll
AFWAL/FIBRC
Wright Patterson AFB, OH 45433

Dr. Ahmed K. Noor
George Washington University - JIAFS
MS/243
NASA Langley Research Center
Hampton, VA 23665

Dr. James J. Olsen
AFWAL/FIB
Air Force Flight Dynamics Laboratory
WPAFB, OH 45433

Mr. Richard F. O'Neill
MZ 22-6960
General Dynamics Convair Division
P. 0. Box 80847
San Diego, CA 92138

Mr. M. A. Ostgaard
AFWAL/FIG
Wright Patterson AFB, OH 45433

Mr. Richard S. Pappa
Structural Dynamics Branch, SDD
MS/230
NASA Langley Research Center
Hampton, VA 23665

Dr. K. C. Park
Lockheed Research Laboratory
Lockheed Missiles & Space Co., Inc.
Sunnyvale, CA 94086

Dr. Donald B. Paul
Air Force Wright Aeronautical Laboratory
AFWAL/FIBE
WPAFB, OH 45433

Dr. Walter D. Pilkey
University of Virginia
Dept. of Mechanical & Aerospace
Engineering, Thornton Hall
Charlottesville, VA 22901

Dr. Larry D. Pinson
SDD, Structural Dynamics Branch
MS/230
NASA Langley Research Center
Hampton, VA 23665

Dr. Robert Plunkett
107 Akerman
University of Minnesota
Minneapolis, MN 55455

Capt. Robert Preston
Air Force Rocket
Propulsion Laboratory
AFRPL/DYA
Edwards AFB, CA 93523

Dr. Lawrence W. Rehfield
Georgia Institute of Technology
Aerospace Engineering
Atlanta, GA 30332

Mr. Robert Reiss
Howard University
Dept. of Mechanical Engineering
Washington, DC 20059

Mr. Howard Reynaud
Dept. Of Communications
Ottawa, Canada

Mr. R. J. Reynolds
General Dynamics Convair Division
P. O. Box 80847
San Diego, CA 92138

Lt. D. Brett Ridgely
Flight Dynamics Laboratory
AFWAL/FIGC
WPAFB, OH 45433

Mr. Richard Russell
Large Space Antenna Systems
Development Office, MS/158
NASA Langley Research Center
Hampton, VA 23665

Dr. Michael Salkind
AFOSR/NA
Bolling Air Force Base
Washington, DC 20332

Ms. Celeste M. Satter
C. S. Draper Laboratory
555 Technology Square
Cambridge, MA 02139

Mr. Leslie Schlam
Perkin/Elmer Corporation
MS/813
100 Wooster Heights Road
Danbury, CT 06810

Professor Thomas I. Seidman
Dept. of Mathematics
University of Maryland-Baltimore County
UMBC - Math
Baltimore, MD 21228

Dr. John R. Sesak
General Dynamics Convair Division
P. O. Box 80847
San Diego, CA 92138

Dr. Keto Soosaar
C. S. Draper Laboratory, MS/70
555 Technology Square
Cambridge, MA 02139

Mr. Timothy G. Shanahan
Martin Marietta
Aerospace, POB 179, D6072
Denver, CO 80201

Mr. Clyde V. Stahle, Jr.
General Electric-Space Division
P. O. Box 8555
Philadelphia, PA 19101

Dr. John Shipley
Harris Corporation, GESD
Bldg. 15, Rm. 500A
P. O. Box 37
Melbourne, FL 32901

Mr. Douglas A. Staley
ANCON Space Technology Corp.
12 Elmbank Road
Thornhill, Ontario, Canada L4J2B7

Mr. C. T. Sun
Purdue University
School of Aeronautics & Astronautics
Grissom Hall
West Lafayette, IN 47907

Mr. Charles P. Shore
Multidisciplinary Analysis &
Optimization Branch, MS/243
NASA Langley Research Center
Hampton, VA 23665

Dr. N. Sundararajan
MS/161, Spacecraft Controls Branch
NASA Langley Research Center
Hampton, VA 23665

Mr. Robert Sierakowiski
AFOSR/NA
Bolling AFB, DC 20332

Dr. Vincent G. Sigillito
Applied Physics Laboratory
The Johns Hopkins University
Johns Hopkins Road
Laurel, MD 20707

Mr. Thomas R. Sutter
Kentron International
3221 N. Armistead Avenue
Hampton, VA 23666

Dr. Theodore R. Tauchert
Dept. of Engineering & Mechanics
University of Kentucky
Lexington, KY 40506

Professor Robert E. Skelton
Purdue University
School of Aeronautics & Astronautics
331 Grissom Hall
West Lafayette, IN 47907

Dr. Earl A. Thornton
Mechanical Engineering & Mechanics Dept.
Old Dominion University
P. O. Box 6369
Norfolk, VA 23508

Dr. Mohan L. Soni
University of Dayton
Research Institute, NCR 326
College Park Drive
Dayton, OH 45469

Mr. Andre Tits
Electrical Engineering Dept.
University of Maryland
College Park, MD 20742

Dr. James Turner
C. S. Draper Laboratory
555 Technology Square
Cambridge, MA 02139

Mr. Peter W. Welch
HR Textron, Inc.
17748 Skypark Boulevard, Suite 150
Irvine, CA 92714

Professor Wallace E. Vander Velde
Dept. of Aeronautics and Astronautics
Room 33-109
Massachusetts Institute of Technology
Cambridge, MA 02139

Prof. James H. Williams, Jr.
Massachusetts Institute of Technology
Room 3-360
77 Massachusetts Avenue
Cambridge, MA 02139

Dr. Vipperla B. Venkayya
AFWAL/FIBR
Air Force Flight Dynamics Laboratory
Air Systems Command
Wright Patterson AFB, OH 45433

Mr. Jeffrey P. Williams
Spacecraft Controls Branch, MS/161
NASA Langley Research Center
Hampton, VA 23665

Mr. Robert L. Wright
MS/364, Systems and Experiments Branch
NASA Langley Research Center
Hampton, VA 23665

Dr. Frank Vigneron
Department of Communications
Ottawa, Canada

Mr. L. R. Vreugde
Perkin-Elmer Corporation
Optical Technology Division
100 Wooster Heights Road
Danbury, CT 06810

Professor Henry T. Y. Yang
School of Aeronautics and Astronautics
Purdue University
West Lafayette, IN 47907

Professor K. David Young
Dept. Mechanical Engineering
& Mechanics
Drexel University
Philadelphia, PA 19104

Dr. Bo Ping Wang
University of Virginia
Dept. of Mechanical & Aerospace
Engineering, Thornton Hall
Charlottesville, VA 22901

Mr. Joseph Walz
Structural Concepts Branch, SDD
MS/230
NASA Langley Research Center
Hampton, VA 23665

Mr. John W. Young
Control Theory & Flight Management
Branch, MS/161
NASA Langley Research Center
Hampton, VA 23665

Mr. Joseph P. Young
Mechanical Engineering Branch
MS/731, GSFC
Greenbelt, MD 20771

Professor Connie J. Weeks
Princeton University
D207 Engineering Quad.
Princeton, NJ 08544

INTRODUCTION

The workshop presentations ranged over many topics in large space structures, including structure-control interaction, structural and structural dynamics modeling, thermal analysis, testing, design, and optimization. The interdisciplinary area of structure-control interaction, which is a challenge to analysts, designers, and test engineers, was clearly emphasized. Not addressed in the workshop was the important subject of structural deployment.

Structure-control interaction is emerging as a separate discipline in which structural dynamicists and controls engineers each become proficient in both areas to accomplish viable designs. Performance requirements dictate an integrated approach to design. The necessity for this merging of structural dynamics and controls disciplines has become apparent because of extreme requirements in potential large space structures applications. Furthermore, research is now ongoing in aeronautics in the areas of active flutter suppression, load alleviation, and reduced static stability, all of which require consideration of the control of structural motion at a rate that excites structural vibration. Presentations on this subject at the workshop revealed the immaturity of the technology. Theoretical considerations dominate research. Most controllers are considered to be ideal, and the effects of various kinds of structural or actuator nonlinearity are not known. The presentation by Lyons and Aubrun of results from experiments on elementary structures with a few sensor-actuator combinations showed some agreement between analysis and test data. Although other experimental work is known to be under way, a reasonable assessment is that several theoretical approaches exist in this area with insufficient experience in their application to form a blending of these methods which can be applied confidently in a practical situation. Only through ground test and analysis programs involving relatively complex structures and associated control systems and through careful space flight experiments will this necessary confidence and experience be achieved. Such programs also will cause appropriate organizational realignments to enhance communications, as well as appropriate merging of the structural dynamics and controls disciplines.

The trends in research in structural analysis and modeling are toward increasing finesse to achieve efficiency. These trends are driven by two considerations: (1) potential large space structures have too many elements to model with the conventional finite element approach, and (2) small, accurate models are a necessity for practical design procedures involving resizing and repeated analyses. One trend is toward models in which structures with many repeating elements are idealized as equivalent continua, followed by analyses that are a blend of classical partial differential equation solutions and approximate techniques. Assumed-function approaches that extend classical Ritz-type methods to nonlinear responses of these idealized structures are being applied with success. None of these new techniques, however, has been incorporated into generally available computer analysis programs. In addition, experience with new structural concepts such as cable-stiffened structures is sparse. With extended experience using large space structure concepts and incorporation of new techniques into practical computer analysis programs, structural analysis and modeling of most forseeable large space structures will become feasible.

Ground testing is perceived as a major challenge in large space structures applications because of gravitational and atmospheric effects. To derive maximum benefit from ground tests, it is necessary to have flight data to substantiate analytical corrections for suspension system, gravitational, and atmospheric effects.

Controversy exists concerning the nature of such flight data. Research-oriented engineers tend to favor basic, relatively inexpensive experiments with specific objectives, whereas project and systems engineers opt for more complex specimens with much greater potential for practical demonstration. As was revealed at the workshop, ground test data from tests of large structures configured for space applications are scarce, and no data exist for space tests. Such data are needed to obtain confidence in the analyses necessary to justify commitment to real applications.

The emphasis in thermal analysis is on obtaining greater analysis efficiency. Very little is being done to verify analytical approaches or to ascertain sensitivities through correlation with tests. Novel approaches to problems such as interelement radiation were revealed. These approaches involve consideration of the probable importance of various geometric effects. Assumed-function approaches are also being developed to enhance efficiency.

Examples of the application of structural optimization procedures in the design of complex structures are rare. Subassemblies can be designed to static load requirements, but the technology for design for dynamic loading is immature. The problem is complex, and research has been under way for over a decade. Discussions at the workshop indicated that real applications will not occur until mission requirements force such a formal approach to design. Large space structure applications seem to provide these requirements.

2

SESSION I

MATHEMATICAL MODELING

Chairman: L. D. Pinson
Secretary: J. M. Housner

ASSESSMENT OF CURRENT STATE OF THE ART IN MODELING
TECHNIQUES AND ANALYSIS METHODS FOR LARGE SPACE STRUCTURES

Ahmed K. Noor
George Washington University Center
NASA Langley Research Center
Hampton, Virginia

INTRODUCTION

Needless to say, a critical and in-depth review of the state of the art in modeling techniques and analysis methods for large space structures would require much more space than can be allotted to this paper. Therefore, this paper focuses on certain aspects of the subject pertaining to the structures discipline. Other disciplines such as thermal analysis and modeling and controls are not covered in this paper.

Figure 1 shows examples of the five categories of large space structures suggested for various applications (see, for example, Refs. 1, 2 and 3). They include

1) Booms and other one-dimensional configurations

2) Planar surfaces

3) Antennas and curved structures

4) Platforms

5) Space stations

Because of their low mass and high stiffness, repetitive lattice trusses have been selected as the primary candidates (Refs. 4 and 5) for most of the large space structures. This paper focuses on modeling techniques and analysis methods for these structures.

RADIAL RIB STRUCTURE
FOLDABLE

TRUSS STRUCTURE
FOLDABLE
NESTABLE STRUTS

HOOP-COLUMN STRUCTURE
FOLDABLE

SPACE PLATFORM

(a)

Figure 1

6

ADVANCED SCIENCE & APPLICATIONS SPACE
PLATFORM

(b)

SPACE STATION
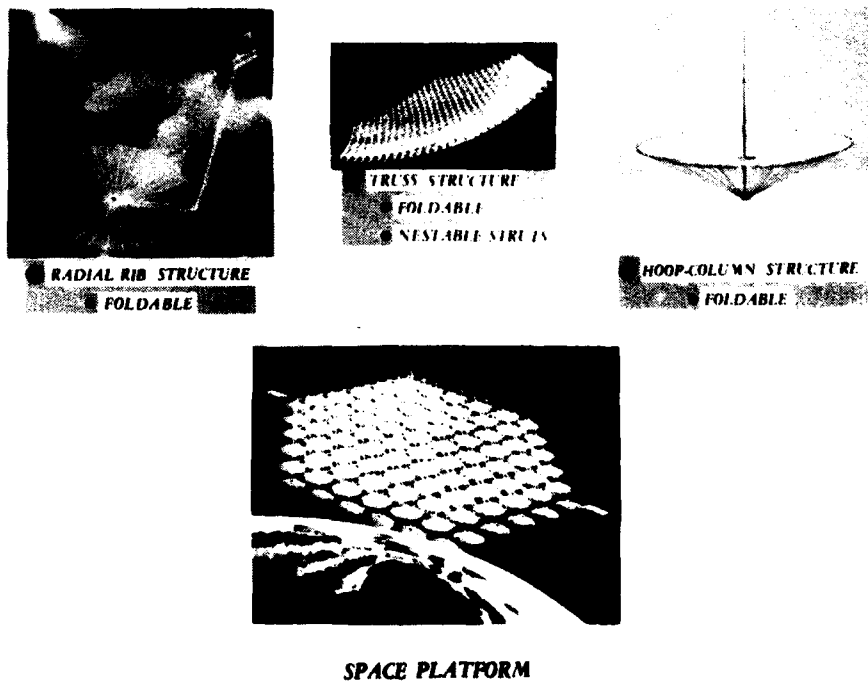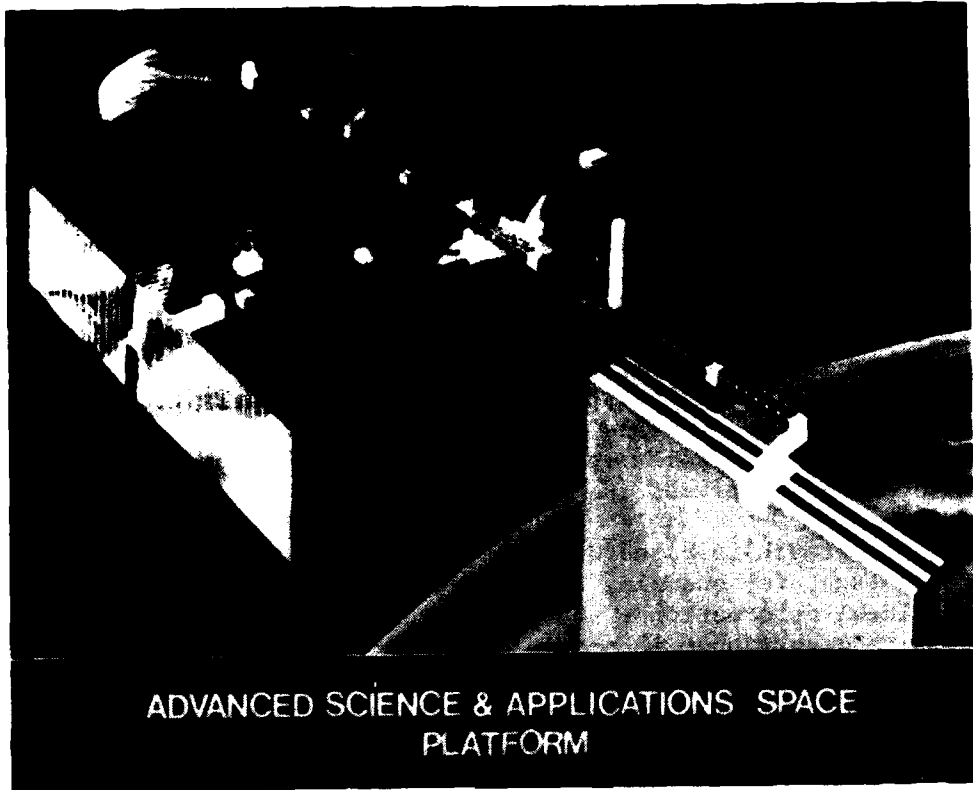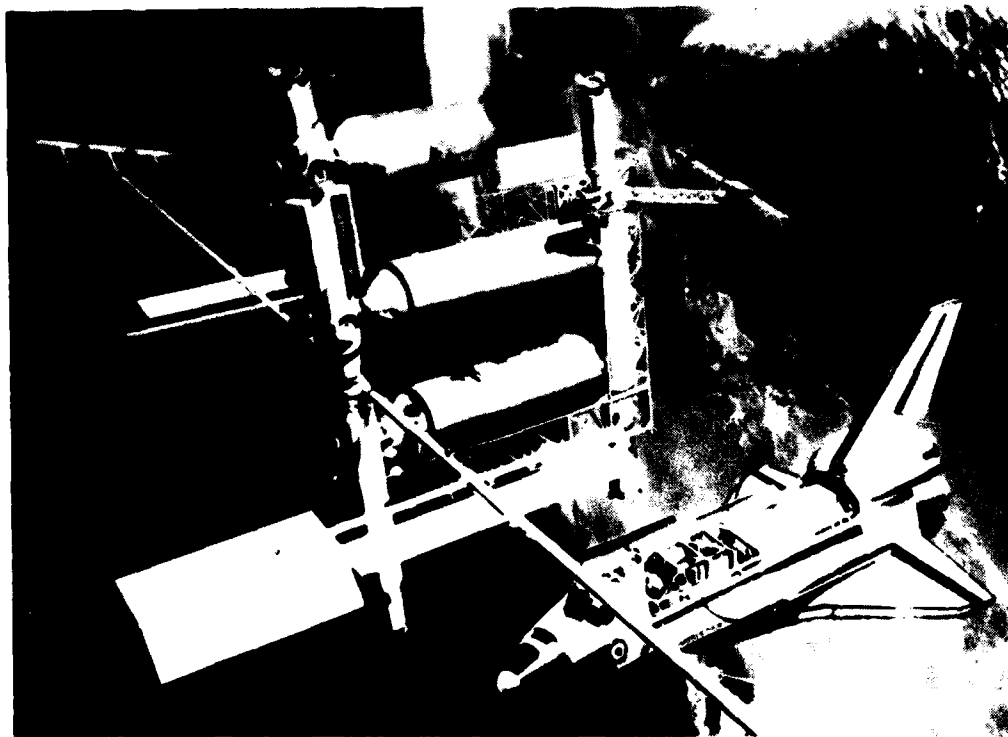
(c)

Figure 1 (Concluded)

CURRENTLY USED APPROACHES FOR ANALYZING
REPETITIVE LATTICES

A review of the state of the art in the analysis, design, and construction of lattice structures until 1976 is given in Refs. 6 and 7. The currently used approaches for analyzing large repetitive lattices can be grouped into four classes as shown in Figure 2.

The first approach is the direct method wherein the structure is analyzed as a system of discrete finite elements. It has the obvious drawback of being computationally expensive for large lattices. This is particularly true when a buckling, vibration, or a nonlinear analysis is required. To remedy this drawback, techniques were developed for substantially reducing the number of degrees of freedom in the buckling and nonlinear analyses (Refs. 8 and 9).

The second approach is based on replacing the actual lattice by a substitute continuum model (see, for example, Refs. 10 through 14). It has the limitations that: a) the local deformation effects are typically not accounted for, and b) ordinary (or classical) continuum is not suitable for lattices with rigid or flexible joints. To overcome these drawbacks, continuum models have been developed which include the local deformation modes (Refs. 15, 16 and 17). For lattices with rigid joints, micropolar continua have been developed (Refs. 18 through 21).

The third approach is the discrete field method which takes advantage of the regularity of the lattice and is based on writing the equilibrium and compatibility equations at a typical joint and then using the Taylor series expansion to replace these equations by differential equations (see, for example, Refs. 22 and 23). This approach works well for simple lattice configurations, but becomes quite involved for lattices with complex geometry.

The fourth group of methods is called the periodic structure approach. This approach is based on either: a) the combined use of finite elements and transfer matrix methods, which is efficient only for rotationally symmetric or simple geometries (Ref. 24), or b) the exact representation of the stiffness of an individual member from which the analysis of beam-like lattices with simply supported edges can be performed (Refs. 25 and 26). The limitations of the periodic structure approach can be removed by combining this approach with the substitute continuum approach. This paper will focus on the reduction methods and improved continuum models.

CURRENTLY USED APPROACHES FOR ANALYZING LARGE REPETITIVE LATTICES

APPROACH	DRAWBACKS	POSSIBLE REMEDIAL ACTIONS
● DIRECT METHOD ● STRUCTURE ANALYZED AS A SYSTEM OF DISCRETE FINITE ELEMENTS	● COMPUTATIONALLY VERY EXPENSIVE FOR LARGE LATTICES	● USE OF REDUCTION METHODS FOR BUCKLING AND NONLINEAR PROBLEMS
● SUBSTITUTE CONTINUUM APPROACH	● LOCAL DEFORMATION EFFECTS NOT ACCOUNTED FOR ● ORDINARY CONTINUUM NOT SUITABLE FOR LATTICES WITH RIGID JOINTS	● INCLUDE LOCAL DEFORMATION MODES IN THE DEVELOPMENT ● USE MICROPOLAR CONTINUA

● DISCRETE FIELD METHOD
 	
    ● EQUILIBRIUM AND COMPATIBILITY EQUATIONS ARE WRITTEN AT A TYPICAL JOINT
 	
    ● TAYLOR SERIES EXPANSIONS ARE USED TO DEVELOP DIFFERENTIAL EQUATIONS
	● DEVELOPMENT AND SOLUTION CAN BE SUBSTANTIAL FOR COMPLEX LATTICE CONFIGURATIONS	

● PERIODIC STRUCTURE APPROACH
 	
    ● SUBSTRUCTURING - COMBINED USE OF FINITE ELEMENTS AND TRANSFER MATRIX METHODS
 	
    ● EXACT REPRESENTATION OF STIFFNESS OF INDIVIDUAL MEMBERS
	● NOT EFFICIENT FOR COMPLICATED CONFIGURATION AND/OR FOR TRANSIENT RESPONSE CALCULATIONS
	
	● LIMITED TO BEAMLIKE LATTICES WITH SIMPLY SUPPORTED ENDS OR RING CONFIGURATION WITH RIGID CENTRAL MAST
		● COMBINE WITH SUBSTITUTE CONTINUUM APPROACH

Figure 2

9

OBJECTIVES AND SCOPE

The objectives of this paper are listed in Figure 3. They are:

1) To review recent progress in continuum modeling and reduction methods which are applicable to large space structures

2) To identify some of the analysis and modeling needs for future large space structures

This paper is divided into three parts. The first part deals with continuum modeling. Both beam-like and plate-like lattices are considered. Linear thermo-elastic static response, free vibrations, and buckling problems are treated. The lattices can have either pin or rigid joints. Continuum models have also been developed for beam-like lattices with open thin-walled section longerons, but will not be considered in this paper. The second part of the paper deals with reduction methods as applied to bifurcation buckling, nonlinear static, and dynamic responses. The third part deals with analysis and modeling needs.

OBJECTIVES

- REVIEW RECENT PROGRESS IN CONTINUUM MODELING AND REDUCTION METHODS WHICH ARE APPLICABLE TO LARGE SPACE STRUCTURES.

- IDENTIFY ANALYSIS AND MODELING NEEDS.

SCOPE

CONTINUUM MODELING

- BEAM-LIKE AND PLATE-LIKE LATTICES WITH DIFFERENT CONFIGURATIONS.

- LINEAR THERMOELASTIC STATIC RESPONSE, FREE VIBRATIONS AND BUCKLING PROBLEMS.

- LATTICES WITH PIN AND RIGID JOINTS.

- BEAM-LIKE LATTICES WITH OPEN THIN-WALLED SECTION LONGERONS.

REDUCTION METHODS

- BIFURCATION BUCKLING, NONLINEAR STATIC AND DYNAMIC RESPONSES.

ANALYSIS AND MODELING NEEDS

- LOADS DETERMINATION

- MODELING AND NONCLASSICAL BEHAVIOR CHARACTERISTICS.

- COMPUTATIONAL MODELS AND ALGORITHMS.

Figure 3

EFFECTIVE THERMOELASTIC CONTINUUM MODEL

The characteristics of an effective continuum model are outlined in Figure 4 for a typical double-layered grid such as the one shown in the figure. It is a continuum having the same amounts of strain and kinetic energies as the original lattice when both are deformed identically. The temperature distribution, loading, and boundary conditions simulate those of the original double-layered lattice grid.

The original three-dimensional double-layered lattice is replaced by a two-dimensional continuum plate model. The last two characteristics are perhaps the most important in terms of new developments. These characteristics are

1) Local deformations are accounted for

2) Lattices with rigid joints are modeled by micropolar continua

- IS A CONTINUUM WHICH HAS SAME AMOUNT OF THERMOELASTIC STRAIN ENERGY STORED IN IT AS ORIGINAL DOUBLE-LAYERED GRID WHEN BOTH ARE DEFORMED IDENTICALLY.

- TEMPERATURE DISTRIBUTION AND BOUNDARY CONDITIONS OF CONTINUUM SIMULATE THOSE OF DOUBLE-LAYERED LATTICE GRID

- THREE-DIMENSIONAL DOUBLE-LAYERED LATTICE IS REPLACED BY TWO-DIMENSIONAL CONTINUUM PLATE MODEL.

- LOCAL DEFORMATIONS ACCOUNTED FOR

- ORDINARY CONTINUUM MODELS FOR LATTICES WITH PIN JOINTS AND MICROPOLAR CONTINUUM MODELS FOR LATTICES WITH RIGID JOINTS

LATTICE STRUCTURE   TWO-DIMENSIONAL CONTINUUM MODEL
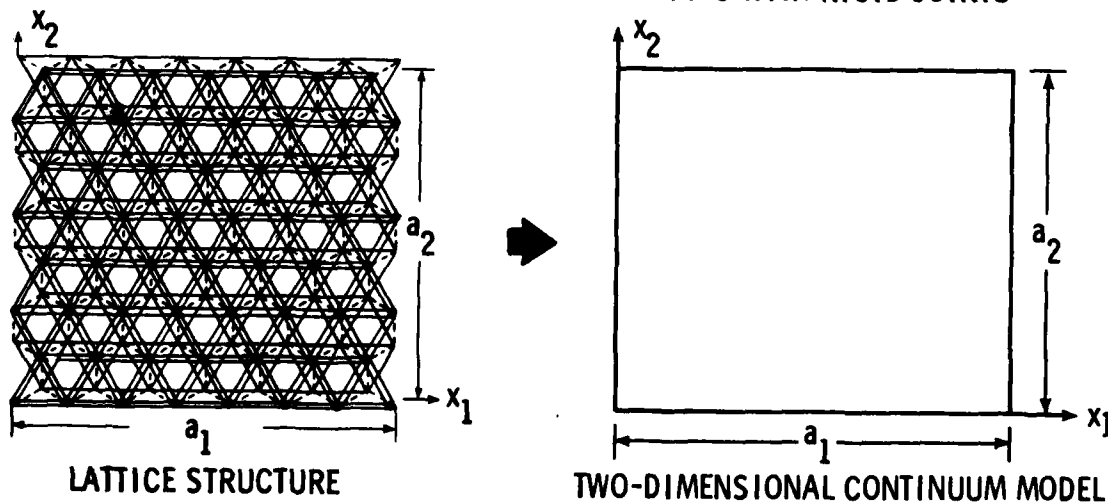
Figure 4

LOCAL DEFORMATIONS IN AXIALLY LOADED PLANAR TRUSS

The local deformation in an axially loaded planar truss is shown in Figure 5. The actual deformation has the zig-zag pattern shown on the top sketch. On the average, however, the chord members remain straight. The classical continuum averages these deformations as shown in the bottom sketch thereby substantially overestimating the axial stiffness. The continuum models developed in Refs. 15, 16 and 17 do account for local deformations such as the one shown here.
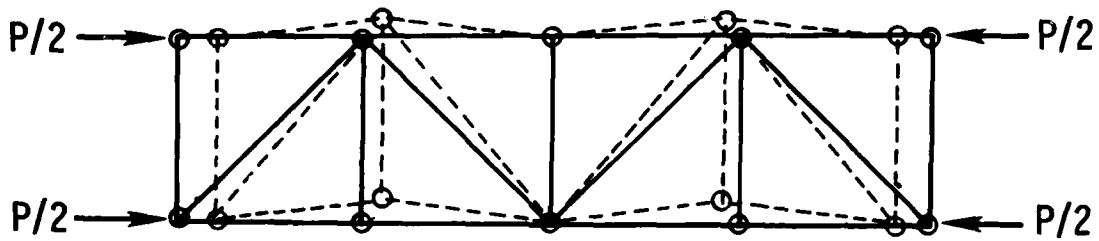
ACTUAL DEFORMATIONS
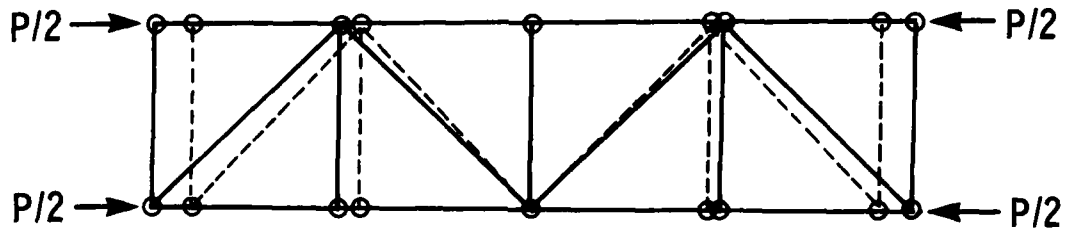
DEFORMATION PREDICTED BY CLASSICAL CONTINUUM MODEL

Figure 5

12

ORDINARY VERSUS MICROPOLAR CONTINUA

A contrast between the ordinary and micropolar continua is made in Figure 6. For an axially loaded pin-jointed truss member the transverse motion is completely characterized by the joint displacements. The member rotation ψ is related to the joint displacements w_i and w_j. Therefore, the appropriate continuum to use in modeling pin-jointed trusses is the ordinary continuum for which the *displacement field completely characterizes the motion of the structure.*

On the other hand, for a rigid-jointed member, the transverse motion is characterized by both the joint displacements w_i, w_j as well as the joint rotations θ_i, θ_j which are independent of the displacements. Therefore, the appropriate continuum to use in modeling rigid-jointed flexural members is one whose motion is *characterized by both a displacement field and an independent rotation field.* The micropolar continuum is such a continuum (Ref. 27).

	TRUSS MEMBER (PIN JOINTS)	BEAM MEMBER (RIGID JOINTS)
DEFORMATION PATTERN		
ROTATIONS	$\psi = \dfrac{1}{L}(w_j - w_i)$	$\psi = \dfrac{1}{L}(w_j - w_i)$ θ_i, θ_j (JOINT ROTATIONS)
APPROPRIATE CONTINUUM	ORDINARY (DISPLACEMENT FIELD ONLY)	MICROPOLAR (INDEPENDENT DISPLACEMENT AND ROTATION FIELDS)

Figure 6

13

BEAM-LIKE LATTICES CONSIDERED IN PRESENT STUDY

    Some typical configurations for the beam-like and plate-like lattice trusses are
shown in Figure 7. The characteristics of the continuum models for these lattices
are given in Refs. 15 and 16.

(a) TRIANGULAR CROSS SECTION

(b) RECTANGULAR CROSS SECTION
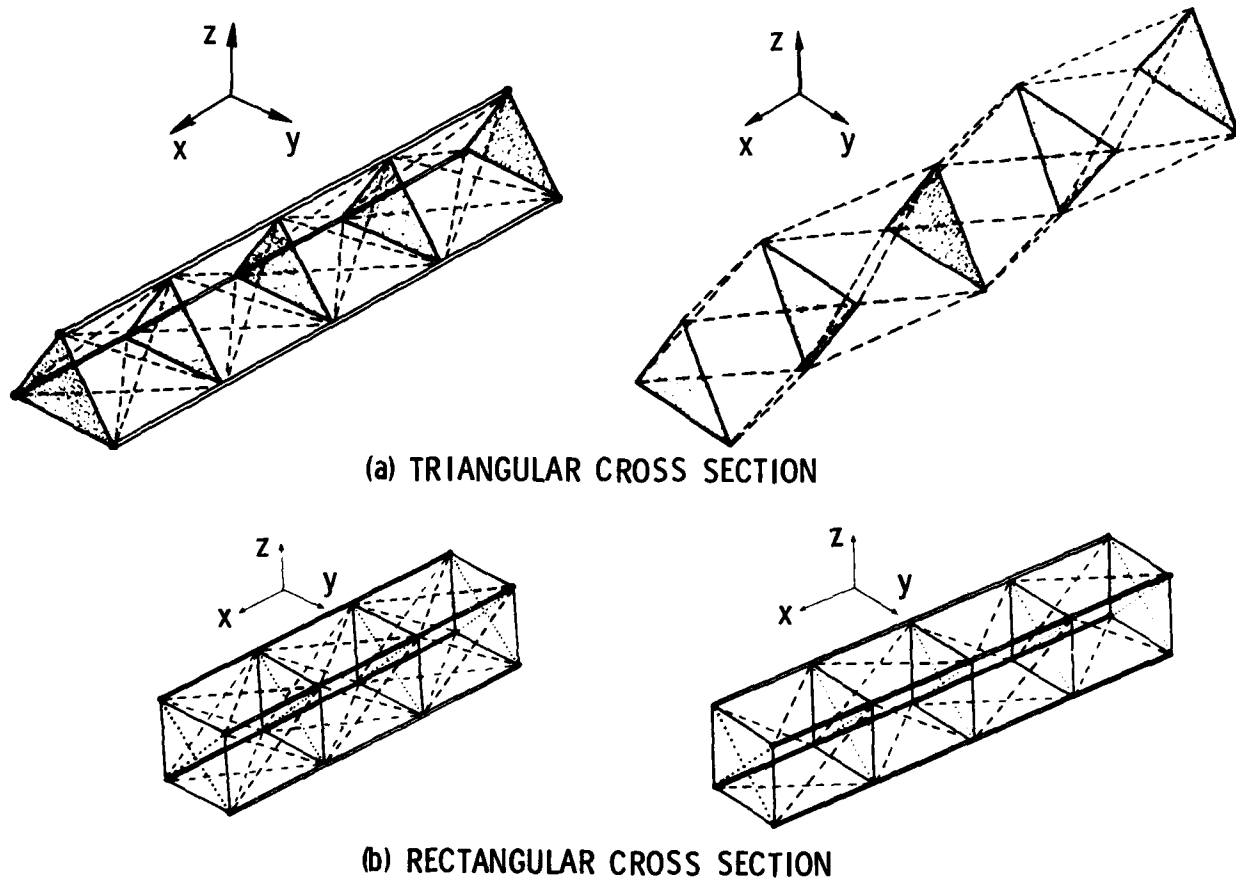
Figure 7

FREE VIBRATIONS OF CANTILEVERED DOUBLE-LACED BEAM

Consider the free vibrations of the cantilevered beam-like lattice with pin joints shown in Figure 8. The continuum model for this structure is a cantilever beam. The stiffness and the mass characteristics of this beam are given in Ref. 15. The accuracy of the lowest seven frequencies obtained by the continuum model is shown in the figure for the two cases of five and twenty bays. The exact frequencies were obtained by a direct finite element analysis of the actual structure. For five bays the maximum error in the third bending frequency is 7 percent and reduces to less than 2 percent for twenty bays. As to be expected, the accuracy of the predictions of the continuum model increases with the increase in the number of bays.

Figure 8

15
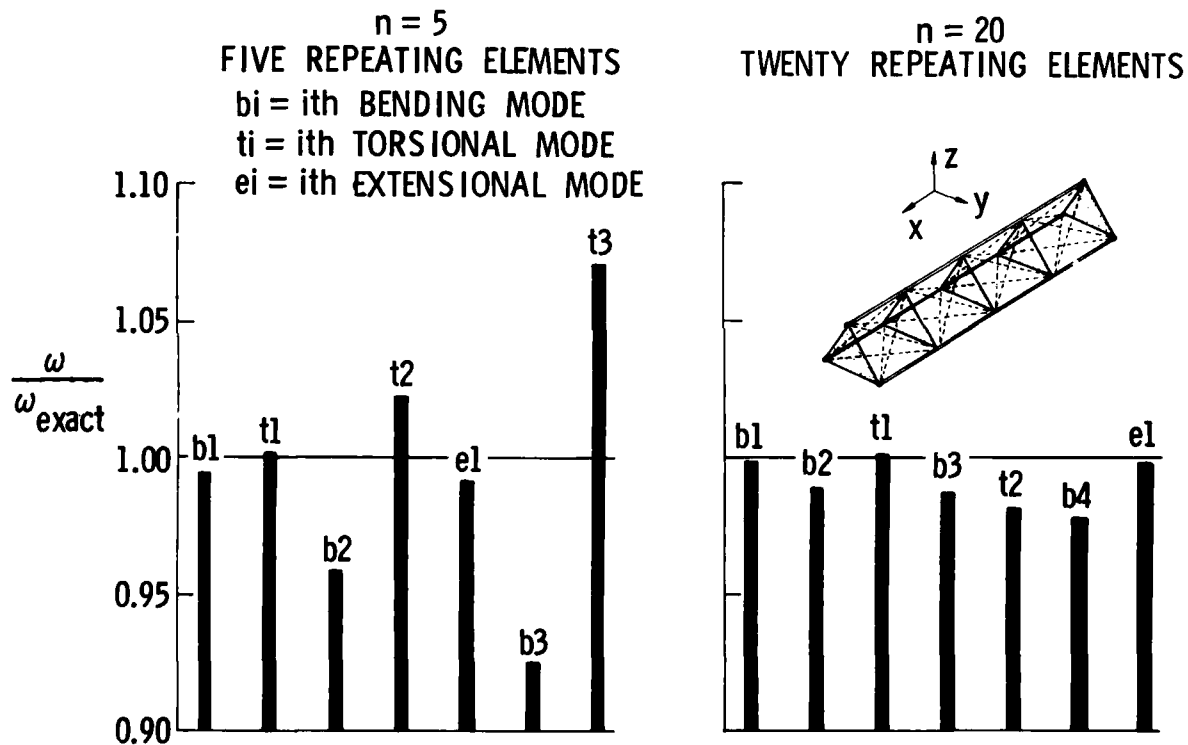
FREE VIBRATIONS OF A SIMPLY SUPPORTED HEXAHEDRAL GRID

The second problem considered is that of the free vibration response of a double-layered hexahedral lattice grid with pin joints shown in Figure 9. The continuum model for this grid is taken to be a square plate whose stiffness and dynamic characteristics are given in Ref. 15.

In order to amplify the effect of local deformations, the areas of the core members of the grid were assumed to be twenty times the areas of the core members. The accuracy of the lowest six frequencies is shown in the figure. The solid lines refer to the continuum which includes local deformations, and the hatched lines are for the case when local deformations are neglected. The importance of including the local deformation is obvious.
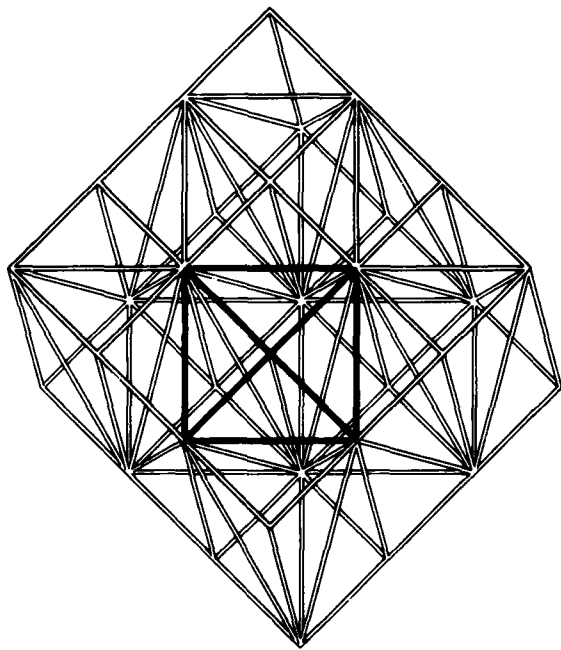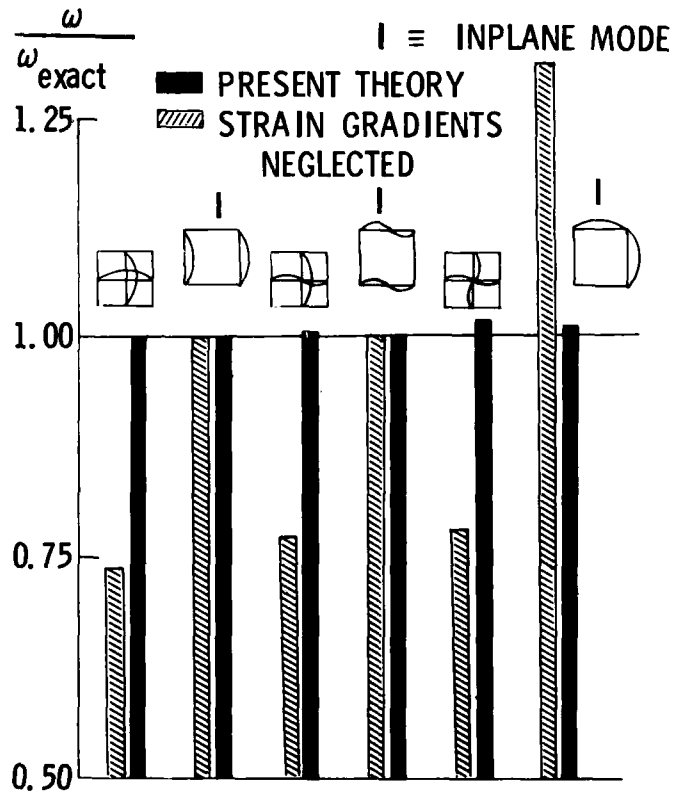
Figure 9

SPATIAL VIERENDEEL GIRDER

This set of results includes the free vibrations and buckling of beam-like lattices with rigid joints. As an extreme case consider the spatial vierendeel girder shown in Figure 10. The continuum model for this structure is a micropolar beam whose stiffness and dynamic characteristics are given in Ref. 21.
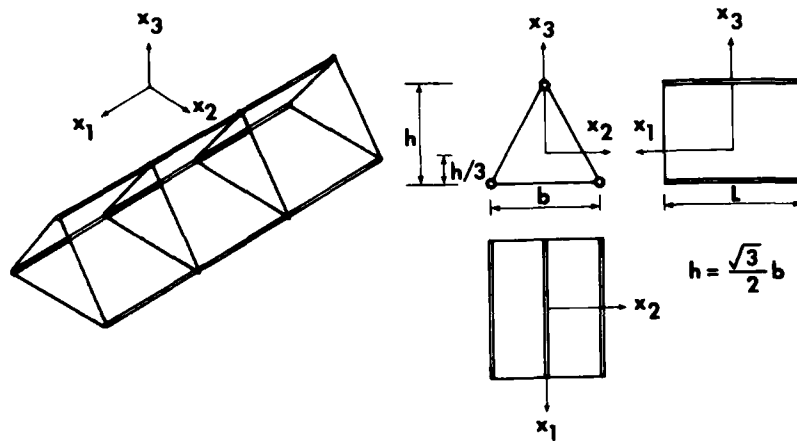
Figure 10

FREE VIBRATIONS OF CANTILEVERED VIERENDEEL GIRDER

The accuracy of the lowest six vibration frequencies obtained by the micropolar continuum models is shown in Figure 11. Two cases are considered, namely, five and twenty bays. For the case of five bays, the maximum error in the third bending frequency is less than 5 percent and for twenty bays the error is well within 0.1 percent.

Accuracy of Micropolar Continuum Solution
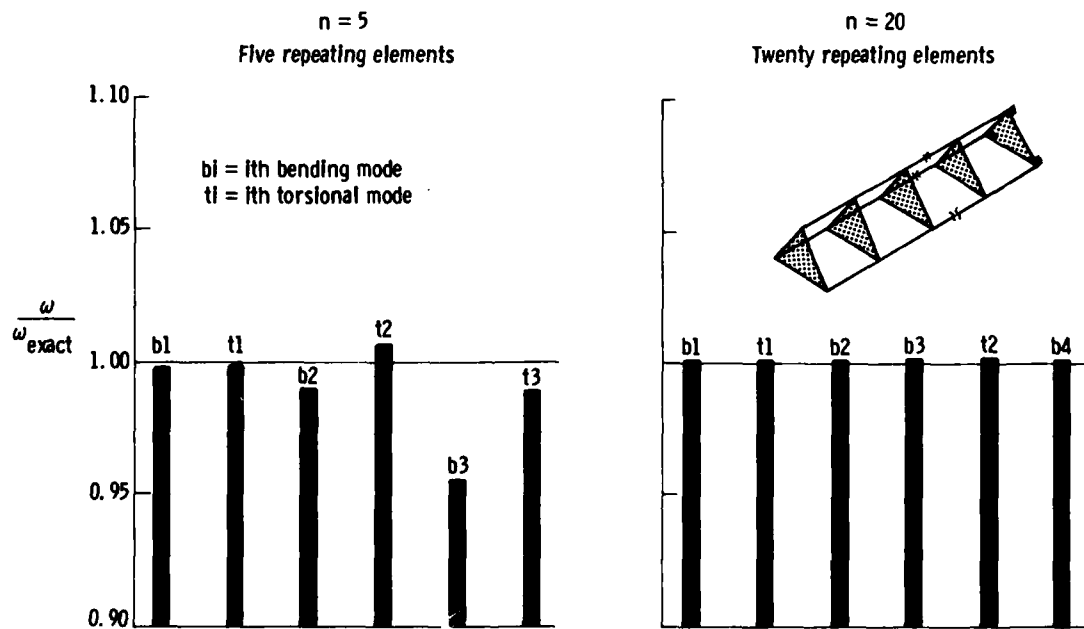
Figure 11

MODE SHAPES FOR CANTILEVERED VIERENDEEL GIRDER

The mode shapes associated with the lowest eight vibration frequencies for a ten-bay cantilevered vierendeel girder are shown in Figure 12. The modes alternate between flexural and torsional as shown. The continuum predictions are given along with the exact frequencies obtained by the direct finite element analysis of the actual lattice structure (shown between parentheses).

$\omega_1 = 2.285$ Hz (2.285)[b]

$\omega_2 = 4.973$ Hz (4.970)[t]

$\omega_3 = 7.553$ Hz (7.554)

$\omega_4 = 14.736$ Hz (14.670)[t]

$\omega_5 = 14.686$ Hz (14.747)[b]

$\omega_6 = 24.542$ Hz (24.253)[t]

$\omega_7 = 24.029$ Hz (24.449)

$\omega_8 = 34.304$ Hz (34.802)[t]
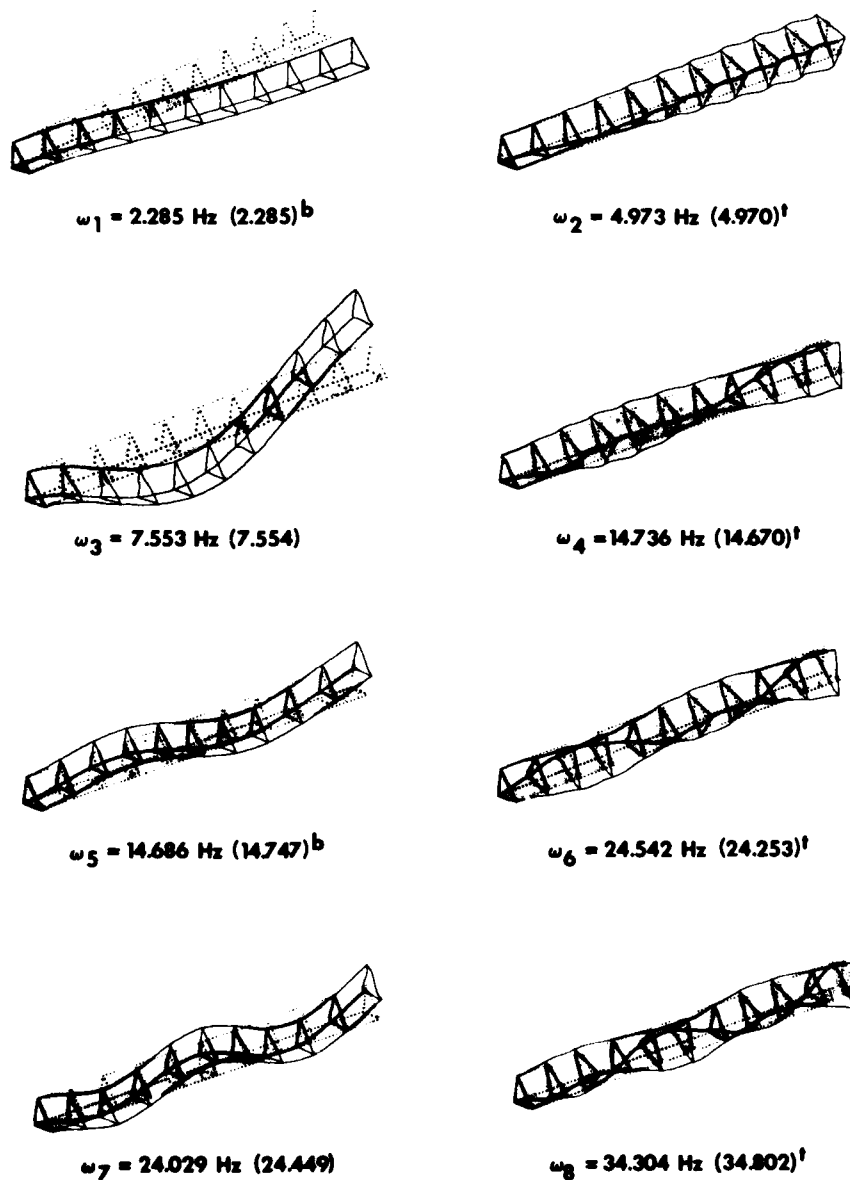
Figure 12

BUCKLING OF CANTILEVERED VIERENDEEL GIRDER

The lowest two bifurcation buckling modes of a ten-bay cantilevered vierendeel girder are shown in Figure 13. The predictions of the micropolar beam model are given along with those obtained by direct finite element analysis of the actual lattice (shown between parentheses).

Ten Repeating Elements
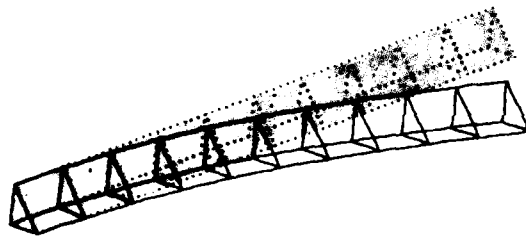
$10^{-3} \times \bar{\lambda}_1 = 1.330$ Newtons (1.330) $10^{-3} \times \bar{\lambda}_2 = 1.807$ Newtons (1.823)
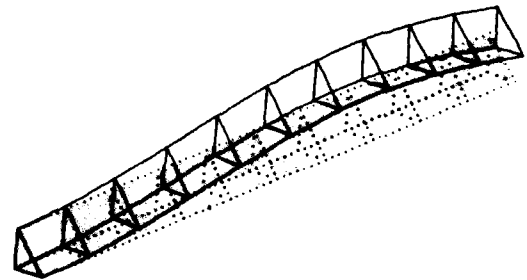
Figure 13

20

REDUCTION METHODS FOR BIFURCATION
BUCKLING AND NONLINEAR ANALYSIS

The second topic considered in this paper is the use of reduction methods for bifurcation buckling and nonlinear analysis. The basic features of reduction methods are outlined in Figure 14. They are techniques for reducing the number of degrees of freedom through the transformation shown. The vector $\{X\}$ represents the original displacement degrees of freedom. The vector $\{\psi\}$ refers to amplitudes of displacement modes and $[\Gamma]$ is a transformation matrix whose columns represent *a priori* chosen global displacement modes.

As to be expected, the effectiveness of reduction methods depends to a great extent on the proper selection of displacement modes. In a number of studies, it was shown that an effective choice of the displacement modes includes the various order derivatives of the displacement vector with respect to the load parameter (Refs. 8 and 9). These vectors are *generated by using the finite element model of the original lattice structure.* The recursion formulas for evaluating the derivatives $\{\frac{\partial X}{\partial p}\}$, $\{\frac{\partial^2 X}{\partial p^2}\}$, $\{\frac{\partial^3 X}{\partial p^3}\}$, ... are obtained by successive differentiation of the original finite element equations. The left-hand sides of the recursion formulas are the same (see Ref. 8). Therefore, *only one matrix factorization is required for the generation of all global functions.* Several numerical experiments have demonstrated the effectiveness of this choice (see Ref. 9).

DEFINITION: ARE TECHNIQUES FOR REDUCING THE NUMBER OF D.O.F. THROUGH THE TRANSFORMATION

$$\{X\}_{n,1} = [\Gamma]\{\psi\}_{r,1} \qquad r << n$$

$\{X\}$ = ORIGINAL DISPLACMENT D.O.F. IN THE FINITE ELEMENT MODEL

$[\Gamma]$ = MATRIX OF GLOBAL DISPLACEMENT MODES

$\{\psi\}$ = REDUCED D.O.F. ~ AMPLITUDES OF DISPLACEMENT MODES

SELECTION OF GLOBAL DISPLACEMENT MODES

$$[\Gamma] = \left[\{\frac{\partial X}{\partial p}\} \quad \{\frac{\partial^2 X}{\partial p^2}\} \quad \{\frac{\partial^3 X}{\partial p^3}\} \cdots \right]$$

p = LOAD PARAMETER

- COLUMNS OF $[\Gamma]$ GENERATED BY USING THE FINITE ELEMENT MODEL OF THE ORIGINAL STRUCTURE
- THEIR GENERATION REQUIRES ONLY ONE MATRIX FACTORIZATION
- NUMERICAL EXPERIMENTS HAVE DEMONSTRATED THEIR EFFECTIVENESS

Figure 14

BASIC EQUATIONS USED IN REDUCTION METHODS FOR BIFURCATION
BUCKLING AND STATIC NONLINEAR PROBLEMS

The basic equations used in reduction methods for bifurcation and static non-
linear problems are given in Figure 15. It is worth noting that the original
displacement unknowns {X} can be on the order of thousands whereas the reduced
unknowns {ψ} are typically twenty or less. This is true regardless of the complexity
of the structure and/or the loading. The details of the computational procedure for
tracing the load-deflection paths in nonlinear static analysis, including identifi-
cation of bifurcation and limit points, are given in Refs. 28 and 29. Application
of reduction methods to nonlinear dynamic problems is discussed in Ref. 9.

		ACTUAL (LARGE) PROBLEM	REDUCED (SMALL) PROBLEM
FUNDAMENTAL UNKNOWNS		$\{X\}$ = INDIVIDUAL DISPLACEMENTS → $\boxed{\{X\} = [\Gamma]\{\psi\}}$ → AMPLITUDES OF DISPLACEMENT MODES	
		● THOUSANDS OF UNKNOWNS	● TWENTY OR LESS
GOVERNING EQUATIONS	BIFURCATION BUCKLING	$\left[[K] + \hat{p}\,[K_G]\right]\{\hat{X}\} = 0$	$\left[[\tilde{K}] + \hat{p}\,[\tilde{K}_G]\right]\{\hat{\psi}\} = 0$
	STATIC NONLINEAR RESPONSE	$[K]\{X\} + \{G(X)\} - p\{P\} = 0$ ~ 1000 EQUATIONS	$[\tilde{K}]\{\psi\} + \{\tilde{G}(\psi)\} - p\{\tilde{P}\} = 0$ ~ 20 EQUATIONS
HOW TO TRACE LOAD-DEFLECTION PATH		● REPEATED SOLUTION OF LARGE SYSTEMS OF SIMULTANEOUS NONLINEAR ALGEBRAIC EQUATIONS	● GENERATION OF [Γ] ● MARCHING WITH SMALL SYSTEM OF EQUATIONS ● ERROR SENSING AND CONTROL (UPDATING [Γ] WHENEVER NEEDED)

$$[\tilde{K}] = [\Gamma]^T[K][\Gamma] \quad , \quad [\tilde{K}_G] = [\Gamma]^T[K][\Gamma] \quad , \quad \{\tilde{G}(\psi)\} = [\Gamma]^T\{G(X)\}$$

Figure 15

APPLICATION OF REDUCTION METHODS TO BIFURCATION
BUCKLING OF A LATTICE TRUSS

As a simple demonstration of the effectiveness of reduction methods to bifurcation buckling problems, consider the thirty-bay cantilevered beam-like lattice truss with pin joints subjected to axial loading. The truss has 372 displacement degrees of freedom. The convergence of the lowest two buckling loads with the increase in the number of global functions or reduced degrees of freedom is shown in Figure 16. With six global functions, i.e., a 6x6 eigenvalue problem, the results obtained by the reduced system are identical to those obtained by the full system of equations to four significant digits.

30-BAY CANTILEVERED BEAM-LIKE LATTICE TRUSS SUBJECTED TO AXIAL LOADING

NUMBER OF BASIS VECTORS	BUCKLING LOAD $p_{cr} \times 10^{-3}$	
	p_1	p_2
3	1.328	328.24
4	1.251	2.191
5	1.258	2.506
6	1.258	2.505
FULL SYSTEM (372 D.O.F.)	1.258	2.505

TYPICAL
REPEATING
ELEMENT

Figure 16

23
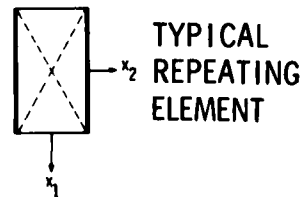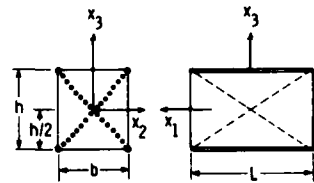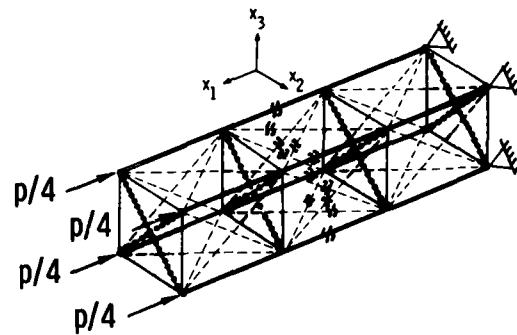
ANALYSIS AND MODELING NEEDS FOR LARGE SPACE STRUCTURES

The third part of the paper deals with the analysis and modeling needs of large space structures. A list of some of the areas where more work is needed in the future is given in Figure 17. The first area in which work is needed is the general deployment/erection analysis capability which includes the elements of both rigid body kinematics and flexible body dynamics.

The second area is that of analysis and modeling of structures with very slender members. This includes members with length to radius of gyration ratio of the order of 1,000. It also includes tension-stiffened and tension-stabilized structures.

Considerably more work is needed on sensitivity analysis, that is the sensitivity of the response of the structure to the various items listed in Figure 17.

Then there is a need for a hybrid continuum/discrete modeling and analysis capability for specialized problems such as stress concentrations.

Finally, accurate determination of thermal, dynamic, and control forces is needed.

- GENERAL DEPLOYMENT/ERECTION ANALYSIS CAPABILITY

  - COMBINED KINEMATIC-STRUCTURAL ANALYSIS (INCLUDING ROTATION, NONLINEAR AND DAMPING CHARACTERISTICS OF JOINTS, AND FLEXIBILITY OF MEMBERS)

  - DETERMINATION OF DEPLOYMENT LOADS (BOTH MECHANICAL AND DYNAMIC)

- ANALYSIS AND MODELING OF LATTICE STRUCTURES WITH VERY SLENDER MEMBERS AND CABLES

  - DYNAMIC CHARACTERISTICS OF STRUCTURES WITH BUCKLED MEMBERS

  - STUDY OF NONLINEAR (LARGE ROTATION) EFFECTS

  - IMPERFECTION SENSITIVITY

  - LEVEL OF MODELING REQUIRED (TENSION-STABILIZED STRUCTURES AND WRINKLED MEMBRANES)

- SENSITIVITY ANALYSIS - SENSITIVITY OF RESPONSE TO:

  - SURFACE INACCURACIES (E.G., CURVED SURFACE STRUCTURES)

  - VARIATIONS IN DESIGN VARIABLES (REQUIRED FOR EVALUATION OF STRUCTURAL CONCEPTS AND FOR OPTIMIZATION)

  - MODELING DETAILS

  - JOINT FLEXIBILITIES AND DAMPING CHARACTERISTICS

  - FAILURE OF SOME MEMBERS (DAMAGE TOLERANCE)

- HYBRID CONTINUUM - DISCRETE MODELING AND ANALYSIS CAPABILITY

- DETERMINATION OF THERMAL, DYNAMIC LOADS AND CONTROL FORCES

  - THERMAL LOADS INCLUDING COMPUTATION OF RADIATION VIEW-FACTORS

  - DYNAMIC LOADS DUE TO DOCKING, MANEUVERING AND ASSEMBLY

Figure 17

24

FUTURE DIRECTIONS FOR MODELING AND ANALYSIS
OF LARGE SPACE STRUCTURES

As far as future directions are concerned, the driving forces are the needs for evaluation of structural concepts, and accurate prediction of strength, stiffness, and fatigue life of large space structures (Figure 18). There are numerous opportunities provided by new advances in computer hardware, firmware, software, CAD/CAM systems, computational algorithms and materials technology.

DRIVING FORCE

- EVALUATE STRUCTURAL CONCEPTS

- PREDICT STRENGTH, STIFFNESS, FATIGUE LIFE AND DAMAGE TOLERANCE

  - MODELING AND ANALYSIS OF LARGE STRUCTURES SUBJECT TO HARSH ENVIRONMENT

  - RELIABILITY AND ERROR ESTIMATES OF SOLUTION

OPPORTUNITIES - PROVIDED BY NEW ADVANCES IN:

- COMPUTER HARDWARE AND FIRMWARE

- COMPUTER SOFTWARE AND CAD/CAM SYSTEMS

- COMPUTATIONAL ALGORITHMS

- MATERIALS TECHNOLOGY

Figure 18

RECENT AND PROJECTED ADVANCES IN COMPUTER
HARDWARE AND SOFTWARE

Some of the recent advances in computer hardware and software are listed in Figure 19. The new computing systems include the supercomputers such as the CRAY 1S and the CDC CYBER 205. The opportunities provided by these large computers are discussed in Ref. 30. There are minicomputers with the new array processors such as the FPS-164 which has 64 bit-length word and a computational speed of the order of 12 MFLOPS (millions of floating point operations per second). Microprocessors are likely to impact large space structures. Then there are the new multiple CPU computers like the APPOLLO computers which have several processors running in an asychronous manner using the same data base.

As far as the user-interface type of hardware is concerned, it is worth mentioning the new verbal (audio) and visual interfaces.

Considerable progress has been made in the software area. Software progress includes relational data bases, which can handle large volumes of data and which are a product of the IPAD technology at NASA Langley (Ref. 31), and the new geometric modeling and graphics systems (such as the AD-2000 and the ANVIL-4000). Perhaps one area which needs more attention is that of artificial intelligence and its exploitation in the design of large space structures.

- NEW COMPUTING SYSTEMS

  - SUPERCOMPUTERS (E.G., CRAY, CYBER 205)

  - MINICOMPUTERS/ARRAY PROCESSORS (FPS-164)

  - MICROPROCESSORS

  - MULTIPLE CPU COMPUTERS (E.G., APPOLLO COMPUTER) - SEVERAL PROCESSORS RUNNING IN AN ASYNCHRONOUS MANNER USING THE SAME DATA BASE.

- HARDWARE - USER INTERFACE

  - GRAPHIC DISPLAY

  - VERBAL (AUDIO) AND VISUAL INTERFACES

- SOFTWARE

  - RELATIONAL DATA BASES (RIM - NASA LANGLEY)

  - GEOMETRIC MODELING AND GRAPHICS SYSTEMS (E.G., AD-2000, ANVIL 4000)

  - ARTIFICIAL INTELLIGENCE

Figure 19

INTEGRATED ANALYSIS AND CAD SYSTEMS

The efficient design of large space structures requires a strong interaction between a number of disciplines including structures, controls, and thermal analysis, among others. In response to this need, integrated analysis and CAD systems have been developed and are currently upgraded to perform this task. Three examples are listed in Figure 20.

- INTEGRATED THERMAL-STRUCTURAL-CONTROL CAPABILITY (BOEING - NASA GODDARD)

- COMPUTER-AIDED DESIGN SYSTEM (GENERAL DYNAMICS, MARTIN MARIETTA - NASA LANGLEY)

- FUTURE DISTRIBUTED/INTEGRATED ANALYSIS DESIGN SYSTEM AT LANGLEY

Figure 20

27

FUTURE DISTRIBUTED/INTEGRATED ANALYSIS DESIGN
SYSTEM AT LANGLEY

A schematic of a future distributed/integrated analysis design system at Langley
is shown in Figure 21. It has an executive and a number of functional modules each
representing one of the disciplines. These models interact through a common rela-
tional information manager (RIM). The planned system, which is already well under
development, would allow the different modules to be executed on different computers
(distributed computing). The computers may even be located at different geographic
locations.
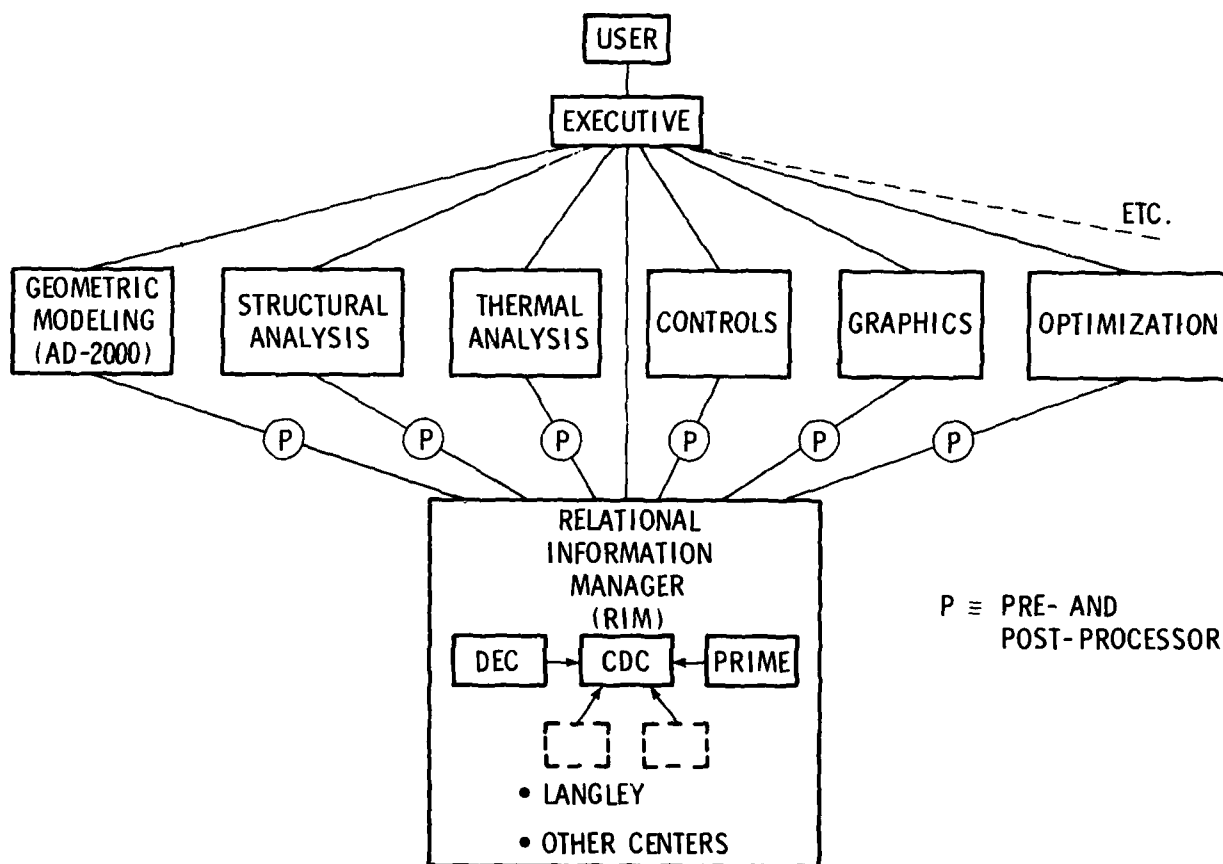
Figure 21

SUMMARY

In summary, three topics are covered in this paper, namely, recent advances in continuum modeling, progress in reduction methods, and analysis and modeling needs for large space structures (Figure 22).

As far as continuum modeling is concerned, an effective and verified analysis capability exists for linear thermoelastic stress, birfurcation buckling, and free vibration problems of repetitive lattices. However, application of continuum modeling to nonlinear analysis needs more development.

Reduction methods have proven to be very effective for bifurcation buckling and static (steady-state) nonlinear analysis. However, more work is needed to realize their full potential for nonlinear dynamic and time-dependent problems.

As far as analysis and modeling needs are concerned, three areas have been identified.

As to be expected, the modeling and analysis of large space structures will be strongly impacted by new advances in computer hardware, software, integrated analysis, CAD/CAM systems, and materials technology.

- **CONTINUUM MODELING**

    - VERIFIED FOR LINEAR STRESS ANALYSIS, BIFURCATION BUCKLING, AND FREE VIBRATION PROBLEMS OF REPETITIVE LATTICES

    - NEEDS DEVELOPMENT FOR NONLINEAR ANALYSIS

- **REDUCTION METHODS**

    - VERIFIED FOR BIFURCATION BUCKLING AND STATIC NONLINEAR PROBLEMS

    - FURTHER DEVELOPMENTS NEEDED FOR NONLINEAR DYNAMIC PROBLEMS

- **ANALYSIS AND MODELING NEEDS**

    - GENERAL DEPLOYMENT/ERECTION ANALYSIS

    - LATTICE STRUCTURES WITH VERY SLENDER MEMBERS AND CABLES

    - SENSITIVITY ANALYSIS

- **IMPACT OF NEW ADVANCES IN COMPUTER HARDWARE, SOFTWARE AND MATERIALS TECHNOLOGY**

Figure 22

REFERENCES

1. Hagler, T.: Building Large Structures in Space. Astronautics and Aeronautics, vol. 14, no. 5, May 1976, pp. 56-61.

2. Card, M. C.; and Boyer, W. J.: Large Space Structures - Fantasies and Facts. Proceedings of the AIAA/ASME/ASCE/AHS 21st Structures, Structural Dynamics and Materials Conference, May 1980, Part 1, pp. 101-114.

3. Brodsky, R. F.; and Morais, B. G.: Space 2020: The Technology, the Missions Likely 20-40 Years From Now. Astronautics and Aeronautics, vol. 20, no. 5, May 1982, pp. 54-73.

4. Bush, H. G.; and Heard, W. L.: Recent Advances in Structural Technology for Large Deployable and Erectable Spacecraft. NASA TM-81905, October 1980.

5. Heard, W. L.; Bush, H. G.; Walz, J. E.; and Rehder, J. J.: Structural Sizing Considerations for Large Space Platforms. Journal of Spacecraft and Rockets, vol. 18, no. 6, Nov.-Dec. 1981, pp. 556-564.

6. Bibliography on Latticed Structures. Journal of the Structural Division, ASCE, vol. 98, no. ST7, July 1972, pp. 1545-1566.

7. Lattice Structures: State-of-the-Art Report. Journal of the Structural Division, ASCE, vol. 102, no. ST11, Nov. 1976, pp. 2197-2230.

8. Noor, A. K.; and Peters, J. M.: Reduced Basis Technique for Nonlinear Analysis of Structures. AIAA J., vol. 18, no. 4, 1980, pp. 455-462.

9. Noor, A. K.: Recent Advances in Reduction Methods for Nonlinear Problems. Computers and Structures, vol. 13, nos. 1-2, 1981, pp. 31-44.

10. Flower, W. R.; and Schmidt, L. C.: Analysis of Space Truss as Equivalent Plate. Journal of the Structural Division, ASCE, vol. 97, no. 12, Dec. 1971, pp. 2777-2789.

11. Heki, K.; and Saka, T.: Stress Analysis of Lattice Plates as Anisotropic Continuum Plates. Proceedings of the 1971 IASS Pacific Symposium, Part II on Tension Structures and Space Frames, 1972, pp. 663-674.

12. Kollar, L.: Analysis of Double-Layer Space Trusses With Diagonally Square Mesh by the Continuum Method. Acta Technica Academiae Scientiarum Hungaricae, Tomus 76 (3-4), 1974, pp. 273-292.

13. Nayfeh, A. H.; and Hefzy, M. S.: Continuum Modeling of the Mechanical and Thermal Behavior of Discrete Large Structures. AIAA J., vol. 19, no. 6, June 1981, pp. 766-773.

14. Sun, C. T.; Kim, B. J.; and Bogdanoff, J. A.: On the Derivation of Equivalent Simple Models for Beam- and Plate-Like Structures in Dynamic Analysis. Proceedings of the AIAA/ASME/ASCE/AHS Structures, Structural Dynamics and Materials Conference, April 1981, pp. 523-532.

15. Noor, A. K.; Anderson, M. S.; and Greene, W. H.: Continuum Models for Beam- and Plate-Like Lattice Structures: AIAA J., vol. 16, no. 12, Dec. 1978, pp. 1219-1228.

16. Noor, A. K.; and Andersen, C. M.: Analysis of Beam-Like Lattice Trusses. Computer Methods in Applied Mechanics and Engineering, vol. 20, no. 1, Oct. 1979, pp. 53-70.

17. Noor, A. K.; and Weisstein, L. S.: Stability of Beam-Like Lattice Trusses. Computer Methods in Applied Mechanics and Engineering, vol. 25, no. 2, Feb. 1981, pp. 179-193.

18. Wozniak, C.: Load Carrying Structures of the Dense Lattice Type, the Plane Problem. Archiwum Mechaniki Stosowanej, vol. 18, 1966, pp. 581-597.

19. Bazant, Z. P.; and Christensen, M.: Analogy Between Micropolar Continuum and Grid Frameworks Under Initial Stress. International Journal of Solids and Structures, vol. 8, no. 3, March 1972, pp. 327-346.

20. Sun, C. T.; and Yang, T. Y.: A Continuum Approach Toward Dynamics of Gridworks. Journal of Applied Mechanics, Transactions of ASME, vol. 40, 1973, pp. 186-192.

21. Noor, A. K.; and Nemeth, M. P.: Analysis of Spatial Beam-Like Lattices with Rigid Joints. Computer Methods in Applied Mechanics and Engineering, vol. 24, no. 1, Oct. 1980, pp. 35-59.

22. Dean, D. L.; and Avent, R. R.: State-of-the-Art of Discrete Field Analysis of Space Structures. Proceedings of the Second International Conference on Space Structures, edited by W. J. Supple, Sept. 1975, pp. 7-16.

23. Dean, D. L.: Discrete Field Analysis of Structural Systems. Springer-Verlag, 1976.

24. McDaniel, T. J.; and Chang, K. J.: Dynamics of Rotationally Periodic Large Space Structures. Journal of Sound and Vibration, vol. 68, no. 3, 1980, pp. 351-368.

25. Anderson, M. S.: Buckling of Periodic Lattice Structures. AIAA J., vol. 19, no. 6, June 1981, pp. 782-788.

26. Anderson, M. S.: Vibration of Prestressed Periodic Lattice Structures. AIAA J., vol. 20, no. 4, April 1982, pp. 551-555.

27. Eringen, A. C.: Linear Theory of Micropolar Elasticity. Journal of Mathematics and Mechanics, vol. 15, no. 6, June 1966, pp. 909-923.

28. Noor, A. K.; and Peters, J. M.: Tracing Post-Limit-Point Paths With Reduced Basis Technique. Computer Methods in Applied Mechanics and Engineering, vol. 28, no. 2, Sept. 1981, pp. 217-240.

29. Noor, A. K.; and Peters, J. M.: Bifurcation and Post-Buckling Analysis of Laminated Composite Plates Via Reduced Basis Technique. Computer Methods in Applied Mechanics and Engineering, vol. 29, Dec. 1981, pp. 271-295.

30. Swanson, J. A.: Opportunities Provided by Large Computers. New and Future Developments in Commercial Finite Element Methods, ed. by J. Robinson, Robinson and Associates, 1981, pp. 436-450.

31. Blackburn, C. L.; Storaasli, O. O.; and Fulton, R. E.: The Role and Application of Database Management in Integrated Computer-Aided Design. Proceedings of the AIAA/ASME/ASCE/AHS 23rd Structures, Structural Dynamics and Materials Conference, May 1982, Part 2, pp. 603-613.

RECENT DEVELOPMENTS IN THERMAL ANALYSIS
OF LARGE SPACE STRUCTURES

R. F. O'Neill
General Dynamics Corporation
Convair Division
San Diego, California

33

LATTICE-TYPE SPACE STRUCTURES CAN EXPERIENCE
ACCUMULATED PENUMBRAL SHADOWING

Thermal analysis of relatively sparse structures in the space environment has customarily omitted consideration of shadowing by up-sun structural members. This convention has been frequently questioned in the case of lattice-type structures supporting very large, near-planar, Earth-facing surfaces (e.g., antennas). For these, significant shadowing can occur whenever the solar vector is nearly tangent to the orbital path. It thus becomes advisable to quantify the shadowing effect, but sparse structures present an exceptional element of complexity. A typical sparse structural assembly, a parabolic expandable truss antenna (PETA), is portrayed in figure 1. In such assemblies, multiple up-sun (i.e., shadowing) members may yield only partial shadowing of an elemental area of interest, with the degree and duration of shadowing being a strong function of the size and density of the structural assembly.
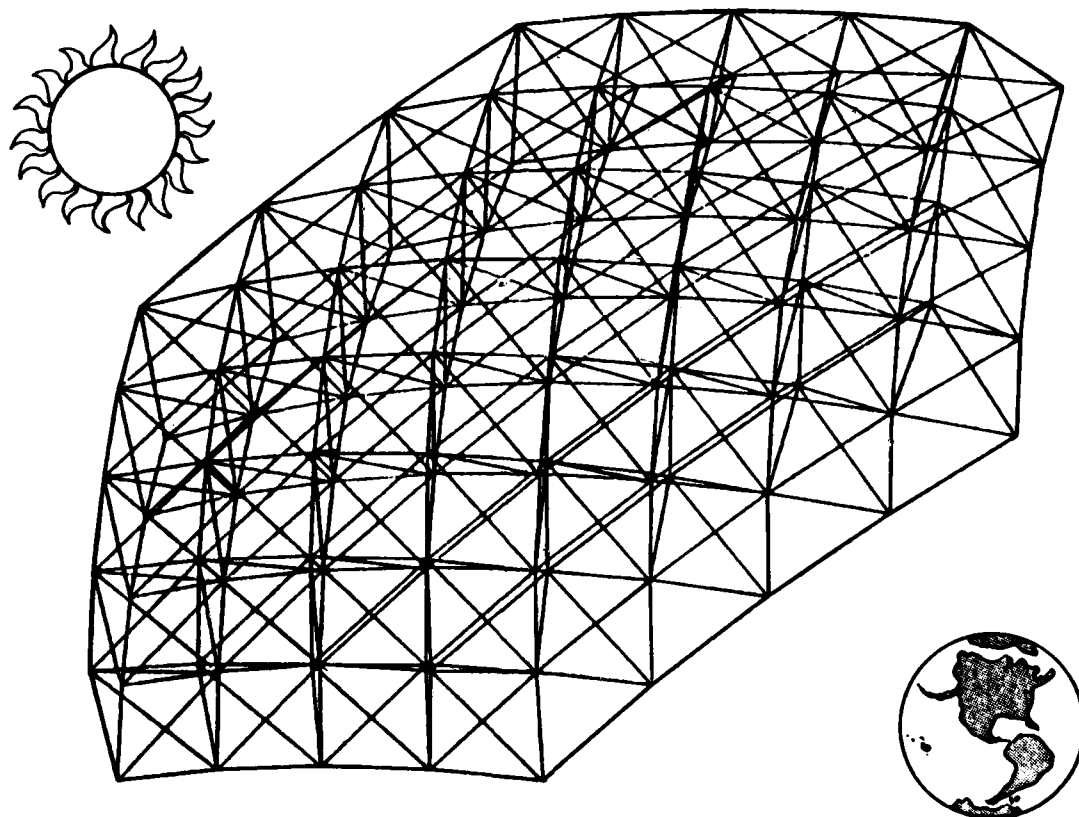
Figure 1

THE TRADITIONAL APPROACH: THERMAL MODELING OF THE ON-ORBIT ASSEMBLY RADIAL ARM

Space heating analysis procedures usually assume either total shadowing or total solar irradiation of individual elemental areas of mapped surfaces. The Vector Sweep program (ref. 1) typifies this approach. While the latter convention is reasonably sound for structural assemblies of which most or all geometric dimensions are of the same order of magnitude, it is less realistic for sparse structures composed of slender members having extremely high length-to-diameter (ℓ/d) ratios. Traditional methods were employed in modeling an on-orbit assembly (OOA) spacecraft structural assembly, as described in reference 2. The analysis model is shown in figure 2. Following computation of radiation view factors for spatially oriented arrays of geometric subelements, incident space-environment heat rates were computed for each subelement at successive points in time throughout the orbit. The heat rate histories were then incorporated in a thermal model of the radial-arm subassembly, which yielded temperature histories for the radial-arm structural elements. The thermal analyzer model nodal arrangement was geometrically identical to the Vector Sweep program subelement arrangement permitting direct incorporation of the Vector Sweep output heat flux histories in the thermal analyzer model. Notwithstanding its level of detail, the thermal model is seen to be limited in scope, in that it can address only a local region of the total structural assembly.
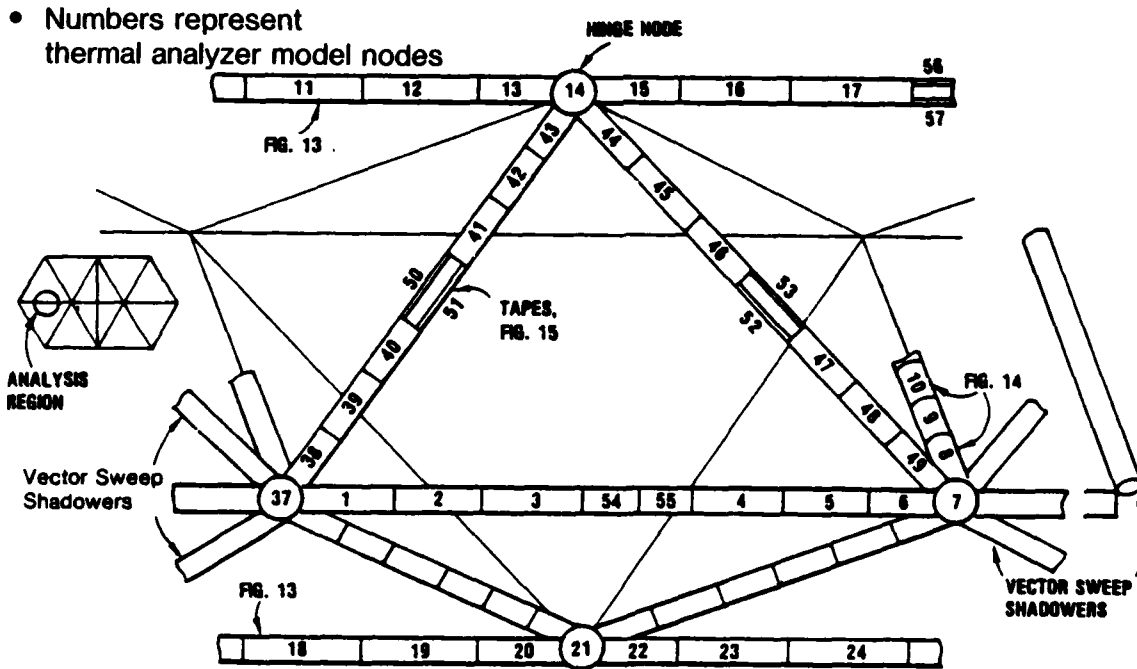
Figure 2

THERMAL RESPONSE AS PREDICTED BY TRADITIONAL METHODS

On-orbit assembly spacecraft radial-arm cross-member temperature histories obtained in the study in reference 2 are shown in figure 3. It will be instructive to make a qualitative comparison of figure 3 with temperature prediction data from the space structure heating (SSQ) procedure, to be presented later. It is seen that only six shadowing members are implied in the figure 3 temperature histories. Thus, accumulated shadowing by multiple, more distant members is not taken into account. This is a commentary on the limited geometric scope of the model of figure 2. Conversely, the total shadowing (rather than penumbral) inferred during the six non-Earth-shadowed intervals is probably excessive.
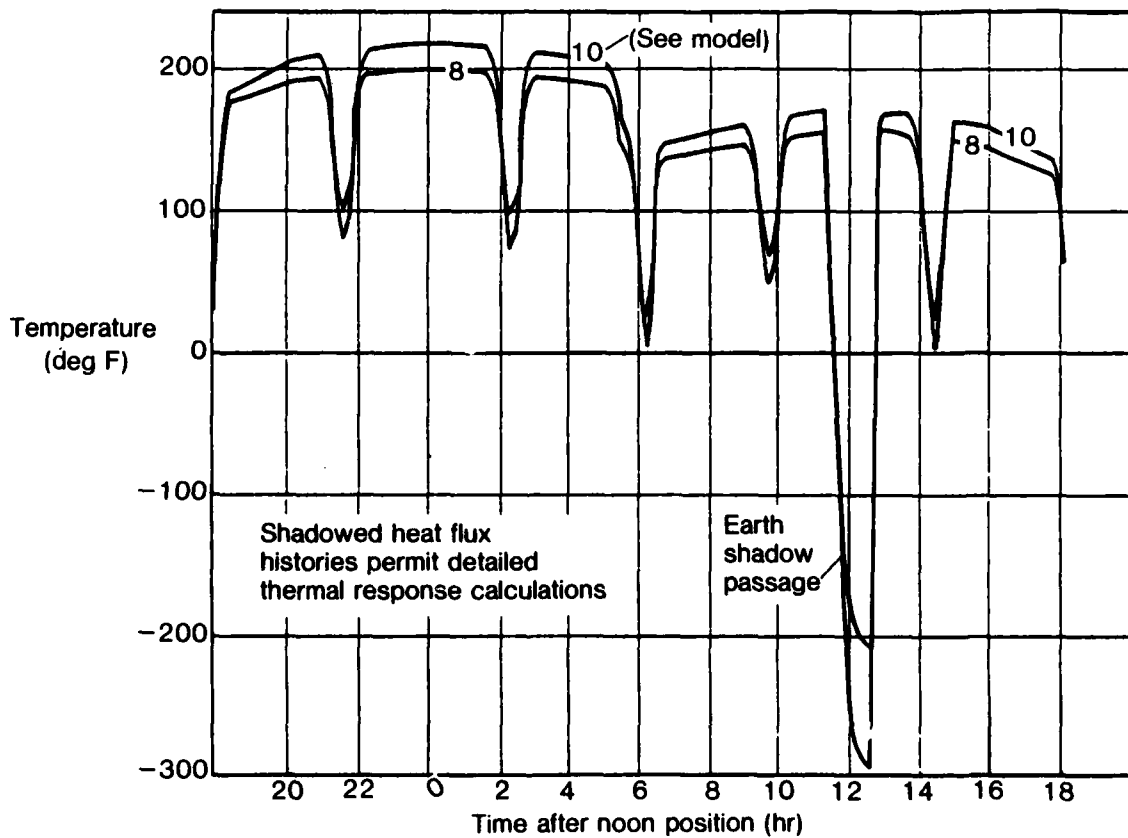
Figure 3

AN ALTERNATE APPROACH: THE SSQ PROCEDURE

It will be seen that typical space structural members can experience intervals of solar shadowing that vary widely in terms of timing, duration and degree, even on a single member. The SSQ program, introduced in reference 3, avoids inordinate computational complexity by confining attention to a single elemental location on a structural member of interest throughout an entire orbital period, proceeding thence to similar treatment of individual alternate locations. The procedure considers a spacecraft in circular orbit and assumes fixed-Earth orientation of the spacecraft. As shown in figure 4, its angular position θ in orbit is measured from an arbitrary datum. Orbital-plane angle of inclination to the Sun vector $\overline{S}$ is defined as β. Also noted in figure 4 is a moving-spacecraft right-handed coordinate system, of which the positive x-axis is in the direction of motion, and the positive z-axis contains the center of the Earth.

CIRCULAR ORBIT,

$$P = \frac{\pi}{30} \sqrt{\frac{(H + 3440)^3}{62750}}$$

$$t = \frac{\theta}{360} P$$
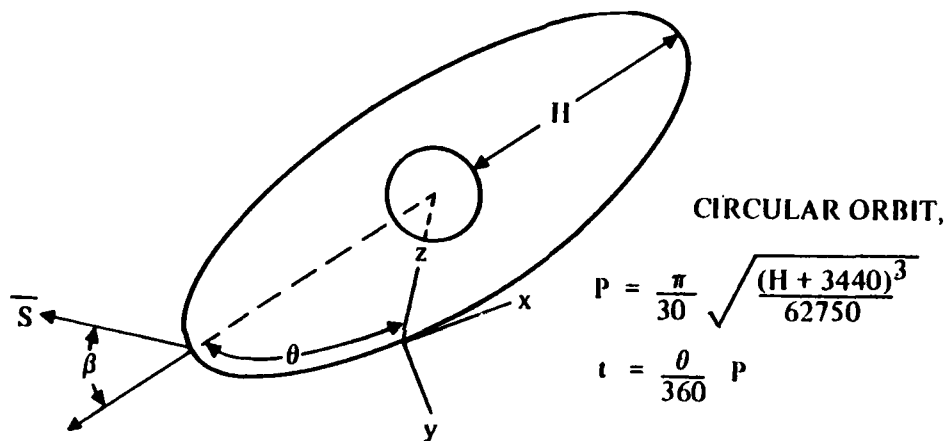
H = ORBIT ALTITUDE, n.mi.

P = ORBIT PERIOD, min

θ = SPACECRAFT ANGULAR POSITION IN ORBIT

β = ORBITAL PLANE INCLINATION TO SUN VECTOR

$\hat{S}$ = COS β SIN θ, SIN β, COS β COS θ

Figure 4

SHADOWING-MEMBER IDENTIFICATION

The SSQ program permits definition of numbered structural node locations in the spacecraft coordinate system, followed by definition of line segments (structural members) in terms of bounding node numbers. Slender structural members are assumed to be cylindrical, and are assigned values of diameter, thermal mass per unit of length, solar absorptance, emittance, and view factor to space. Partially or totally opaque bodies are also defined in terms of bounding line segments, and the latter surfaces are assigned transmissivities that may vary as functions of solar angle of incidence.

Following selection of a structural element of interest i, all spacecraft coordinate data are transformed (without rotation) to an i-centered coordinate system. The latter data thus define potential shadowing members j. As shown in figure 5, the locus of the spacecraft-Sun vector progressing about element i through a complete orbit describes a cone with its apex at the i-centered system origin. Potential shadowers are represented as line segments. Simultaneous solution of line and cone equations yields sets of intercepts $(x, y, z)_j$ which are then examined for residence between limiting values $(x, y, z)_{1,j}$ and $(x, y, z)_{2,j}$. Qualifying sets define individual members that actually do shadow element of interest i, permitting definition of the orbital position θ at which shadowing occurs. At this point, shadowing members j are retained in a new k array, in order of increasing θ_k.
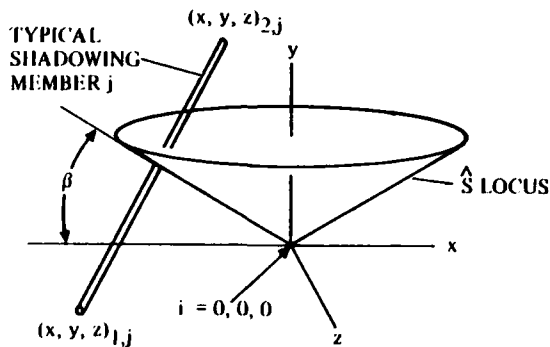
- SHADOWER j COORDINATES TRANSLATED TO i = 0, 0, 0 SYSTEM

- $L_j = \sqrt{(x_2 - x_1)_j^2 + (y_2 - y_1)_j^2 + (z_2 - z_1)_j^2}$

  $a_j = \left(\frac{x_2 - x_1}{L}\right)_j, \quad b_j = \left(\frac{y_2 - y_1}{L}\right)_j, \quad c_j = \left(\frac{z_2 - z_1}{L}\right)_j$

- SHADOWER: $\left(\frac{x - x_1}{a}\right)_j = \left(\frac{y - y_1}{b}\right)_j = \left(\frac{z - z_1}{c}\right)_j$

- $\hat{S}$ LOCUS: $x^2 + z^2 - y^2/\tan^2\beta = 0$

Figure 5

38

SHADOW ORIENTATION

It now becomes necessary to examine the orientation of shadows θ_k as viewed from the element of interest i. As seen in figure 6, shadows traversing the visible solar disc can be classified as being essentially horizontal or nonhorizontal. The latter distinction becomes an important discriminator in computing individual shadowing durations. The two shadow classifications are compared in figure 6, in which assumed values for the radius of and distance to the Sun are shown: 375,735 n.mi., and 80,884,432 n.mi., respectively. Of major significance, the end points of a so-called horizontal shadow are assumed to enter and leave the visible solar disc, but it is assumed that the end points of a nonhorizontal shadow are never visible.


Figure 6

39
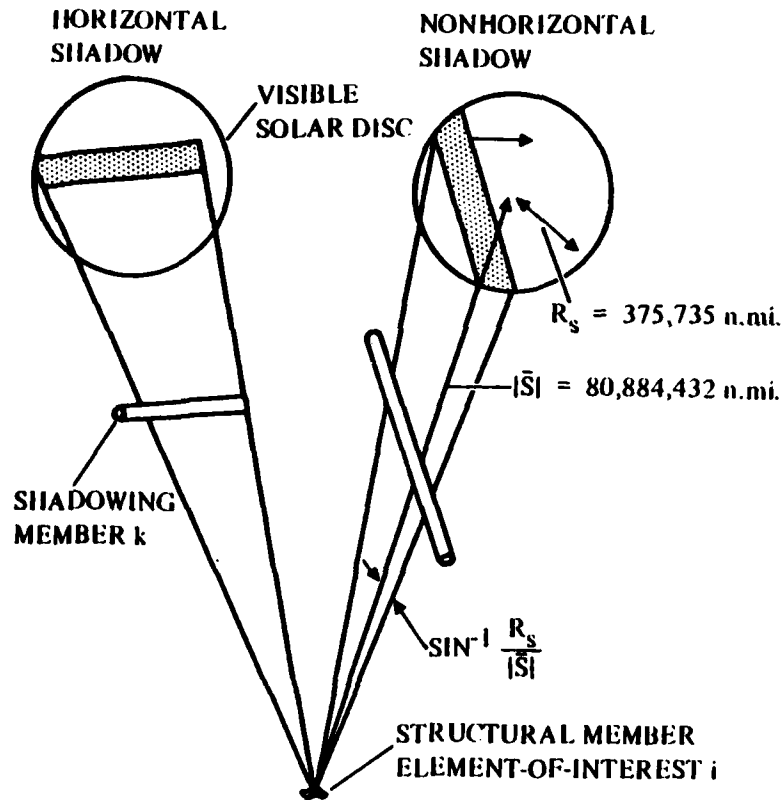
INCLINATION ANGLE φ' DETERMINES SHADOW CLASSIFICATION

Development of the test for classifying shadow orientation is shown in figure 7. Unit vector $\hat{p}$ normal to $\hat{S}$ and $\bar{L}_k$ is obtained by normalizing the product $\bar{L}_k$ x $\hat{S}$. Incidence angle ϕ_k is the angle described by $\hat{n}_k$ and the projection of $\bar{L}_k$ on a plane normal to $\bar{S}$. Angle ϕ_k is employed later in computing the duration of non-horizontal shadow intervals. The scalar projection of $\bar{L}_k$ on $\hat{n}_k$ is $(\bar{L} \cdot \hat{n})_k$, and $(\bar{L} \cdot \hat{n} \tan \phi)_k$ divided by $(\bar{L} \cdot \hat{n})_k$ is the slope of the $\bar{L}_k$ projection normal to $\bar{S}$. As shown in figure 7, $(\bar{L} \cdot \hat{n} \tan \phi)_k$ divided by the absolute value of vector $(\bar{\ell}_1 + \bar{L} \cdot \hat{n})$ $\hat{n})_k$ is the tangent of angle ϕ_k'. This angle is an indicator of horizontal versus non-horizontal shadow orientation; i.e., for $\phi_k' = 2 \tan^{-1} (R_S/|\bar{S}|)$, member k would barely qualify as nonhorizontal (see figure 6). At this point, a reasonable assumption is imposed to define a horizontal shadow in terms of $R_S/|\bar{S}|$, as shown in figure 7.

$\bar{p}_k = \bar{L}_k \times \hat{s}$

$\phi_k = \sin^{-1} |\hat{p} \cdot \hat{n}|_k$

$\phi_k' = \tan^{-1} \left| \dfrac{\bar{L} \cdot \hat{n} \tan \phi}{|\bar{\ell}_1 + (\bar{L} \cdot \hat{n})\hat{n}|} \right|_k$

$\bar{L}_k$ lies along shadowing member

$\hat{p}_k$ = unit vector $\perp$ to $\hat{S}$ and $\bar{L}_k$

$\hat{n}_k$ = unit vector $\perp$ to $\hat{S}$ and $\parallel$ to orbit plane

ϕ_k = $\angle$ of incidence to $\hat{n}$ of $\bar{L}_k$ projection $\perp$ to $\hat{S}$

$\dfrac{R_S}{|\bar{S}|}$ $\geqslant$ TAN ϕ_k' for horizontal shadow

$\geqslant L_k \dfrac{\sin (\cos^{-1} |\hat{L}_k \cdot \hat{S}|)}{|\ell_1 + (\bar{L} \cdot \hat{n})\hat{n}|_k}$ if ϕ_k GE 89°
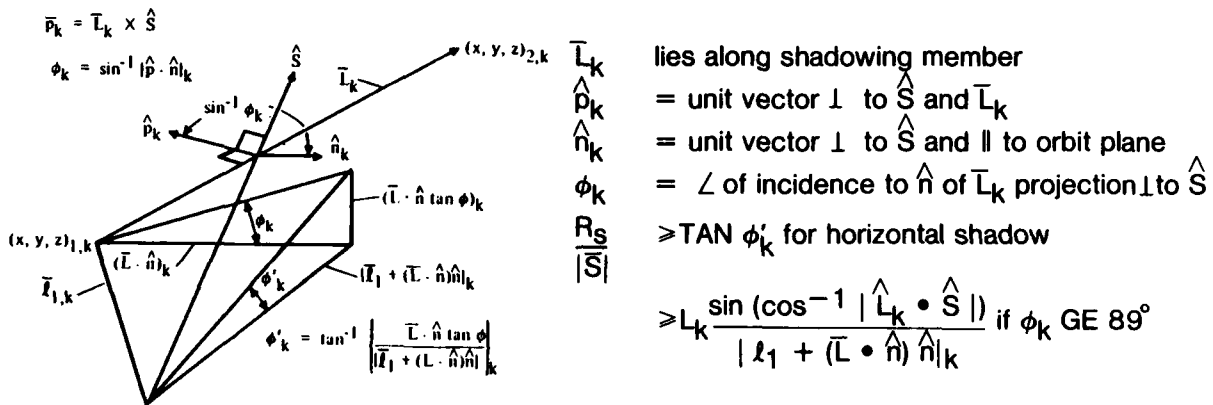
Figure 7

SHADOWING INTERVAL DURATION

It now becomes necessary to compute the durations required for each shadow to traverse the visible solar disc. Methods employed to compute shadowing interval durations are illustrated in figure 8, in which the following terms are introduced:

θ_B = Beginning of interval

θ_E = End of interval

$\Delta\theta = \theta_E - \theta_B$

d = Shadowing member width

ℓ = Distance to intercept at θ

Horizontal shadow maximum durations are evaluated in terms of the projection of an extremely long shadower on a celestial unit sphere. Nonhorizontal shadow durations are related to their inclination angles ϕ to the orbit plane, the lower limit being twice the bracketed term (a verticle shadow). However, the value that θ_B and θ_E for both horizontal and nonhorizontal shadows cannot exceed is always limited by the shadower end coordinates.

• **Horizontal shadow**

• **Nonhorizontal shadow**

$$\Delta\theta_k \leq \frac{2}{\sin\phi} \left[\sin^{-1} \frac{R_s}{|\bar{S}|} + \sin^{-1} \left(\frac{d}{2\ell} \right)_k \right]$$

Path of sun projection on celestial unit sphere

$$A = \cos^2 \left[\beta - \sin^{-1} \frac{R_s}{|\bar{S}|} - \sin^{-1} \left(\frac{d}{2\ell} \right)_k \right]$$

$$B = \cos^2 \left[\beta + \sin^{-1} \frac{R_s}{|\bar{S}|} + \sin^{-1} \left(\frac{d}{2\ell} \right)_k \right]$$

$$\Delta\theta_k \leq 2\sin^{-1} \left[\frac{B^2 - A^2}{A^2 (B^2 - 1)} \right]^{1/2}$$

• **But, both shadow types**

$$\text{Min } \theta_B \geq \left[\sin^{-1} \frac{-x_1}{\sqrt{x_1^2 + z_1^2}} \right.$$

$$\text{and } \cos^{-1} \frac{-z_1}{\sqrt{x_1^2 + z_1^2}} \left. \right] - \sin^{-1} \frac{R_s}{|\bar{S}|} - \sin^{-1} \left(\frac{d}{2\ell} \right)_k$$

$$\text{Max } \theta_E \leq \left[\sin^{-1} \frac{-x_2}{\sqrt{x_2^2 + z_2^2}} \right.$$

$$\text{and } \cos^{-1} \frac{-z_2}{\sqrt{x_2^2 + z_2^2}} \left. \right] + \sin^{-1} \frac{R_s}{|\bar{S}|} + \sin^{-1} \left(\frac{d}{2\ell} \right)_k$$

Figure 8

41
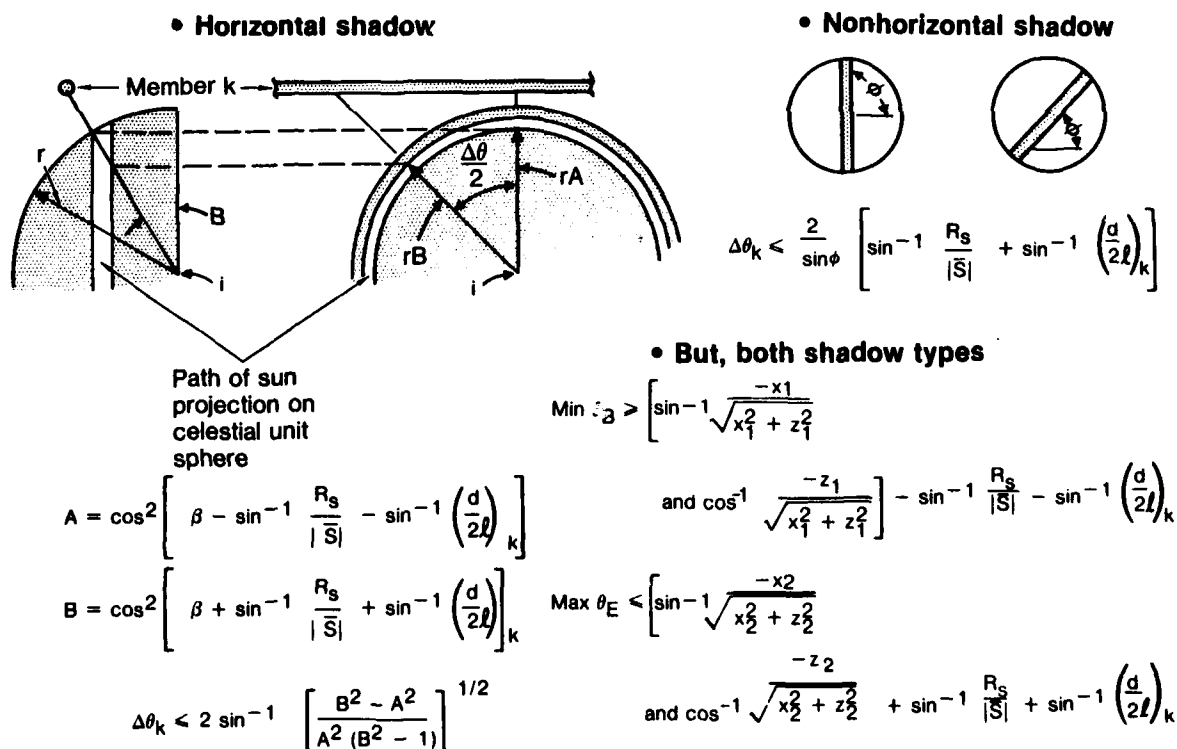
MERGED SHADOWS

At this point, the k array of shadowing members is ordered in terms of increasing θ_k. Many adjacent shadows (or portions of horizontal shadows) probably merge to form a single larger shadow. These conditions must be recognized and adjusted. The method employed for merged horizontal shadows is illustrated in figure 9. Merged nonhorizontal shadows are accommodated by similar procedures. The latter adjustments permit creation of a new "m" array of discrete shadowers as would be viewed from the "i" element-of-interest, and each shadower is defined in terms of an effective distance ℓ, an effective width d, and bounding angles θ_B and θ_E.
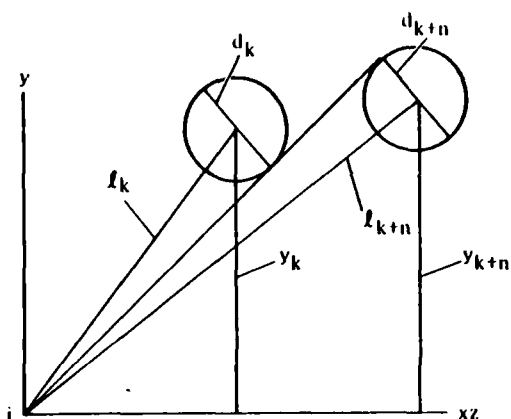
• IF $\left| \sin^{-1}\left(\dfrac{y}{\ell}\right)_k - \sin^{-1}\left(\dfrac{y}{\ell}\right)_{k+n} \right| \leq \sin^{-1}\left(\dfrac{d}{2\ell}\right)_k + \sin^{-1}\left(\dfrac{d}{2\ell}\right)_{k+n}$

LET $a = \text{MAX OF } \left(\sin^{-1}\dfrac{y}{\ell} + \sin^{-1}\dfrac{d}{2\ell}\right)_{k,k+n}$

LET $b = \text{MIN OF } \left(\sin^{-1}\dfrac{y}{\ell} - \sin^{-1}\dfrac{d}{2\ell}\right)_{k,k+n}$

• CREATE NEW MEMBER kk

$\ell_{kk} = \ell_k$ $\qquad\qquad \theta_B)_{kk} = \text{MAX OF } \theta_B)_{k,k+n}$

$d_{kk} = \ell_k |(a-b)|$ $\qquad \theta_E)_{kk} = \text{MIN OF } \theta_E)_{k,k+n}$

Figure 9

42

SIMULTANEOUS NONMERGED SHADOWS

The SSQ program now creates a new m array of merged and nonmerged shadowing members, ordered in terms of increasing θ_B. Overlapping $\Delta\theta_m$ intervals represent subintervals in which more than one distinct shadow is contained within the visible solar disc. It is therefore necessary to create an n array of subintervals of which $\Delta\theta_n = (\theta_E - \theta_B)_n$, and in which the contributing members m are identified. A graphic representation of this procedure is contained in figure 10.


n SET	m SETS CONTAINED
n	m, m+1
n+1	m, m+1, m+2
n+2	m+1, m+2
n+3	m+1, m+2, m+3
n+4	m+3

Figure 10

43
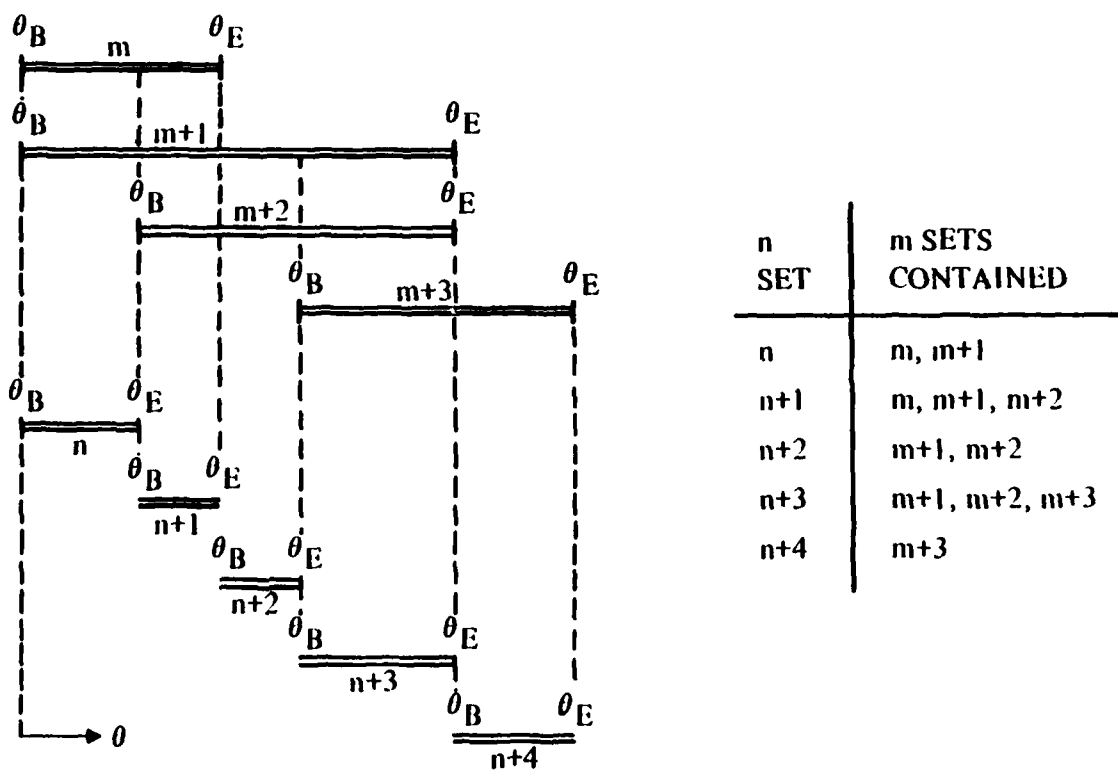
INTEGRATION OF SHADOW PROJECTIONS ON THE SOLAR DISC

Penumbral solar heat flux is computed by integration of projected shadows m on the visible solar disc, as portrayed in figure 11. A solar disc area reduction factor $SHAD_m$ is computed as shown in figure 11. Horizontal shadows are currently assumed to reside in the center of the solar disc (constant b_m). For nonhorizontal shadows, $SHAD_m$ is computed at eight equally spaced θ points within each $\Delta\theta_m$ interval. Earth-shadowing simulation is superimposed by additional solar flux attenuation during penumbra passage (assumed linear with θ) and by total eclipse during umbra passage.

$$SHAD)_m = \frac{1}{\pi R_s^2}\left[(b\text{-}R_s)\sqrt{2bR_s\text{-}b^2} - (a\text{-}R_s)\sqrt{2aR_s\text{-}a^2}\right]_m \cdots$$
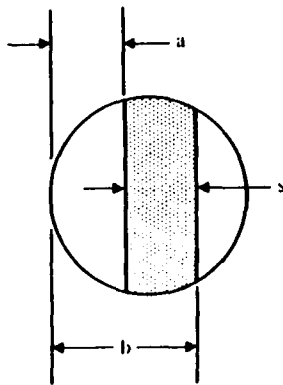
$$\cdots + \frac{1}{\pi}\left[\sin^{-1}\left(\frac{b-R_s}{R_s}\right) - \sin^{-1}\left(\frac{a-R_s}{R_s}\right)\right]_m$$

$R_s = 375,735$

$|\bar{S}| = 80,884,432$

$s_m = |S|\left(\frac{d}{l}\right)_m$

$a_m = (b\text{-}s)_m$

IF $b_m \le s_m$, $a_m = 0$

IF $b_m \ge 2R_s$, $b_m = 2R_s$

EVALUATE $SHAD)_m$ OVER $\Delta\theta_m$ RANGE, $\left(\frac{\Delta\theta}{8}\right)_m$ INTERVAL

FOR HORIZONTAL SHADOWS, $b_m = R_s + \frac{1}{2}s_m$, CONSTANT

FOR NONHORIZONTAL SHADOWS, $b_m = \left(\frac{\theta - \theta_b}{\Delta\theta}\right)_m (2R_s + s_m)$

Figure 11

44

COMPUTATION OF SHADOWED INCIDENT SOLAR FLUX

If selected lines j are identified as bounding an opaque or semiopaque surface, only two such lines can be intercepts. During the resulting interval $\theta_{j+n} - \theta_j$, solar flux is further attenuated by a constant or variable transmissivity τ, or can be eclipsed. Solar angle of incidence γ to a transmissive surface is computed as shown in figure 12, in which the two intercepted bounding lines are represented as vectors L_j and $\bar{L}_{j+n}$, and a vector triple product is formed to compute the solar incidence angle. Also shown in figure 12 is the total solar flux incident to element i, but attenuated by (1) the summation of SHAD terms, (2) the transmissivity of a semiopaque intervening surface, and (3) angle of incidence to structural element i, in which S is the solar heat flux constant, an input term.

$$\gamma = \cos^{-1}\left|\frac{\hat{L}_j \times \hat{L}_{j+n} \cdot \hat{S}}{|\hat{L}_j \times \hat{L}_{j+n}|}\right|$$

TRANSMISSIVITY $\tau = f(\gamma)$

$$q_s = \left(1 - \sum_m SHAD\right)_n \tau S \sqrt{1 - (\hat{S} \cdot \hat{L}_i)^2}$$
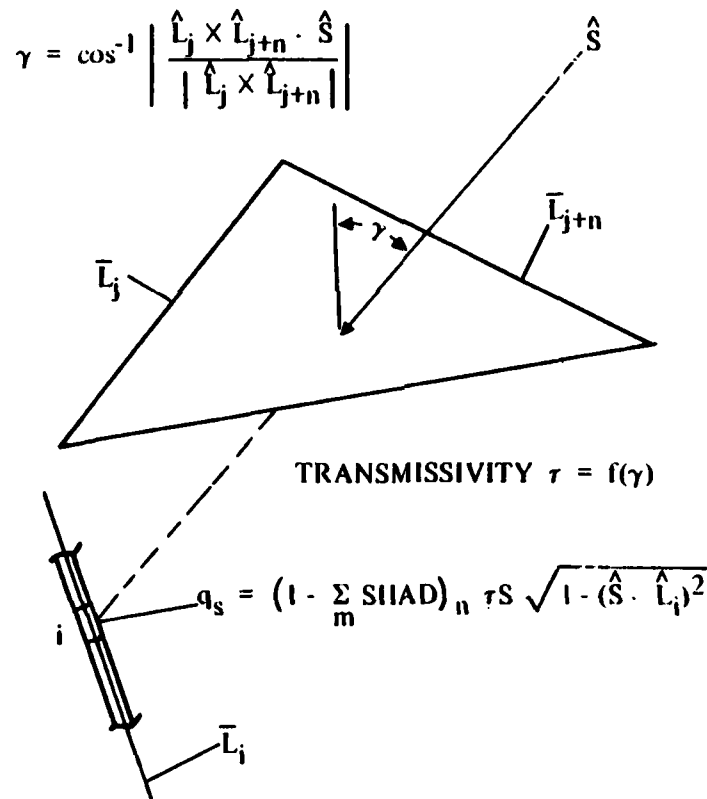
Figure 12

HEAT FLUX SUMMATION AND RESULTING THERMAL RESPONSE

Incident Earth thermal and albedo radiation fluxes are computed in the SSQ program, but shadowing of these diffuse fluxes is not considered. Earth thermal heat flux q_E is calculated as shown in figure 13, in which ρ is the Earth albedo factor (input), and F_E is a geometric factor for thermal radiation to a cylinder. It is contained in the program as tabular functions of altitude (an input term) and structural member angle of inclination to an Earth radius vector. Earth albedo radiation q_A is also computed as noted in figure 13, in which

$$H = \text{altitude}$$
$$R = \text{Earth radius}$$
$$\cos \theta_s = \cos \beta \cos \theta$$

Arrays of solar, Earth thermal, and Earth albedo heat flux incident to structural member i are contained in printed output and are also available for graphic display.

Total absorbed heat flux can be employed in computing the thermal response of an elemental length of structural member of interest i. A differential energy balance is used, in which mc is the elemental thermal mass, t is time (a function of θ), q is total absorbed heat flux, σ is the Stefan-Boltzmann constant, F_S is the element view factor for radiation to space, ϵ is the emittance of the element, and α is its solar absorptance. The closed-form solution in temperature T is evaluated at successive points of time.

• HEAT FLUX SUMMARY

$$q = \alpha q_s + \alpha q_A + \epsilon q_E$$

$$q_s = \left(1 - \sum_m \text{SHAD}\right)_n \tau S \sqrt{1 - (\hat{S} \cdot \hat{L}_i)^2}$$

$$q_E = \frac{S}{4}(1 - \rho) F_E$$

$$q_A = \rho S F_E \left(0.86 + 0.14 e^{0.53 \frac{H}{R}}\right) \cos \theta_s$$

• STRUCTURAL ELEMENT THERMAL RESPONSE

$$mc \frac{dT}{dt} = qd - \sigma F_s d\epsilon \pi T^4$$

$$\frac{A + T}{A - T} = Be^{\left(F + G - 2 \tan^{-1} \frac{T}{A}\right)}$$

$$A = \left(\frac{q}{\pi \sigma F_s \epsilon}\right)^{\frac{1}{4}} \qquad F = 2 \tan^{-1} \frac{T_1}{A}$$

$$B = \frac{A + T_1}{A - T_1} \qquad G = \frac{4 \pi d A^3 \sigma F_s \epsilon}{mc}(t - t_1)$$

Figure 13

46

SSQ PROGRAM OUTPUT OPTIONS INCLUDE
HEAT FLUX AND TEMPERATURE PLOTS

The SSQ program is coded in FORTRAN V for the CDC CYBER 172 computer, and can be operated in either the batch or interactive mode. The input format is orderly and uncomplicated. Printed output can be limited to heat flux and temperature prediction data or can include expanded data identifying shadowing members, merged shadowers, and shadowing members (m array) contained in multiple shadowers (n array). DISSPLA software is employed in the graphic output subroutine. Tektronix terminal visual and/ or hard copy and FR80 hard-copy output are available. Typical FR80 graphic output features are shown in figure 14. SSQ program heat flux output can easily be formatted as required for input to other thermal-analysis programs. Temperature output can also be formatted to accommodate the input requirements of structural-analysis programs such as LASS (ref. 4) or NASTRAN.


Figure 14

47
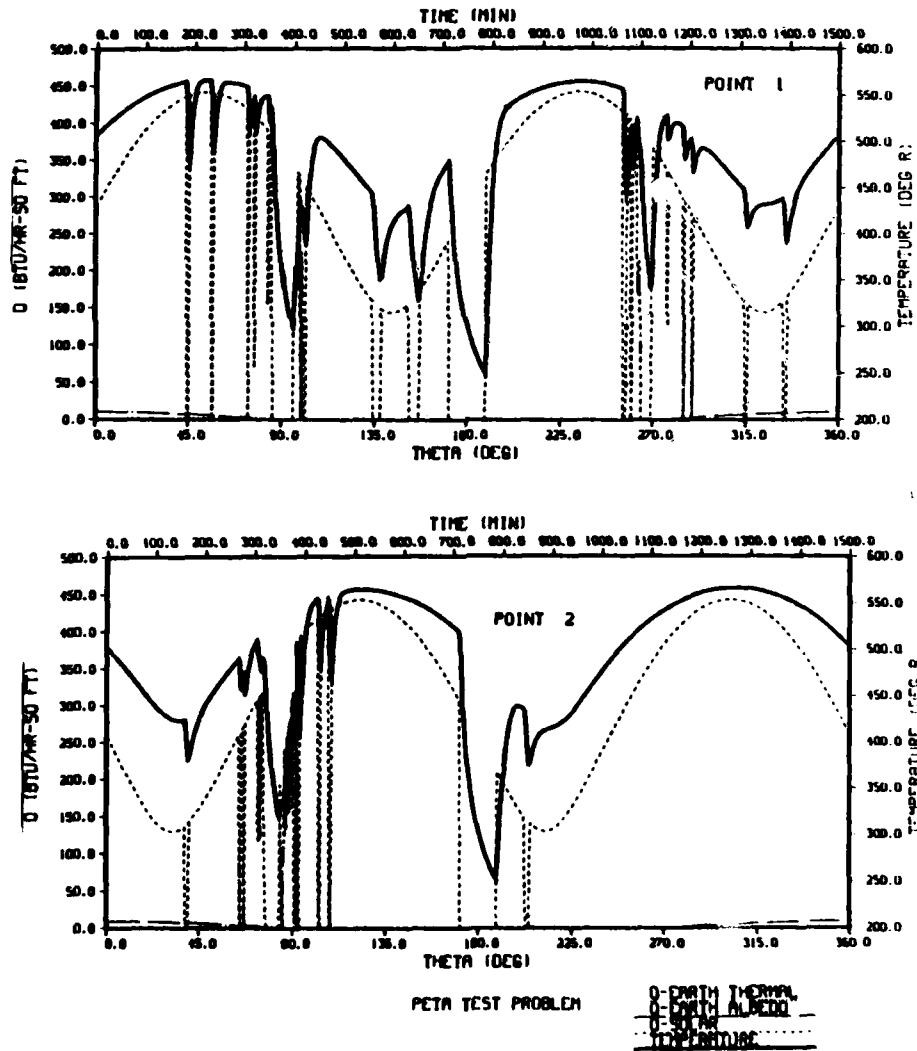
SELECTION OF GENERIC MEMBERS

It is possible to achieve substantial simplification of the SSQ shadowing-member-identification routine, and we can greatly reduce the task of computing incident heat flux histories. For example, shadowed heat flux incident to each of 978 members of a 12-bay PETA structure throughout a complete orbit can be constructed from results computed for only 108 members. As shown in figure 15, the PETA structure contains nine basic member orientations that recur throughout the entire assembly. It is shown in figure 5 that the locus of the subvehicle vector about any point throughout a complete orbit is a cone of half angle $(\pi/2-\beta)$, of which β is the solar vector angle of incidence to the orbital plane. An array of members spanning the entire spacecraft, and inclined β degrees from the orbital plane, will contain 108 members, 12 each of nine generic orientations. Analysis of the members in this array will permit computation of shadowed heat flux histories for all members in the entire spacecraft. Exceptions will be shadowing effects caused by major external space hardware. As will be seen, the latter effects can be computed separately and superimposed on selected heat flux histories, where appropriate.
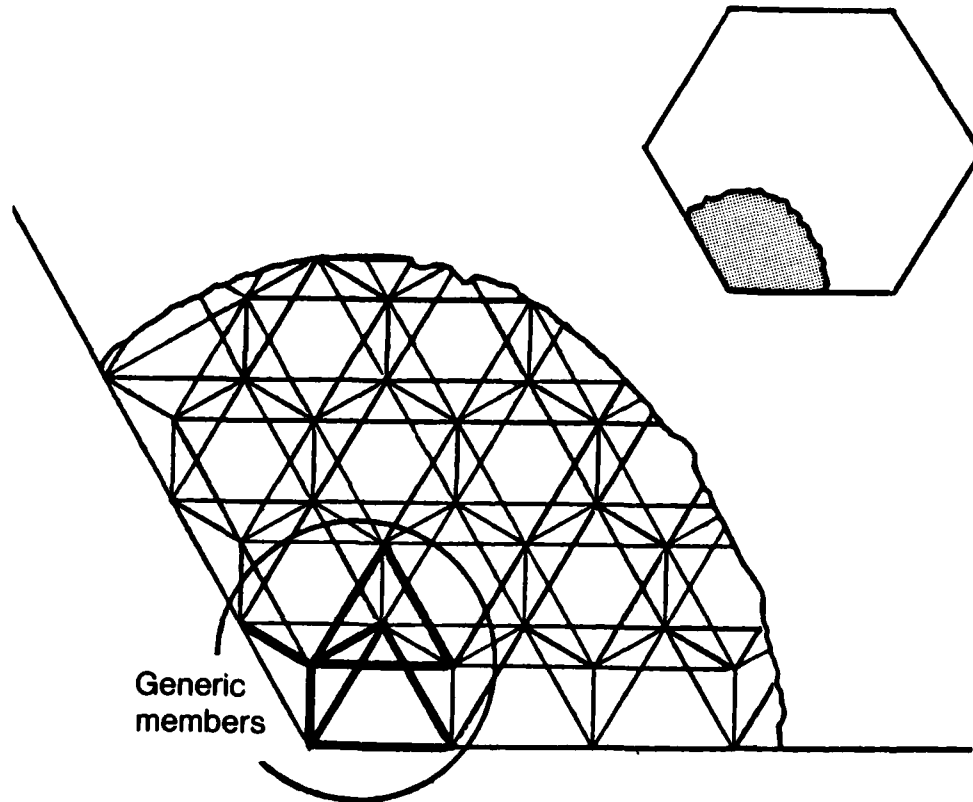

Generic members

Figure 15

CONSTRUCTING A HEAT FLUX HISTORY DATA BASE

Following identification of a 12-bay transverse array of 108 generic members in the PETA structure (fig. 16) and their respective shadowing members, it is proposed to compute shadowed incident heat flux histories for five (tentatively) equally spaced locations on each of nine generically oriented members (fig. 15) of the 12-bay generic member array. This data will comprise a heat flux history data file in which each heat flux history is identified in terms of (1) one of the nine basic member orientations, (2) one of the five equally spaced member locations, and (3) distance from the spacecraft leading and trailing edges. The data file will permit construction of heat flux histories for any or all structural members on the spacecraft, as illustrated in figure 16. Consider a member residing at d_1, equidistant from the leading and trailing edges, as shown in figure 16(b). Incident heat flux to all points on this member will have been already assembled in the data file for the entire orbit ($0 \leq \theta \leq 2\pi$). But figure 16(c) portrays a member location, d_2 from the leading edge and d_3 from the trailing edge. Incident heat flux to points on this member will be contained in the d_2 record for the orbit interval ($0 \leq \theta \leq \pi$), and in the d_3 record for the orbit interval ($\pi \leq \theta \leq 2\pi$). Heat flux histories for all members can thus be constructed rapidly, especially since many members will reside at identical locations with respect to the leading and trailing edges of the spacecraft. In the absence of additional major shadowing, such members will have identical heat flux (and temperature) histories.
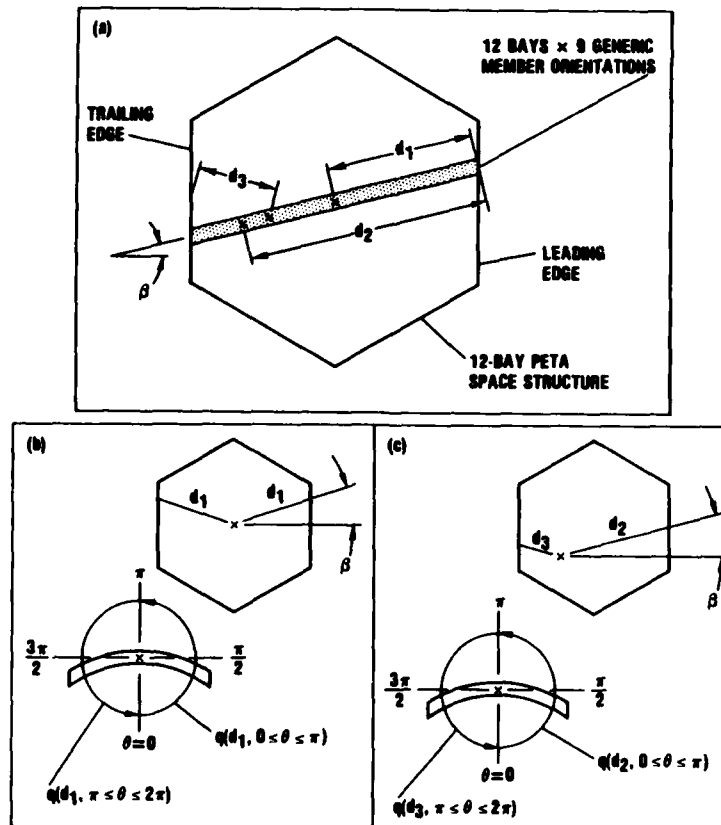

Figure 16

MAJOR BODY SHADOWING

Heat flux attenuation by major shadowing space hardware, if any, must be taken into account before member thermal response can be computed. Shadows cast by these external bodies will traverse the spacecraft surface, and the shadow path is parallel to the orbital plane only if β is zero. It will be necessary to identify all structural members any part of which resides within the limits of a shadow path. Major shadowing computations can thus be limited to the latter members. A typical shadowing situation is portrayed in figure 17. Of the shadowing-body coordinate data, the maximum and minimum y values correspond to points 2 and 3, respectively. At least one end of potentially shadowed members must have a y coordinate no greater than y_2. For members meeting the latter test, let point 1 be either end of the structural member, and

$$\beta'_{max} = \sin^{-1} \frac{y_2 - y_1}{\sqrt{(x_2 - x_1)^2 + (y_2 - y_1)^2 + (z_2 - z_1)^2}}$$

$$\beta'_{min} = \sin^{-1} \frac{y_3 - y_1}{\sqrt{(x_3 - x_1)^2 + (y_3 - y_1)^2 + (z_3 - z_1)^2}}$$

If $\beta'_{max} > \beta > \beta'_{min}$ for either end of the member, shadowing of a member will occur. Also, if both $\beta' > \beta$ on one end of the member while both $\beta' < \beta$ on the other end, shadowing will exist. Shadowing intervals for all shadowed points can be computed by the methods of figure 8. Major body shadowing effects must now be superimposed on the heat flux data records of figure 16.
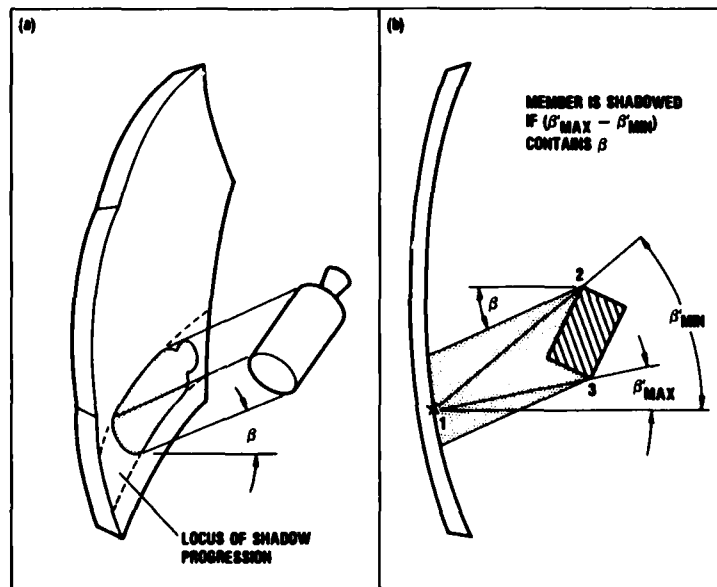

Figure 17

LIMITING THE SCOPE OF TEMPERATURE COMPUTATIONS

Judicious selection of an orbit for which β is zero (e.g., an equatorial orbit, 21 March or 21 September) and a preferred PETA attitude can permit temperature computation for all members of a 12-bay PETA structure in terms of only 163 members (plus members subject to major body shadowing). Effects of the choice of PETA attitude and β on the task of computing member temperatures are illustrated in figure 18. Dark-shadowed regions of the PETA profiles represent areas in which the temperature histories of all members can be generated by computing the temperatures of a single transverse array of generic members. Light-shaded areas are those in which each member has one, and only one, thermally identical member in the opposite light-shaded area. Thus, the PETA orientation of figure 18a (β = 0) would require temperature history computation for exactly half of the total number of PETA members. The same PETA orientation with β ≠ 0, shown in figure 18b, would yield a limited central region in which all temperature histories are represented in a single transverse generic-member array, but the above-noted light-shaded temperature correspondence is limited to members situated on the vertical counterline. All members in the unshaded regions of figure 18c would require individual temperature computation. The PETA orientation of figure 18d (β = 0) yields a large central region in which all member temperature histories occur in a single transverse generic-member array. The latter advantage is largely repeated in the orientation of figure 18e (β ≠ 0). However, the lower light-shaded region members of figure 18e will each be thermally identical to those of the upper light-shaded region. Temperature histories need only be computed for structural members in the shaded region of figure 18e, which will include an array of generic members at the top of the region. Thus, 163 members can thermally model all 978 members in the 12-bay PETA structure. Added to this, as noted earlier, are the members that must be subjected to major body shadowing.


Figure 18

51
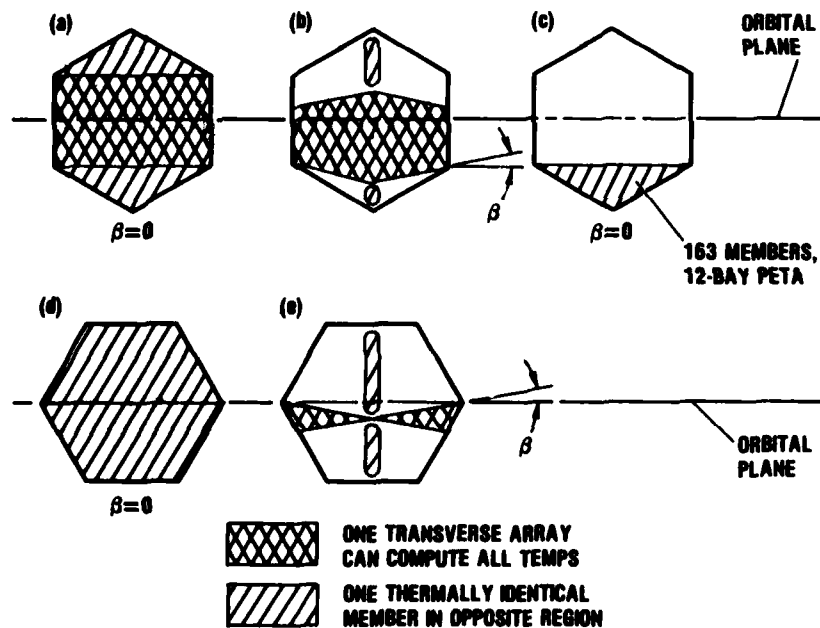
SSQ IS FAST AND EFFICIENT

Assuming a 12-bay PETA analysis application, it is feasible to create one or more data files containing temperature histories for multiple points on each member of the entire PETA structure, although the individual members will far outnumber the temperature histories. The latter records would be indexed in terms of (1) types of generic members (figure 19), (2) location on the member, and (3) distances from the spacecraft leading and trailing edges. Additionally, specific temperature records might be identified solely in terms of specific elements of the structure. It would then be possible to create a detailed and accurate transient temperature profile of the entire structure by simply constructing a directory assigning identification of specific heat flux and temperature records to each member of the structure. To this point, a CYBER 720 CP time expenditure of only 3,380 seconds is estimated for the entire structure, exclusive of plotting. This data base can be employed as the basis for developing rapid-estimation thermal-analysis algorithms, possibly amenable to interactive execution.

- Analysis of a 6-bay, 240-member PETA required only 4.14 CP seconds per elemental point (CYBER 720)

- 108 generic members can model incident heat flux histories, & 163 members can model temperature histories for an entire 12-bay, 978-member PETA structure. Estimated CYBER 720 CP time is 3,600 seconds

- Major body shadowing effects require added computation

- Graphic output requires added expenditure

Figure 19

52

DEVELOPING A RAPID-ESTIMATION ALGORITHM

It is anticipated that examination of the thermal-response data base will reveal the existence of large groups of structural members that experience similar temperature histories. This would permit the analyst to assign the latter members to analogous modules for purposes of subsequent simplified analyses. Thus, thermal analysis of a single member might reasonably yield the thermal response of all members of the module subset. Members subjected to major body shadowing will experience incident heat flux histories differing markedly from those of the 108 generic heat flux schedules of the 12-bay PETA structure, necessitating separate identification and analytical treatment of these members. Therefore, it is probable that the location of analogous modules would be much affected by the location of major shadows. Moreover, variations in the latter conditions might be expected from mission to mission, or at different times in a single mission. Examples of these conditions might include the arrival of an upper-stage propulsion system, or the continuing reorientation of large solar panels. Thus, if we are working with a specific algorithm, and later elect to relocate a large shadowing solar panel, we would probably wish to redesign the thermal-analysis algorithm. Application-peculiar shadowing effects therefore suggest the possible desirability of partial or total batch execution of a baseline thermal analysis as a necessary prerequisite for redesigning thermal-analyses algorithms. A visual search of the graphic data for general temperature excursion trends may not be the only means of deducing simplified thermal-analysis algorithms. It would be relatively simple to record such statistical data as extreme values, mean values, frequencies, and ranges. Whatever the nature of the simplified algorithm, the first step in its development must be execution of the baseline SSQ code. (See fig. 20.)

- Identify generic structural members

- Create an incident heat flux data base

- Superimpose major body shadowing effects

- Create a temperature history data base

- Create simplified thermal analysis algorithms

  - Examine the temperature data base

  - Identify key members

  - Identify statistical data & trends

Figure 20

REFERENCES

1. O'Neill, R. F., and Moutrie, C. L.: Vector Sweep Program, Computer Program P3523A. General Dynamics Convair Division Report CASD/LVP 74-015, March 1974.

2. O'Neill, R. F.: Thermal Control Design Analysis of an On-Orbit Assembly Spacecraft. Paper No. 79-0917, AIAA Conference on Advanced Technology for Future Space Systems, May 1979.

3. O'Neill, R. F.: Space Structure Heating (SSQ), A Numerical Procedure for Analysis of Shadowed Space Heating of Sparse Structures. Paper No. 81-1179, AIAA 16th Thermophysics Conference, June 1981.

4. Leondis, Alex: Large Advanced Space Systems Computer-Aided Design and Analysis Program. NASA CR-159191-2, 1980.

CONTROL OF LARGE SPACE STRUCTURES:
STATUS REPORT ON ACHIEVEMENTS AND
CURRENT PROBLEMS

M. G. Lyons
Integrated Systems, Inc.
Palo Alto, California

J. N. Aubrun
Lockheed Palo Alto Research Laboratory
Palo Alto, California

55

LSS CONTROL OBJECTIVES

The principal objectives for LSS control are listed below. The general objectives range from basic deployment and maneuvering, where some vibration modes may be suppressed, to disturbance rejection for very high performance imaging applications. The controls selected generally must produce some combination of eigenvalue/eigenvector and loads modification in order to achieve the mission objectives.

GENERAL

- Deployment management and maneuvering

- Pointing, stabilization, dimensional control

- Wave front error management (static and dynamic)

- Disturbance rejection

SPECIFIC

- Stiffness (natural frequency) modification

- Damping augmentation

- Eigenvector modification

- Disturbance load modification

  - Maneuvering

  - Steady state

STATE-OF-THE-ART ASSESSMENT AND PROBLEMS

The ultimate mechanization for LSS controls depends on development within at least the four areas shown below. The principal difficulties now appear to be a lack of funded experimental efforts and inadequate signal processing and actuation hardware. The requirements for integrated spacecraft control, including structures, algorithms, sensors/actuators, and architectures, are still not generally acknowledged by the systems planners. Large high-performance vehicles cannot meet mission performance goals without such an approach.

STUDY AREA	ACHIEVEMENTS	CURRENT PROBLEMS
1. Deployment and maneuvering control analysis	– Maneuvering algorithms and demonstrations – Multibody software – Deployment ground tests	Control requirements and demonstrations for controlled deployment largely ignored
2. Synthesis/analysis tools and methods for robust control designs	– Basic SAS well understood – Robust control design methods developed (stability) – Experimental verification	– Interface to structural dynamics – CAD software for rapid design – Robust high performance (low sensitivity)
3. Identification/adaptive methods for high performance	– Algorithms well developed – Self-tuning methods applied to some S/C & helicopter systems	– Few experimental tests – Dependence on FFT methods – Adaptive methods largely untested – Real-time mechanizations difficult
4. System architectures/ mechanizations	– A/P systems demonstrated closed-loop (200 Hz) – High throughput multiprocessor/ parallel processor architectures in development – Hardware tests in progress	– No integrated control philosophy for space structures – Experimental tests still unplanned – Existing A/P architectures inadequate – Inadequate actuator research

PLATE EXPERIMENT: GENERAL SCHEMATIC

This picture describes the circular plate suspension and the actuator/sensor devices attached to it. The "trapeze" type suspension allows quasi-free motions of the plate in all directions, minimizing the interaction with flexible modes. The spring and mass system provides isolation against vibrations coming through the mounting bracket. This bracket is attached to a frame bolted on the 14-foot optics table.
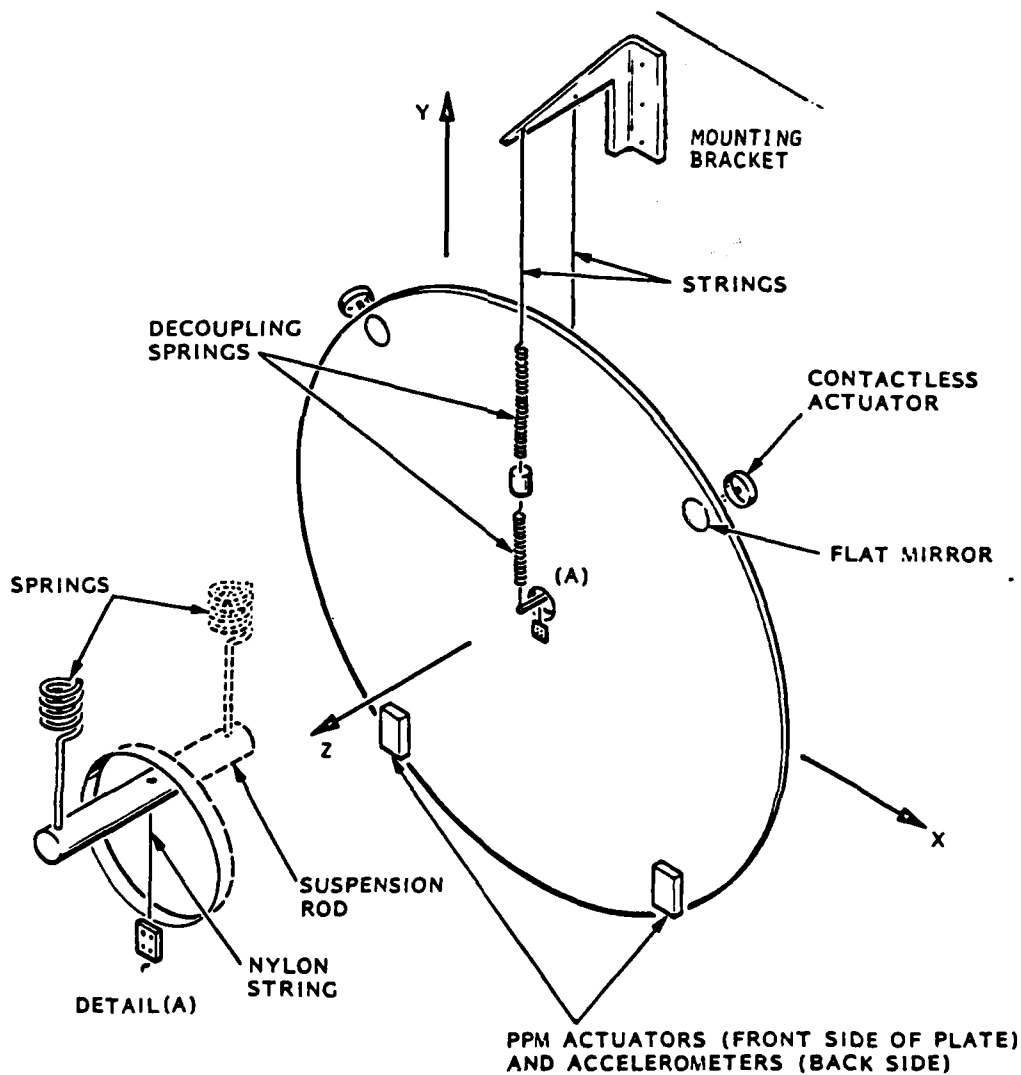
ANGULAR OPTICAL SENSING SYSTEM

This chart shows how the local rotation of the plate is measured at the mirror locations. The laser beams (obtained by splitting a single input beam) are reflected by the mirrors and fall upon the 2-axis linear detectors. The (x', y') positions of the spots produce pairs of proportional signals. The x' deflection showed on the chart corresponds to a rotation of the mirror about the x' axis of the plate, and the position y' corresponds in the same way to a rotation about the y' axis.
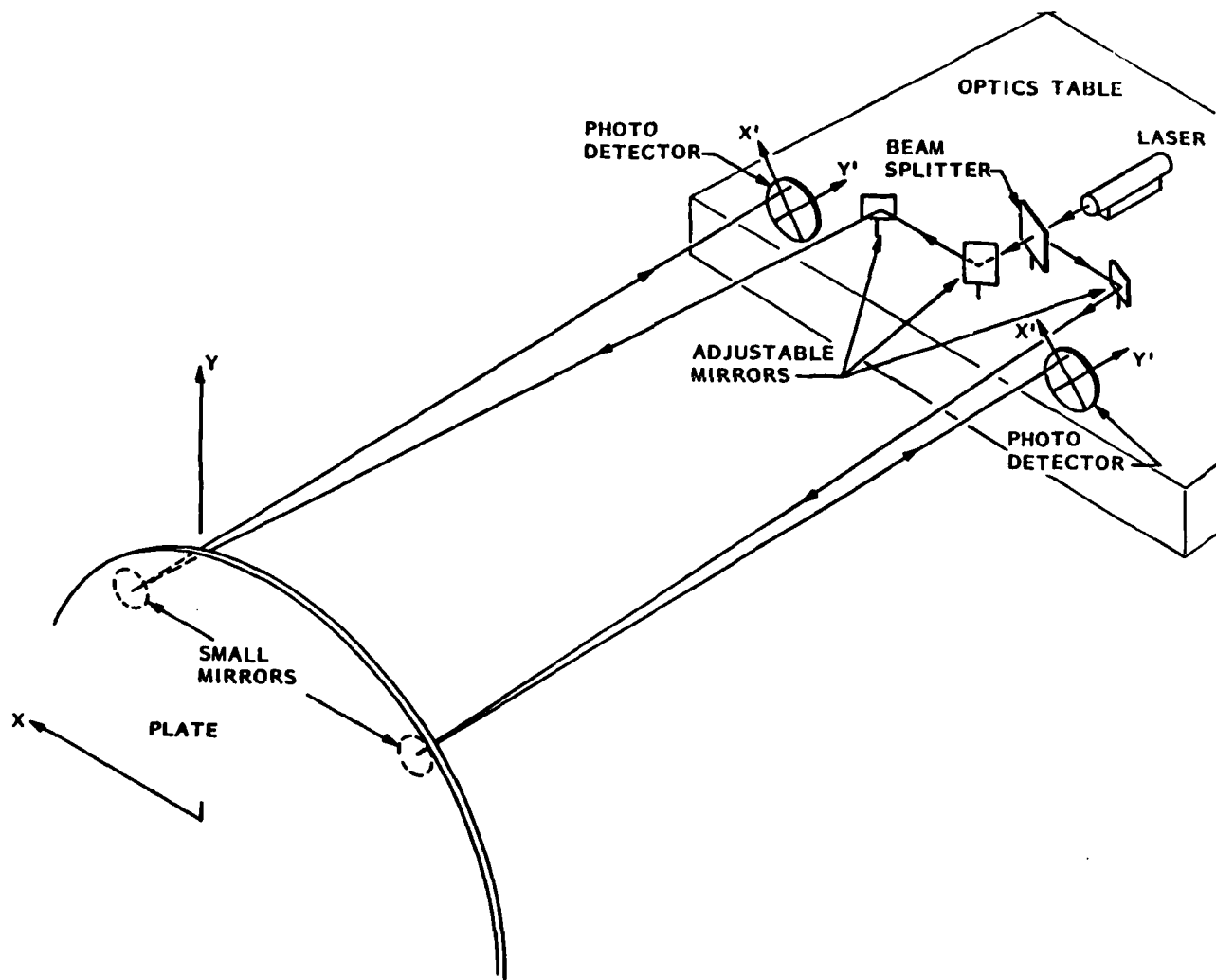
PLATE EXPERIMENT SENSORS AND ACTUATORS

This chart depicts the nature and location of the actuators and sensors used on the circular plate experiment. The actuators are of two types:

1. Contactless Actuators – Magnetic forces are exerted on a small magnet attached to the plate. This provides the necessary actuation for absolute pointing.

2. Pivoted Proof-Mass Actuators (PPM) – Reaction forces are exerted by moving a small mass connected to the plate by an electrodynamic motor. Only AC forces can be produced this way.

Sensors are of the angular type (deflection of a light beam by a small mirror is sensed by a linear photo detector) or of the linear displacement type (measured via phase difference of the return light from a corner mirror using microphase detectors). In addition, accelerometers are used to measure vibrations along the Z axis.

SENSORS

① , ② : INERTIAL SENSING/
ACCELEROMETERS
(1 D.O.F. Z-MEASUREMENT)

③ , ④   OPTICAL SENSING/MIRRORS
⑤ , ⑥ '   (2 D.O.F. $\theta_{x'}$, $\theta_{y'}$ ANGULAR
MEASUREMENT

(x', y') ARE 45° W.R.T.
(x, y)

⑦ – ⑩ : MICROPHASE OPTICAL SENSOR
(Z DISPLACEMENT)

ACTUATORS

A_1, A_2 : PIVOTED PROOF-MASS

A_3, A_4, A_5 : CONTACTLESS ACTUATORS
(5 MAY BE USED TO SIMULATE DISTURBANCES)

60
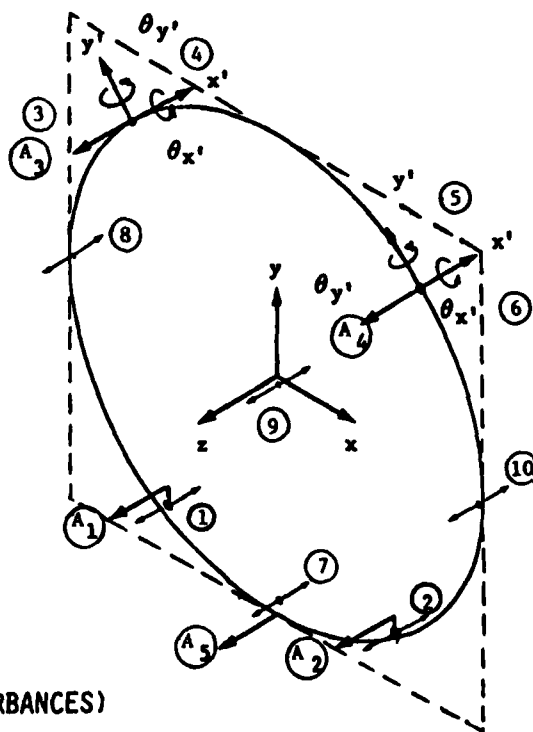
OVERALL SYSTEM CONFIGURATION

This chart shows the interaction and interfaces between the various processors and the test structure. Control gains generated by control synthesis programs on the UNIVAC 11-10 are transmitted directly to the STI/DEC 11-23 microprocessor system and stored on disk. These gains can then be loaded, when needed, in the Array Processor (AP) before starting control experiments. The AP has its own A/Ds and DACs and thus carries out the control of the specimen independently of the rest of the system. It can however be directed by the 11-23 to either start or stop controlling, or to acquire a time-slice of data for later examination by the 11-23 software. Also, the 11-23 can concurrently run dynamic characterizations of the specimen (either open- or closed-loop) since it can acquire sensor data and send excitation signals via its own A/Ds and DACs.

61
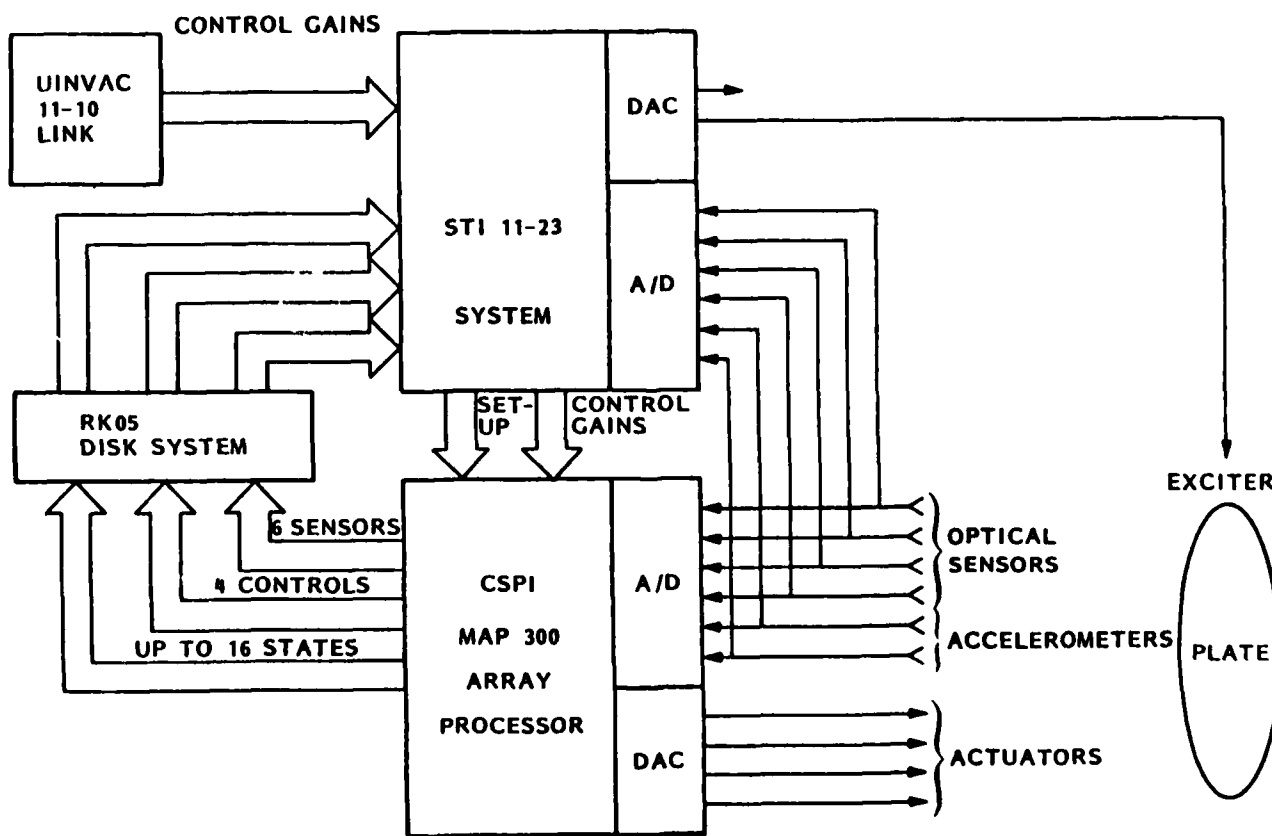
CONTROL EXPERIMENT PROCEDURE

This chart is a flowchart showing the various operations involved in the structural control experiments. From the finite element analysis, a linear model is derived which is used as a basis for control synthesis programs. These programs generate a set of gain matrices which are stored in the 11-23 and may be manually updated if needed. The appropriate set is loaded in the array processor. Then the control algorithm is started and the AP controls the specimen and may acquire data. This data is stored on disk and can be analyzed off-line by the 11-23 or transmitted to a larger computer (VAX, UNIVAC 11-10) for further processing. Also, while the AP is running, dynamic characterization may be carried out by the 11-23.
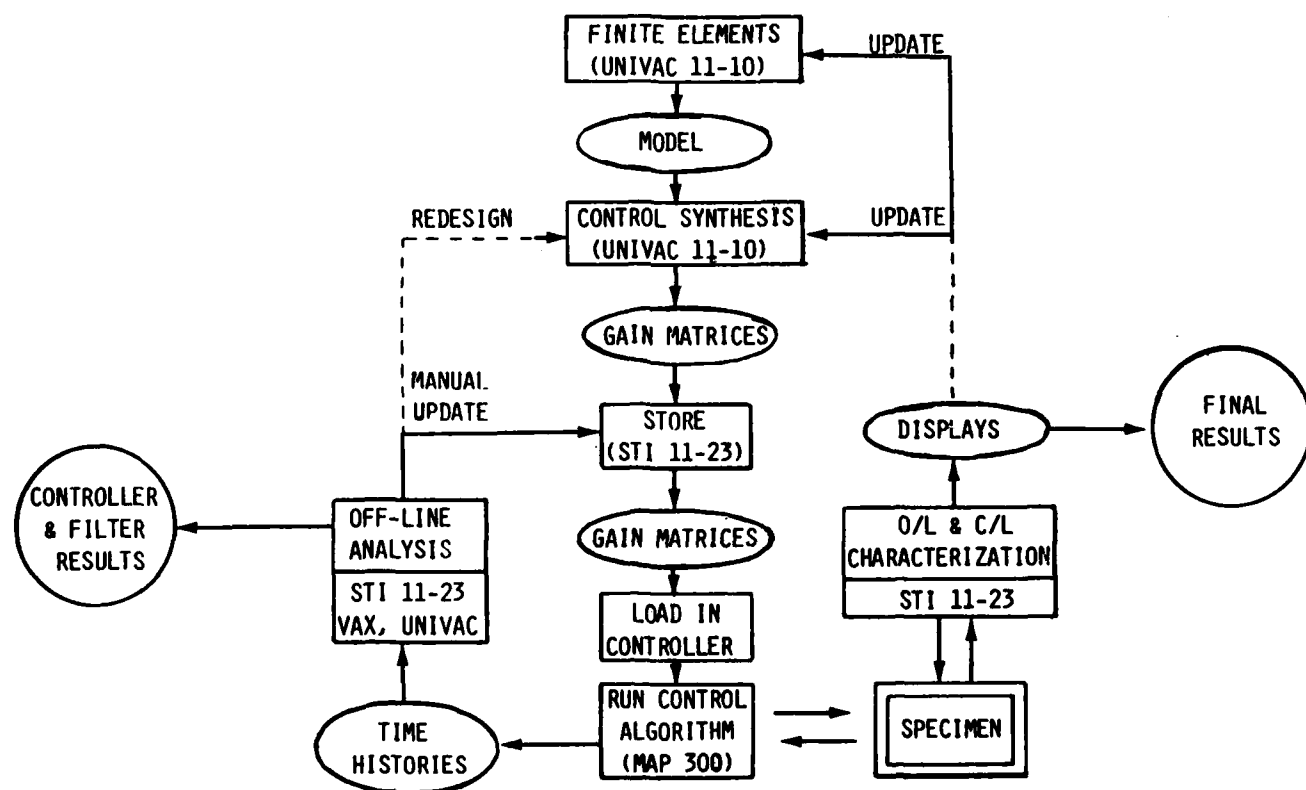
CIRCULAR PLATE RESPONSE TO STEP TORQUE

This chart shows the angular rotations of the plate about its x' and y' axes when a step torque is applied about the x' axis. The controller is digital as described in the previous chart. The integral part of the controller makes the angle return to zero, exactly cancelling the disturbance (DC) torque. The next chart shows the steady-state pointing error. The rms value is about 5 μrad.
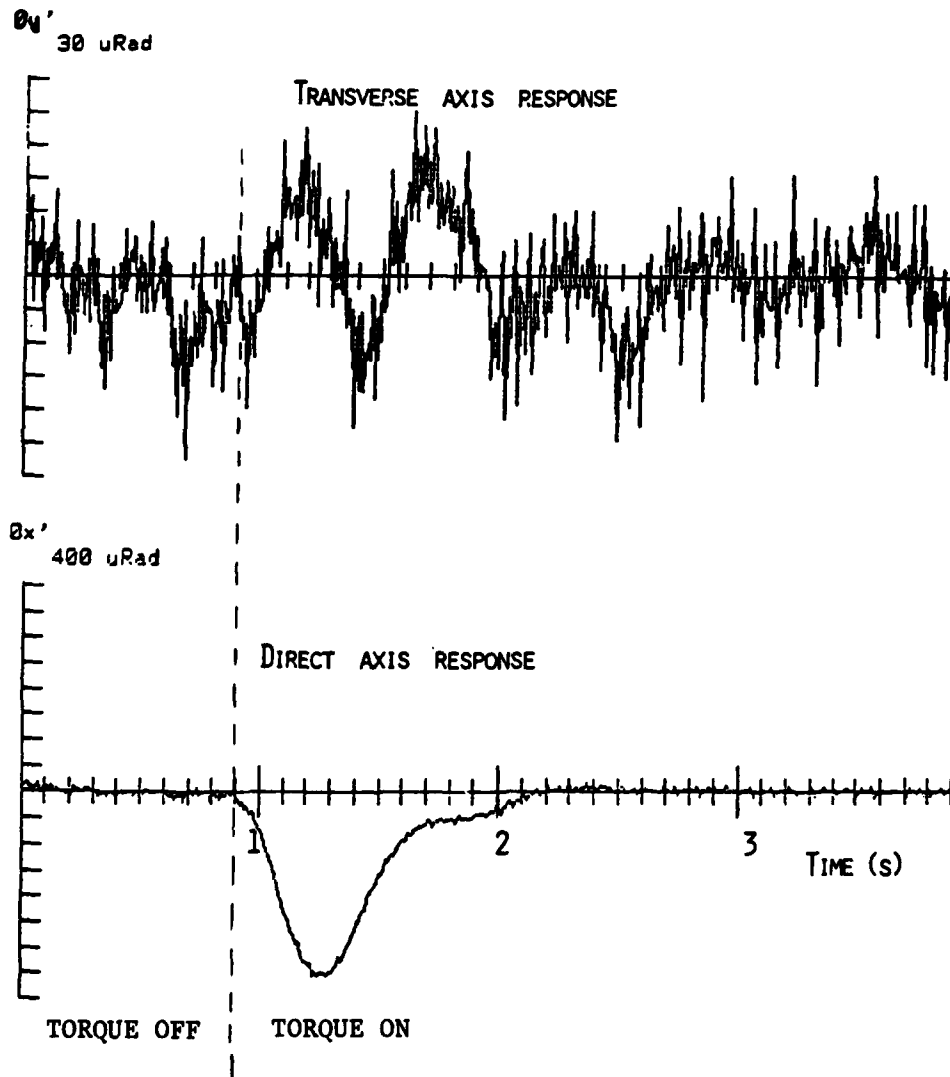
CIRCULAR PLATE: CLOSED-LOOP TEST (HAC 3RB)
MEASURED AND ESTIMATED OPTICAL SENSOR OUTPUT

This chart shows comparisons between estimated and measured sensor signals.
The sensor estimates are obtained by reconstruction from the state estimates.
Errors in the translational mode estimate are more obvious in the velocity
comparisons.
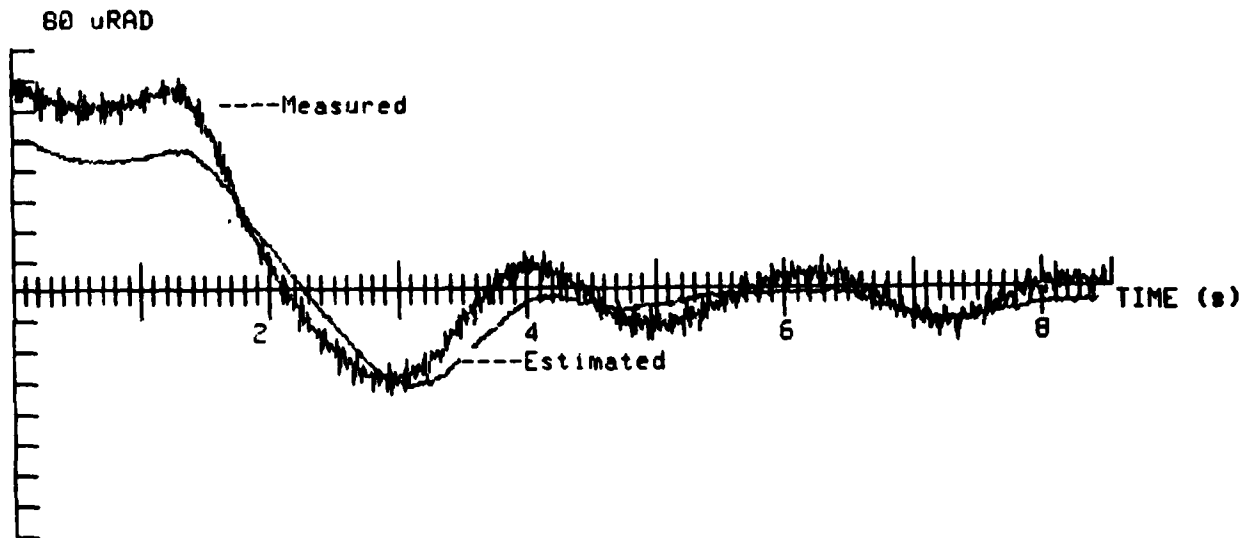
CIRCULAR PLATE: CLOSED-LOOP TEST (3RB, 2F)

In this chart, a direct comparison between closed-loop and open-loop responses is made showing the faster decay introduced by the control system. Also the steady-state amplitude has been reduced by a factor of 2. The controller controls two flexible modes and uses the two top actuators only.
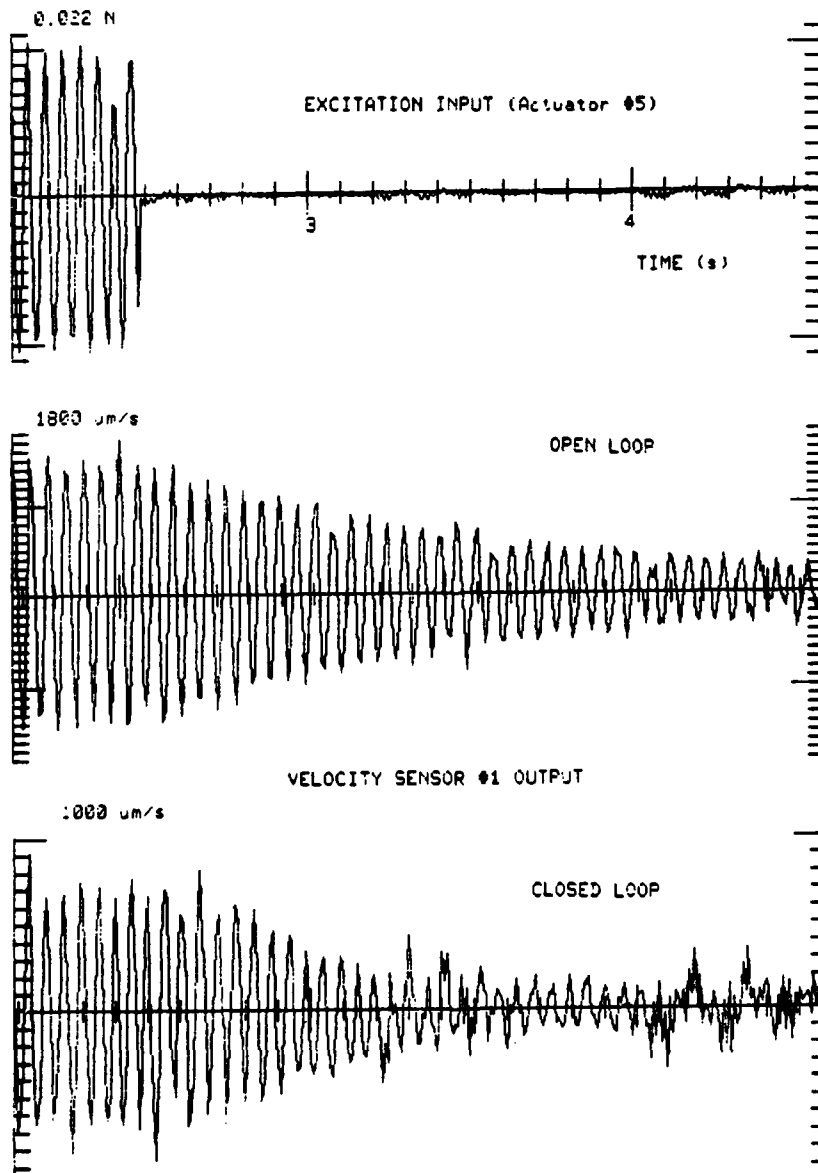
INVESTIGATIVE TECHNIQUES

The least-squares method gives biased estimates of parameters when the input measurement is contaminated by noise. The instrumental-variables technique was developed to minimize the bias in estimates. In addition, unlike least squares, the instrumental-variables method does not require solution to a nonlinear programming problem. The instrumental-variable estimates are, therefore, obtained in a single step.

The recursive prediction error methods based on discrete ARMA models update estimates at each data point. The algorithms include recursive maximum likelihood, recursive least squares, recursive instrumental variables, and extended Kalman filter (corrected). These have been used successfully in signal processing and process control and monitoring applications.

ALGORITHM	ADVANTAGES	DISADVANTAGES
Frequency Domain Instrumental Variables	•Always converges •Requires no starting values •Data can be averaged for use with low signal-to-noise ratio •Number of active modes can be easily determined	•Not minimum variance •Can only be block recursive •Requires solution to a polynomial equation •Difficult to make it robust
Recursive Maximum Likelihood	•Minimum variance •Always converges •Easy to incorporate robustness against data dropouts	•Requires solution to a polynomial equation to compute damping ratios and frequencies •Discrete ARMA leads to poles near the unit circle

OPEN-LOOP INPUT AND SPECTRUM FOR PLATE IDENTIFICATION

The plate open- and closed-loop systems are excited, in these tests, by a square wave driving a CEM actuator. The corresponding FFT shows that model excitation energy desirable for system ID is not ideal for this excitation.

Time, sec

Freq, Hz
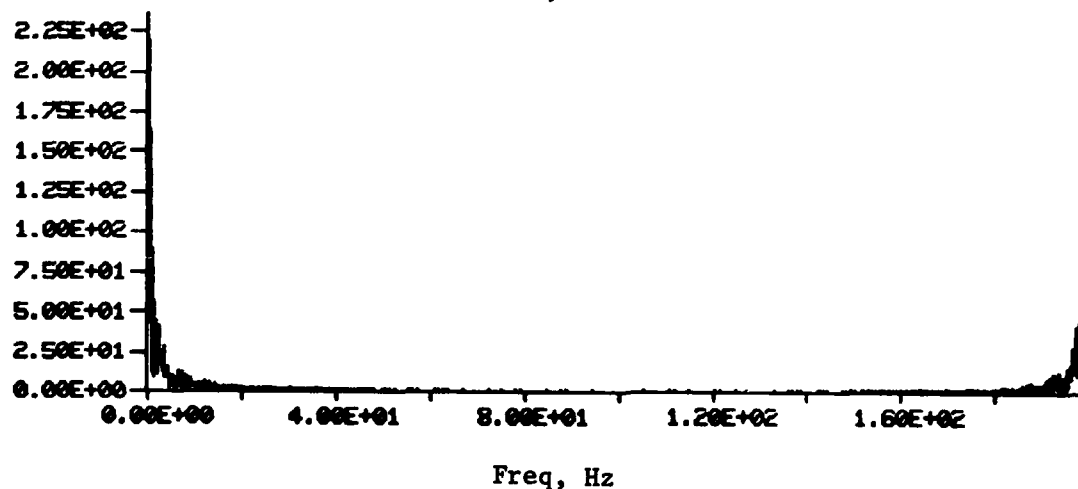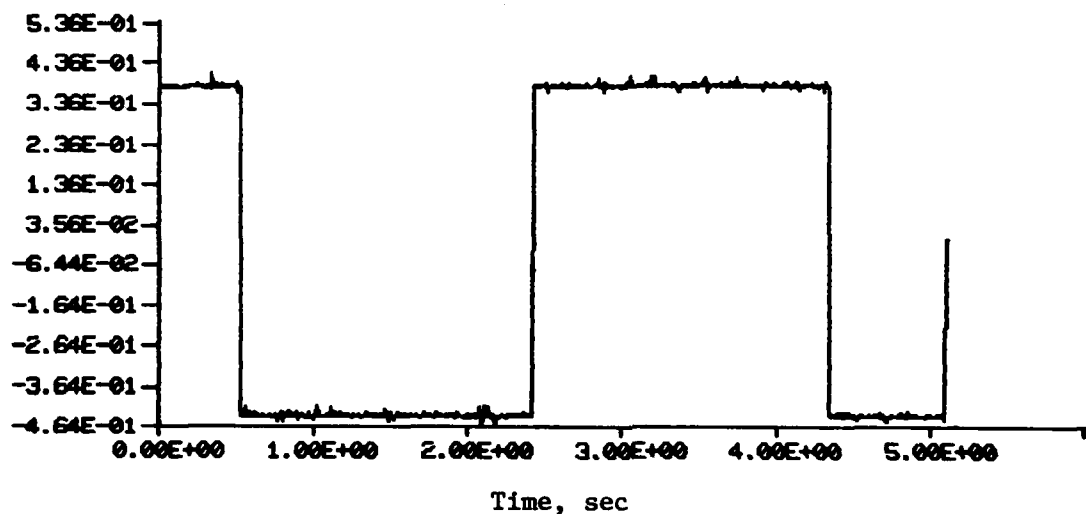
VELOCITY FFT COMPARISON (CH. 1)

Open- and closed-loop FFT's of the velocity measurements show damping for the closed loop. The attitude controller destabilizes this plant. Signal-to-noise, however, makes damping ratio evaluation from the FFT difficult.
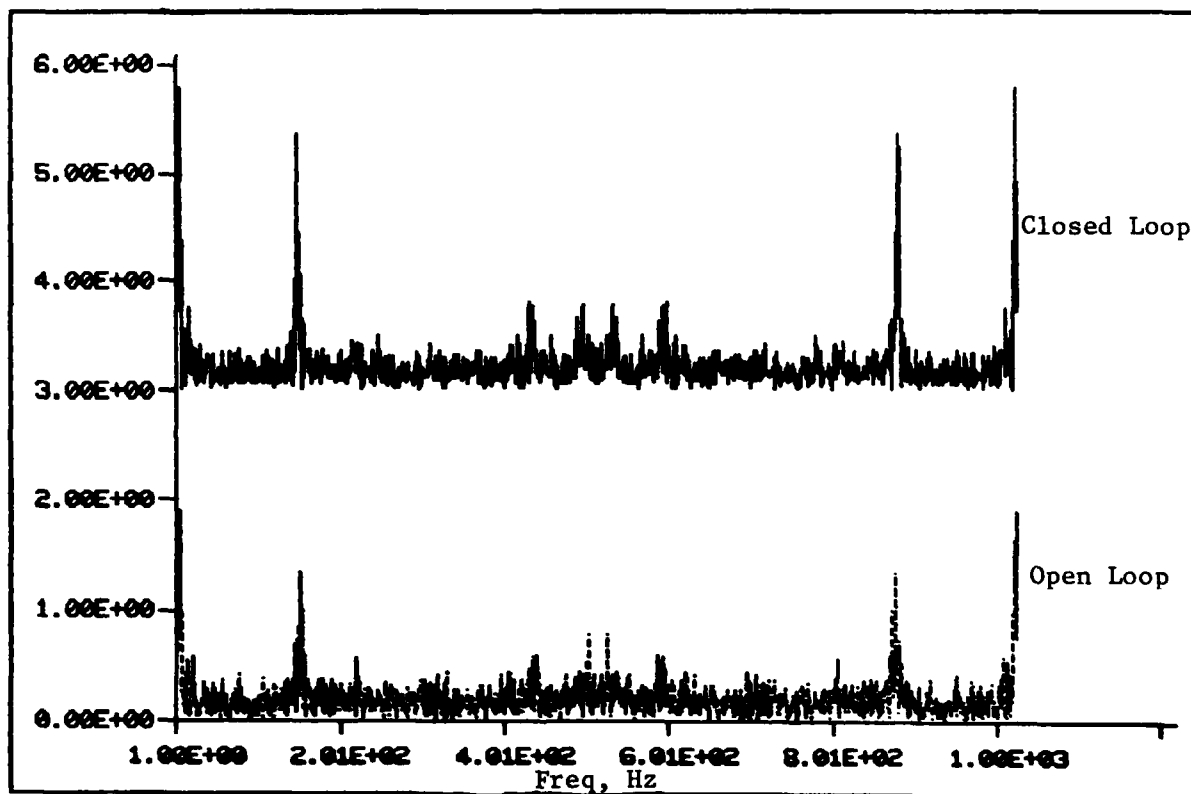
OPEN-LOOP 20TH ORDER ID (POLES ONLY)

Open-loop transfer function reconstruction, after model identification, is shown below. The effect of the zeros is quite pronounced.

Open-Loop Audio-Regressive Part
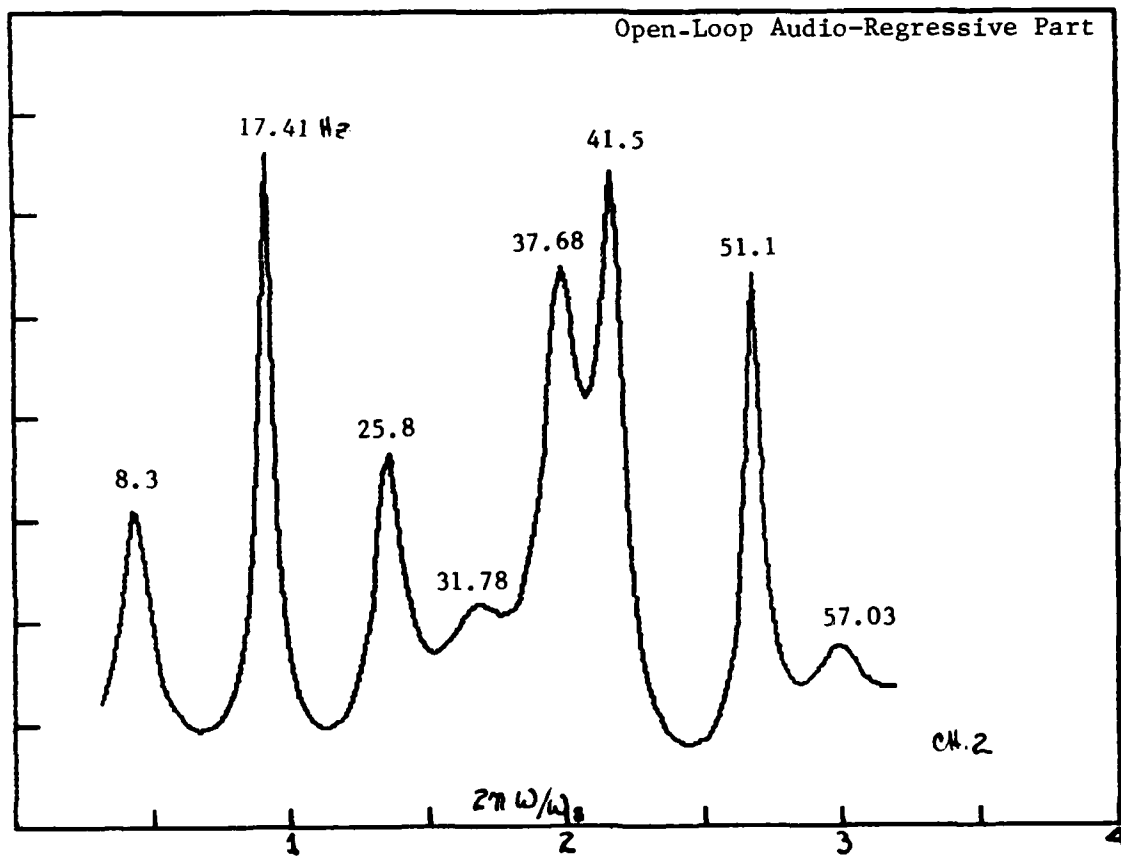
CLOSED-LOOP DAMPING RATIO VERSUS MODAL FREQUENCY

Here, damping ratio is plotted versus modal frequency for some of the higher frequency modes. Variations from about 30 percent to nearly undamped are observed. All modeled modes and damping ratios are shown.
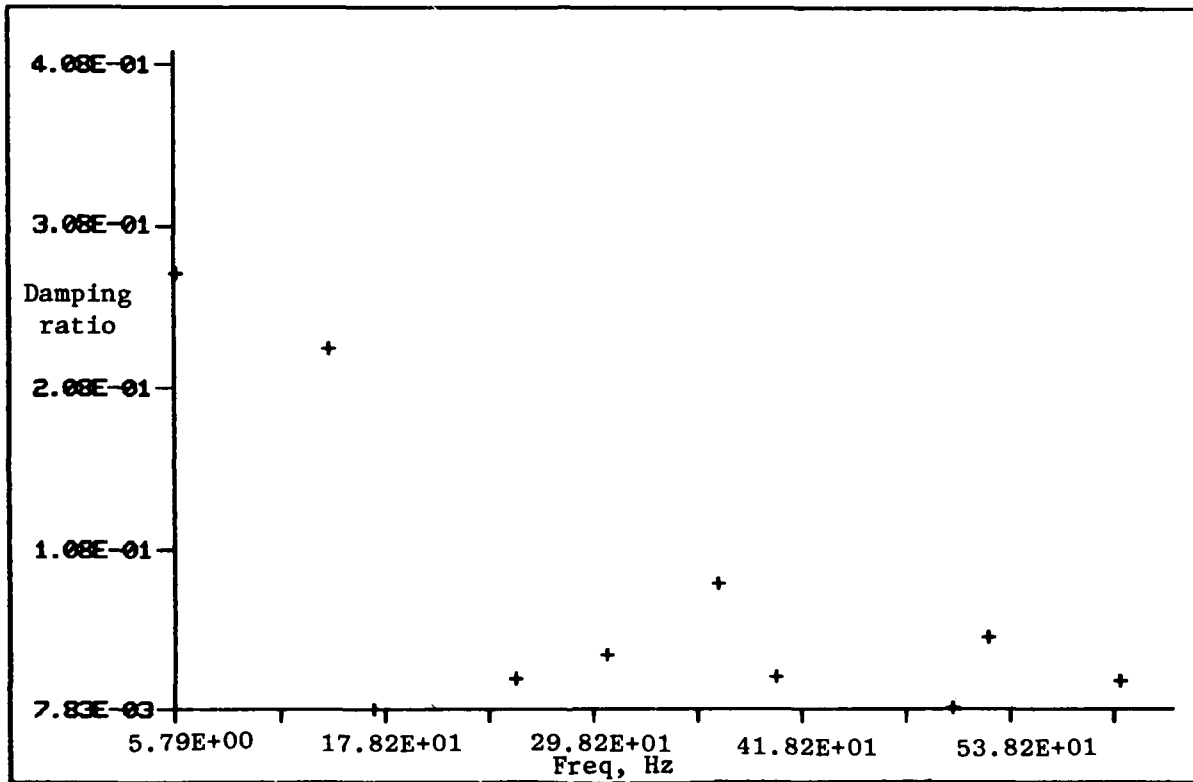
COMPARISON OF DAMPING RATIO VERSUS MODEL ORDER

Damping ratio comparisons shown here clearly indicate the reduced damping induced by the attitude controller.

Open-Loop 16th-Order Model			Open-Loop 20th-Order Model	
Frequency (Hz)	Damping		Frequency (Hz)	Damping
17.26	0.0228		17.41	0.0224
51.27	0.0072		51.1	0.0092
25.83	0.0174		25.8	0.0333
			31.8	
			41.5	

● Damping ratio estimates sensitive to model order for high Q modes

Closed-Loop 20th-Order Model	
Frequency (Hz)	Damping
17.17	0.0078
50.45	0.0092
25.21	0.0267

STRUCTURAL MODELLING AND CONTROL DESIGN UNDER INCOMPLETE PARAMETER INFORMATION: THE MAXIMUM-ENTROPY APPROACH

D. C. Hyland
MIT Lincoln Laboratory
Lexington, Massachusetts

LSS CONTROL METHODOLOGY REQUIREMENTS

Figure 1 indicates the overall objectives of the work considered here. Besides the obvious basic requirement for a LSS control design methodology, there are several additional requirements needed to avoid excessive development cost and possible design impasses. Actually, these additional requirements are not demanded merely from a desire for mathematical elegance but are often essential for the attainment of the basic objective. Ideally, as the right of the figure indicates, we should like to devise a rigorous, one-step design procedure which renders inadvertent design of non-robust controllers unlikely or impossible and directly addresses the effects of modelling uncertainty in large-order systems. The present paper concerns a new modelling approach which succeeds in attaining many of these desirable features. Put most briefly, our approach proceeds by adhering to the following two ground rules:

1. Incorporate parameter uncertainties directly into the design model (v . minimum data/maximum entropy models).

2. With a high-order stochastic design model, design implementable (fixed-order) compensation which is optimal "on the average." (Our work has concentrated on mean-square optimization because of its simplicity and relative familiarity).

AVOIDANCE OF DESIGN IMPASSE

- AD HOC, CUT-AND-TRY PROCEDURES MINIMIZED OR ELIMINATED (Rigorous, One-Step Design Procedure)

BASIC REQUIREMENT

ACCEPTABLE PERFORMANCE AT REASONABLE ACTUATION LEVELS

- GUARANTEE ELEMENTARY SYSTEM PROPERTIES (Robust Stability) — WITHOUT SERIOUS PERFORMANCE DEGRADATION (Inadvertent Design Of Unstable Controller Rendered Unlikely Or Impossible)

- APPLICABLE TO LARGE ORDER SYSTEMS WITH MODELLING INACCURACIES (Direct Design Under Imperfect System Information)

Figure 1

74

CONSEQUENCES OF THE CONVENTIONAL MODELLING PHILOSOPHY

The underlying motivation and ultimate ramifications of the above ideas can be explained by contrasting current design strategies with the present approach (Figs. 2,3).

Most schemes so far proposed invoke (at least implicitly) the existence of a very high order and allegedly accurate design model which presumes complete information on the values of all structural parameters. As Fig. 2 indicates, this initial modelling step engenders a number of seemingly impenetrable obstacles. The first and most serious obstacle, "large dimension", is connected with the difficulties imposed upon optimization computations by the large dimension of the plant model. There are basically two ways to circumvent this obstacle. The left-hand path shown in Fig. 2 proceeds by limiting the amount of system information retained in the model, i.e., by model simplification employing any one of a number of techniques. Following this model reduction step, an "optimal" control design can be computed by means of a suitable LQG-based algorithm. At this point one has a design but no assurance (arising from the underlying mathematics of the design formulation) of stability and/or robust performance in the face of inevitable spillover effects and parameter errors. Thus, it is usually necessary to "hedge" about a nominal LQG-based design in order to recover essential system properties - and this involves lengthy and complicated design iterations.

Another approach to the treatment of the dimensionality problem is suggested by the right-hand path in Fig. 2. Here, one seeks to limit the system information incorporated in the control by designing a "simple" control of inherently energy dissipative form. This manages to handle the problems of spillover and other forms of modelling error but is limited to relatively low performance. The reason is to be found in the inescapable trade-off between robustness and performance; one can be "safe" everywhere in parameter space but cannot simultaneously achieve excellent performance for any particular parameter values.

Thus, there is difficulty in securing a control which is both robust and optimal (in some well-defined sense). Moreover, since the two generic design approaches described here do not rigorously guarantee desirable properties, much checking and design iteration is required. Finally, each attempt to circumvent a particular obstacle seems to lead to further difficulties (for example the problem of large dimensionality appears to necessitate modal truncation, but this step, in turn, raises the specter of spillover instabilities, etc.).

The absence of theoretical simplicity and the plethora of ad hoc design steps generally indicate that something is wrong - some fundamental element of realism has been ignored. The view advanced here is that what is at fault is not to be found in the detailed design strategies of Fig. 2 (since these are logically driven by the initial premise) but rather arises from the presumption of a completely accurate, deterministic structural model. Actually, due to numerous sources of modelling error, and in advance of extensive testing and identification, there exists considerable *a priori* uncertainty in the structural parameters. Moreover, one typically has very little data with regard to the deviations of parameters from their nominal values. Thus, if one rules out the possibility of (off-line) identification of all parameters of a very large order system and attempts to devise a control which satisfactorily handles most parameter uncertainties at their *a priori* levels, then realism demands that such a control design be predicated upon a stochastic model which incorporates the kind of extremely limited statistical information actually available.

Such a stochastic structural model is one major development of the work reviewed herein. In contrast to the customary deterministic model, the minimum data/maximum entropy model directly incorporates the least possible (in the sense to be described later) *a priori* parameter information. The approach taken here is to adopt this model as the basic design model (thus incorporating the effects of parameter uncertainty at a fundamental level) and design mean-square optimal controls (that is, choose the control law to minimize the average of a quadratic performance index over the parameter ensemble).

DETERMINISTIC STRUCTURAL MODEL
(Presumes Complete Information)

LIMIT INFO.
RETAINED IN
MODEL

LIMIT INFO.
INCORPORATED
BY CONTROLLER

LARGE DIMENSION

SIMPLIFICATION

* TRUNCATION (Aggregation)
* DECOMPOSITION (Perturbation)

etc

MODEL SIMPLIFICATION

"OPTIMAL" DESIGN FOR REDUCED MODEL

POSITIVE REAL DESIGN, AND/OR RATE-OUTPUT FEEDBACK

SPILLOVER INSTABILITIES AND SIMILAR DIFFICULTIES

MODELLING UNCERTAINTIES
(Robustness)

PERFORMANCE REQUIREMENTS
(The Need For Optimality)

Figure 2

76

RAMIFICATIONS OF MAXIMUM-ENTROPY MODELLING

Figure 3 sketches the major consequences of this approach when applied to the typical case in which all but a modest number of system states are associated with high levels of parameter uncertainty. First, the maximum entropy modelling philosophy throws new light on the dimensionality problem. Although the number of "poorly known" states may be very large, their statistical response is extremely simple and, in particular, the second-moment response of such states may often be computed from closed-form expressions. In other words, the process of averaging over the parameter ensemble automatically induces a kind of "stochastic simplification". Since we consider averaged quadratic functionals as performance measures, this feature extends also to the optimization problem (as will be illustrated below). Thus, the control corresponding to the poorly known portion of the system can be determined in advance of burdensome computations and a mean-square optimal design is possible for very large order systems.

We note that use of the maximum entropy model as the design model gives rise to new forms of optimality conditions, representing generalizations of the familiar Riccati equations of LQG. In formulating the optimality conditions for implementable compensation, we have proceeded by climbing a ladder; each successive rung is a controller form of increasing complexity and realism.

Even with implementation constraints imposed, the present approach has the potential to treat very high order system models. Thus, since spillover effects ultimately arise from model truncation and the consequently artificial division of the full-order system, "spillover" becomes a phantom within the present context.

Finally, the essential design model is as unpresumptive of prior information as possible and thus envelops the actual parameter statistics in that it is "maximally chaotic". Moreover, the optimization formulation implicitly imposes robustness constraints, as will be illustrated shortly. Thus, by virtue of the intrinsic mathematical properties of the original design model, it is possible to secure an optimal and robust design with little or no design iteration.
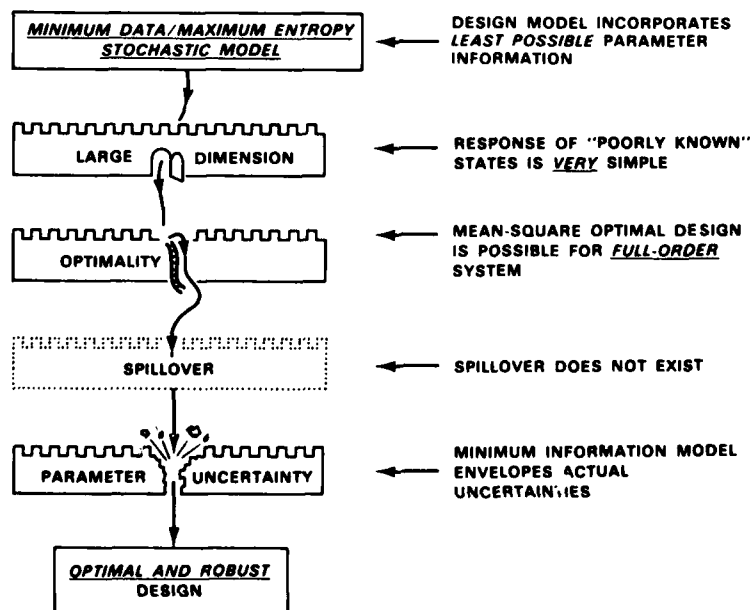
Figure 3

LIMITATIONS OF DETERMINISTIC DESIGN: THE NEED TO
QUANTIFY PRIOR UNCERTAINTY

Now let us explore the basic ideas of the maximum-entropy modelling approach, outline what is involved in its implementation, and then illustrate the various prop-
erties described above.

First, consider a structure whose parameters may be found in some "parameter space" as sketched in Fig. 4.a. Standard LQG-based approaches implicitly assume that all system maps are known and, consequently, produce a design which is optimal (with respect to a quadratic performance measure) only for a single point (associated with the nominal values) in parameter space. However, due to actual in-mission changes, mathematical modelling errors arising from truncations implicit in the finite element method, etc., all system parameters are <u>not</u>, in fact, known. Thus, to put the matter in the most general terms, a structural model can never encompass the "truth" – rather a model should be regarded as a mathematical statement of what and how much is known. Considered as such, a model must not only specify nominal values but must also contain an admission of prior ignorance regarding parameter deviations from expected values. An admission of prior uncertainty can be quantified by supposing the param-
eters to be distributed according to some probability law (see Fig. 4.b, where the shading indicates the region of significant probability).

MODAL PARAMETER SPACE

$$\bar{A}, \bar{B}... \text{ GIVEN}$$
$$\dot{x} = \bar{A}x + \bar{B}u$$
$$\text{MIN: } J = \int_{t_0}^{t_1} dt \left[x^T R_1 x + u^T R_2 u \right]$$
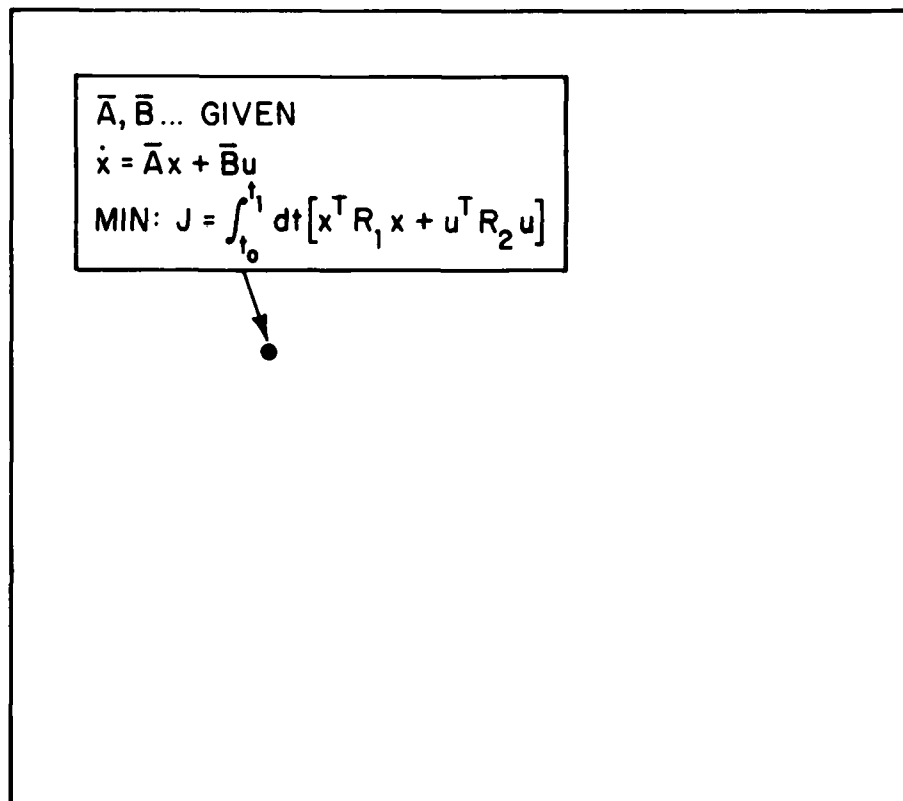
Figure 4.a

MINIMUM EXPECTED COST DESIGN: INCOMPLETENESS OF PRIOR PROBABILITIES AND THE MAXIMUM ENTROPY IDEA

Thus, one might be tempted, as suggested in Fig. 4.b, to assume that all necessary probability distributions are given and proceed to design a control which is optimal "on the average" by minimizing the expected value of a quadratic cost. However, the problem is more difficult than this because, in practice, a complete probability model is never available from empirical determinations. Rather, we need to induce a complete probability model from a highly incomplete set of available data. A fundamental logical requirement is that this be done in a manner which avoids inventing data which does not exist! In other words, it is necessary to construct a complete probability assignment which is consistent with the data at hand but admits the greatest possible prior ignorance with regard to all other data. This is the heart of the maximum entropy modelling idea. The appropriate quantitative procedure has been given by Jaynes (Refs.1,2): first define a measure of prior ignorance, i.e., the entropy ("entropy" as in information theory not thermodynamics), then determine the probability law which maximizes this functional subject to the constraints imposed by available data.

$p[A, B, ...]$ GIVEN

$\dot{x} = Ax + Bu$

MIN: $\bar{J} = E[J]$
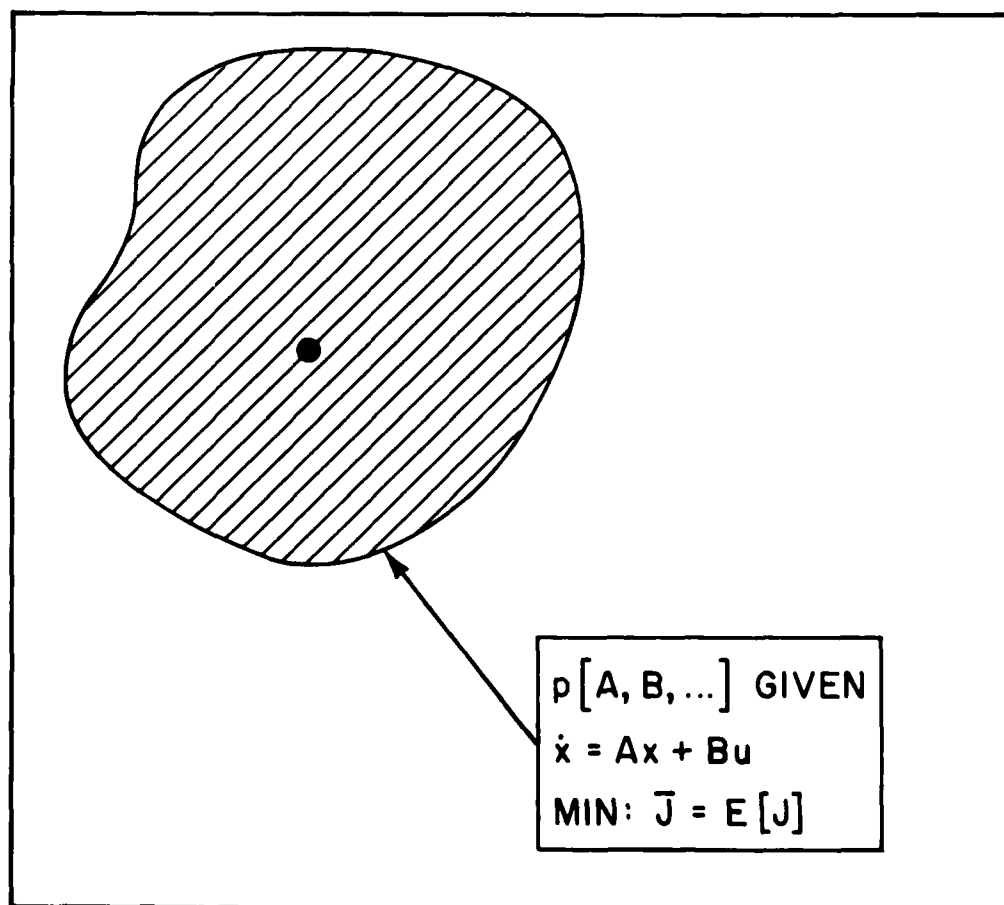
Figure 4.b

THE MINIMUM DATA/MAXIMUM ENTROPY DESIGN APPROACH

Having overcome the difficulties imposed by incomplete available data, it should be noted that for flexible mechanical systems one may identify a "minimum data set" which is just sufficient to induce any well-defined maximum entropy model. In other words, all admissible sets of available data must include the minimum set, and lack of any element of this minimum set will cause the induced maximum entropy model to "blow up" in certain crucial respects. Since, in practice, one is provided with little or no prior statistical data, it is not only design conservative, but also realistic to acknowledge as available data only the minimum data set.

Thus, as sketched in Fig. 4.c, our stochastic design approach involves three main stages (see Refs. 3-5). First, the minimum data set is constructed and appropriate numerical values are assigned; next, a maximum-entropy probability model is induced from the minimum data (giving the basic design model), and, finally, a mean-square optimal design is determined under the maximum-entropy statistics. This procedure gives us a mechanism for incorporating incomplete system information within the control design. Moreover, as Fig. 4.c suggests, the maximum-entropy model is maximally dispersed in parameter space, and one can guarantee that the resulting design will very greatly reduce the probability of severe performance degradation in the face of parameter deviations.
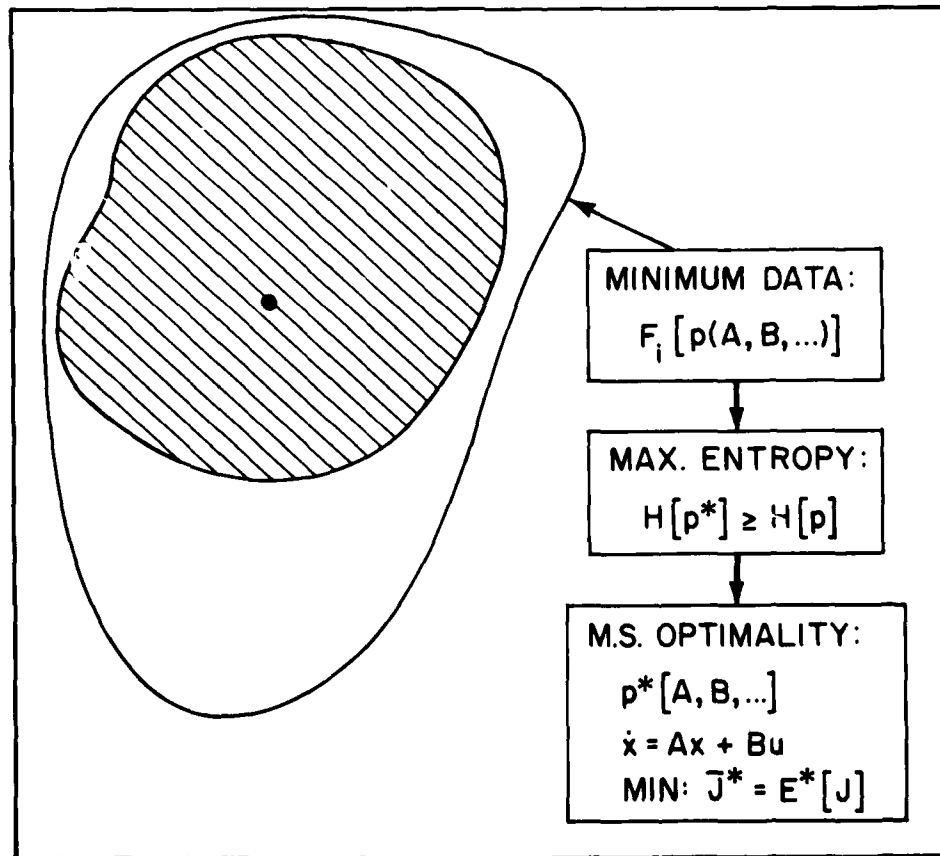
Figure 4.c

MAXIMUM-ENTROPY APPROACH: SPECIFIC FEATURES
FOR STRUCTURAL SYSTEMS

Figure 5 indicates more specific features of the maximum-entropy approach as applied to linear mechanical systems. In the state-space equation at the top of the figure, x denotes the state vector of the plant and any dynamic compensation that might be employed, and the dynamics map is the sum of a deterministic portion, $\bar{A}$, representing the nominal parameter values and a zero-mean random portion, α. With this form of representation, the formulation is presently capable of encompassing most of the more serious sources of modelling error in structural systems. In particular, α may represent general uncertainties in the stiffness matrix and in the placement and alignment of actuators and sensors (see Refs.6 and 7).

A suitable measure (which is particularly familiar in information theory) of *a priori* ignorance is given in the figure, where p(x) denotes the probability density of the state. Actually, since entropy is only a <u>relative</u> measure of information, its definition is not unique, and the expression given below is one of several possibilities (note that Refs.3 and 5 defined entropy measures directly upon the parameter space). Although each possibility is particularly suited to a specific purpose, all these entropy definitions lead to the same results. In particular, besides specification of nominal parameter values and an enumeration of those scalar structural parameters whose independent variation is to be included in α, the minimum data set consists of the "uncertainty relaxation times". Each of these time scales is associated with a particular uncertain scalar parameter, and is simply and explicitly defined in terms of familiar statistical quantities (see Refs.3 and 5 for details). Qualitatively speaking, the relaxation times give the time scales over which the effects of the associated uncertainties upon second-moment response are manifested, and their reciprocals constitute fundamental measures of the magnitudes of parameter deviations.

The maximum-entropy model induced by this data set is a rather special form of Stratonovich state-dependent noise (see Ref.8), and it yields a modified Lyapunov equation for determination of the state covariance matrix, $Q \triangleq E[xx^T]$. The linear operator, D[.], appearing at the bottom of Fig. 5, is a mapping of the class of symmetric matrices onto itself, and it constitutes the principal modification. Since the matrix elements of D[Q] are inversely proportional to the relaxation times, this "stochastic Lyapunov equation" reduces to the ordinary Lyapunov equation in the deterministic limit (wherein all relaxation times are infinite). Since Q is the only response quantity directly relevant to mean-square performance, optimality conditions are obtained in the form of "stochastic Riccati equations" involving analogous modifications of the standard Riccati equation. Thus, these new forms of optimality conditions contain the familiar results for deterministically parametered systems as a special case.

$$\dot{x} = (\bar{A} + \alpha)x + w$$

UNCERTAIN QUANTITY:	α (Uncertainty in Stiffness Matrix, Sensor/Actuator Locations, etc.)
MEASURE OF a priori IGNORANCE (Entropy):	$H \triangleq -E\,[\ln p(x)]$
MINIMUM DATA SET:	"RELAXATION TIMES" = T_{kj} (Formed from Characteristic Functions of Random Parameters)
MIN. DATA/MAX. ENTROPY MODEL: (for $Q \triangleq E\,[xx^T]$)	$H_{MAX} = \frac{1}{2} \ln |Q|$ $\dot{Q} = \bar{A}Q + Q\bar{A}^T + D[Q] + V$ $(D[\cdot] \propto 1/T)$

Figure 5

EFFECTS OF PARAMETER UNCERTAINTY: INCOHERENCE

Although inaccessible to us in practice, a complete probabilistic description of the structure nevertheless exists in principle. The maximum-entropy model may be viewed as an approximation to this complete probability law which extracts only certain salient features which are to be modelled with fidelity. This naturally leads to the question: What features of the actual parameter statistics are preserved in the maximum entropy model? (Obviously, the relaxation times are preserved, but what is their physical meaning?)

To provide an answer, let us consider the effects of parameter uncertainty on second-moment response of mechanical systems generally - not necessarily under the maximum entropy model. First, for purposes of illustration, Fig. 6 shows a simple system of two (weakly) coupled oscillators in which the stiffnesses k_1 and k_2 are subject to uncertainty. When the magnitudes of the deviations are significant and largely independent of the detailed probability distributions of k_1 and k_2, the cross-correlation coefficient (defined in the figure, where $(\overline{.})$ denotes an average over the parameter ensemble) of the two oscillators approaches a value of order T after a time period of order T following some initial state. Here T is the minimum of the relaxation times associated with k_1 and k_2. This tendency of uncertainty to suppress cross correlation among distinct modes has been termed the "incoherence" effect, and the situation depicted in Fig. 6 may be generalized in an obvious manner to the case of n(n > 2) oscillators.
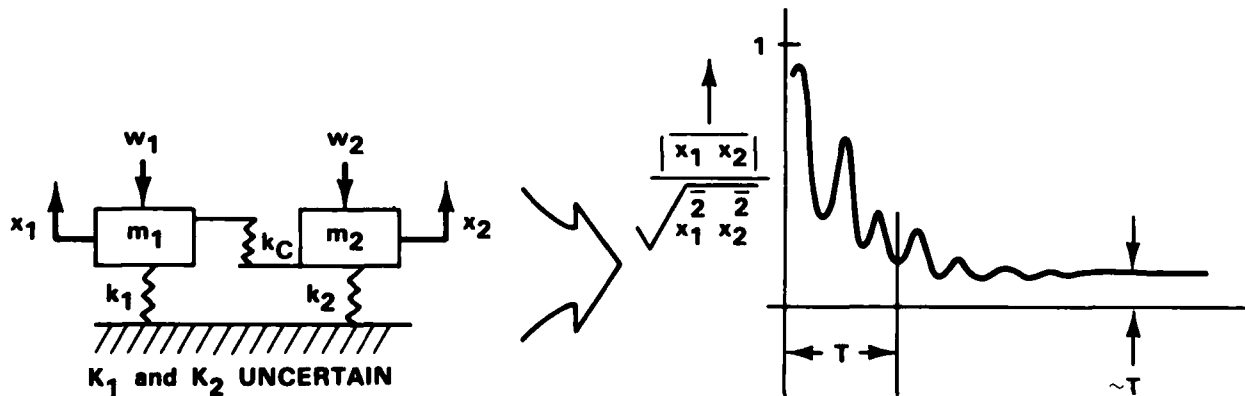
$$T \triangleq MIN(T_1, T_2)$$

$$T_1, T_2 \triangleq RELAXATION\ TIMES\ OF\ K_1\ and\ K_2$$

Figure 6

82

EFFECTS OF PARAMETER UNCERTAINTY: ISOTROPY

Next consider the same system as in Fig. 6 but with uncertainty only in the coupling spring stiffness (Fig. 7). Besides the incoherence effect, averaging over the parameter ensemble introduces a net power flow between the uncoupled oscillators which tends to equalize their separate mechanical energies. For sizable uncertainty levels and over a time of order T_c following some initial state, the system relaxes to a special statistical equilibrium wherein the relative energy difference is proportional to T_c. Here again, T_c is the relaxation time (as defined in Ref.5) associated with the random portion of k_c. Thus, for very large uncertainty (T_c small), this "isotropy" effect produces equality of energies and, from the point of view of their second-moment response, the two oscillators are largely indistinguishable. This sort of thermal equilibrium is established in an analogous manner for a large-order system wherein uncertainties exist which tend to couple nominally uncoupled modes.

The effects just discussed have been known (separately) for some time (see, for example, Refs.9-11) and are <u>real</u> - not artifacts of the maximum-entropy modelling approach. Rather, the magitudes and associated time scales of these effects are precisely what the maximum-entropy model <u>preserves</u> and <u>faithfully models</u>.
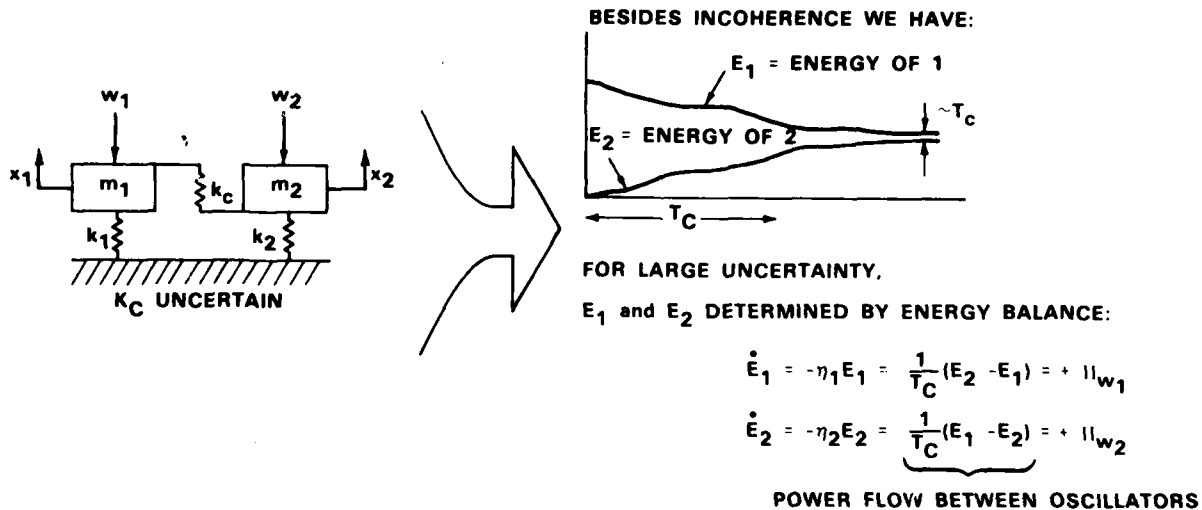
Figure 7

IMPACT OF UNCERTAINTIES ON MEAN-SQUARE OPTIMAL DESIGN

The great importance of accurate modelling of incoherence and isotropy arises from the fact that these effects engender distinct qualitative regimes wherein mean-square optimal control design is dramatically affected. To illustrate this, consider the mean-square optimal design of full-state feedback regulation (relevant equations are indicated at the top of Fig. 8) for a high-order stochastic model which incorporates the "actual" parameter statistics. Also suppose that modes are arranged in order of increasing uncertainty levels. By virtue of the incoherence effect, there emerges an "incoherent range" wherein the modes are (to a close approximation) mutually uncorrelated and uncorrelated with lower order modes. The remaining (low order) modes retain significant cross-correlation and constitute the "coherent range". In addition, for sufficient uncertainty in the structural stiffness, there may exist an "isotropic subrange" (where approximate equality of modal energies holds) within the incoherent range. Clearly, since the performance index can be expressed as a linear function of the second moments, the contribution of all the incoherent modes is of the form of a weighted sum of mean squares of the separate states (as indicated in Fig. 8). This reduction to a sum of mean squares has a profound effect on the control design because it implies that any control effort devoted to shifting modal frequencies and/or closed-loop eigenvectors is wasted. In consequence, mean-square optimal design demands an inherently robust positive real or rate feedback controller for the incoherent modes. Obviously, this dramatic qualitative effect cannot be ignored.

Now the maximum entropy model not only models the above qualitative regimes faithfully, but in addition, the associated optimality condition (the stochastic Riccati equation) automatically produces an inherently energy dissipative rate feedback control for the highly uncertain, incoherent modes. Moreover, the incoherent range control design is in close conformity with the asymptotic solution of the stochastic Riccati equation for large uncertainty levels. Since, in many instances, this asymptotic solution can be given in closed form, one may regard the mean-square optimal design for the very poorly known states as being known in advance of burdensome computations.

$$\dot{x} = (A - BK) x + w$$

$$J = \int \omega t \, E\left[x^T(R_1 + K^T R_2 K) x\right]$$

MODAL ORDER AND/OR FREQUENCY ⟶

◄—COHERENT ⟶ ◄——— INCOHERENT ⟶ └——— ⟶

DISSIPATIVE

◄— ISOTROPIC —►

$$J = \sum_{k,i} \mathcal{J}_{c_{ki}} \overline{x_k x_i} \quad + \quad \sum_k \hat{\mathcal{J}}_{kk} \overline{x_k^2} \quad + \quad \left(\sum_k \hat{\hat{\mathcal{J}}}_{kk}\right) \overline{x_{ls}^2}$$

| HIGH PERFORMANCE CONTROL | POSITIVE-REAL OR CENTRALIZED RATE FEEDBACK | DEMANDS, COLOCATION AND RATE OUTPUT FEEDBACK |

SECOND-MOMENT STATISTICS
GIVEN IN CLOSED FORM
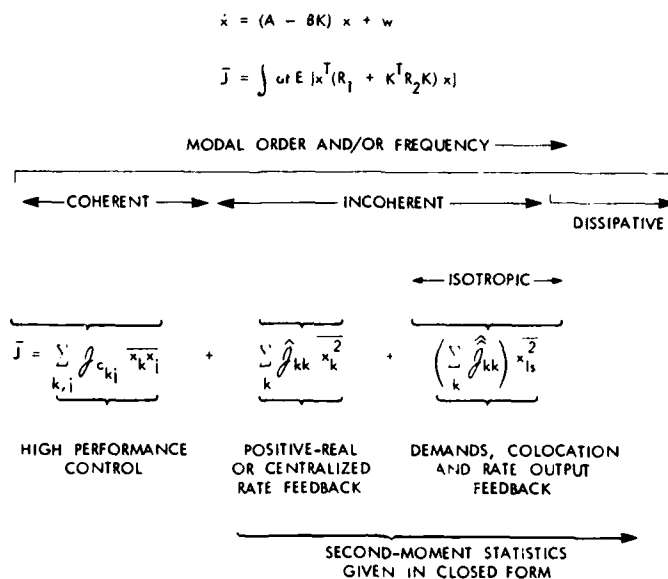
NOTE: THESE REGIMES ARE REAL AND ARE FAITHFULLY PRESERVED
IN THE MAX. ENTROPY MODEL

Figure 8
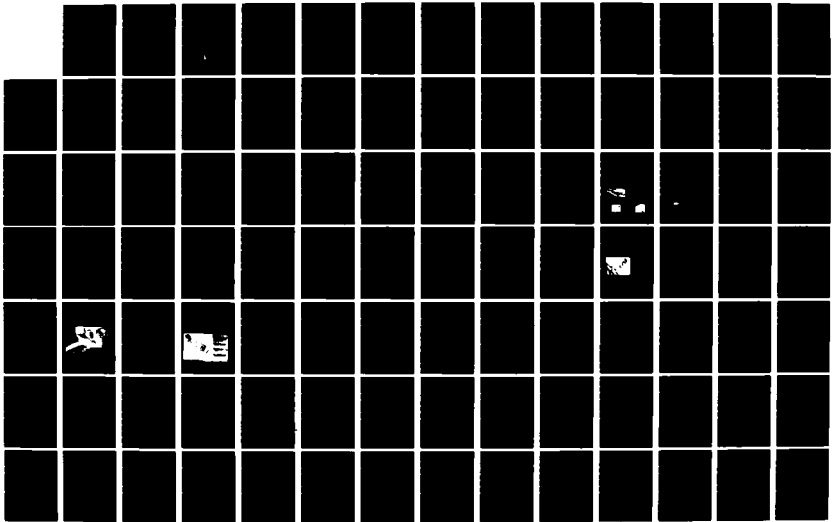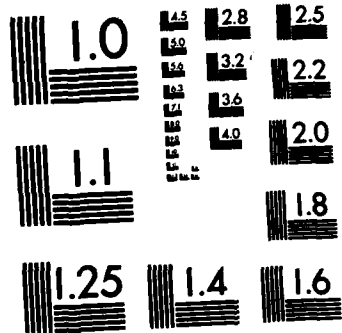
MICROCOPY RESOLUTION TEST CHART

NATIONAL BUREAU OF STANDARDS-1963-A

NUMERICAL EXAMPLE FOR THE REGULATOR PROBLEM

As a specific example, consider the regulator design for a simply supported Bernoulli-Euler beam with one force actuator depicted in Fig. 9. Here an energy weighting is imposed on the state in the performance index, and we denote by the scalar ρ the relative control input weighting. (For complete details regarding this example, including closed-loop poles, sensitivity studies, etc., see Ref. 12). Uncertainties only in the open-loop frequencies are considered, and frequency deviations from the nominal values, ω_k, are taken to be Gaussian. The corresponding relaxation times, T_k, are seen to be inversely proportional to the relative standard deviations, σ_k. To provide a simple model which reflects progressive degradation in modelling accuracy with increasing modal order, we take the σ_k to increase with nominal frequency.

EXAMPLE: SIMPLY SUPPORTED BEAM WITH FORCE ACTUATOR
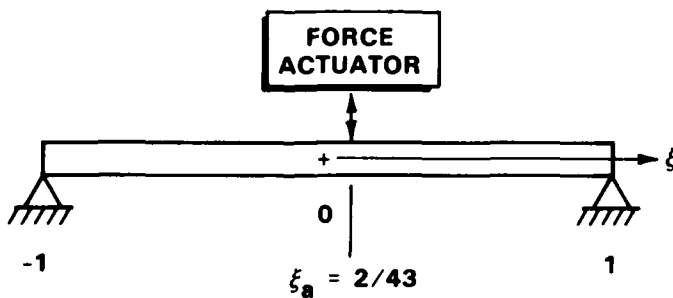
* NONDIMENSIONAL EQUATIONS
  OF MOTION $(\bar{\omega}_n = n^2)$

* "ENERGY" STATE-WEIGHTING

* UNCERTAINTIES IN OPEN-LOOP
  FREQUENCIES:

$$T_K = \frac{\sqrt{\pi}}{2} (\sigma_K \ \bar{\omega}_K)^{-1}$$

σ_K = STANDARD DEVIATION
OF Kth MODE FREQUENCY

* SIMPLE UNCERTAINTY MODEL:

$$\sigma_K = \sigma \bar{\omega}_K$$

FORCE
ACTUATOR

ξ

0

-1

$\xi_a = 2/43$

1

Figure 9

DESIGN RESULTS AND QUALITATIVE INTERPRETATIONS - STOCHASTIC SIMPLIFICATION

For specific values of damping, ρ, and uncertainty level, Fig. 10 shows the mean-square optimal design for a 100-mode model. For clarity, we show the gain magnitudes scaled by means of ρ. The position and velocity gains for each mode are shown pairwise, the labelling of the abscissa referring to the mode number. Note also that a different ordinate scale was used for the last 50 modes to more clearly display the details.

This design was obtained in less than 10 seconds computation time in the following manner. First, rigorous bounds for the deviation of the solution of the stochastic Riccati equation from the asymptotic solution are available from Ref. 3, and these show that the asymptotic solution incurs negligible error (4th significant digit) for the 25th mode and that the error declines rapidly for all higher modes. Consequently, the solution of the full-order design equation for the last 75 modes was obtained with virtually no computational effort. Detailed computations were required only for the first 25 modes. Thus, because of the special structure of the stochastic Riccati equation, the results shown represent a highly accurate solution for the full 100-mode model.

The above features illustrate a general principle which emerges also in numerous additional examples: *Under a system model which incorporates limited a priori information, it is always possible to so arrange matters that the burden of mean-square optimal design computation is similarly limited.*

Also note from Fig. 10 that the design algorithm has automatically produced a reasonably high gain (> 20-percent damping), which is a virtually deterministic LQ design for those modes (the first three) associated with low uncertainty and an inherently robust rate feedback control for the poorly known modes. These regimes were not secured on an ad hoc basis but are limiting qualitative features of a global design which is guaranteed stable and optimal.

STOCHASTIC BEAM PROBLEM — GAIN MAGNITUDES
### ($\eta = 0.005$, $\rho = \sigma = 0.1$)
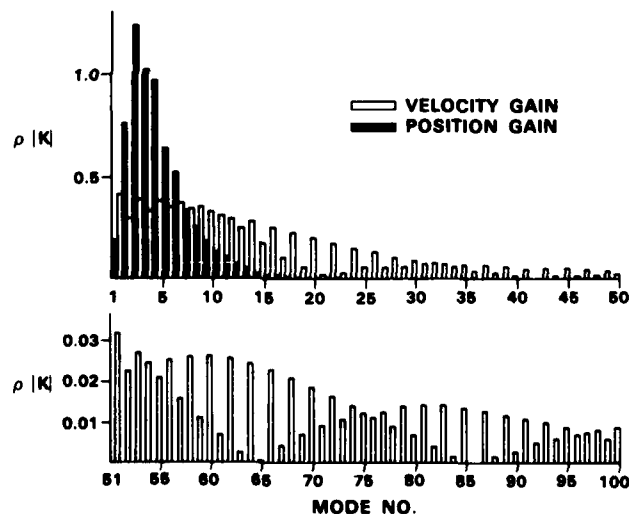
Figure 10

STOCHASTIC STABILITY AND ROBUSTNESS PROPERTIES

With regard to stability, various theoretical assurances are available for the maximum-entropy approach. Figure 11 sketches the basic rationale for many of the stability and robustness proofs. First, for a variety of controller forms, unique solutions have been shown to exist for all uncertainty levels. As part and parcel of such demonstrations, it is necessarily shown that the mean-square optimal performance, $\bar{J}^*$, is bounded. But, under certain mild geometric conditions, this is impossible unless the closed-loop system is second-moment stable (and hence almost surely stable). In addition, one has assurance of robustness with respect to deterministic system stability concepts. By Lyapunov arguments and associated singular value bounds, the range in parameter space for which stability is obtained can be shown to be comparable to the modelled uncertainty levels (as will be illustrated presently).

The above properties thus imply that by allowing the modelled uncertainty levels to increase without bound, one may use the maximum-entropy optimality conditions to discover (or rather, rediscover!) particularly robust controller forms. As Fig. 11 indicates, this is indeed the case. We may summarize much of this work by stating: *Under the maximum-entropy model, and in the presence of very great parameter uncertainty, the mean-square optimal control is a control which is inherently energy dissipative.*

MEAN-SQUARE OPTIMALITY

$$\Downarrow$$

ROBUSTNESS UNDER MODELLED UNCERTAINTIES

(1) SOLUTIONS TO OPTIMALITY CONDITIONS EXIST FOR ALL <u>UNCERTAINTY</u> LEVELS

(2) $\bar{J} = \int dt \, E[x^T R_1 x + u^T R_2 u]$ CAN BE MINIMIZED <u>ONLY IF</u> $\bar{J}^* < \infty$

(3) $\bar{J}^* < \infty$ <u>ONLY IF</u> SYSTEM IS SECOND MOMENT STABLE

$$\Downarrow$$

● GUARANTEED STOCHASTIC STABILITY

● PARAMETER SPACE STABILITY RANGE ∝ MODELLED UNCERTAINTY LEVELS

● POSITIVE REAL OR RATE OUTPUT FEEDBACK CONTROL FOR LARGE UNCERTAINTIES

Figure 11

87

EXAMPLE ILLUSTRATING ROBUSTNESS PROPERTIES - STABILITY STUDIES

To illustrate the relative stability properties of the stochastic design, consider the simple two-mass system in Fig. 12 (for complete details and further results see Ref. 13). With a single force actuator and displacement sensor located at mass 1, it is desired to suppress the displacement response of mass 2 (thus the steady-state performance index, J_s, is as indicated in the figure). We assume that only the frequency of the single elastic mode is uncertain and is subject to normally distributed variation with standard deviation, σ, relative to its nominal value, ω. Of course, since only one parameter is uncertain, the range of stability in parameter space can be shown particularly simply for this example.

The assumed observation noise, w_2, requires design of a full-order dynamic compensator (observer) for this system. The relevant mean-square optimality conditions for the maximum-entropy model are given in Ref. 13. These were solved for a range of values of σ. Each such compensator design corresponding to a given modelled uncertainty (a given σ value) was then interconnected with a perturbed structural model with modal frequency $\omega(1 + \delta)$. Thus δ is the deviation of the frequency relative to the nominal value, ω. Stability was then checked for the closed-loop system over a range of values of δ.

TWO-MASS SYSTEM
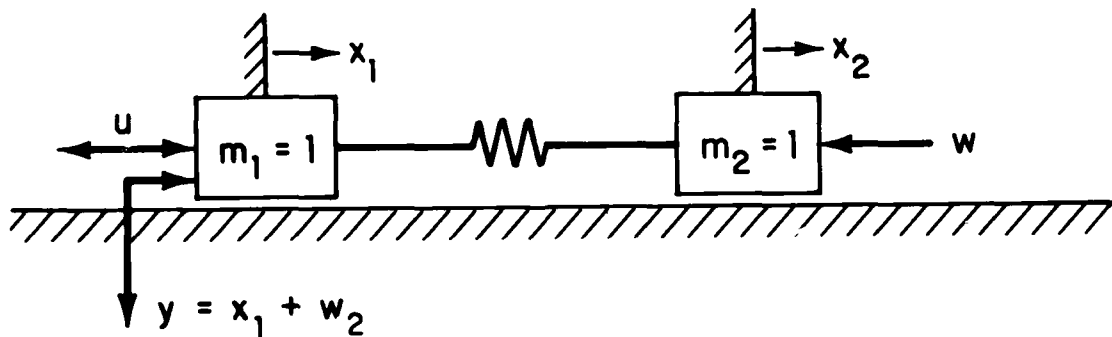
PERFORMANCE INDEX: $\bar{J}_s = E\left[x_2^2 + u^2\right]$

ASSUMING FREQUENCY
IS GAUSSIAN: $T = \dfrac{\sqrt{\pi}}{2}\,(\sigma\,\bar{\omega})^{-1}$

Figure 12

EXAMPLE PROBLEM – STABILITY BOUNDARIES

The results of the stability study are summarized in Fig. 13. Thus, for example, the deterministic, LQG design ($\sigma = 0$) is unstable for relative frequency variations between –10 percent and –50 percent and greater than +30 percent. On the other hand, progressive increase of the modelled uncertainty level dramatically widens the stability range. In fact, as the figure makes evident, stability is guaranteed for $\delta \leq \sigma$. Note that if δ is randomly distributed but of bounded variation, σ may always be chosen to guarantee stability. On the other hand, if δ is randomly distributed with unbounded variation, appropriate choice of σ can still reduce the probability of instability to any desired level. Thus, a striking illustration of the general robustness results discussed is evident. Similar stability studies have been performed and analogous results achieved in other much more complicated examples (see Refs. 13-14).

(Unstable Region Shaded)
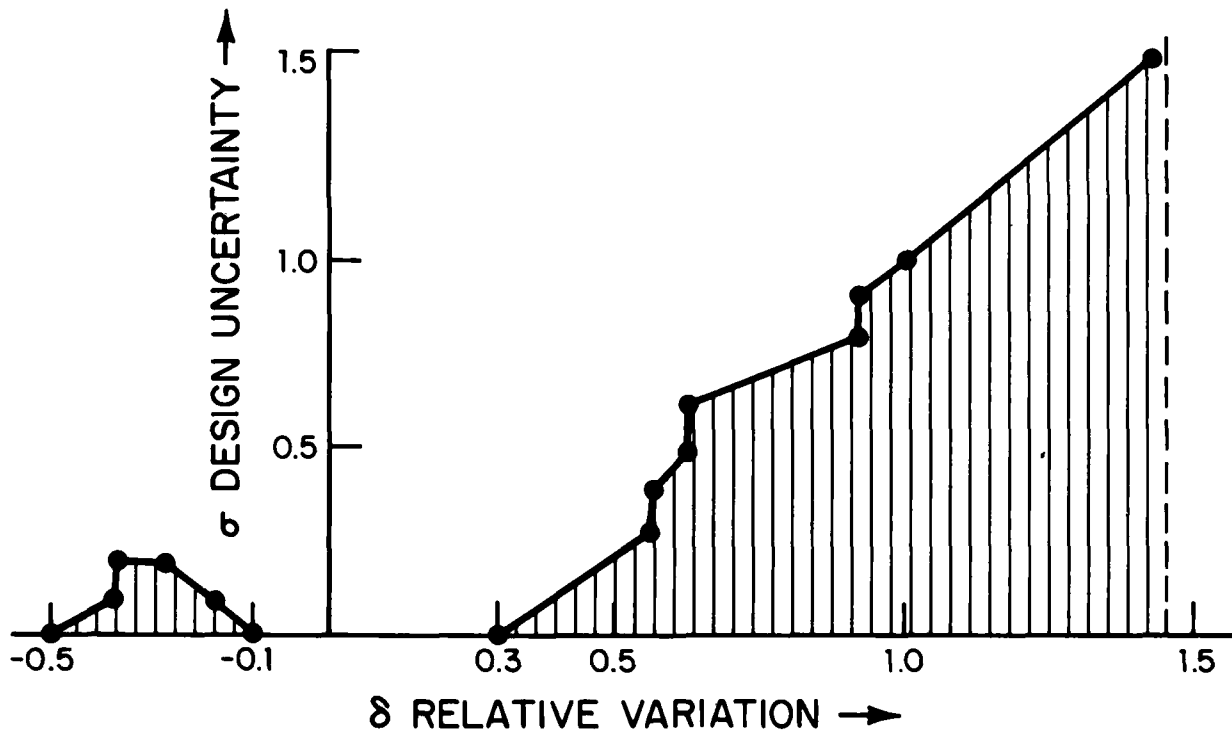
Figure 13

MEAN-SQUARE OPTIMAL DESIGN: IMPOSITION OF
IMPLEMENTATION CONSTRAINTS

The remainder of this paper considers various optimization issues. As noted, we attained a maximum-entropy formulation for implementable compensation by first considering the simplest controller form, i.e., full-state feedback regulation, and then by progressively removing idealized restrictions. This stage-by-stage development is summarized in Fig. 14. As mentioned, the maximum-entropy model conjoined with mean-square optimization gives rise to new forms of optimality conditions. For example, determination of the mean-square optimal regulator requires solution of the stochastic Riccati equation (for its definition and basic properties, see Refs. 3, 4, 5 and 15). This equation reduces to the standard Riccati equation in the deterministic limit, but, as the foregoing beam example illustrates, new convergence properties are exhibited in the presence of uncertainty.

Next, the unrealistic restriction of full-state feedback was removed and state information was assumed available only through a limited number of sensor outputs. Assuming non-singular observation noise, the case of full-order dynamic compensation was considered and appropriate optimality conditions derived in Refs. 13 and 14. These results show that in the presence of uncertainties, the separation principle no longer holds. Indeed, the optimality conditions determining the regulator and observer gains (k and F, respectively in Fig. 14) are determined by two coupled stochastic Riccati equations together with two additional Lyapunov equations. The appended Lyapunov equations serve to determine two auxilliary cost matrices which characterize the error "leaking through" from regulator to observer (and vice versa) due to the action of parameter uncertainty. Despite this additional complexity, efficient numerical procedures for solution of the full optimality conditions have been developed and successfully applied to a variety of example problems (of which the two-mass system considered above is the simplest case). Finally, it should be noted that various desirable features observed for the regulator problem, i.e., stochastic simplification and the automatic emergence of a simple, dissipative control for the poorly known modes, are also obtained in this less idealized setting.

The next and final stage in the development of suitable optimality conditions removes the assumption that the compensator order is equal to that of the plant. Clearly, while the structure is of infinite dimension, on-board software limitations force the compensator order to be rather modest. Thus it is necessary to design a mean-square optimal, dynamic compensator whose order ($N_q, N_q \leq 2n$) is preassigned by the designer. This is the problem of optimal, linear, fixed-order dynamic compensation and quite apart from the inclusion of parameter uncertainty effects; the results presented in Ref. 16 are new. In place of the purely computational approach which combines gradient calculation with parameter optimization algorithms, Ref. 16 provided, for the first time, explicit optimality conditions for fixed-order compensation. As in the case of full-order compensation, these conditions amount to two Riccati-like and two Lyapunov-like equations. A qualitatively new feature, however, is that these equations determine not only the optimal gains but also a projection (idempotent matrix) which defines the N_q-dimensional observation and control subspaces of the compensator. This "optimal projection" essentially characterizes the geometric structure of a reduced-order model of the plant which is employed internally by the compensator. For example, the usual modal truncation approach to model reduction is tantamount to the assumption that the projection is of the canonical form $\begin{bmatrix} I_{N_q} & 0 \\ 0 & 0 \end{bmatrix}$ in the modal coordinate basis. However, in most instances, the true optimal projection is far more general than this, and, in contrast to all previous approaches, the conditions of Ref. 16 determine both the gains and the optimal compensator structure with its associated reduced-order model.

Various theoretical properties of the fixed-order compensation optimality conditions are elaborated in Ref. 17. In particular, solutions of these equations give rise to a control for which closed-loop stochastic stability and mean-square optimality are guaranteed. Moreover, solutions exist of a highly simplified asymptotic form for those high-order, poorly known modes constituting the incoherent range. Thus, as in the regulator problem, the optimization computations can be carried out for very large order systems.

CONTROLLER FORM	VARIATIONAL PROBLEM	OPTIMALITY CONDITIONS
FULL STATE FEEDBACK	("A" is Uncertain and Treated Under the Max. Entropy Model) $$\text{MIN: } J = \int_{t_o}^{t_1} dt\, E\, [x^T R_1 x + u^T R_2 u]$$ $$\dot{x} = Ax + Bu + w_1 \quad ; \quad x \in R^{2n}$$ $$u = -kx \quad ; \quad u \in R^{\ell}$$	• SPECIAL FEATURES STOCHASTIC RICCATI EQ'S • NEW CONVERGENCE PROPERTIES WITH INCREASING MODEL ORDER
FULL-ORDER COMPENSATION	SAME AS ABOVE, EXCEPT: $$u = -kq \quad ; \quad u \in R^{\ell}$$ $$\dot{q} = \alpha q + Fy \quad ; \quad q \in R^{2n}$$ $$y = Cx + w_2 \quad ; \quad y \in R^{P}$$	COUPLED STOCHASTIC RICCATI EQ'S • NO SEPARATION PRINCIPLE
FIXED-ORDER COMPENSATION	SAME AS ABOVE, EXCEPT $$q \in R^{N_q} \quad , \quad N_q \leqslant 2n$$	COMPENSATOR STRUCTURE DETERMINED BY OPTIMAL PROJECTION

Figure 14

91

GENERALITY OF THE OPTIMAL PROJECTION APPROACH TO FIXED-ORDER COMPENSATION

A further property of the formulation of Ref. 16 is its considerable generality, as indicated in Fig. 15. Although the original derivation assumed nonsingular observation noise and thus permitted no direct sensor feedback, the conditions of mean-square optimal output feedback can be recovered from the equations of Ref. 16 as a special limiting case. Also if N_q is set equal to the plant dimension, the optimality conditions immediately reduce to those of Ref. 13. If, in addition, no parameter uncertainty exists, the full-order compensation optimality conditions directly yield the uncoupled Riccati equations of LQG theory. Finally, a variety of LQG-based techniques with their assorted model reduction schemes can be seen as special approximations to the present optimality conditions (see Ref. 17 for further details regarding the relations between the optimal projection and modern modal control approaches). Thus, the optimal projection formulation has the conceptual scope needed to assess the relative merits of the various more specialized design schemes that have been advanced in the recent past.


**FIXED-ORDER COMPENSATION
THROUGH OPTIMAL PROJECTION**

M.S. OPTIMAL, FULL-ORDER COMPENSATION

LQG

M.S. OPTIMAL OUTPUT FEEDBACK
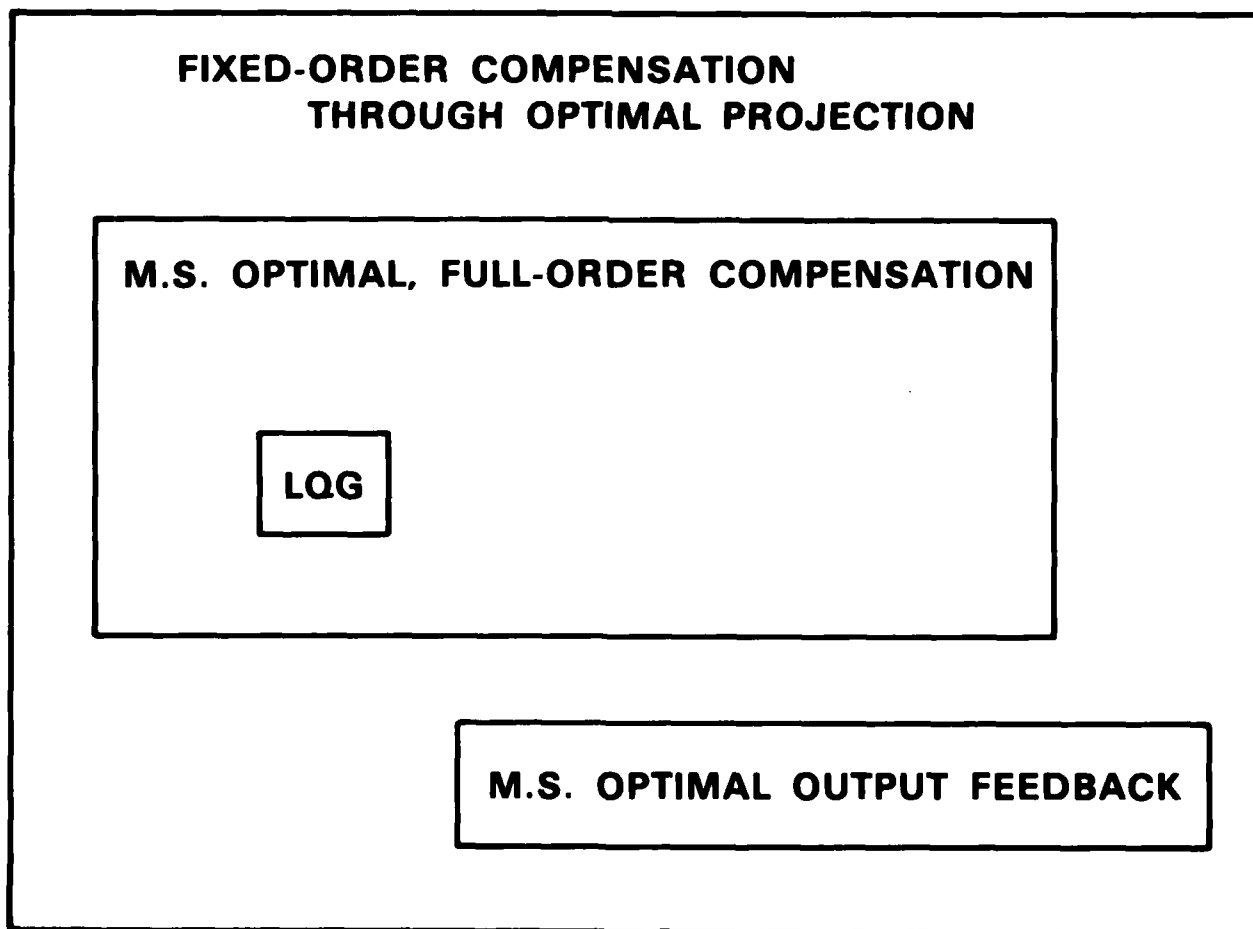
Figure 15

MAXIMUM-ENTROPY MODELLING CONJOINED WITH OPTIMAL PROJECTION: TOWARD MECHANIZED DESIGN SYNTHESIS

   Although numerical techniques for solution of the fixed-order compensator opti-
mality conditions are based primarily upon software previously developed for full-
order compensation, it remains to consolidate this software and explore fixed-order
design for representative example problems. The theoretical properties mentioned
certainly provide strong impetus for completing this task, and our immediate object
is the design synthesis software package indicated in Fig. 16. Given a high-order
plant model (specified nominal values and uncertainty relaxation times), together with
quadratic control objectives and a specified compensator order, this software package
would handle the optimization computations via a two-level iterative method employing
efficient relaxation techniques for the incoherent regime. Because of the guaranteed
system properties listed at the bottom of Fig. 16, the need for direct human interven-
tion in the control design process would be largely eliminated. The designer's
burden is thereby greatly reduced, and all that is required on his part is a familiarity
with the meaning and impact of uncertainty relaxation times and some design experience
with quadratic optimization.

MODELLING

- NOMINAL VALUES
- RELAXATION TIMES

OBJECTIVES

STATE AND
CONTROL INPUT
WEIGHTING MATRICES

DESIGN SYNTHESIS

BOUND DEVIATIONS FROM
ASYMPTOTIC SOLUTION
AND DELIMIT COHERENT
RANGE

SOLVE FULL OPTIMALITY
CONDITIONS BY TWO-LEVEL
METHOD

- MEAN-SQUARE OPTIMAL DESIGN
- NOMINAL SYSTEM IS STABLE

- STOCHASTIC SYSTEM IS 2nd MEAN AND ALMOST SURELY STABLE
- ROBUST STABILITY UNDER *MODELLED* UNCERTAINTY LEVELS

Figure 16

UNIFIED STRUCTURE/CONTROL DESIGN SYNTHESIS

The contemplated design optimization package would be of particular usefulness in performing trade-off studies needed for the overall structure/control design synthesis (see Fig. 17). In the very earliest design stages, the theory underlying the control design package can be used to delimit the various qualitative regimes and bound the best achievable mean-square performance for several candidate structural design concepts. This would allow computationally simple performance trade-off studies - including the effects of *a priori* modelling uncertainties, actuator/sensor placement, etc. Such studies would permit the early elimination of those structural concepts which are not feasible in view of the performance requirements. In general, the control design approach outlined here would help to guide the structural design according to the inherent capabilities and limitations of fixed-order compensation.

In the later stages of design (with a reasonably well-defined structural concept), the control synthesis software could be used to achieve a dynamic controller of lowest order which meets performance requirements. If the resulting compensator order also satisfies on-board computational constraints, a final linear system design is achieved which produces acceptable performance despite parameter uncertainties taken at their *a priori* levels. In this case, the need for parameter identification would be obviated. Generally, however, *a priori* uncertainties may be so large that the robustness level produced by the control design synthesis package is too high to permit good mean-square performance. Here, the design synthesis package of Fig. 16 can be employed iteratively to establish the gradients of performance with respect to the various relaxation times. This would permit one to enumerate those (relatively few) "crucial" structural parameters that must be identified in order to secure the required performance. Considerable simplification thereby results for identification algorithms, since only the crucial parameters need be addressed.
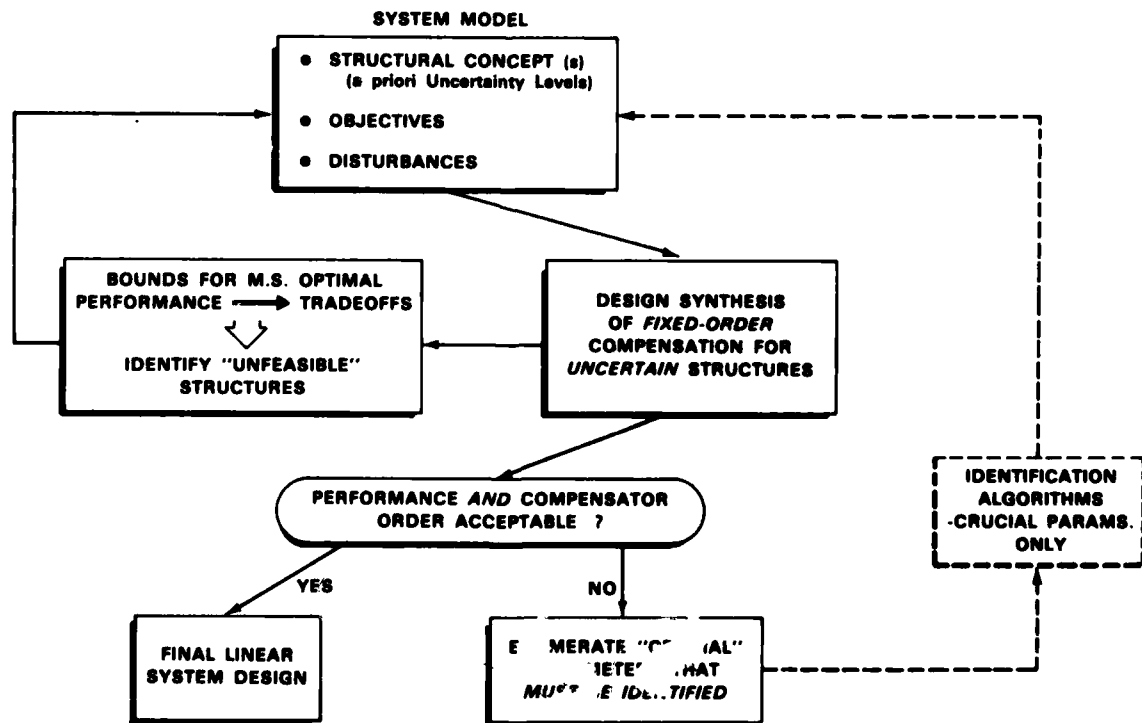

Figure 17

REFERENCES

1. Jaynes, E. J., "New Engineering Applications of Information Theory," Proceedings of the First Symposium on Engineering Applications of Random Function Theory and Probability, edited by J. L. Bogdanoff and F. Kozin (Wiley, New York, 1963), pp. 163-203.

2. Jaynes, E. J., "Prior Probabilities," IEEE Trans. Systems Sci. Cybern., SEC-4, 227 (1968).

3. Hyland, D. C., "Optimal Regulation of Structural Systems With Uncertain Parameters," MIT, Lincoln Laboratory, TR-551, 2 February 1981, Defense Documentation Center AD-A099111/7.

4. Hyland, D. C., "Active Control of Large Flexible Spacecraft: A New Design Approach Based on Minimum Information Modelling of Parameter Uncertainties," Proceedings of the Third VPI&SU/AIAA Symposium on Dynamics and Control of Large Space Platforms, Blacksburg, Va., June 1981.

5. Hyland, D. C., "Minimum Information Stochastic Modelling of Linear Systems With a Class of Parameter Uncertainties," No. 9474, IEEE American Control Conference, Arlington, Va., June 1982.

6. Hyland, D. C., "Maximum Entropy Stochastic Approach to Control Design for Uncertain Structural Systems," No. 9475, IEEE American Control Conference, Arlington, Va., June 1982.

7. Hyland, D. C., "Robust Spacecraft Control Design in the Presence of Sensor/ Actuator Placement Errors," No. 82-1405, AIAA Astrodynamics Conf., San Diego, California, August 1982.

8. Stratonovich, R. L., "A New Form of Representation of Stochastic Integrals and Equations," SIAM J. Contr. 4, 362 (1966).

9. Kistner, A., "On the Moments of Linear Systems Excited by a Coloured Noise Process," in Stochastic Problems in Dynamics, edited by B. L. Clarkson (Pitman, London, 1977), pp. 36-53 .

10. Ungar, E. E., "Statistical Energy Analysis of Vibrating Systems," Trans. ASME, J. Eng. Ind. 89, 626 (1967).

11. Lyon, R. H. and Maidanik, G., "Power Flow Between Linearly Coupled Oscillators," J. Acoust. Soc. Am. 34, 623 (1962).

12. Hyland, D. C. and Madiwale, A. N., "Minimum Information Approach to Regulator Design: Numerical Methods and Illustrative Results," Proceedings of the Third VPI&SU/AIAA Symposium on Dynamics and Control of Large Space Platforms, Blacksburg, Va., June 1981.

13. Hyland, D. C. and Madiwale, A. N., "A Stochastic Design Approach for Full-Order Compensation of Structural Systems With Uncertain Parameters," No. 81-1830, AIAA Guid. & Contr. Conf., Albuquerque, New Mexico, August 1981.

14. Hyland, D. C., "Mean-Square Optimal, Full-Order Compensation of Structural Systems With Uncertain Parameters," MIT, Lincoln Laboratory, TR-626.

15. Hyland, D. C., "Optimal Regulator Design Using Minimum Information Modelling of Parameter Uncertainties: Ramifications of the New Design Approach," Proceedings of the Third VPI&SU/AIAA Symposium on Dynamics and Control of Large Space Platforms, Blacksburg, Va., June 1981.

16. Hyland, D. C., "Optimality Conditions for Fixed-Order Dynamic Compensation of Flexible Spacecraft With Uncertain Parameters," No. 82-0312, AIAA Aerospace Sciences Mtg., January 1982.

17. Hyland, D. C., "Mean-Square Optimal, Fixed-Order Compensation-Beyond Spillover Suppression," No. 82-1403, AIAA Astrodynamics Conf., San Diego, California, August 1982.

SESSION II

ANALYSIS METHODOLOGY

Chairman: V. B. Venkayya
Secretary: John Gubser

A COMPUTATIONAL APPROACH TO THE CONTROL OF
LARGE-ORDER STRUCTURES

L. Meirovitch
Department of Engineering Science and Mechanics
Virginia Polytechnic Institute and State University
Blacksburg, Virginia

EQUATIONS OF MOTION FOR THE STRUCTURE

Kinetic Energy: $T(t) = \frac{1}{2} \int_D m(P) \dot{u}^T(P,t) \dot{u}(P,t) dD(P)$

    $u(P,t)$ = displacement vector
    $m(P)$ = mass density
    D = domain of extension of the structure
    P = nominal point

Potential Energy: $V(t) = \frac{1}{2} [u, u]$

    $[\ ,\ ]$ = energy inner product (Ref. 1)

Virtual Work: $\delta W = \int_D f^T(P,t) \delta u(P,t)\ dD(P)$

    $f(P,t)$ = distributed force (actually explicit function of state rather than of
           spatial position and time)
    $\delta u(P,t)$ = virtual displacement

Extended Hamilton's Principle: $\int_{t_1}^{t_2} (\delta L + \delta W) dt = 0,$

                                    $\delta u(P,t) = 0,\ t = t_1,\ t_2;\ P \in D$

    $L = T - V$ = Lagrangian

Partial Differential Equation of Motion for the Structure (Ref. 1):

$$Lu + M\ddot{u} = f\ ,\quad P \in D$$

    L = Differential operator matrix with entries of order $2p$
    M = Mass matrix

Boundary Conditions: $B_i u = 0\ ,\quad P \in S;\quad i = 1, 2, \ldots, p$

    B_i = Differential operator matrices with entries of maximum order $2p-1$
    S = Boundary of D

STRUCTURE DISCRETIZATION BY THE FINITE ELEMENT METHOD

Linear Transformation: $u(P,t) = L(P) q(t)$

    $L(P)$ = matrix of interpolation functions (Ref. 1)
    $q(t)$ = vector of nodal coordinates

Discretized Kinetic and Potential Energy: $T = \frac{1}{2} \dot{q}^T M \dot{q}\ ,\ V = \frac{1}{2} q^T K q$

    $M = \int_D L^T(P) ML(P)\ dD(P)$ = mass matrix, $M = M^T$, $M > 0$
    $K = [L(P), L(P)]$ = stiffness matrix, $K = K^T$, $K \geq 0$

Discretized Virtual Work: $\delta W = Q^T \delta q$

$Q = \int_D L^T(P)\underline{f}(P,t)dD(P)$ = nodal force vector

Discretized Equations of Motion: $M\ddot{\underline{q}} + Kq = \underline{Q}$

Equations have appearance of an n-degree-of-freedom discrete system.

NATURE OF THE DISCRETIZED SYSTEM

A discretized model is a truncated model meant to represent a distributed structure.

Eigenvalue Problem of Order n: $K^{(n)}\underline{q}_r^{(n)} = \lambda_r^{(n)} M^{(n)}\underline{q}_r^{(n)}$, $r=1,2,\ldots,n$

$K^{(n)}$, $M^{(n)}$ = $n \times n$ stiffness and mass matrices

$\lambda_r^{(n)}$ = computed eigenvalues, $\lambda_1^{(n)} \leq \lambda_2^{(n)} \leq \ldots \leq \lambda_n^{(n)}$

$\underline{q}_r^{(n)}$ = n-dimensional eigenvectors

Eigenvalue Problem of Order n + 1: $K^{(n+1)}\underline{q}_r^{(n+1)} = \lambda_r^{(n+1)} M^{(n+1)}\underline{q}_r^{(n+1)}$

$$r = 1,2,\ldots,n+1$$

$$\lambda_1^{(n+1)} \leq \lambda_2^{(n+1)} \leq \ldots \leq \lambda_{n+1}^{(n+1)}$$

Inclusion Principle (Ref. 1): $\lambda_1^{(n+1)} \leq \lambda_1^{(n)} \leq \lambda_2^{(n+1)} \leq \lambda_2^{(n)} \leq \ldots \leq \lambda_n^{(n+1)} \leq \lambda_n^{(n)} \leq \lambda_{n+1}^{(n+1)}$

Convergence Property: $\lim_{n\to\infty} \lambda_r^{(n)} = \lambda_r$, $r=1,2,\ldots,n$

Paradox: By increasing n, more computed eigenvalues tend to be accurate, but new ones are added at the high end of the spectrum, and the latter ones tend to be wildly in error.

Conclusion: No discretized model can yield a complete and accurate representation of a distributed structure.

MODAL EQUATIONS OF MOTION FOR CONTROL

Consider an n-degree-of-freedom discretized model, but drop superscript (n),

λ_r = computed eigenvalues, $\underline{q}_r$ = computed eigenvectors

Computed Eigenfunctions for Distributed Structure: $\underline{\phi}_r(P) = L(P)\underline{q}_r$, $r=1,2,\ldots,n$

Structure is self-adjoint $\longrightarrow$ modes are orthogonal (Ref. 1) and can be normalized

$$\underline{q}_s^T M\underline{q}_r = \delta_{rs}, \quad \underline{q}_s^T K\underline{q}_r = \lambda_r \delta_{rs}, \quad r,s = 1,2,\ldots,n$$

Consequence: $\int_D \underline{\phi}_s^T(P)M\underline{\phi}_r(P)\,dD = \delta_{rs}$, $\int_D \underline{\phi}_s^T(P)L\underline{\phi}_r(P)\,dD = \lambda_r\delta_{rs}$, $r,s = 1,2,\ldots,n$

Expansion Theorem (Ref. 1): $\quad u(P,t) = \sum\limits_{r=1}^{N} \underset{\sim}{\phi}_r(P) u_r(t)$

$u_r(t)$ = modal coordinates
N = number of modes retained in the model, $N \ll n$

Modal Equations: $\quad \ddot{\underset{\sim}{u}}(t) + \Lambda \underset{\sim}{u}(t) = \underset{\sim}{f}(t)$

$\underset{\sim}{u}(t) = [u_1(t) \; u_2(t) \; \ldots \; u_N(t)]^T$ = modal displacement vector

$\underset{\sim}{f}(t) = [f_1(t) \; f_2(t) \; \ldots \; f_N(t)]^T$ = modal control vector

$\Lambda = \text{diag}\,[\lambda_1 \; \lambda_2 \ldots \lambda_N] = \text{diag}\,[\omega_1^2 \; \omega_2^2 \; \ldots \; \omega_N^2]$ = matrix of eigenvalues

ω_r = natural frequencies

Modal Controls: $\quad f_r(t) = \int_D \underset{\sim}{\phi}_r^T(P) \underset{\sim}{f}(P,t)\,dD, \quad r=1,2,\ldots,N$

COUPLED MODAL CONTROLS

Feedback Control Vector: $\quad \underset{\sim}{f} = \underset{\sim}{f}(\underset{\sim}{u}, \dot{\underset{\sim}{u}})$

Distributed Controls in Terms of Discrete Actuators: $\quad \underset{\sim}{f}(p,t) = \sum\limits_{j=1}^{M} \underset{\sim}{F}_j(t)\,\delta(P-P_j)$

$\underset{\sim}{F}_j(t)$ = discrete-point controls, $j=1,2,\ldots,M$

Modal Controls: $\quad f_r(t) = \sum\limits_{j=1}^{M} \int_D \underset{\sim}{\phi}_t^T(P) \underset{\sim}{F}_j(t)\delta(P-P_j)dD = \sum\limits_{j=1}^{M} \underset{\sim}{\phi}_r^T(P_j) \underset{\sim}{F}_j(t), \quad r=1,2,\ldots$

Control Spillover (Ref. 2) Into Unmodeled Modes: $\quad f_r(t) \neq 0, \quad r=N+1, N+2, \ldots$

Modal Feedback Control: $\quad \underset{\sim}{f} = B\,\underset{\sim}{F}$

B = Modal Participation Matrix, $\quad B = \begin{bmatrix} B_1 \\ B_2 \\ \vdots \\ B_N \end{bmatrix}, \quad B_r = [\phi_r^T(P_1) \; \phi_r^T(P_2) \ldots \phi_r^T(P_M)]$

Modal Equations: $\quad \ddot{\underset{\sim}{u}}(t) + \Lambda \underset{\sim}{u}(t) = B\,\underset{\sim}{F}(t)$

N modeled modes $\Big\langle$ $\begin{array}{l} N_C \text{ controlled modes} \\ N_R \text{ residual modes} \end{array}$, $N = N_C + N_R$

Modal Equation in Partitioned Form: $\begin{bmatrix} \ddot{u}_C \\ \hline \ddot{u}_R \end{bmatrix} + \begin{bmatrix} \Lambda_C & 0 \\ \hline 0 & \Lambda_R \end{bmatrix} \begin{bmatrix} u_C \\ \hline u_R \end{bmatrix} = \begin{bmatrix} B_C \\ \hline B_R \end{bmatrix} \underset{\sim}{F}$

Feedback Control Vector: $\quad \underset{\sim}{F} = G_1\, \dot{\underset{\sim}{u}}_C + G_2\, \underset{\sim}{u}_C$

$G_1, \; G_2$ = control gain matrices

102

Closed-Loop Modal Equations:
$$\begin{bmatrix} \ddot{u}_C \\ \hline \ddot{u}_R \end{bmatrix} + \begin{bmatrix} -B_C G_1 & | & 0 \\ \hline -B_R G_1 & | & 0 \end{bmatrix} \begin{bmatrix} \dot{u}_C \\ \hline \dot{u}_R \end{bmatrix}$$

$$+ \begin{bmatrix} \Lambda_C - B_C G_2 & | & 0 \\ \hline -B_R G_2 & | & \Lambda_R \end{bmatrix} \begin{bmatrix} u_C \\ \hline u_R \end{bmatrix} = 0$$

Closed-loop poles of the controlled modes are determined by $-B_C G_1$ and $\Lambda_C - B_C G_2$.

Closed-loop poles of the residual modes are determined by Λ_R.

Conclusion: Closed-loop poles of the residual modes are not affected by feed-back controls; therefore, <u>control spillover into the residual modes cannot destablize these modes</u>.

CONTROL IMPLEMENTATION USING OBSERVERS

State Equations of Motion:
$$\begin{bmatrix} \dot{v}_C \\ \hline \dot{v}_R \end{bmatrix} = \begin{bmatrix} A_C & | & 0 \\ \hline 0 & | & A_R \end{bmatrix} \begin{bmatrix} v_C \\ \hline v_R \end{bmatrix} + \begin{bmatrix} B_C' \\ \hline B_R' \end{bmatrix} F$$

Feedback Control Vector: $F = G_C v_C \qquad G_C = [G_1 \quad G_2]$

$v_C = [\dot{u}_C^T \quad u_C^T]^T$ = modal state vector

$$A_C = \begin{bmatrix} 0 & | & -\Lambda_C \\ \hline I & | & 0 \end{bmatrix}, \quad A_R = \begin{bmatrix} 0 & | & -\Lambda_R \\ \hline I & | & 0 \end{bmatrix}, \quad B_C' = \begin{bmatrix} B_C \\ \hline 0 \end{bmatrix}, \quad B_R' = \begin{bmatrix} B_R \\ \hline 0 \end{bmatrix}$$

Displacement Measurements Vector: $y(t) = Cu(t) = C_C u_C(t) + C_R u_R(t)$

Velocities Measurements Vector: $y(t) = C\dot{u}(t) = C_C \dot{u}_C(t) + C_R \dot{u}_R(t)$

$$C = \begin{bmatrix} \Phi(P_1) \\ \Phi(P_2) \\ \vdots \\ \Phi(P_K) \end{bmatrix}$$

$\Phi(P_i)$ = modal matrix evaluated at $P = P_i$

K = number of sensors

Output Vector: $y(t) = C_C' v_C + C_R' v_R$

The term $C_R' v_R$ gives rise to <u>observation spillover</u> (Ref. 2).

Lunenberger Observer:
$$\begin{bmatrix} \dot{\hat{v}}_C \\ \hline \dot{\hat{v}}_R \end{bmatrix} = \begin{bmatrix} A_C & | & 0 \\ \hline 0 & | & A_R \end{bmatrix} \begin{bmatrix} \hat{v}_C \\ \hline \hat{v}_R \end{bmatrix} + \begin{bmatrix} B_C' \\ \hline B_R' \end{bmatrix} F + \begin{bmatrix} K_C \\ \hline K_R \end{bmatrix} (y - \hat{y}),$$

$$\hat{y} = C_C' \hat{v}_C + C_R' \hat{v}_R$$

$\hat{v}_C$, $\hat{v}_R$ = estimates of v_C, v_R

K_C, K_R = observer gain matrices, chosen so that $\hat{v}_C$ approaches v_C exponentially

$\hat{y}$ = observer output

Feedback Control Vector: $F = G_C \hat{v}_C$

Error Vectors: $e_C = \hat{v}_C - v_C$, $e_R = \hat{v}_R - v_R$

State and Error Equations Combined:

$$
\begin{bmatrix} \dot{v}_C \\ \hline \dot{v}_R \\ \hline \dot{e}_C \\ \hline \dot{e}_R \end{bmatrix}
=
\begin{bmatrix}
A_C + B_C'G_C & 0 & B_C'G_C & 0 \\ \hline
B_R'B_C & A_R & B_R'G_C & 0 \\ \hline
0 & 0 & A_C - K_C C_C' & -K_C C_R' \\ \hline
0 & 0 & -K_R C' & A_R - K_R C_R'
\end{bmatrix}
\begin{bmatrix} v_C \\ \hline v_R \\ \hline e_C \\ \hline e_R \end{bmatrix}
$$

Conclusion: Observation spillover exists but cannot destabilize the system if the observator gains are chosen properly.

CONTROLLABILITY AND OBSERVABILITY

Controllability Matrix: $C = [B_C' \mid A_C B_C' \mid A_C^2 B_C' \mid --- \mid A_C^{2N_C-1} B_C']$

For system to be completely controllable, C must be of rank $2N_C$ (Ref. 3).

Controllability Matrix for Discretized Model:

$$
C =
\begin{bmatrix}
B_C & 0 & \Lambda_C B_C & 0 & \Lambda_C^2 B_C & & 0 \\
0 & B_C & 0 & -\Lambda_C B_C & 0 & --- & (-1)^{N_C-1} \Lambda_C^{N_C-1} B_C
\end{bmatrix}
$$

For system to be completely controllable, all rows of B_C must be nonzero.

Observability Matrix: $0 = [C'_C{}^T \mid A_C^T C'_C{}^T \mid (A_C^T)^2 C'_C{}^T \mid (A_C^T)^{2N_C-1} C'_C{}^T]$

For system to be completely observable, 0 must have rank $2N_C$ (Ref. 3).

Observability Matrix for Discretized Model:

$$
0 =
\begin{bmatrix}
C_C^T & 0 & -\Lambda_C C_C^T & & \Lambda_C^2 C_C^T & & 0 \\
0 & -\Lambda_C C_C^T & 0 & \Lambda_C^2 C^T_C & 0 & --- & \Lambda_C^{N_C-1} C_C^T
\end{bmatrix}
$$

For system to be completely observable, all columns of C_C must be nonzero.

MODAL FILTERS (IN SPACE)

Second Part of Expansion Theorem: $u_r(t) = \int_D \phi_r^T(P) M u(P,t) \, dD$

$$r = 1, 2, \ldots$$

$$\dot{u}_r(t) = \int_D \phi_r^T(P) M \dot{u}(P,t) \, dD$$

$u(P,t)$, $\dot{u}(P,t)$ = distributed measurements

Integrals filter out contributions from modes $\neq r$, hence, the term <u>modal filters</u> (Ref. 4).

Discrete Measurements: Use K sensors to produce discrete measurements. Then, use the finite element method to generate estimates $\hat{u}(P,t)$, $\hat{\dot{u}}(P,t)$ of $u(P,t)$, $\dot{u}(P,t)$.

Modal Filters for Discrete Measurements: $\hat{u}_r(t) = \int_D \phi_r^T(P) M \hat{u}(P,t) \, dD$

$$\hat{\dot{u}}_r(t) = \int_D \phi_r^T(P) M \hat{\dot{u}}(P,t) \, dD \qquad r = 1, 2, \ldots, N_C$$

Finite Element Approximation: $\hat{u}_i(P,t) = L^T(P) y_i(t)$, $\hat{\dot{u}}_i(P,t) = L^T(P) \dot{y}_i(t)$, $P \in D_i$

$$i = 1, 2, \ldots, K-1$$

$y_i(t)$, $\dot{y}_i(t)$ = nodal measurements vectors

Modal Filters: $\hat{u}_r(t) = \sum_{i=1}^{K-1} \int_{D_i} \phi_r^T(P) M \hat{u}_i(P,t) \, dD = \sum_{i=1}^{K-1} I_{ri} y_i(t)$, $\hat{\dot{u}}_r(t) = \sum_{i=1}^{K-1} I_{ri} \dot{y}_i(t)$

$$I_{ri} = \int_{D_i} \phi_r^T(P) M L^T(P) \, dD \text{ (computed off-line)}$$

INDEPENDENT MODAL SPACE CONTROL (IMSC) METHOD

(i) <u>Control of Distributed Structures by Distributed Actuators</u>

Infinite Set of Modal Equations: $u_r + \omega_r^2 u_r = f_r$, $r = 1, 2, \ldots$

Special Case of Modal Feedback Controls: $f_r = f_r(u_r, \dot{u}_r)$, $r = 1, 2, \ldots$

Note: The rth modal control depends only on the rth modal coordinate and velocity.

Consequence: System becomes <u>completely decoupled</u>; therefore, the control for each mode can be designed independently of any other mode.

Synthesis of Actual Distributed Controls from Modal Controls (Ref. 4):

$$f(P,t) = \sum_{r=1}^{\infty} M(P) \phi_r(P) f_r(t)$$

Note: If only N_C modes are to be controlled, then set $f_r = 0$ $(r > N_C)$, which implies <u>no control spillover into the uncontrolled modes</u>.

105

Linear Controls: $f_r = G_{r1}\dot{u}_r + G_{r2}u_r$, $r = 1, 2, \ldots$

$\quad$ G_{r1}, G_{r2} = modal gains

Nonlinear, On-Off Controls (Ref. 5): $f_r = \{-k_r, \; \dot{u}_r > d_r; \; 0, \; |\dot{u}_r| < d_r; \; k_r, \; \dot{u}_r < -d_r\}$

$\quad$ k_r = control gain parameter $\qquad\qquad\qquad r = 1, 2, \ldots$

$\quad$ $2d_r$ = magnitude of dead-band region

(ii) <u>Control of Distributed Structure by Discrete Actuators</u>

Equations for Control of N_C Modes: $\ddot{\underset{\sim}{u}}_C + \Lambda_C \underset{\sim}{u}_C = \underset{\sim}{f}_C = B_C \underset{\sim}{F}$

Synthesis of Actual Controls from Modal Controls: $\underset{\sim}{F} = B_C^{\dagger} \underset{\sim}{f}_C$, $\quad M < N_C$

$$\underset{\sim}{F} = B_C^{-1} \underset{\sim}{f}_C \; , \quad M = N_C$$

In the latter case, the number of actuators must be the same as the number of controlled modes.

Equations for Uncontrolled Modes: $\ddot{\underset{\sim}{u}}_U + \Lambda_U \underset{\sim}{u}_U = B_U \underset{\sim}{F} = B_U B_C^{-1} \underset{\sim}{f}_C$

<u>Control spillover</u> into the uncontrolled modes does exist.

No instability is possible.

(iii) <u>Control of Discretized Structures by Distributed Actuators</u>

Same as (i), except, that $\underset{\sim}{f}(P,t) = \sum_{r=1}^{N_C} M(P) \underset{\sim}{\phi}_r(P) f_r(t)$

<u>No control spillover</u> into the uncontrolled modes exists.

(iv) <u>Control of Discretized Structures by Discrete Actuators</u>

Same as (ii).

<center>COMPUTATIONAL ALGORITHMS FOR CONTROL</center>

(i) <u>Pole Allocation</u>

$\quad$ Select Closed-Loop Poles ρ_k $(k = 1, 2, \ldots, 2N_C)$

$\quad$ State Equation for Single Input: $\dot{\underset{\sim}{v}}_C = A_C \underset{\sim}{v}_C + \underset{\sim}{b}_C' F(t)$

$\quad$ Single Input Feedback: $F(t) = \underset{\sim}{g}_C^T \underset{\sim}{v}_C$

$\quad\quad$ $\underset{\sim}{g}_C$ = gain vector

$$g_C = \sum_{j=1}^{2N_C} \frac{\prod\limits_{k=1}^{2N_C} (\rho_k - \lambda_j) \underset{\sim}{v}_j}{\underset{\sim}{v}_j^T \underset{\sim}{b}_C' \prod\limits_{\substack{k=1 \\ k \neq 1}}^{2N_C} (\lambda_k - \lambda_j)}$$

$\underset{\sim}{v}_j$ $(j=1,2,\ldots,2N_C)$ = left eigenvectors of A_C

General Multi-Input Control Is Not Feasible.

Dyadic Control (Inputs Are Proportional to One Another): $\underset{\sim}{F}(t) = G_C \underset{\sim}{v}_C(t)$

G_C = gain matrix

$$G_C = \underset{\sim}{h} \sum_{j=1}^{2N_C} \frac{\prod\limits_{k=1}^{2N_C} (\rho_k - \lambda_j) \underset{\sim}{v}_j^T}{\underset{\sim}{v}_j^T B_C' \underset{\sim}{h} \prod\limits_{\substack{k=1 \\ k \neq 1}}^{2N_C} (\lambda_k - \lambda_j)}$$

Closed-Loop Poles for IMSC: $\quad \rho_r = \alpha_r \pm i\beta_r, \quad r=1,2,\ldots,N_C$

Modal Controls: $\quad f_r(t) = (\omega_r^2 - \alpha_r^2 - \beta_r^2)u_r(t) + 2\alpha_r \dot{u}_r, \quad r=1,2,\ldots,N_C$

(ii) Linear Optimal Control

Performance Index for Coupled Controls: $\quad J = \int_0^{t_f} (\underset{\sim}{v}_C^T Q \underset{\sim}{v}_C + \underset{\sim}{F}^T R \underset{\sim}{F})\, dt$

$\quad$ Q, R = Weighting matrices

Optimal Control Vector: $\quad \underset{\sim}{F}(t) = -R^{-1} B'^T K(t) \underset{\sim}{v}_C(t)$

$\quad K(t) = 2N_C \times 2N_C$ matrix satisfying the Riccati equation

$$\dot{K} = -KA_C - A_C^T K - Q - KB'R^{-1}B'^T K$$

Steady-State Case: $\dot{K} = 0$

Nonlinear algebraic matrix Riccati equation can be transformed to eigensolution of a real general matrix.

Algorithm requires 600 N_C^3 multiplications for convergence.

Transient Case: $\dot{K} \neq 0$

Nonlinear matrix Riccati equation can be transformed into a $4N_C \times 4N_C$ linear matrix equation, which must be integrated on-line. Process requires ample computer capacity, which may make real-time implementation impossible.

107

Performance Index for IMSC: $J = \sum_{r=1}^{N_C} J_r$

J_r = independent modal performance indices

$$J_r = \int_0^{t_f} (v_r^T Q_r \, v_r + f_r^2 \, R_r/\omega_r^2)dt, \quad r=1,2,\ldots,N_C$$

Q_r = 2 × 2 diagonal matrix, R_r - scalar

Solve N_C Matrix Riccati Equations of Order 2.

Steady-State Case Requires $N_C^3/2$ Operations, Fewer by a Factor of 1200 Than Coupled Controls.

Transient Case Implementation in Real Time Is Possible.

COMPARISON OF COUPLED CONTROLS AND IMSC

Advantages of Coupled Controls: Fewer actuators, provided controllability is ensured.

Advantages of IMSC:

   a) Larger choice of control techniques, including nonlinear control
   b) Lower computational effort (Table 1)
   c) Lower computer storage requirement
   d) Lower control energy (Ref. 6)
   e) Locations of actuators not important (Ref. 7)
   f) Provable robustness (Ref. 8)

Some of these advantages are illustrated in Figures 1-5.

	Number of Actuators	Time (s)
Coupled Controls	4	176.5
	6	127.1
	8	104.5
	10	100.0
	12	87.7
IMSC	12	2.3

Table 1.- Computational effort required to solve the Riccati equation.
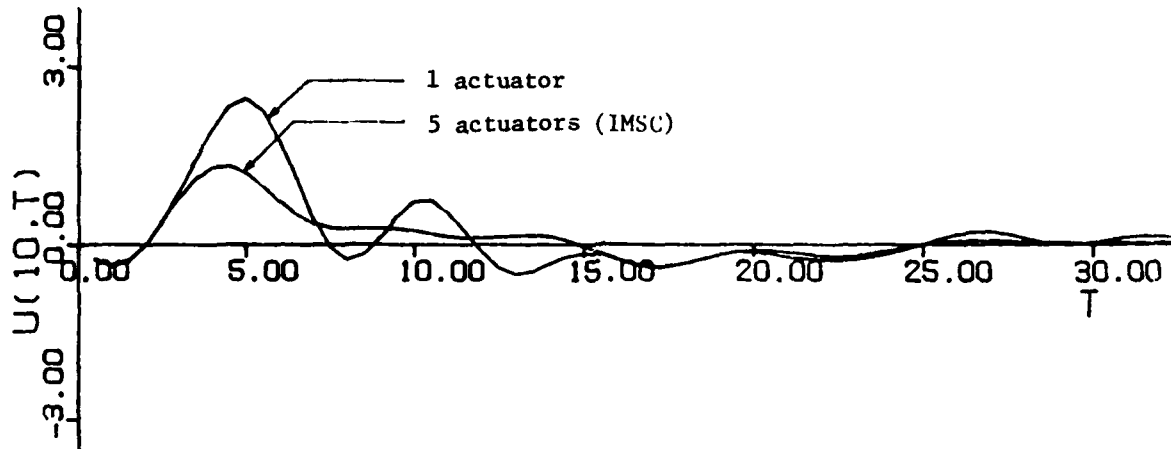
Figure 1.- Displacement at the end of the bar - pole allocation.
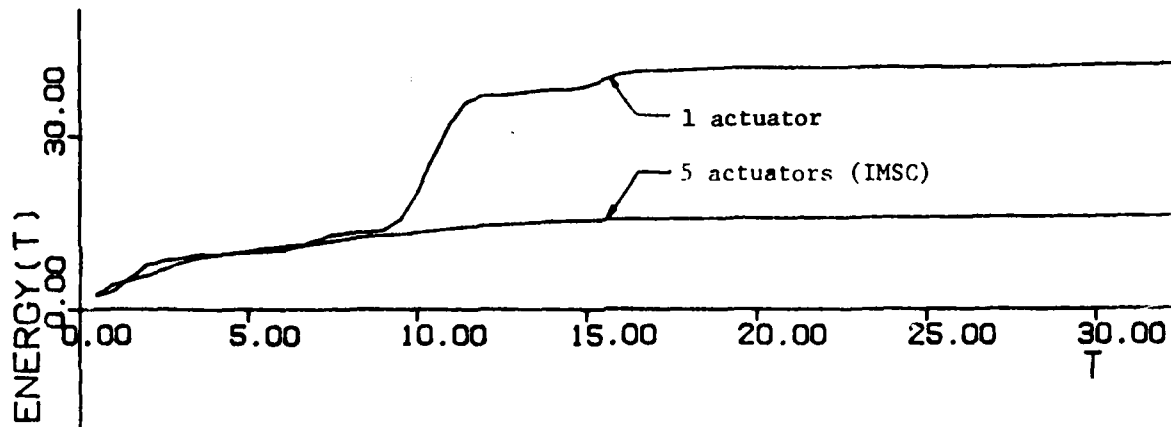

Figure 2.- Energy required for the controlled modes - pole allocation.
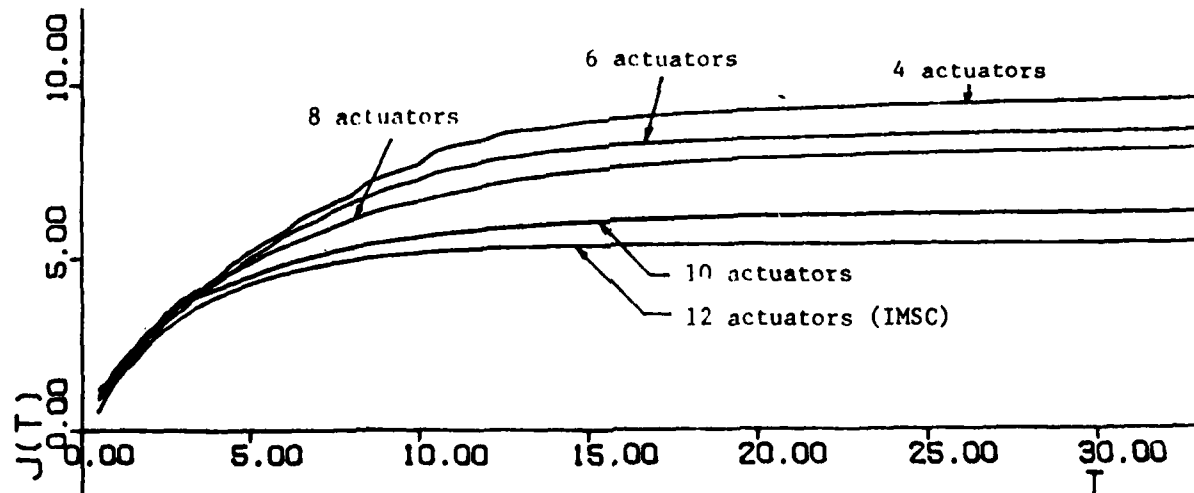
Figure 3.- Performance index - coupled and independent controls.

109
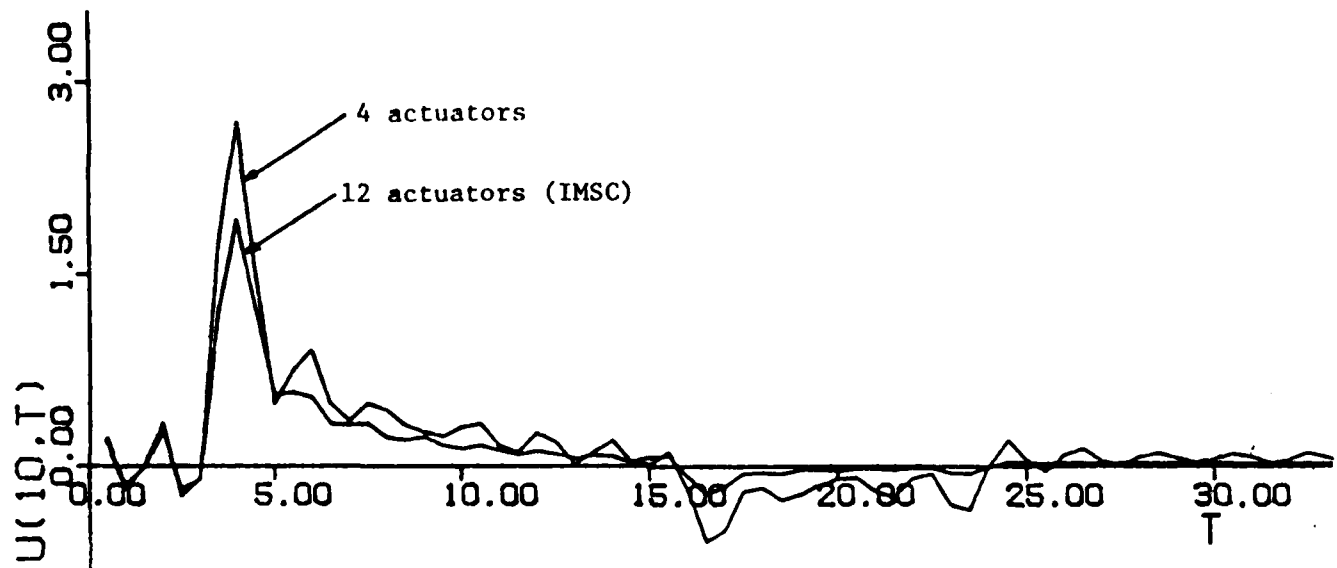
Figure 4.- Displacement at the end of the bar - optimal control.
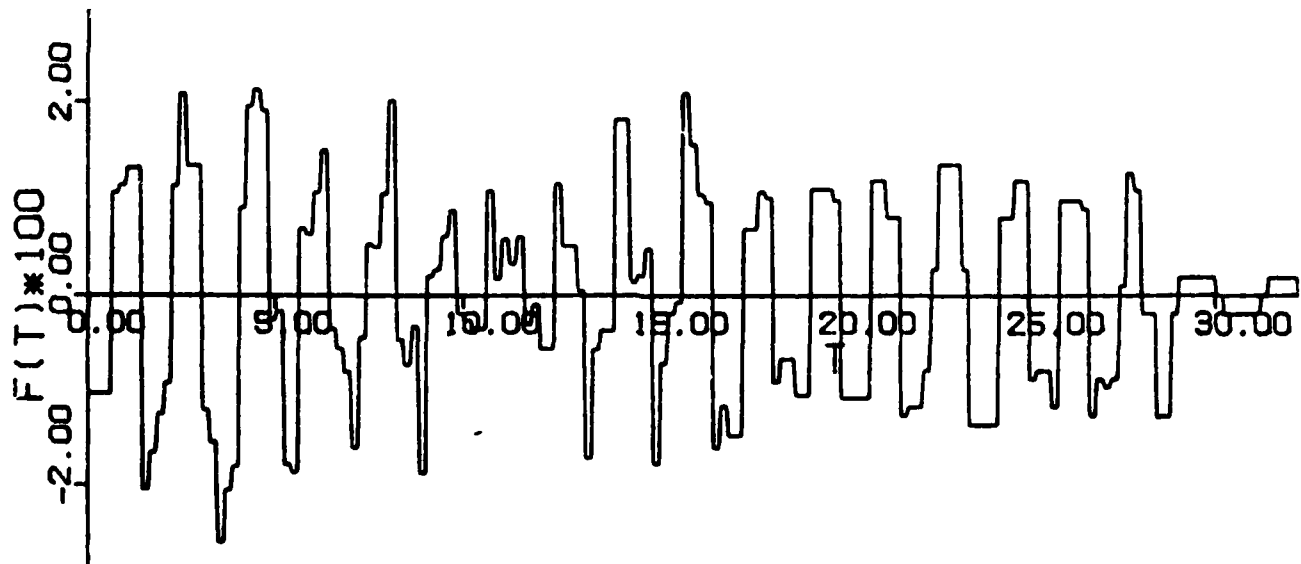
Figure 5.- Force in the 12th actuator - nonlinear control.

110

REFERENCES

1. Meirovitch, L.: Computational Methods in Structural Dynamics. Sijthoff-
        Noordhoff Co. (The Netherlands), 1980.

2. Balas, M. J.: Active Control of Flexible Systems. Journal of Optimiza-
        tion Theory and Applications, vol. 25, no. 3, 1978, pp. 415-436.

3. Anderson, B.D.O.; and Moore, J.B.: Linear Optimal Control. Prentice-Hall,
        Inc., 1971.

4. Meirovitch, L.; and Baruh, H.: Control of Self-Adjoint Distributed-Parameter
        Systems. Journal of Guidance, Control, and Dynamics, vol. 5, no. 1,
        1982, pp. 60-66.

5. Meirovitch, L.; and Öz, H.: Computational Aspects of the Control of
        Large Flexible Spacecraft. Proceedings of the 18th IEEE Conference
        on Decision and Control, December 1979, pp. 220-229.

6. Meirovitch, L.; Baruh, H.; and Öz, H.: A Comparison of Control Techniques
        for Large Flexible Systems. AAS Paper No. 81-195, 1981.

7. Baruh, H.; and Meirovitch, L.: On the Placement of Actuators in the Control
        of Distributed-Parameter Systems. Proceedings of the 22nd AIAA Dynamics
        Specialists Conference, April 1981, pp. 611-620.

8. Meirovitch, L.; and Baruh, H.: Control Sensitivity of Distributed Systems
        to Changes in Parameters. AIAA Paper No. 82-0313, 1982.

ANALYSIS AND TESTING
OF LARGE SPACE STRUCTURES

C. V. Stahle
Space Systems Division, General Electric Company
Valley Forge, Pennsylvania

GROUND TEST CONSIDERATIONS

Figure 1 outlines key considerations for performing ground tests of LSS. The large
size combined with the loading due to gravity will make testing of the complete struc-
ture difficult. Gravitational stiffening, suspension effects, virtual air mass, pre-
loads, and air damping will alter the dynamic characteristics. Low resonant fre-
quencies and high modal densities within the frequency range of interest combine with
small motions and accelerations to make testing difficult. Mechanism complexities
and nonlinearities associated with space-erected/assembled structures cause struc-
tural complexity regardless of other considerations. From these considerations it ap-
pears that ground testing of a complete LSS will be difficult if not impossible.

- LARGE SIZE

- GRAVITY - STIFFENING, LOADING

- AIR MASS, DAMPING

- LOW RESONANT FREQUENCIES

- HIGH MODAL DENSITY

- SMALL MOTIONS/ACCELERATIONS

- SUSPENSION EFFECTS

- MECHANISM COMPLEXITIES

- NONLINEARITIES

GROUND TESTING WILL BE VERY
DIFFICULT IF NOT IMPOSSIBLE

Figure 1

GROUND TEST APPROACHES

Figure 2 outlines some approaches to ground testing. Scale model testing can overcome the size and gravity effects but does not assure detailed representation. Element tests provide a means of supplementing model tests and will be particularly effective for items such as joints. Substructure testing appears to be the most promising, enabling dynamic behavior of actual structure to be measured while overcoming some of the concerns (e.g., size, gravity, modal density). Intentional linearization of the structure will be helpful in minimizing test problems associated with small orbital motions. A separate analysis of the test configuration will probably be required in that some ground test effects will undoubtedly be present. Most likely, tests will be directed toward verification of analysis using either models or partial structures.

- PERFORM SCALE MODEL TESTS

- PERFORM ELEMENT TESTS

- TEST SUBSTRUCTURES

- LINEARIZE STRUCTURES

- PERFORM SEPARATE ANALYSIS OF GROUND TEST ARRANGEMENTS

> TESTS WILL BE DIRECTED TOWARD
> ANALYTICAL VERIFICATION USING
> MODEL OR PARTIAL STRUCTURES

Figure 2

ROLL-UP SOLAR ARRAY MODAL TEST

The modal test of a roll-up solar array performed at GE, Figure 3, indicates test approaches which have been used. The test was performed in the large vacuum chamber (32 feet diameter by 54 feet high). The array was hung downward to eliminate suspensions and preclude excessive gravity loading. Sinusoidal base motion was used to excite the array. Special low-frequency test equipment was used including an oscillator/analyzer that would provide a "hyperbolic" sweep (log rate increasing with frequency to provide constant resonant sweep distortion). Air caused a 60-percent reduction in the fundamental frequency and an order of magnitude change in damping. Gravity, included in the analysis, shifted the fundamental resonant frequency by a factor of 2. Low-frequency sinusoidal testing was found to be tedious and very time consuming.

SHAKER

ELECTRO-
OPTICAL
TRACKERS

WALKWAY

BLANKET
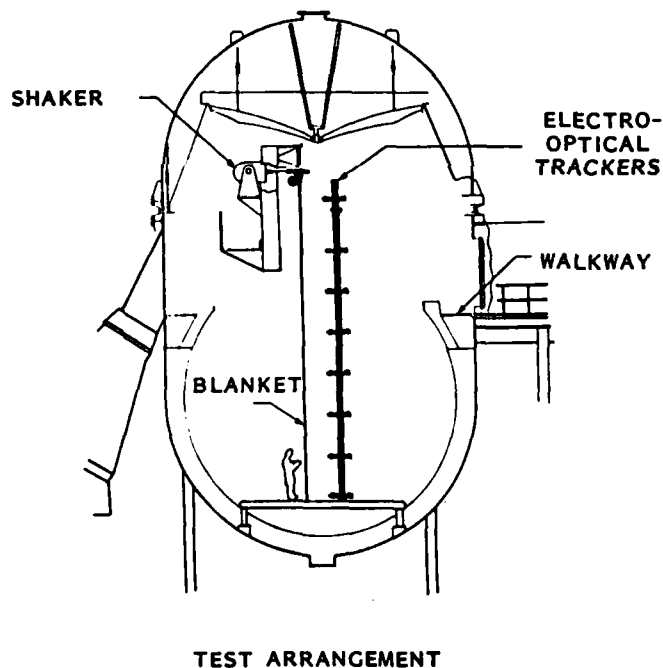
- DC COUPLED HIGH-DISPLACEMENT VACUUM RATE VIBRATION EXCITER

- LOW-FREQUENCY SWEEP OSCILLATOR

    .008 Hz

    LINEAR, LOGARITHMIC OR HYPERBOLIC SWEEP

- NONCONTACTING VACUUM RATED SENSORS

- CO/QUAD RESPONSE MEASUREMENT

- BASE MOTION EXCITATION

- NO SUSPENSION EFFECTS

- ANALYSIS INCLUDED GRAVITY

- AERODYNAMIC EFFECTS SHIFTED THE FUNDAMEN RESONANCE 60 PERCENT

- GRAVITY SHIFTED THE FUNDAMENTAL RESONAN BY A FACTOR OF 2

TEST ARRANGEMENT

Figure 3

116

DESIGN DEVELOPMENT AND VERIFICATION

The development and verification process for LSS will differ from that currently being used for spacecraft as indicated in Figure 4. Present practices rely primarily on ground tests to verify the design and verify workmanship for the flight unit using a prototype (qual) structure. Testing of the complete LSS will not be practical. Ground tests will be used primarily to verify analysis, and the use of a prototype structure will be eliminated to reduce cost. A key feature will be that the ground test verification role will be replaced by analysis. Consequently, major emphasis must be placed on the development of accurate analytical methods.
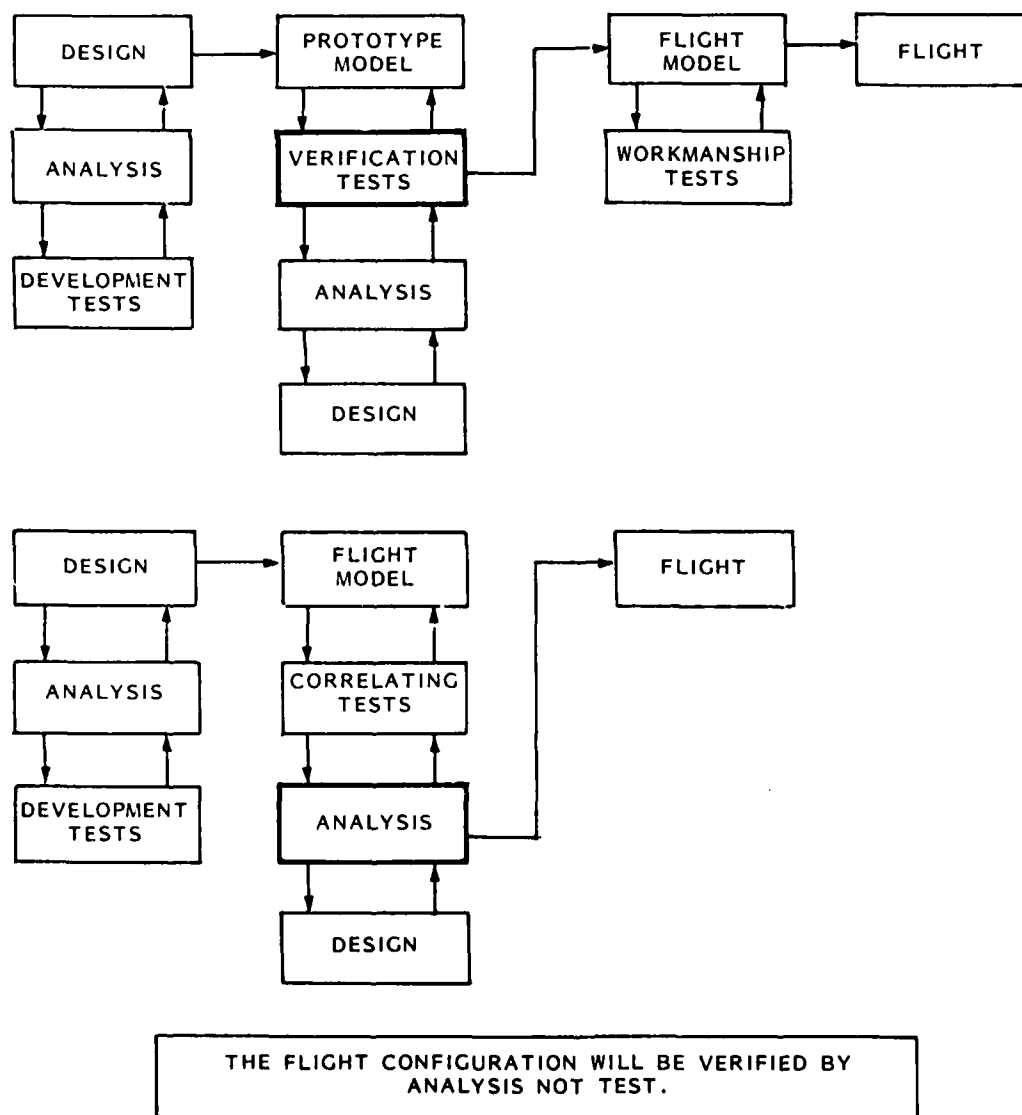

Figure 4

ANALYSIS CONSIDERATIONS

The analytical considerations can be grouped in the areas of structural interactions and complexity as indicated in Figure 5. The structural interactions can involve motion-dependent forces caused by orbital rates, the control system, and solar radiation. All of these interactions have been experienced by spacecraft. Spacecraft with highly flexible gravity gradient rods exhibited destructive orbital interaction, and the performance of other spacecraft was degraded by thermal "flutter." Structural analysis complexities include FEM modeling of distributed mass systems requiring large DOF or condensation, modeling adequacy for mechanism joints, inaccuracies arising from normal mode analysis of structures having nonproportional damping, and analysis of nonlinear structures such as those using tensioning members. Comprehensive LSS analysis will require complex models and use modified equations of motion that include interactions.

- **STRUCTURAL INTERACTIONS**

    - ORBITAL

    - CONTROLS

    - THERMAL

- **STRUCTURAL COMPLEXITY**

    - DISTRIBUTED MASS

    - MECHANISM MODELING

    - DAMPING

    - NONLINEARITIES

ANALYSIS WILL REQUIRE COMPLEX MODELS WITH MODIFIED EQUATIONS

Figure 5

ANALYTICAL APPROACHES

Analytical approaches which could be used are outlined in Figure 6. To evaluate interactions, a combination of computer codes that treat each structural interaction in detail and a comprehensive code that treats all interactions simultaneously appears to provide a tractable approach. Specified codes would be used to support the structural design and would be more detailed, more readily implemented, and less expensive to run. The comprehensive analysis would build on the specialized design support analyses and be used to verify the design. Attractive approaches to modeling of the complex LSS configurations include substructuring, modal synthesis, and experimentally based models. Modal models are attractive in that they provide frequency truncation. An integrated modeling approach that considers experimental verification should be used to maximize confidence in the analytical predictions.

- **DEVELOP STRUCTURAL INTERACTION CODES**

  - **ORBITAL**

  - **THERMAL**

  - **CONTROL**

  - **COMBINED**

- **DEVELOP COMPLEX MODELS OF STRUCTURE**

  - **SUBSTRUCTURE ANALYSIS**

  - **MODAL SYNTHESIS**

  - **EXPERIMENTALLY BASED MODELS**

> SPECIALIZED AND COMPREHENSIVE
> ANALYSES USING MODAL MODELS
> COMBINE TO PROVIDE A TRACTABLE
> APPROACH

Figure 6

119

TANDEM SPACECRAFT ANALYSIS AND TEST APPROACH

The analysis and test approach being used for a tandem-launched spacecraft is shown in
Figure 7 and illustrates a substructuring approach. The spacecraft are launched two at
a time with the one inverted relative to the other. The analytical model is assembled
from six substructures: two identical main bodies, four identical solar array stacks.
The modal test will provide solar array modes and main body modes that can be used to
synthesize the tandem spacecraft pair. One solar array stack was tested and two main
body tests will be performed. Residual mass and flexibility from the FEM will be used
with the test modes to assemble the spacecraft pair. Tests of a single solar array
and main body simplify the modal tests and reduce the amount of test hardware required.
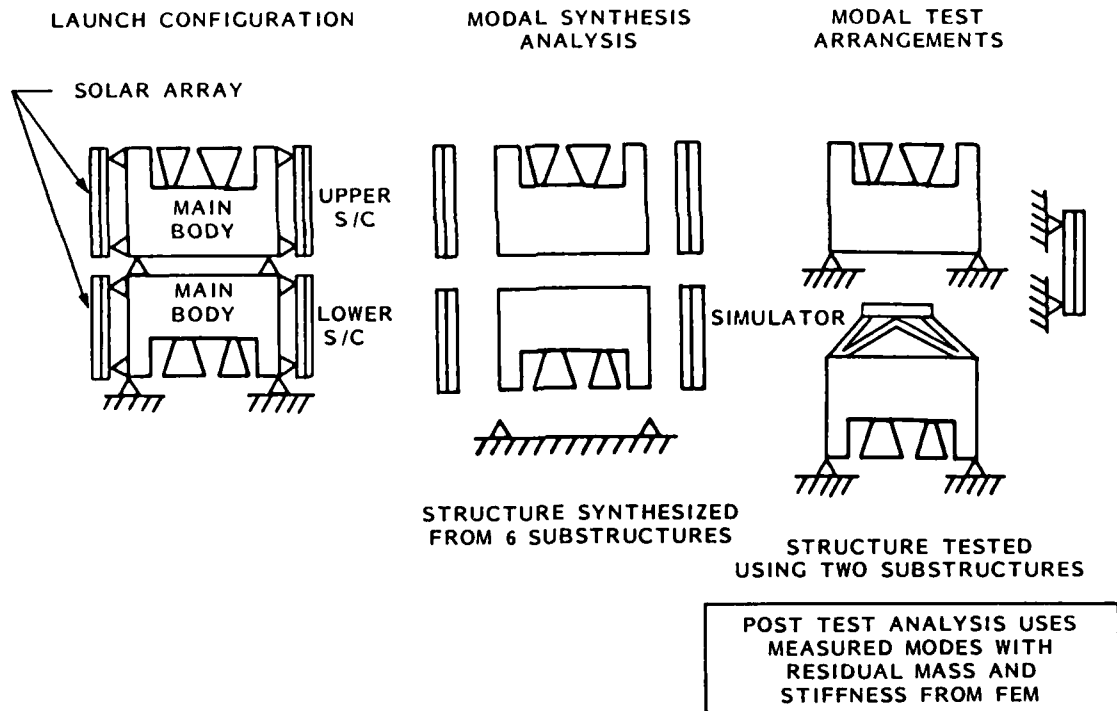
Figure 7

RESEARCH AREAS

Some research areas are outlined in Figure 8. The first area is the development of
analytical codes that will enable accurate prediction of orbital dynamics behavior in-
cluding structural interactions with orbital, thermal, and control excitations. As in-
dicated previously, specialized codes and a comprehensive code are suggested to sup-
port spacecraft design and verify orbital performance. Ground and orbital test sub-
stantiation of the codes is an essential part of code development. Much of this
activity is currently planned or is in progress.

Because of the increased reliance on analysis, it is essential that testing and methods
of using experimental data to enhance analysis accuracy be developed. Also, because
complete structures will probably not be ground tested, the development of methods for
using data generated with partial structures is essential. Specific items needing
research are (1) methods of using modal test data to improve FEM models, (2) methods
of correcting test data to eliminate ground test effects, (3) limits for ground tests
which assure adequate data for correlation with analysis, (4) methods of performing
modal tests (ground or orbital) when modal density is high, and (5) methods of analysis
and testing using substructures. Damping should be examined as a means of reducing
structural dynamic sensitivity.

- ● ANALYTICAL CODE DEVELOPMENT

    - COMPREHENSIVE (STRUCTURE, ORBITAL, CONTROL, THERMAL).

    - SPECIALIZED (STRUCTURE-ORBITAL, STRUCTURE-CONTROL, ETC.)

    - TEST VERIFIED (GROUND, ORBITAL)

- ● ANALYSIS/TEST CORRELATION METHODS

- ● SUBSTRUCTURE ANALYSIS/TEST METHODS

- ● TEST METHODS

- ● DAMPING

Figure 8

THERMAL ANALYSIS CONSIDERATIONS FOR
LARGE SPACE STRUCTURES

Howard M. Adelman and Charles P. Shore
NASA Langley Research Center
Hampton, Virginia

# THERMAL-STRUCTURAL ANALYSIS CONSIDERATIONS FOR VARIOUS MISSIONS

Some of the aerospace vehicles which have been the subject of NASA research are shown in figure 1. Each vehicle is associated with a different set of thermal loading circumstances. These circumstances determine the need for thermal-structural analysis tools. The supersonic transport concept presented minimal analytical difficulties, and it was found that existing analysis tools were adequate. The hypersonic transport design included an actively cooled structure to dissipate high heat loads of long duration. This configuration required analyses to account for strong coupling among thermal, structural, and fluid behavior. Studies of this vehicle led to the development of an integrated thermal-structural analysis approach and integrated finite elements in which the temperatures and thermal input to the structural analysis are computed together in a consistent manner (ref. 1). Thermal-structural analysis of the Space Shuttle orbiter during entry was probably the most severe challenge to thermal-structural analysis techniques to date. Shuttle analysis requirements led to research to implement faster transient techniques, improved modeling methods, and use of advanced computer hardware (ref. 2). For large space structures, the impact on thermal structural analysis methods appears to be a need to efficiently handle radiation heat transfer effects including view factors, solar flux, and shadowing. Additionally, prediction and control of the thermal deformations of sensitive components such as antennas will influence both analysis and optimization methods.


SUPERSONIC TRANSPORT

ANALYSIS TOOLS ADEQUATE

HYPERSONIC TRANSPORT

COOLED STRUCTURE · THERMAL/FLUID/STRUCTURE
HIGHLY COUPLED LED TO INTEGRATED
FINITE ELEMENT ANALYSES

SHUTTLE

ANALYSIS STRAINED METHODS
INTERPOLATION USED LED TO RESEARCH IN FASTER
ALGORITHMS, USE OF ADVANCED COMPUTERS, ETC.

SPACE STRUCTURES
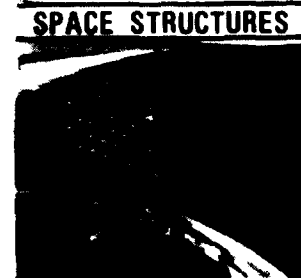
RADIATION DOMINATED SHAPE CONTROL NEEDED

Figure 1

124

BASIC PROBLEM IN THERMAL-STRUCTURAL ANALYSIS

Much of the recent Langley research in thermal-structural analysis methods was
motivated by problems encountered in the design of the Space Shuttle orbiter (fig.
2) for which it was necessary to have knowledge of the histories of temperature and
thermal stress due to the time-dependent reentry aerodynamic heating. The straight-
forward approach would be to use a finite element and/or lumped-parameter model of
large sections or complete components of the vehicle structure. However, due to the
shear size of the required model and the high cost and long computer run times, it
was necessary to model small portions of the structure, indicated in black, and
interpolate results to obtain temperatures in the unmodeled (white) portions of the
orbiter. About 90 percent of the temperatures used in stress calculations were
obtained by interpolation. There was some uncertainty and uneasiness associated
with the use of interpolation. Examination of analysis requirements indicated that
certain complicating factors listed on the figure were primarily responsible for the
excessive resources required for the analysis. Research described in reference 2
was motivated by the need to reduce the resources associated with the cited factors.


Figure 2

125
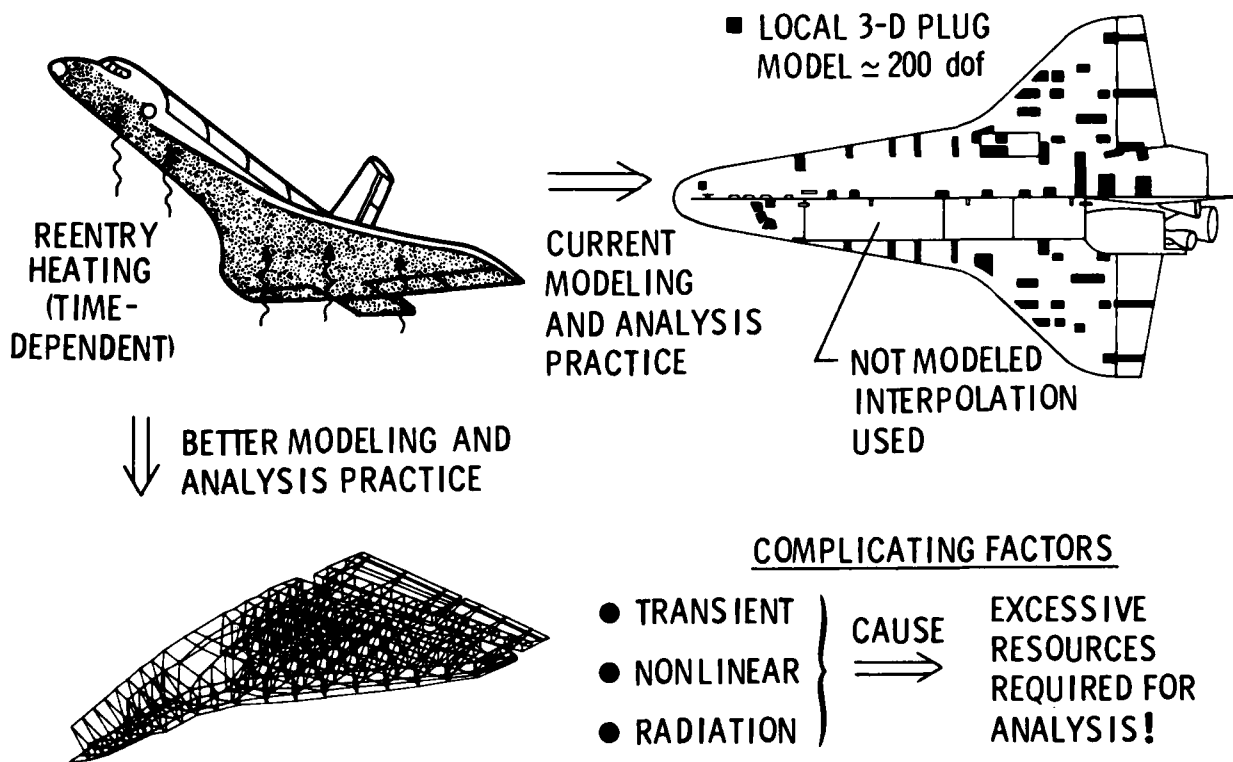
ASPECTS OF THERMAL ANALYSIS OF LARGE SPACE STRUCTURES

As a guide to subsequent discussions of research opportunities in thermal-structural analysis of large space structures, figure 3 depicts various aspects of the analysis. Key areas of analytical deficiencies include efficient view factor and flux calculations and proper accounting for interactions. Two important interactions cited are the need to simultaneously monitor and control the temperature distribution and shape of flexible orbiting structures such as antennas and the need to account for the coupling between thermal deformations and radiation view factors in flexible structures.
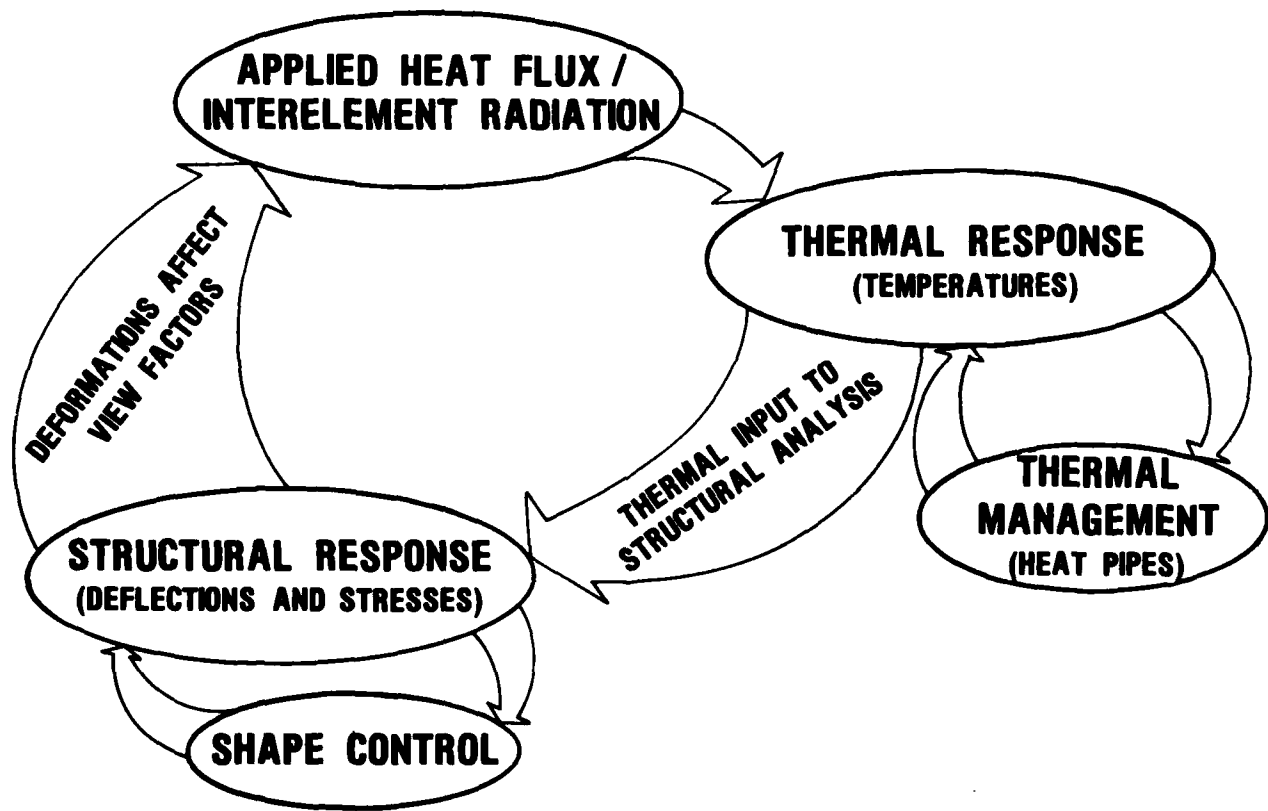

Figure 3

MOTIVATING QUESTIONS AND ISSUES

Previous experience in thermal-structural analysis activities for aircraft and space transportation vehicle structures suggests that in thermal-structural analysis of large space structures (including space stations), a number of critical questions and issues tend to guide research. As indicated in figure 4, computer time and cost are important factors. Consequently, improved solution methods (algorithms) and use of simplified analysis and modeling techniques, such as isothermal finite elements, are of interest. The roles of advanced computer hardware, such as interactive minicomputers and super mainframes, need to be assessed by comparative analyses. Two issues are cited: (1) the need exists to demonstrate new promising analysis tools on real problems of sufficient size and complexity to ensure that good performance is not restricted to small academic problems; and (2) a certain dichotomy exists, namely, much of the research is carried out in the integrated thermal-structural finite element context while much practical thermal analysis uses lumped-parameter methods. Significantly more dialogue between the two communities is needed to ensure that needed and usable research is being carried out.

QUESTIONS

HOW CAN WE OVERCOME EXCESSIVE REQUIREMENTS OF COMPUTER TIME AND COST FOR THERMAL ANALYSIS OF LSS?

HOW DETAILED MUST ANALYSES AND MODELING BE FOR ACCEPTABLE RESULTS?

WHAT IS THE ROLE OF ADVANCED COMPUTER HARDWARE?

ISSUES

NEED TO DEMONSTRATE TECHNIQUES ON REAL PROBLEMS IN ORDER TO ASSURE CREDIBILITY.

NEED FINITE ELEMENT - LUMPED-PARAMETER DIALOGUE

Figure 4

127

MOTIVATION FOR USING FINITE ELEMENTS

Recent thermal-structural research activities at Langley have been based on finite element analyses (fig. 5). The primary consideration for using finite element methods has been the need for integrated thermal-structural analysis and optimization of heated structures. Use of finite elements permits a high degree of compatibility between thermal and structural models and avoids the cumbersome data transfer often required between lumped-parameter grids for temperatures and finite element grids for thermal stress analyses. Further, the graphics available in finite element codes permit rapid model checking and verification. The SPAR finite element computer program is used extensively at Langley for both thermal and structural analyses. It is a production level program with a modular configuration which gives a high degree of flexibility in terms of processor execution sequence. The modularity and the flexibility also enhance the program for interactive computing. Because of these features, SPAR is utilized as a test bed for implementation of new methods at Langley.

● THERMAL-STRUCTURAL INTEGRATED ANALYSES

● COMPATIBILITY

● EASE OF DATA TRANSFER

● MODEL VERIFICATION AND CHECKING

SPAR PROGRAM USED AT LANGLEY
- INTERACTIVE MODE
- FLEXIBLE AND MODULAR
- TEST-BED FOR NEW METHODS
- PRODUCTION LEVEL PROGRAM

Figure 5

128

DEVELOPMENT OF THERMAL-STRUCTURAL ANALYSIS METHODOLOGY

The Langley approach to improved thermal-structural analysis methodology consists of several parts (fig. 6). To begin, needs are identified from various sources including industry and academic contacts and from working aircraft and spacecraft problems. Once a need has been identified, ideas are conceived to satisfy the need, and the methodology is developed to implement these ideas. The methodology is then evaluated on small well-defined problems in study computer codes. After the methodology reaches sufficient maturity, it is installed in SPAR and exercised on sufficiently complicated problems to demonstrate the benefits derived from the new methodology. An example of this approach is the recent addition to SPAR of the GEARIB set of solution algorithms as described in reference 2. When the new methodology is independent of the analysis method (i.e., finite element or lumped parameter) it should also be useful in lumped-parameter programs, such as MITAS or SINDA.

OVERALL APPROACH
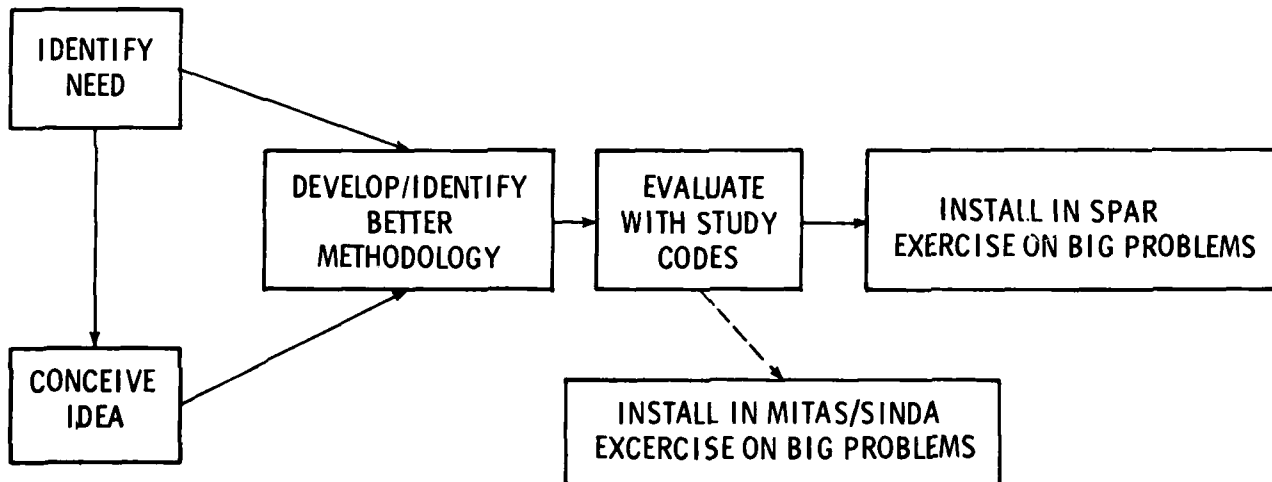
Figure 6

ELEMENTS OF RESEARCH PROGRAM FOR THERMAL ANALYSIS AND OPTIMIZATION

The list of research tasks shown in figure 7, apart from the division into analysis and optimization, falls into three categories: (1) items which are generic and ongoing (solution methods for transient temperatures, integrated analysis methods, evaluation of advanced computer hardware, sensitivity analysis, and thermal-structural optimization); (2) items which are ongoing but will receive increased attention because of their importance to large space structures (approximate analysis techniques, improved radiation analysis); and (3) new areas of work (finite element modeling and analysis techniques for heat pipes).

ANALYSIS

- SOLUTION METHODS FOR TRANSIENT TEMPERATURES
- INTEGRATED ANALYSIS METHODS
- APPROXIMATE ANALYSIS TECHNIQUES
- IMPROVED RADIATION ANALYSIS

- EVALUATION OF ADVANCED COMPUTER HARDWARE
- MODELING TECHNIQUES FOR HEAT PIPES

OPTIMIZATION

- SENSITIVITY ANALYSIS
- THERMAL-STRUCTURAL OPTIMIZATION

Figure 7

130

TRANSIENT THERMAL ANALYSIS TIME REDUCED BY IMPROVED SOLUTION METHOD

One important element of the Langley research program has been the implementation and verification of efficient solution algorithms. A promising set of implicit algorithms denoted GEARIB has been installed in SPAR. The desirable feature of the GEARIB technique is the ability to adaptively vary the step size throughout the temperature history. As indicated in figure 8, various algorithms were used to trace the 3500-second temperature history in a section of the Shuttle orbiter wing. Two models were considered: a two-dimensional section through the wing depth and a one-dimenstional plug through the center of the two-dimensional model. Calculations for each model were carried out using explicit Euler and implicit backward differences as well as GEARIB. The explicit algorithm is burdened by the need to take small time steps (i.e., 0.1 seconds) to avoid numerical instability. The backward differences algorithm uses a larger but fixed time step of 1.0 second (determined by accuracy considerations). The GEARIB algorithm, by adaptively changing its time step to as much as 218 seconds, obtained solutions with significantly less computer time than the two previous methods. Additional results (not shown) were obtained using a lumped-parameter thermal analyzer (MITAS) and indicated that for consistent models, solution methods, and accuracy levels, SPAR and MITAS solution times are comparable. Thus, it is expected that use of GEARIB in this type of analyzer would lead to efficiency improvements similar to those obtained in the finite element program.
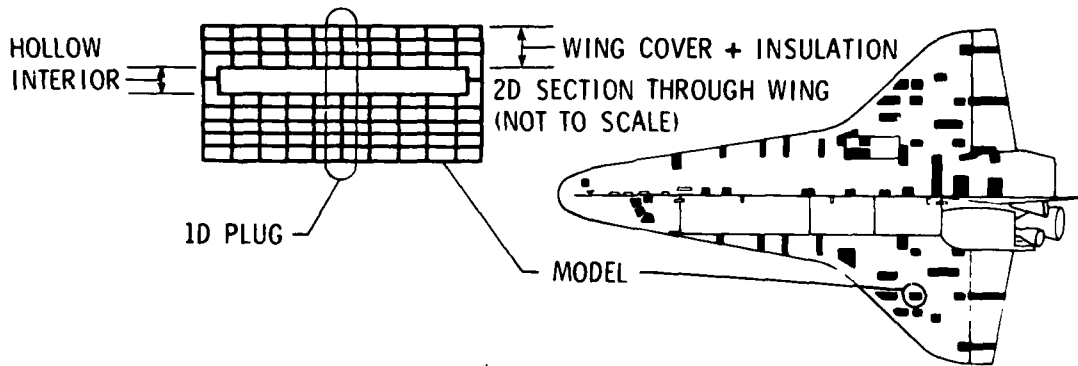
SOLUTION TIMES* FOR 3500 s TEMPERATURE HISTORY				
MODEL	1D PLUG		2D SECTION	
METHOD	TIME STEP	SOLUTION TIME	TIME STEP	SOLUTION TIME
EULER-EXPLICIT	0.1	1723	0 1	3205
BACKWARD DIFFERENCES-IMPLICIT FIXED TIME STEP	1.0	256	1.0	1145
GEARIB-IMPLICIT VARIABLE TIME STEP	0.85-218	63	0.1-225	245

*ALL TIMES IN SECONDS

Figure 8

131

REDUCED-BASIS METHOD FOR TRANSIENT THERMAL ANALYSIS

Along with implementing improved solution algorithms such as GEARIB, work has been initiated to develop approximate analysis techniques which have potential for significant reductions in solution effort. One such method is the reduced-basis technique which combines the classical Rayleigh-Ritz approximation with contemporary finite element methods to retain modeling versatility as the degrees of freedom are reduced (ref. 3). The effectiveness of the method depends upon representation of local temperatures by a few modes or basis vectors. The reduced-basis technique has been successfully applied to the problem illustrated in figure 9. This problem represents a 58-in. segment of the lower surface of the Space Shuttle wing and consists of a 119-mil.-thick aluminum skin covered by 1 in. of insulation. The combined structure was modeled with two-dimensional, finite elements with 84 node points (84 degrees of freedom). A heat pulse reasonably representative of Shuttle reentry was applied to the surface and produced temperatures where radiation becomes appreciable. Additionally, the thermal properties of the insulation are nonlinear functions of temperature and ambient pressure so that the heat transfer equations are highly nonlinear. A total of 23 thermal mode shapes were selected from solutions of two thermal eigenvalue problems: the first based on material properties evaluated for uniform temperatures of 560°R, and the second based on temperatures from a steady-state problem with averaged heating and thermal properties. The resulting temperatures are compared with temperatures obtained from a SPAR thermal analyzer solution of the full system of 84 equations. The temperature histories shown on the figure agree very well and indicate that the reduced-basis technique can approximate temperatures from the full system within 20°R over the entire heat pulse. Efforts are continuing to find the minimum number of basis vectors for acceptable temperatures and to demonstrate the technique for larger problems.
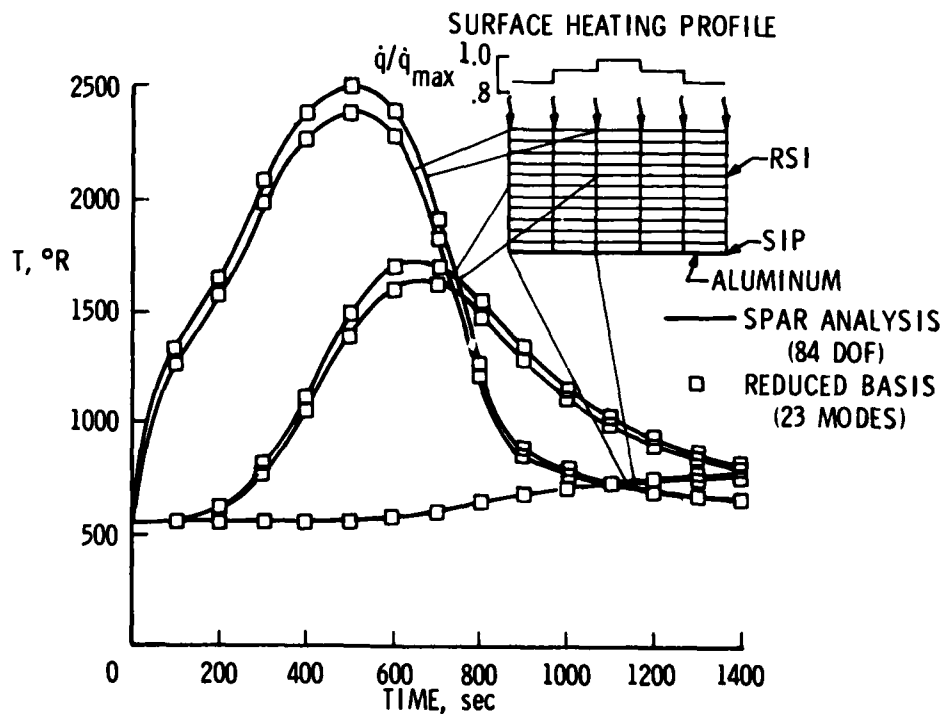

Figure 9

ORBITING TRUSS SPACE STRUCTURE FOR TESTING INTEGRATED FINITE ELEMENTS

Development of integrated finite elements has recently been focused on elements with radiation heat transfer (ref. 4). The next three figures reproduced from reference 4 describe some recent results from that work. The test problem for evaluating the integrated elements is shown in figure 10. A three-member module of an orbiting space truss is shown. A typical truss member receives solar, Earth-emitted and Earth-reflected heating and emits thermal energy to space. In a geosynchronous orbit, solar heating predominates. Incident normal flux to a truss member varies significantly as a member changes orientation with respect to the solar flux vector. As the orbiting structure enters and emerges from the Earth's shadow, significant changes in incident heating occur. Member temperatures and structural deformations depend strongly on the time-dependent heating and member material and surface properties.


Figure 10

133
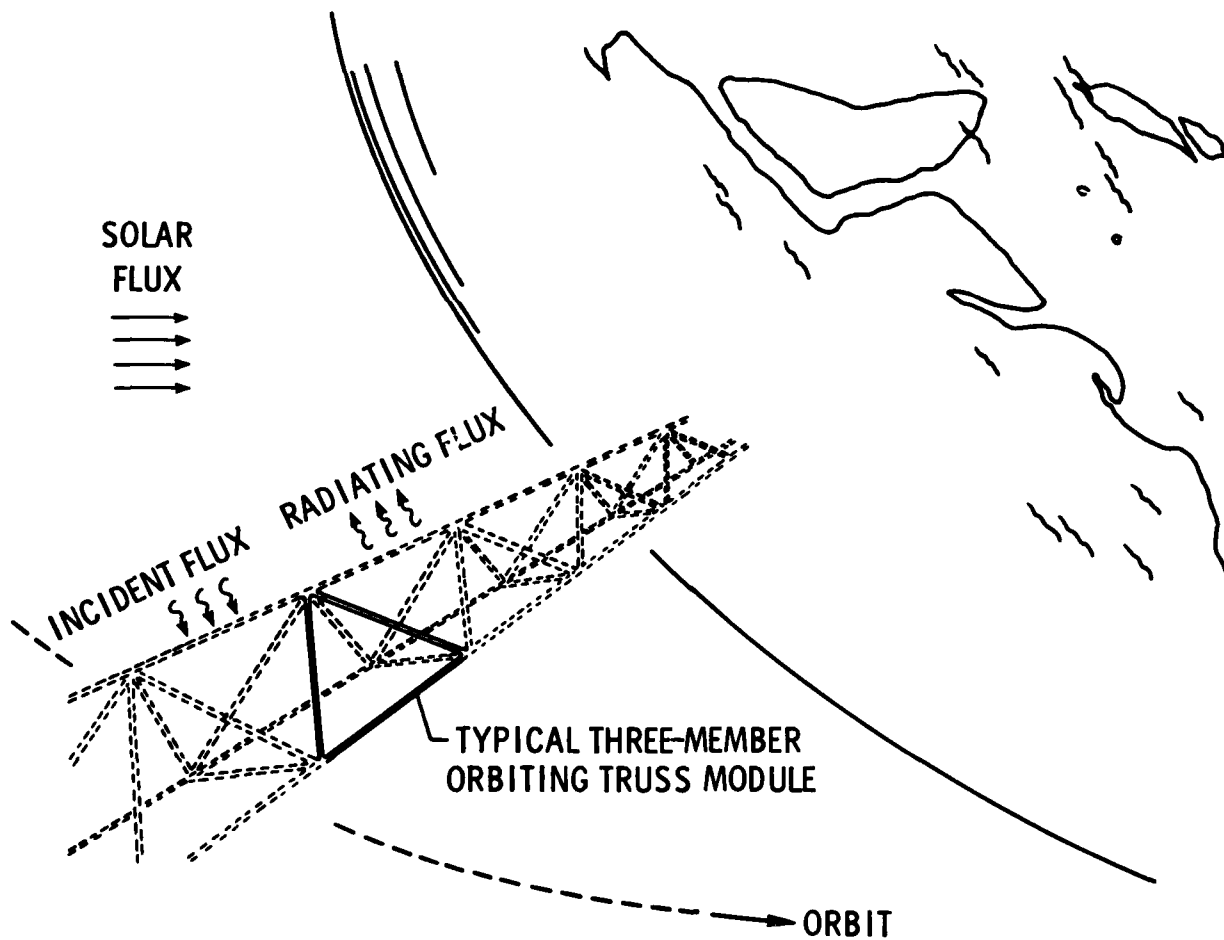
COMPARATIVE TEMPERATURE DISTRIBUTION OF A THREE-MEMBER ORBITING TRUSS

Temperature distributions from conventional and integrated finite elements for the three-member truss are shown in figure 11 for a typical orbital position of the truss space structure. The term integrated element refers to a thermal element formulation using a nodeless variable to obtain a quadratic temperature variation in a two-node element so that accurate thermal forces may be obtained for thermal stress analyses using two-node structural elements. Solutions were obtained for models using a single conventional and a single integrated finite element to represent each truss member. A solution using 10 conventional elements per member is used as a baseline for comparing conventional finite elements with integrated finite elements. The conventional elements did not give a good representation of interior member temperatures. The nodeless variable elements predicted member temperature distributions and nodal temperatures very accurately with small deviations from the reference solution.


Figure 11

134
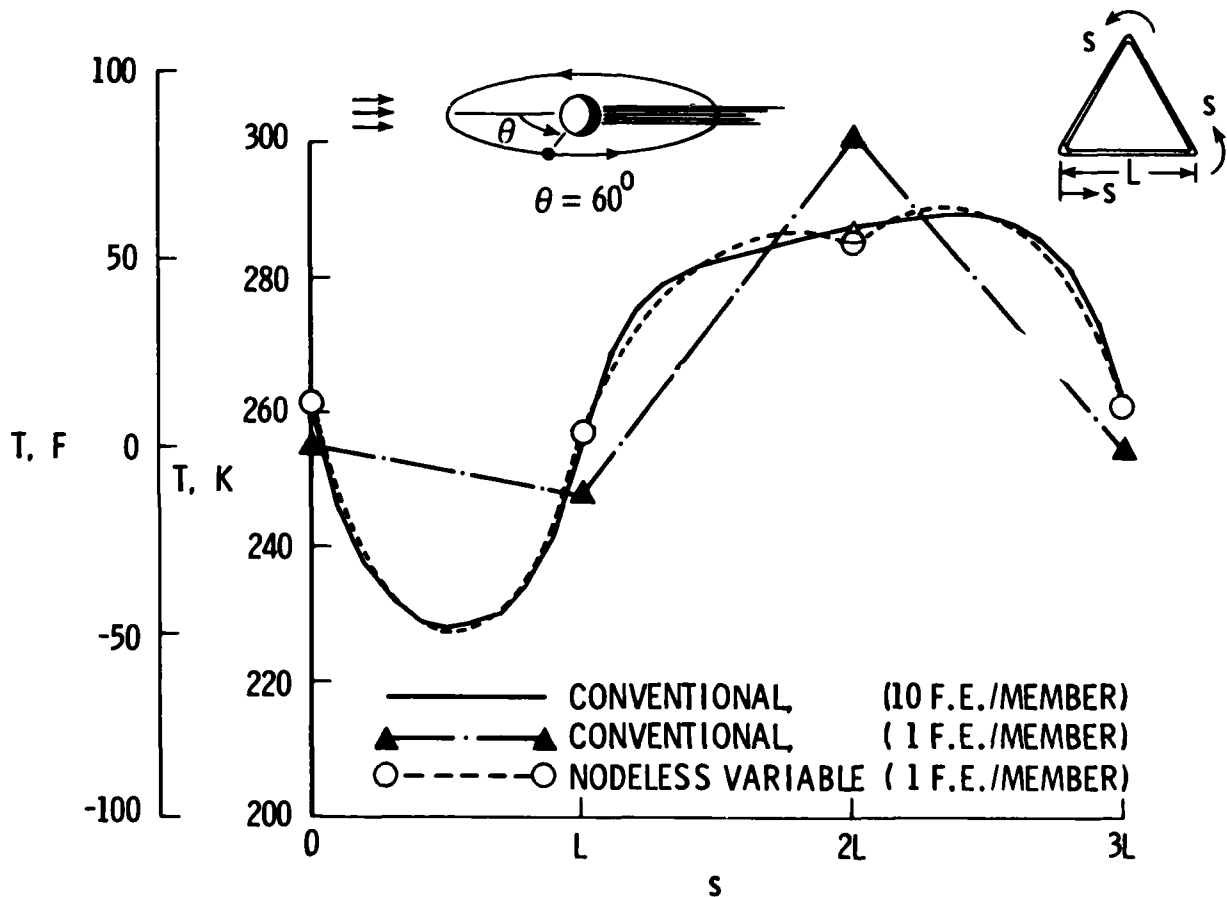
COMPARATIVE DISPLACEMENTS OF A THREE-MEMBER ORBITING TRUSS

Histories of a typical member elongation for one orbit are compared for the various finite element models (fig. 12). The member elongation as computed from the one element per member conventional model temperature distributions show up to 44 percent deviation from the reference solution. These discrepancies arise because the linear temperature distributions predicted by the conventional elements give a poor representation of the average member temperature. Since the nodeless variable elements represent temperature distributions very accurately, the elongation predicted from these temperatures shows excellent agreement with the reference solution with the largest discrepancy less than 1 percent.


Figure 12

135
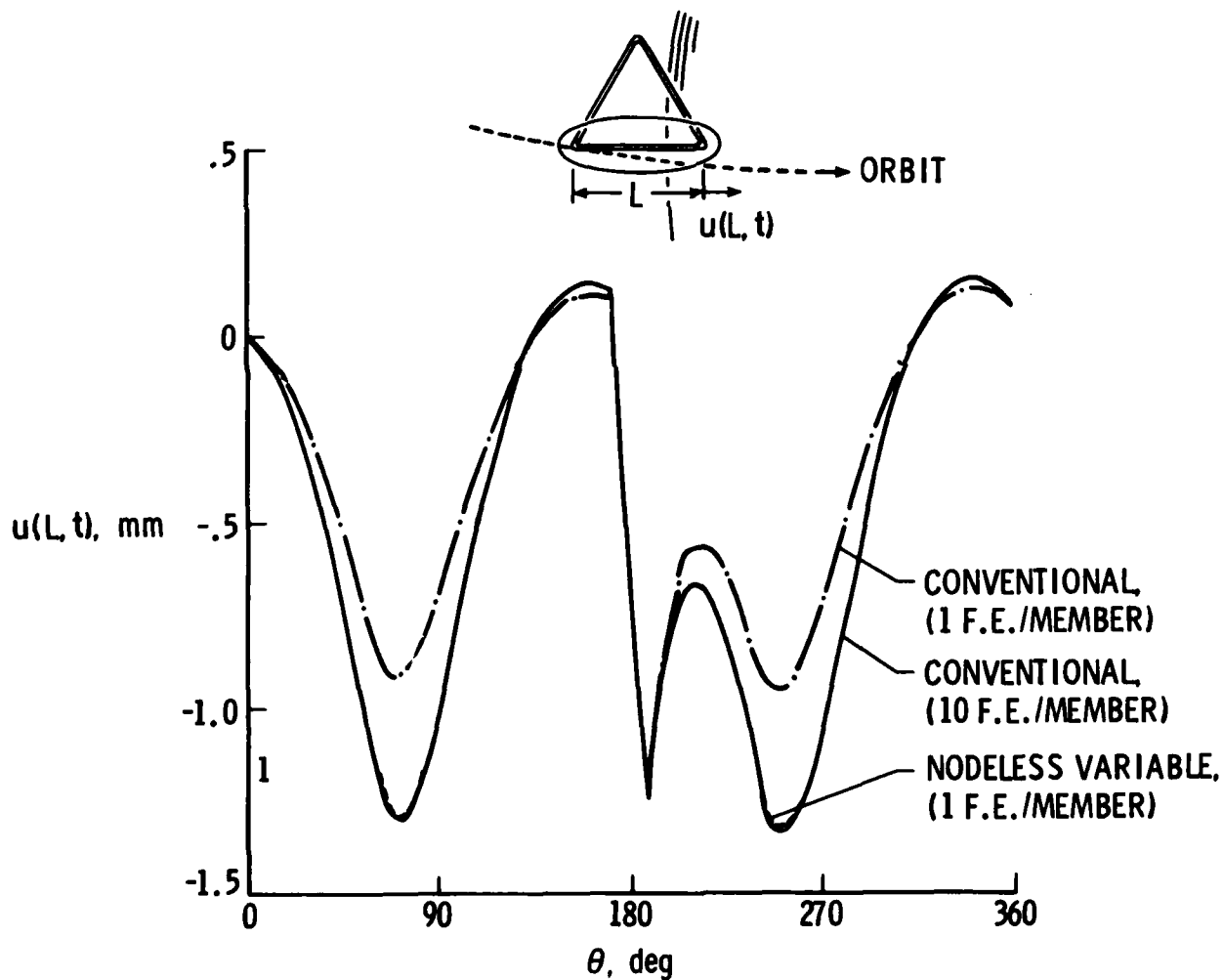
CHARACTERISTICS OF ISOTHERMAL TRUSS ELEMENT

Although the rather rigorous integrated elements discussed in the previous figure are in the research stage and hold promise for future applications, less rigorous state-of-the-art analysis procedures are being applied which employ engineering assumptions. For example, several modeling simplifications are often utilized in thermal analysis of space trusses (ref. 5). For finite element analysis of space trusses, the simplifications are embodied in the isothermal truss element (fig. 13). The isothermal element neglects conduction, radiation exchange with other elements, and interelement shadowing. The element temperature is determined by a balance of radiation heat transfer between solar and Earth-reflected (albedo) energy and radiation from the element to space. The figure typifies the temperature distributions obtained with the isothermal element. Temperatures around the triangular substructure of the orbiting truss are compared. The exact temperature distribution is given by the piecewise linear representation. The isothermal elements obtain good overall element temperatures but miss the details near the ends of the element. Consequently, use of isothermal elements can be useful for overall temperature distributions and deformations but would not be expected to be sufficient for detailed deflections or stresses, particularly at the joints between trusses.

- ENERGY EMITTED
- INCIDENT HEATING

● CHARACTERISTICS

- NEGLECTS CONDUCTION, INTERELEMENT RADIATION AND INTERELEMENT SHADOWING
- GOOD AVERAGE MEMBER TEMPERATURES
- PERMITS SIGNIFICANT MODEL SIZE REDUCTION
- MISSES DETAILED DISTRIBUTIONS
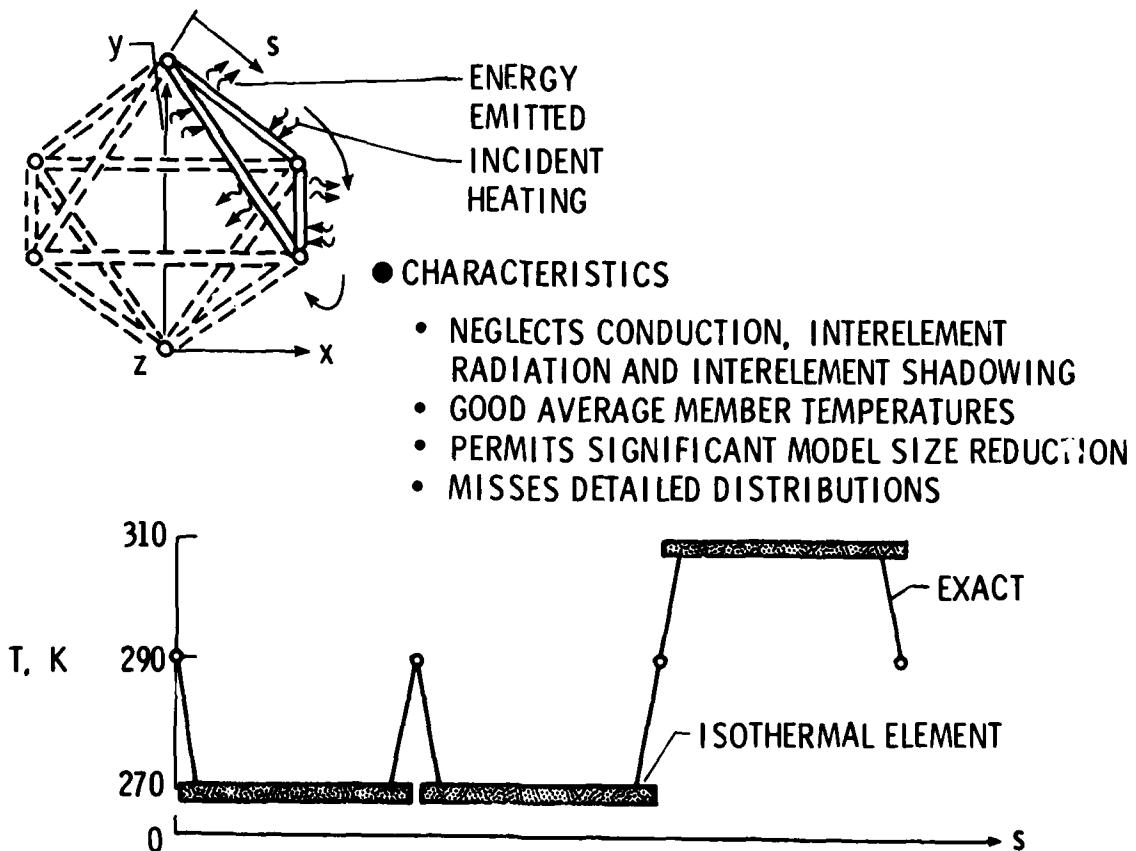
Figure 13

EVALUATION OF APPROXIMATE THERMAL MODELING
AND ANALYSIS TECHNIQUES FOR SPACE TRUSSES

As indicated previously, thermal analyses of space trusses have often relied on simplifying assumptions associated with the isothermal element concept. As indicated in figure 14, there is a need to evaluate the errors associated with a number of simplifications including the neglect of conduction, interelement radiation and shadowing as well as the use of quasi-steady analyses (neglect of transient effects). In addition, two approximate analysis techniques will be evaluated: namely, the reduced-basis method (fig. 9 and ref. 3) and a thermal modal decomposition method. The test problem being used for the first set of evaluations is a truss model obtained from reference 5.

- APPROXIMATIONS TO BE EVALUATED

  - MODELING APPROXIMATIONS

    - NEGLECT CONDUCTION
    - NEGLECT INTERELEMENT RADIATION
    - NEGLECT INTERELEMENT SHADOWING
    - ISOTHERMAL ELEMENTS

- ANALYSIS APPROXIMATIONS

  - REDUCED-BASIS METHOD
  - (RAYLEIGH-RITZ)
 - THERMAL MODES
  - QUASI-STEADY ANALYSIS

Figure 14

137
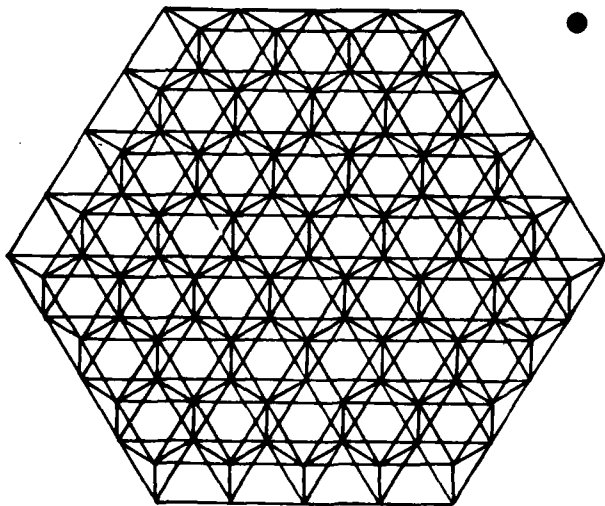
LONG DURATION EXPOSURE FACILITY RADIATION THERMAL ANALYSIS

Along with many of the complicating factors associated with the thermal analysis of the Shuttle orbiter (fig. 2), radiation heat transfer effects have a large impact on analysis needs for large space structures. Recent experiences at Langley in computing view factors for a future Shuttle payload demonstrate the need for efficient calculations of radiation view factors. The Long Duration Exposure Facility (LDEF) is depicted in figure 15. The model shown included 440 panels and 124 occluding surfaces, and required 60,000 view factors. Thermal analysis of this structure required 32 hours of CPU time using an in-house, developed computer program on a CDC 6600 computer and indicates that radiation analysis of large space stuctures such as a space station is likely to severely strain current techniques. The results of this analysis along with other similar experiences for Shuttle components suggest the need to take a look at more efficient programs such as TRASYS (ref. 6) and to attempt to improve techniques used for radiation analysis.


Figure 15

138
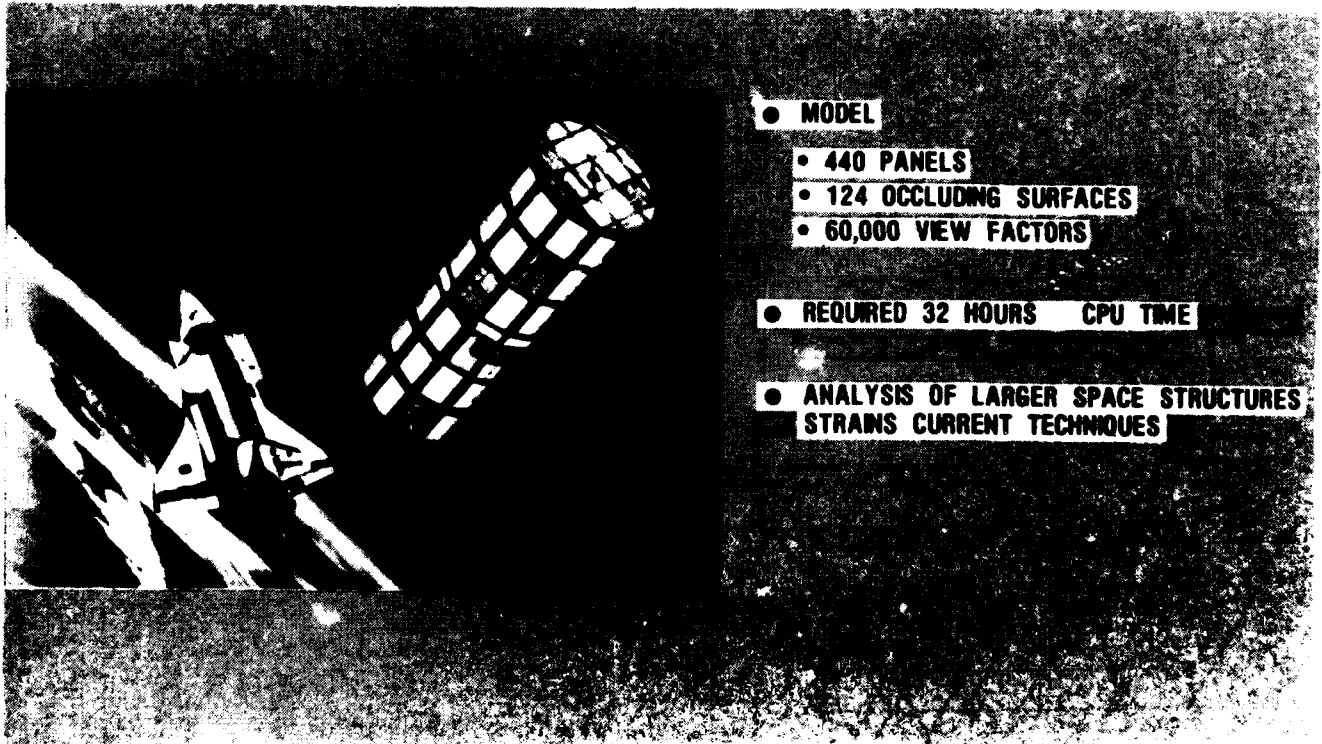
RADIATION THERMAL ANALYSIS RESEARCH

Since complex space station geometry and heating-induced geometry changes will strongly influence radiation heating and interelement radiation exchange, improved methods for calculating view factors and heat fluxes are needed. The TRASYS program has undergone significant upgrading as described in reference 7 and will be evaluated. This program is used extensively at Johnson Space Center for Shuttle and spacecraft applications. Langley is also developing improved radiation capability under a grant with the University of Washington. As indicated in figure 16, improved numerical and code capabilities will be demonstrated in a study code and will include such effects as shadowing, reflections, reradiation, adiabatic surfaces, planes of symmetry, solar flux, and penumbral effects. Techniques currently being considered to improve efficiency are double area integration, contour integration, and Monte Carlo methods. After the improved capabilities have been demonstrated for small problems, the SPAR thermal analyzer will be updated to include the improvements. The goal is to develop in SPAR the capability to compute radiation view factors and fluxes, then temperatures and deformations, and finally feed those deformations back to the view factor calculation to obtain the view factors for the deformed structure. Results from part of this effort may also be incorporated in lumped-parameter thermal analyzers, and some products of the research could be incorporated in TRASYS or TRASYS-type programs.

- OBJECTIVE

  - IMPROVE EFFICIENCY TO CALCULATE VIEW FACTORS AND FLUXES

- APPROACH

  - DEVELOP IMPROVED NUMERICAL AND CODE CAPABILITIES
  - DEMONSTRATE WITH STUDY CODE
  - INCLUDE SHADOWING, REFLECTIONS, RERADIATION, ADIABATIC SURFACES, PLANES OF SYMMETRY, SOLAR FLUX, PENUMBRAL EFFECTS

- TECHNIQUES

  - DOUBLE AREA INTEGRATION
  - CONTOUR INTEGRATION
  - MONTE CARLO

- RESULTS

  - EFFICIENT NUMERICAL AND COMPUTER TECHNIQUES
  - INCORPORATION IN SPAR THERMAL ANALYZER
  - TRANSFERABLE TO LUMPED-PARAMETER ANALYSES

Figure 16

ROLE OF ADVANCED COMPUTER HARDWARE

Discussions involving advanced computer hardware at a recent NASA symposium, Computational Aspects of Heat Transfer in Structures (ref. 2), brought out several observations on the role of advanced computer hardware (fig. 17). Significant reductions in run times were achieved for the unmodified SPAR thermal analyzer on a CYBER 203 and for SINDA on the CRAY. The discussions also indicated that the effort required to restructure (vectorize) large operational codes to take full advantage of vector processing requires such a large personnel investment that it is not generally cost effective. There might be justification for building a vectorized program from the beginning provided the community of potential users was significant. Benefits mentioned for minicomputers were their interactive capability and virtual memory which permits solution of large problems. Benefits mentioned for the supercomputers were their large in-core capacity which permits rapid solution of extremely large problems.

- ● SIGNIFICANT REDUCTION IN RUN TIME ACHIEVED (SPAR ON CYBER-203, SINDA ON CRAY)

- ● RESTRUCTURING PROGRAMS FOR VECTOR COMPUTERS NOT COST EFFECTIVE

- ● BENEFITS FROM MINIS (INTERACTIVE, VIRTUAL MEMORY)

- ● BENEFITS FROM SUPER COMPUTERS (LARGE CAPACITY)

Figure 17

140

THERMAL ANALYSIS OF 30-METER PRECISION DEPLOYABLE ANTENNA

One of the early examples used to evaluate finite element thermal analysis on the CYBER 203 computer was the antenna structure shown in figure 18. This was a fairly small model, containing only 55 grid points and 183 elements, but did have the complexities of interelement radiation and shadowing. A transient analysis was performed for one geosynchronous orbit and solution times on the CYBER 175 and CYBER 203 computers were compared. The 31-percent savings of computer time was considered significant but not entirely satisfying since greater savings had been anticipated. It was decided that since the program operated in the scalar mode and the program had not been restructured to take better advantage of the vector processing capability of the CYBER 203, the time saving was as much as could be expected. This reasoning, however, led to a subsequent task of performing some vectorized programming to assess the benefit of vector processing by the CYBER 203.
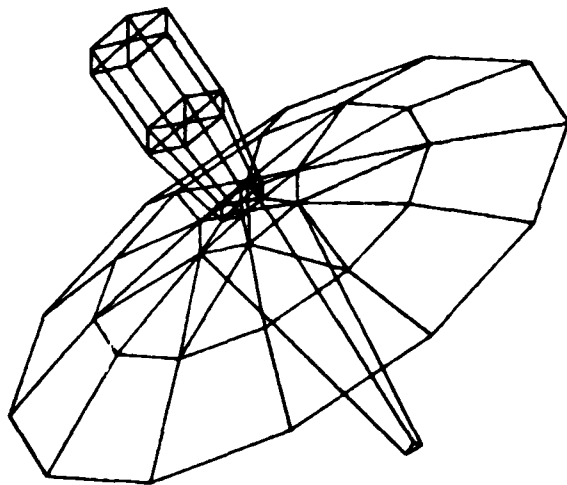
- 55 GRID POINTS
- 183 ELEMENTS
- INTERELEMENT RADIATION
- TIME-DEPENDENT SHADOWING
- TEMPERATURE HISTORY FOR 24 HOURS
  DT = .01 hr

| SOLUTION TIME,* sec	
CYBER 175	CYBER 203
46.4	32.1

*SCALAR MODE

TEMPERATURE HISTORY
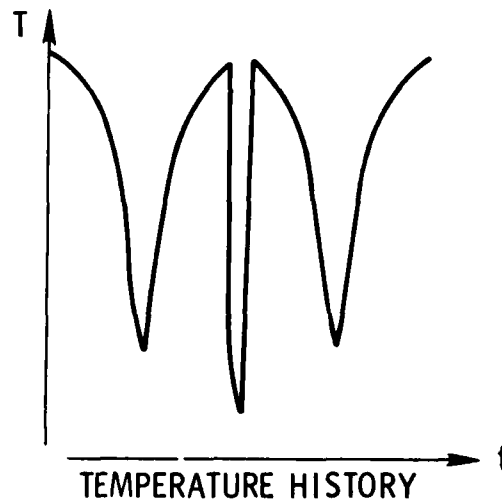
Figure 18

IMPACT OF VECTORIZATION ON SOLUTION TIME ASSESSED

A pilot program was written to determine the benefits of the vector processing capability of the CYBER 203. The program solves for the transient temperatures in an insulated cylinder modeled with SPAR solid thermal elements. Figure 19 shows the vectorization stages that have been completed. The CYBER 203 run time in the scalar mode is shown in the first line of the table. The next entry displays the benefits from obvious conversions of DO loops to explicit vector calls and the vectorization of scaling the element conductivity matrices. The subroutines which factor and solve the symmetric banded system of equations were replaced by a vectorized subroutine from the CYBER 203 system math library. The answers produced were identical, and the time required for this operation was cut by almost two-thirds. The library routine uses a vector length of half the bandwidth plus one. For the insulated cylinder model this was 26. A larger bandwidth would produce more savings here. The single most time-consuming operation is the multiplication of the conductivity matrix, denoted K, by the temperature vector, denoted by T. The reprogramming of this operation so that relatively long vectors were operated on (ref. 8) was responsible for the largest time savings and brought the total solution time down to 33 seconds, a reduction to nearly one-third the original solution time.

PROBLEM: 1000 sec TEMPERATURE HISTORY OF 800 NODE CYLINDER, DT = 2.0 sec

LEVEL OF VECTORIZATION	CPU TIME
ORIGINAL - NO VECTORIZATION	92
EXPLICIT VECTOR CALLS FOR OBVIOUS LOOPS AND SCALING	85
VECTORIZED ROUTINE FOR SOLUTION OF EQUATIONS (MATH LIBRARY ROUTINE)	65
VECTORIZED K T OPERATION	33

REGION OF APPLIED HEATING
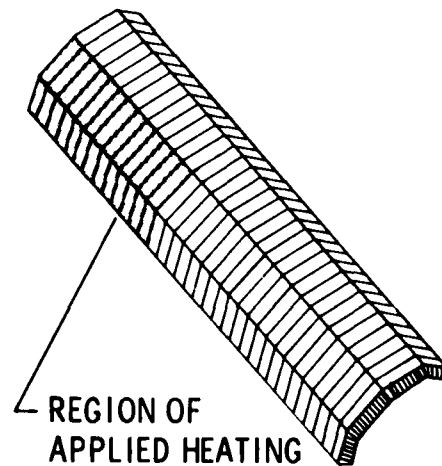
Figure 19

PROPOSED APPLICATIONS OF HEAT PIPES TO AEROSPACE STRUCTURES

The use of heat pipes for reducing temperature gradients and the associated deformations and stresses has been proposed for a number of applications (fig. 20) such as a heat-pipe-cooled leading edge for the Shuttle Orbiter wing (ref. 9) and a heat pipe sandwich panel radiator concept for the orbiter payload bay doors. For large space antennas, a heat pipe sandwich panel has been proposed for the reflector structure (ref. 10). Finally, heat pipes have been proposed for thermal management on space station concepts (ref. 11). These proposed applications lead to the question of whether existing capability is adequate to handle detailed analyses of heat pipe thermal performance.

Figure 20

143
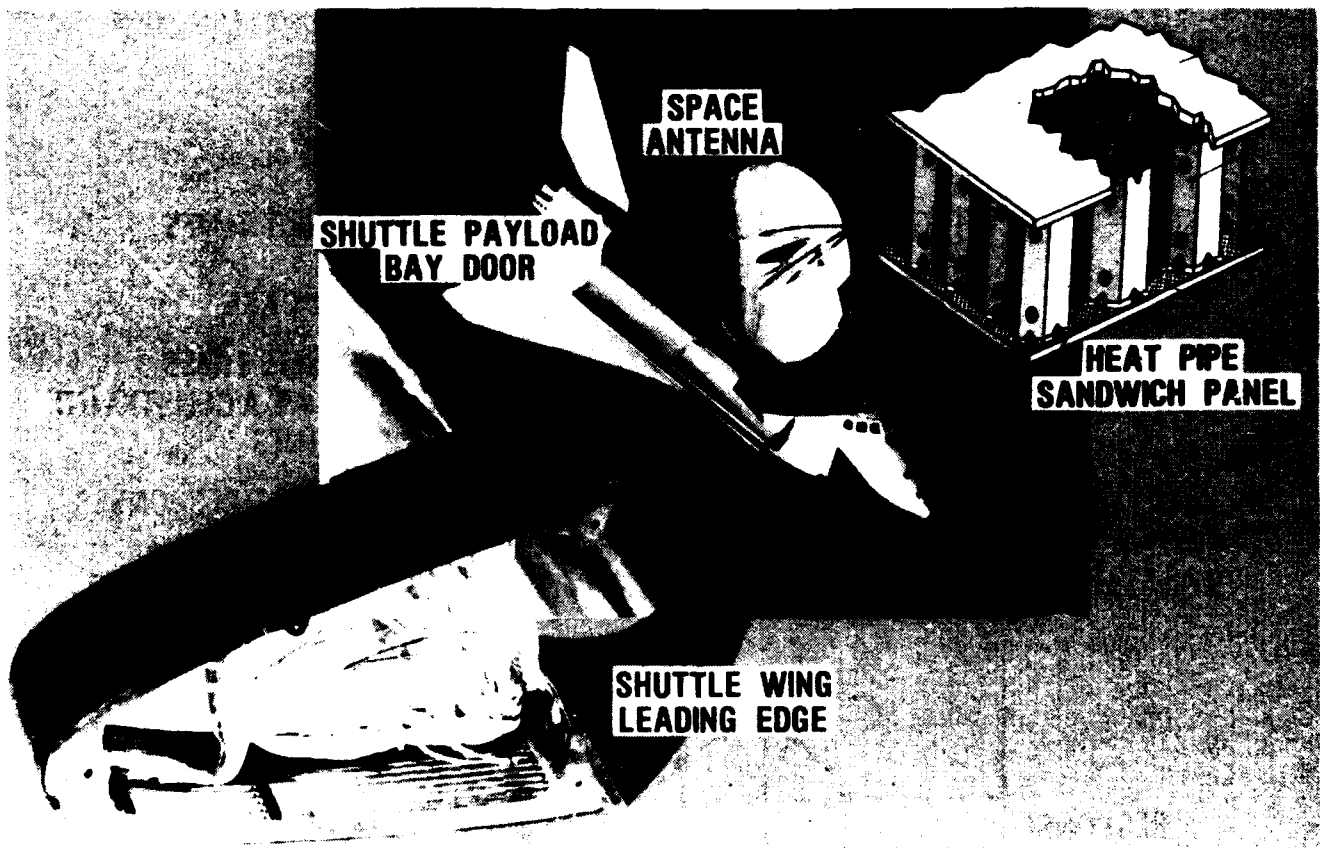
CONSTRAINT TRACKING FOR TRANSIENT THERMAL RESPONSE

An important aspect of space structure analytical design will be the
requirement that time-dependent temperatures and stresses be less than specified
allowable values (constraints) for all appropriate values of time for all orbits.
The traditional approach for such problems has been to calculate response quantities
for a few "time slices" and design the structure so that constraints are satisfied
for each time slice (fig. 21). An extension of this approach called "discrete
times" calculates response quantities at many discrete times which span the time
domain (ref. 12). The response for each discrete time is treated as a separate
constraint and the structure is designed to satisfy all the constraints. For the
example shown, two such constraints are not satisfied and the structure must be
resized. A third method to handle time-dependent constraints known as the "critical
times" method is to calculate times when the largest response for a given design
occurs, size to satisfy the constraints for those times, and periodically update the
critical times as the optimization proceeds (ref. 13).

| APPROACH	DESCRIPTION
● USUAL TIME SLICING	CALCULATE RESPONSE AT DISCRETE TIMES TREAT EACH AS A LOAD CASE DESIGN TO SURVIVE EACH LOAD CASE
● DISCRETE TIMES METHOD (ref. 12)	CALCULATE RESPONSE AT DISCRETE TIMES TREAT RESPONSE AT EACH TIME AS A CONSTRAINT SIZE TO SATISFY ALL CONSTRAINTS
● PREDICTED CRITICAL TIMES METHOD (ref. 13)	CALCULATE TIME (S) WHEN LARGEST RESPONSES OCCUR SIZE TO SURVIVE AT THOSE TIMES

DESCRETE TIMES METHOD
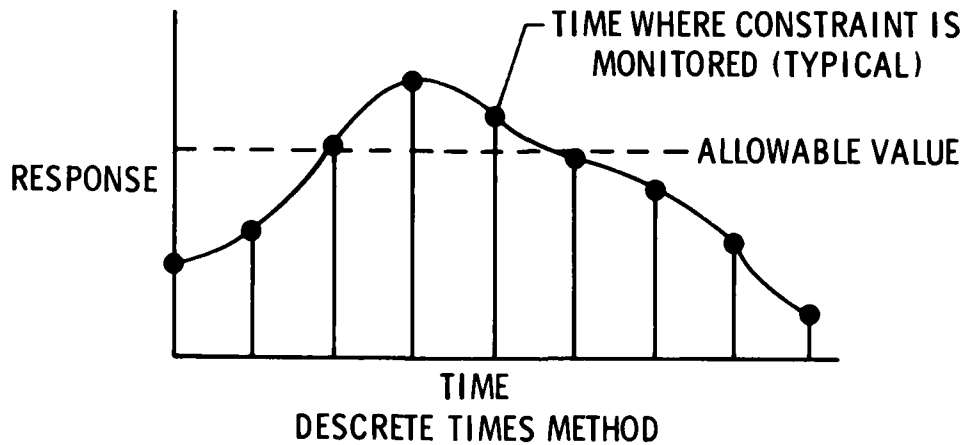
Figure 21

OPTIMUM DESIGN FOR THERMAL DISTORTION CONSTRAINTS

Large flexible space structures such as antennas and optical systems typified by the Space Telescope (fig. 22) require the consideration of extremely tight constraints on temperatures, temperature gradients, and thermal deformations. For example, part of the optical control system in the Space Telescope is permitted no more than a 0.0005°F temperature difference over an 18-inch span. Typical methods for controlling temperatures and deformations in the telescope include the use of thermal coatings and heaters. A contractual effort is being initiated with the Perkin-Elmer Corporation to adapt mathematical optimization procedures to the problem of automatically selecting parameters such as coating locations, heater locations, and sizes to meet specified tolerances on the deformations and temperatures of orbiting structures. This effort will build on the work of the principal investigator's doctoral dissertation (ref. 14) which has already been used to influence design procedures for the Space Telescope. As part of this work, thermal analysis techniques will be modified as required to assure that the high precision needed in computed temperatures is achieved.


Figure 22

145
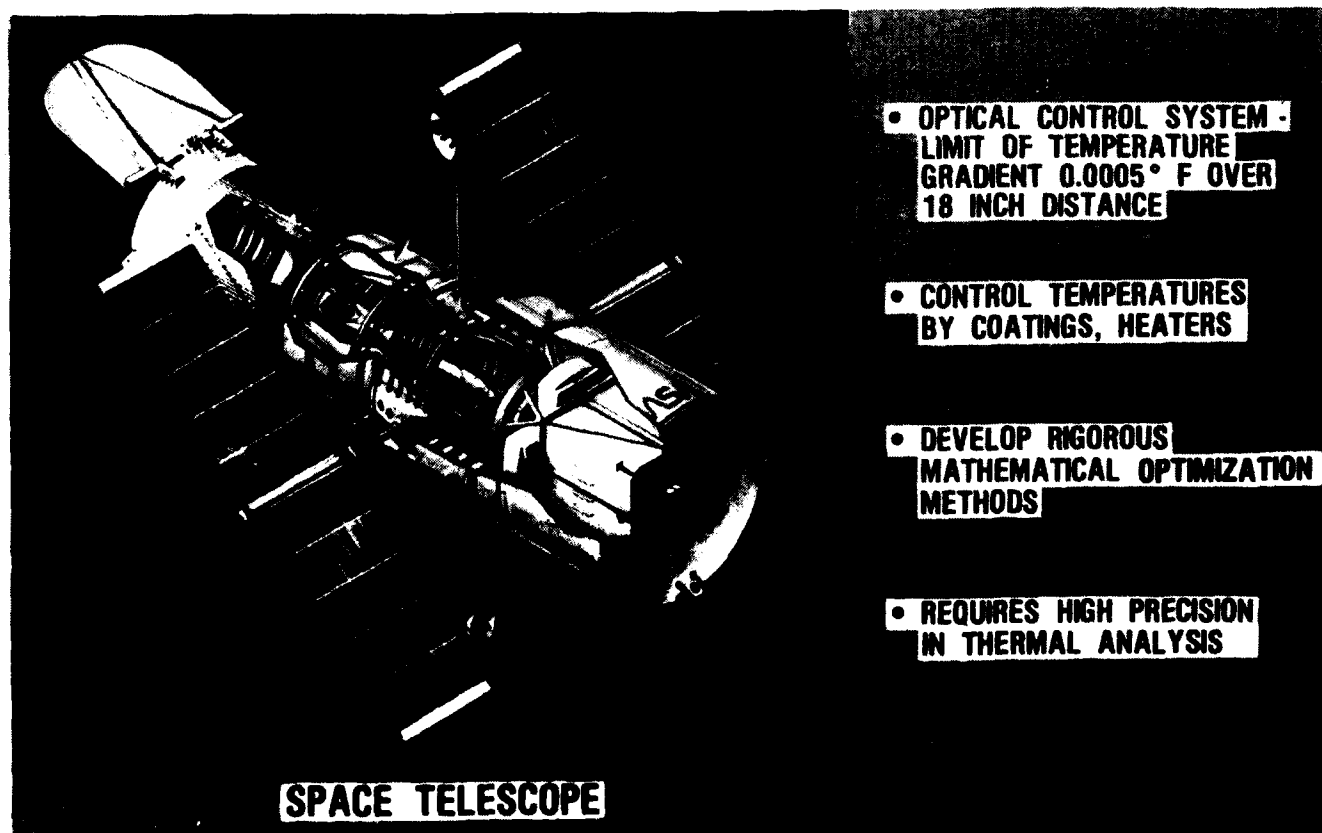
SUMMARY

This paper has intended to discuss a number of issues and needs relative to thermal analysis of large space structures and space stations (fig. 23). Some indications of trends in the Langley thermal-structural analysis research program consistent with the issues and needs are also presented. The main heat transfer mechanism in space is radiation; consequently, there is a need for a strong thrust on improved radiation analysis capability. Also the important interactions among temperatures, deformations, and controls need to be accounted for. Finite element analysis capability seems to be lagging behind lumped-parameter capability for heat pipe analysis. Briefly, the Langley plan will include improving radiation analysis capability, evaluating the errors involved in certain approximate analysis and modeling techniques for large space trusses, and continuing the development of integrated thermal-structural finite elements with an emphasis on radiation heat transfer. Work will be initiated to develop finite element analysis techniques for heat pipes. Finally, optimization research activities will be oriented toward methods to design flexible orbiting structures to account for thermal and thermal-deformation requirements.

- THERMAL ANALYSIS NEEDS OF LSS PRESENT RESEARCH OPPORTUNITIES:

  - RADIATION ANALYSIS

  - INTERACTIONS: TEMPS, DEFORMATION, CONTROLS, ETC.

  - HEAT-PIPE MODELING, ANALYSIS, OPTIMIZATION

- PLANS

  - ORIENT THERMAL-STRUCTUAL ANALYSIS ACTIVITY TO LSS

  - MAJOR THRUST ON RADIATION ANALYSIS IN SPAR

  - EVALUATE SIMPLIFIED MODELING AND ANALYSIS TECHNIQUES

  - CONTINUE INTEGRATED FINITE ELEMENT DEVELOPMENT

  - INITIATE FE HEAT-PIPE MODELING AND ANALYSIS RESEARCH

  - INITIATE OPTIMIZATION APPLICATIONS TO LSS

Figure 23

REFERENCES

1. Thornton, E. A.; Dechaumphai, P.; and Wieting, A. R.: Integrated Thermal Structural Finite Element Analysis for Applications to Hypersonic Transport Design. AIAA Paper No. 80-0717, 1980.

2. Adelman, H. M., ed.: Computational Aspects of Heat Transfer in Structures, NASA CP-2216, 1982.

3. Shore, C. P.: A Reduced Basis Technique for Transient Thermal Analysis. NASA CP-2216, 1982, pp. 133-146.

4. Thornton, E. A.; Dechaumphai, P.; and Wieting, A. R.: Integrated Finite Element Thermal-Structural Analysis With Radiation Heat Transfer. AIAA Paper No. 82-0703, May 1982.

5. Garrett, L. B.: Interactive Design and Analysis of Future Large Spacecraft Concepts. NASA TP-1937, 1981.

6. Jensen, C. L.; and Goble, Richard G.: Thermal Radiation Analysis System (TRASYS II) Users Manual. NASA CR-159273-1, 1979.

7. Vogt, R. A.: Recent Development in Thermal Radiation Analysis System (TRASYS). NASA CP-2216, 1982, pp. 243-251.

8. Robinson, J. C.; Riley, K.; and Haftka, R. T.: Evaluation of the SPAR Thermal Analyzer on the CYBER-203 Computer. NASA CP-2216, 1982, pp. 405-424.

9. Camarda, C. J.; and Masek, Robert V.: Design, Analysis, and Tests of a Shuttle-Type Heat Pipe-Cooled Leading Edge. Journal of Spacecraft and Rockets, vol. 18, no. 1, January-February 1981, pp. 71-78.

10. Basiulus, A.; and Camarda, C. J.: Design, Fabrication and Test of Liquid Metal Heat-Pipe Sandwich Panels. AIAA Paper No. 82-0903, 1982.

11. Space Operations Center: A Concept Analysis. NASA TM-81062, 1979.

12. Adelman, H. M.: Preliminary Design Procedure for Insulated Structures Subjected to Transient Heating. NASA TP-1534, 1979.

13. Haftka, R. T.; and Shore, C. P.: Approximation Methods for Combined Thermal/ Structural Design. NASA TP-1428, 1979.

14. Costello, Frederick A.: Optimization Technique for Spacecraft Thermal Control. PhD. Dissertation, University of Penn., 1965.

SESSION III

OPTIMIZATION FOR CONTROLLABILITY

Chairman: M. A. Ostgaard
Secretary: V. B. Venkayya

ALGORITHM DEVELOPMENT FOR THE CONTROL DESIGN
OF FLEXIBLE STRUCTURES

Robert E. Skelton
Purdue University
School of Aeronautics and Astronautics
West Lafayette, Indiana

ABSTRACT

In feedback control problems it has recently been established that there is *an optimum controller order* for a given mission (set of control objectives) [1]. The conclusion is that it is possible to make the model too simple (something everyone knows), and *it is possible to make the model too complex!* The engineering explanation for this phenomenon is that models of too low order have large effects from errors in model order, whereas models of too high order have large effects from errors in parameters. One might think that parameter identification methods could be added to remove this latter difficulty. But, alas, it is well known in identification theory [2]-[9] that overparameterization actually degrades the performance (convergence) of the identification algorithms. Hence, further research is needed to determine methods to find the *optimum* controller complexity (controller order *and* controller parameterization). That is, the modeling problem and the control problem must be united within some integrated systematic approach.

The method currently under investigation for accomplishing this is component cost analysis [1]. Component cost analysis determines the critical components in a dynamic system, and varied applications of these concepts lead to an algorithm which *integrates* the following design problems.

- Which *components* of the system structure should be redesigned and what parameters of the redesign are important to change?

- Which *sensors and actuators* should be redesigned; where should the sensors and actuators be located; what type of sensors and actuators should be used?

- Which *parameters* will be most critical to identify?

- What *controller order* and *associated optimum controller bandwidth* is optimum?

- What *sample rate* should be selected for digital control?

1.0 INTRODUCTION

Flexible structures and their dynamics have been studied for over a century. However, only recently has there been an interest in the active control of flexible structures. Such interest was piqued in the 1960's by a flexibility-induced instability in the USA's first satellite [10] and, more recently, by sophisticated requirements for precision-controlled structures in space for astronomy, communication networks, near-Earth scientific studies, and space solar-power alternatives [11]. The rapid development of computers and control theory in the 1960's has encouraged active control applications for other structures as well, such as flutter suppression in aircraft [12], and active damping of bridges and tall buildings [13]. This is not to say that active control is needed in every structure, however, and there is no clear way to make the decision of when and how much control effort is needed in a structure. There is a need to study the dynamical properties of the mechanical system with a view toward discerning what improvements in performance can easily be made by redesigning the structure and what improvements must be left for active control functions. This *beneficial* interaction of the dynamics and control disciplines in the development of a rotational design methodology has not yet occurred to any mature degree. Usually the structure designs and the control designs occur sequentially. This luxury cannot be afforded in the future. Stringent requirements force us to provide better coordination between structure design, control design, and controller software design.

Some of the reasons that the control of flexible spacecraft can be a difficult task are briefly described by the following three problems.

(i) The Model Error Problem

The space structure is usually constructed of lightweight materials, and thus the assembled structure is very lightly damped. This uniqueness of light damping for the space structure makes the control design extremely sensitive to modeling errors, since the slightest perturbation of truncated modes by control action can shift these eigenvalues into the right half-plane. Also there is the usual uncertainty in the computation of the modal data. This problem is especially critical for spacecraft since modal data uncertainties cannot be removed before flight, due to the difficulty of testing the extremely lightweight structure in a 1-g environment.

(ii) The Limited Controller Software Problem

The practical limitations of memory and speed of onboard computers mean that only controllers of constrained dimension can be considered. These constraints can severely reduce the performance capabilities of the controlled system due again to the effect of modeling errors imposed by the controller order constraints. (An infinite dimensional system controlled by finite controllers immediately suggests that the standard "optimal" state feedback solutions are not going to be realized). Thus, limited software serves only to compound the model error problem by constraining the order of the controller and by adding delays in the feedback loop.

(iii) The Performance Requirement Problem

Of course the model error problem and the limitations of software pose no serious threat to the mission if the performance requirements are quite lenient. Thus, the degree to which (i) and (ii) pose problems is directly related to the severity of the performance requirements. Therefore, early research on the subject sought to help with the trade-offs between performance and modeling errors (including those induced by controller software limitations).

2.0 MODELS OF SPACE STRUCTURES

Those portions of the structure resembling beams, plates, and membranes might reasonably be idealized as a material continuum. The resulting partial differential equations (PDEs) contain all the modal data over an infinite spectrum [14]. Other parts of the structure might contain trusses or complicated connections which require a finite element formulation of the model, resulting in a set of ordinary differential equations (ODEs) [15]-[17]. Also, the dynamics of actuators and sensors are usually described by ODEs. This combination of distributed-parameter models (PDEs) and lumped-parameter models (ODEs) must eventually be reduced to a finite set of ODEs. The discretization of the PDEs must be accomplished so that the frequency spectrum over which each of the subsystems (actuators, sensors, substructure 1, substructure 2, etc.) are modeled is consistent. Otherwise, troublesome dynamical interactions between subsystems might be unintentionally concealed at the outset. Thus, *each* of the substructure models might be truncated prior to the assembly of the composite model (2.1).

$$M'\ddot{q} + C'\dot{q} + G'\dot{q} + K'q = B'u_a$$

$$y = \begin{pmatrix} P'q \\ R'\dot{q} \end{pmatrix}$$

structures, S_{STR} (2.1a)

$$\dot{x}_a = A_a x_a + B_a u + w_a$$
$$u_a = C_a x_a + v_a$$

actuators, S_a \hfill (2.1b)

$$\dot{x}_s = A_s x_s + B_s y + w_s$$
$$z = C_s x_s + v$$

sensors, S_s \hfill (2.1c)

where the inertia or "mass" matrix $M' = M'^T > 0$ is positive, definite, and symmetric; the stiffness matrix $K' = K'^T \geq 0$ is positive, semidefinite, and symmetric; the internal energy dissipation due to damping is $\dot{q}^T C' \dot{q}$ and $C' = C'^T \geq 0$ is positive, semidefinite, and symmetric; and any gyroscopic term is due to $G' = -G'^T$, which is skew-symmetric. The disturbance models assumed for w_a, v_a, w_s, v are all zero-mean white noise processes. The dimensions of the vector are $x_s \in R^s$, $x_a \in R^a$, $q \in R^N$, $u_a \in R^{m_a}$, $u \in R^m$, $y \in R^{n_y}$, $z \in R^{n_z}$. The coordinate transformation

$$q = T\eta \tag{2.2a}$$

is often made to put the structural subsystem S_{STR} in the coordinates

$$\ddot{\eta} + Z_1 \dot{\eta} + Z_2 \eta = Bu_a \quad , \quad B \triangleq T^T B', \quad Z_2 \triangleq T^T K' T \quad , \quad Z_1 \triangleq T^T [C' + G']T \tag{2.2b}$$

$$y = \begin{bmatrix} P\eta \\ R\dot{\eta} \end{bmatrix} \quad , \qquad P \triangleq P'T \ , \qquad R \triangleq R'T \tag{2.2c}$$

Let the first n_r elements of q and η be associated with rigid-body (zero frequency) modes of the structure. Then these matrix partitions apply

$$Z_2 \triangleq T^T K' T \triangleq \text{block diag} \quad [0 \ \omega^2] \ , \quad \omega^2 \triangleq \text{diag} \ [\omega_1^2, \ \ldots, \ \omega_N^2] = T_e K' T_e \tag{2.2d}$$

$$T^T M' T = I \ , \quad T = [T_r \ T_e], \ T^T C' T = \text{block diag} \ [0 \ \Delta] \ , \quad \Delta \geq 0 \tag{2.2e}$$

$$T^T G' T = \begin{bmatrix} G'_{rr} & G'_{re} \\ G'_{er} & G'_{ee} \end{bmatrix} , \quad \begin{array}{l} \eta_r^T = [\eta_r^T \ \eta_e^T] \ , \qquad R = [R_r \ R_e] \\[2mm] P_r = [P_r \ P_e] \ , \qquad B^T = [B_r^T \ B_e^T] \end{array} \tag{2.2f}$$

where the zero in (2.2e) holds if the rigid modes are undamped, and $G'_{rr} = -G'^T_{rr}$, $G'_{er} = -G'^T_{er}$, $G'_{ee} = -G'^T_{ee}$. Now (2.2) becomes

$$\ddot{\eta}_r + G'_{rr} \dot{\eta}_r + G'_{re} \dot{\eta}_e = B_r u_a \tag{2.3a}$$

154

$$\ddot{n}_e + G'_{er}\dot{n}_r + G'_{ee}\dot{n}_e + \Delta\dot{n}_e + \omega^2 n_e = B_e u_a \qquad (2.3b)$$

$$y = \begin{pmatrix} P_r n_r + P_e n_e \\ R_r \dot{n}_r + R_r \dot{n}_e \end{pmatrix} \qquad \begin{matrix}(2.3c)\\[20pt](2.3d)\end{matrix}$$

There are N nearly elastic modes with frequencies

$$\{\omega_1 \le \omega_2 \le \cdots \le \omega_N\} \qquad (2.4)$$

and eigenvectors

$$T_e = [t_1, t_2, \cdots, t_N] \qquad (2.5)$$

3.0 ON THE STRUCTURE OF MODELING ERRORS

Let the composite model (2.1) be written in state form

$$\dot{x} = Ax + Bu + Dw + f, \qquad x^T \overset{\Delta}{=} (n^T, \dot{n}^T, x_a^T, x_s^T)$$
$$z = Mx + v + g, \qquad w^T = (w_a^T, w_s^T, v_a^T) \qquad , \ x \in R^n, \ n \doteq 2n_a + a + s \qquad (3.1)$$

where nonlinearities f and g might be added to the model for performance evaluation purposes, but might be ignored during control design. The associated parameters (A,B,D,M) may be deduced from (2.1), (2.2). There may be *several* stages of model simplification between the most general model used for simulation and performance evaluation before flight and the model upon which the control design is based. To simplify the discussion, we discuss only two models. In this section, model (3.1) will represent the physical system (admittedly in this case, the state X is infinite-dimensional and the parameters A,B,D,M are not precisely known). The reduced model used for controller design is

$$\dot{x}_R = A_R x_R + B_R u + D_R w_R \qquad (x_R \in R^r) \qquad (3.2)$$

$$z_R = M_R x_R + v_R$$

and we postpone the discussion of how (3.2) might be derived. Our current interest concerns the characterization of the differences between *any* two models (3.2) and (3.1). In order to match identically the measurements z(t) actually obtained from the *physical* system, one could define vector functions of time $e_x(t)$, $e_z(t)$ as those which drive the state and measurement equations in such a way

$$\dot{x}_R = A_R x_R + B_R u + D_R w_R + e_x(t) \qquad (3.3)$$

$$z = M_R x_R + e_z(t)$$

that $z(t)$ matches the actual measurements. Such model error vectors have been shown [18] to be composed of four parts

$$\begin{pmatrix} e_x \\ e_z \end{pmatrix} \overset{\Delta}{=} e = e_\Delta + e_t + e_d + e_n \tag{3.4}$$

where e_Δ is due only to parameter errors, e_t is due to errors in model order, e_d is due to neglected disturbances and e_n is due to neglected nonlinearities. Of course, none of these e_Δ, e_t, e_d, e_n can be known *a priori*. Parameter adaptive control and identification methods [19]-[21] strive to drive $e_\Delta(t)$ to zero. Such methods can be effective *when e_Δ is the dominant source of error* in (3.4). Terms contributing to e_t depict the coupling between retained and truncated equations in the (infinite-dimensional) model underlying the physical system. Much attention [22]-[24] has been devoted to the reduction of the "spillover" terms e_t (and their corresponding closed-loop consequences). Such approaches can be effective *if e_t happens to be the dominating term* in (3.4). Orthogonal filters [25], [26] make fewer assumptions about $e(t)$, save that it is square integrable. This more general characterization of model error has the potential advantage of simultaneously accommodating errors of the type (3.4), but the method also has disadvantages in the design stage. The method requires the selection and storage of a set of independent functions (to be used for fitting the actual error function), and the choice of these functions is not unique. One choice is to use elements of the state transition matrix for a higher order model as in [27]. Another choice is to use orthogonal functions as in [25].

Having described the *nature* of the modeling errors, we wish now to be more explicit about their *effects*. These effects will now be described, first in terms of stability and then in terms of a quadratic performance metric.

4.0 STABILITY AND PERFORMANCE IN THE PRESENCE OF MODELING ERRORS

4.1 Stability and Modeling Errors

Let

$$u = G \hat{x}_R$$

$$u(s) = [G(sI - A_R - B_R G + F M_R)^{-1} F] z(s) \tag{4.1}$$

$$\dot{\hat{x}}_R = A_R \hat{x}_R + B_R u + F(z - M_R \hat{x}_R)$$

describe the dynamical controller used to control the system (3.1). G is usually chosen to stabilize $[A_R + B_R G]$ and F is usually chosen to stabilize $[A - FM]$, although the controller poles, $\lambda_j[A_R + B_R G - FM]$, $j = 1, \ldots, r$, should also be stable [28]. There is no unique relationship between the parameters of the controller (4.1) and the evaluation model of the system (3.1). The controller parameters (A_R, B_R, M_R) may or may not be related to some reduced-order model obtained from (3.1). For example, the simpler model (A_R, B_R, M_R) might have been derived directly from physical laws, but using an *idealization** of the system that was simpler than the idealization that led to (3.1). For these reasons the phrase "parameter errors" has no unique meaning. In fact, none of the terms in the decomposition (3.4) is unique.

---

*By *idealization* we mean the set of hypotheses within which the dynamical system is assumed to move. For example, different idealizations of the same system might include: an elastic material continuum, a set of connected rigid bodies, a rigid body.

156

It has been established [29], [30] that

(a) ● *When the controller gain GF in (4.1) is "small enough", the modeling errors will not destabilize the closed-loop system which is open-loop asymptotically stable.*

(b) ● *When the controller gain GF in (4.1) is "large enough", the modeling errors will always destablize the closed-loop system.*

(c) ● *In the absence of structural damping (C' = 0 in (2.1a)), a stablizing linear feedback controller (4.1) does not exist.*

The interesting conclusions concerning (c) are that: (i) the undamped structure is used *most often* in model development for control design, and (ii) the small and highly uncertain structural damping that every real space structure will have is what makes control possible. For successful application, every control scheme relies upon and presumes the existence of a finite amount of structural damping in the open-loop system.

Rate feedback "guarantees" to add some damping in the system under the presumption of infinite bandwidth sensors and actuators [30], but too much rate feedback actually *degrades* output performance (such as the line-of-sight errors in a telescope). See [31] for a spacecraft example of this phenomenon.

4.2 Performance and Modeling Errors

We cite here the performance available with and without modeling errors. If one chooses G and F in (4.1) to be optimal for the model (A_R, B_R, M_R) with noise intensities W_R and V_R respectively for the zero-mean white noise processes $w_R(t)$ and $v_R(t)$, and *if there were no model errors* $e(t) = 0$, then the trade-off between the optimal output performance

$$y_{MS} \overset{\Delta}{=} \lim_{t \to \infty} E\|y\|_Q^2 \qquad (Q > 0) \tag{4.2a}$$

and the optimal input performance

$$u_{MS} \overset{\Delta}{=} \lim_{t \to \infty} E\|u\|_{R_0}^2, \qquad R = R_0\rho > 0 \tag{4.2b}$$

(where ρ is an arbitrary weighting scalar chosen by the designer) would be "hyperbolic" in the sense of Fig. 1.

The output of the reduced model is $y_R = C_R x_R$. Under the assumptions of controllability of (A_R, B_R) and observability of both (A_R, C_R), and (A_R, M_R) [32]

$$G = \frac{1}{\rho} R_0^{-1} B_R^T K, \qquad 0 = K A_R + A_R^T K + C_R^T Q C_R - G_R^T R G_R \qquad (4.3a)$$

$$F = P M_R^T V_R^{-1}, \qquad 0 = P A_R^T + A_R P + D_R W_R D_R^T - F V_R F^T \qquad (4.3b)$$

and small ρ leads to large control gains. In the presence of inevitable modeling errors, Fig. 1 illustrates the eventual (and perhaps rapid) degradation in output performance with increasing control authority (decreasing ρ). This result is not predicted, of course, by the standard linear quadratic Gaussian (LQG) theory since the theory relies upon the absolute fidelity of the mathematical model. Methods to combat such model error effects are the subjects of many papers, but satisfactory solutions have yet to emerge. For the lower order controllers, the low control efforts in Fig. 1 give large errors and the large controls give large errors. Thus, there exists an optimum level of control effort which is a function of controller order.

For any performance metric of the form (4.2), the relationship between stability and the value of the performance metric V is established as follows. Denote the closed-loop plant matrix by A, and the output matrix by C, and ignore nonlinearities f and g. Then for the *closed*-loop system

$$\dot{x} = A x + \mathcal{D} w \qquad (4.4a)$$

$$y = C x, \qquad V \overset{\Delta}{=} \lim_{t \to \infty} E \|y\|_Q^2, \qquad Q > 0, \qquad y^T \overset{\Delta}{=} (y^T, u^T) \qquad (4.4b)$$

If the matrix pair (A, C) is observable and $(A, \mathcal{D})$ is disturbable then V is finite only if A is stable [32]. Thus, relative stability information is contained in the magnitude of V, and we have the result:

Proposition 1: Stability margins with quadratic performance metrics

If observability and disturbability are properties of the closed-loop system (4.4) then y_{MS} serves both as a stability margin and a quadratic performance metric.

Thus, the calculation

$$y_{MS} = \text{tr } P C^T Q C, \qquad 0 = P A^T + A P + \mathcal{D} W \mathcal{D}^T \qquad (4.5)$$

provides an acceptable performance evaluation if the triple $(A, C, \mathcal{D})$ is disturbable, observable. There are three problems which prevent the use of proposition 1 in *guaranteeing* stability of physical systems.

(1) The "physical" system is infinite dimensional.

(2) Observability and disturbability tests are impossible to do with precision on a digital computer, even for a finite-dimensional model.

(3) The physical system is never observable in the following sense.

158

Proposition 2: Unobservability of physical systems

As mathematical models increase in complexity, describing more and more completely the dynamical details of the physical process, the model eventually includes unobservable states with respect to any finite dimensional output vector y.

Proposition 2 explains the sense in which physical systems are never completely observable. This proposition is intuitively verified by imagining that microscopic phenomena such as molecular motions are not going to be observable in the rate gyro measurements. Even though one may not be interested in such trivial examples as molecular motions, the useful point of propositions 1 and 2 is that as far as *stability* is concerned there is no clear way to know when minute motions become "nontrivial". Thus, the propositions serve to remind us that one can never *guarantee* stability of the physical system. This point may be made from another view. Since stability is a *mathematical* property of a *mathematical* model, interpretations of stability for the underlying *physical system* must be accompanied by precise statements of the type of modeling errors ignored. Thus, the term "stability guarantees" refers only to properties of the assumed model, and these comments must be kept in mind when reading the "stability" results of this (or any other) report.

5.0 COMPONENT COST ANALYSIS

The central idea to be discussed in this section is to exploit the precise statement of the optimal control problem in order to predict which system components will make the largest contributions in the total quadratic performance criterion. These components are retained, and the balance is discarded from the model. A "component" of the system can be any subset of coordinates designated by the analyst. For example, all of those coordinates associated with a particular substructure (antenna, solar panel, etc.) might be called one "component" for the purpose of assigning a value to the component for its contribution in the total performance criterion. The general ideas of such "component cost analysis" (CCA) are described in [1, 33-36]. As another example, each *modal* coordinate might be designated as a "component". In this event the procedure becomes *modal* cost analysis (MCA), and the result is that the contribution of each mode is determined for the given quadratic performance criterion. MCA has been applied to models of flexible structures in [37].

5.1 Performance Objectives

The performance o⌐ the dynamical system must be judged by a specific criterion. One may require specific pole locations, focusing only on stability, but that leaves the question of eigenvectors and output performance imprecisely specified. Stability is clearly not a sufficient design goal. The linear quadratic Gaussian (LQG) problem has the advantage that poles *and* zeros are involved in the design specification and that the motion of specific variables of interest can be penalized directly by inserting these variables into the cost function to be minimized. On the other hand, these specified variables may be regulated satisfactorily while other variables become unbounded. The earlier *Proposition 1* states that observability is sufficient to prevent this situation, but it may not be known whether all the potentially unstable motions are observable in the selected variables for minimization. Thus, in oversimplified terms, the "classical" approach is to "design for stability" (and then we must check for performance), whereas the LQG approach is to "design for performance" (and then we must check for stability). Insights into the best of both methods are required for successful designs. In this section the LQG methods are presented.

We define by the vector y the collection of all variables we wish to directly control. For example, if attitude control of the rigid body [described by η_r in (2.3a)] is the objective, then one might choose $y \overset{\Delta}{=} \eta_r$. Alternately, if vibration suppression is the only objective, then $y \overset{\Delta}{=} \dot{\eta}_e$ might be chosen. The choice of a weighting matrix Q in (4.2) is often dictated by energy considerations. As an illustration the choices $\{Q \overset{\Delta}{=} I, y \overset{\Delta}{=} \dot{\eta}_e\}$ lead to $y^T Q y \overset{\Delta}{=}$ kinetic energy in elastic modes. The potential energy in elastic modes is characterized by the choice $\{Q \overset{\Delta}{=} \omega^2, y \overset{\Delta}{=} \eta_e\}$. The expected value operator E is required in (4.2) due to the presence of random "noisy" disturbances in the actuators and sensors (2.1). The control mean-square effort u_{MS} is added to the performance metric, where the scalar ρ is an arbitrary weighting scalar which trades off control performance y_{MS} versus control effort u_{MS}. In practice, ρ must be chosen so that u_{MS} does not exceed the physical bounds of the actuators or structure load design constraints.

The objective of component cost analysis is to decompose the performance metric V into "component costs" V_i,

$$V = y_{MS} + \rho\, u_{MS} = \sum_{i=1}^{n_c} V_i \tag{5.1}$$

where n_c is the number of components in the system and V_i is in the *in situ* contribution of component i. We choose in the next section to define "components" of the open-loop system as "modal" coordinates and their sensitivities. In section 5.3 we choose to define a "component" of the closed-loop system as a state of the dynamical controller. In each case we intend to assign a relative importance to each component by determining its ranking in the manner

$$V_1 \geq V_2 \geq V_3 \geq \cdots \geq V_{n_c} \tag{5.2}$$

and truncate components with small component costs V_i from the system. The next two sections give the necessary mathematics.

5.2 Modal Cost Analysis

Ignoring the sensor and actuator dynamics in this section, and considering the nongyroscopic system,

$$\ddot{\eta}_e + \Delta\dot{\eta}_e + \omega^2 \eta_e = B_e w_a, \qquad \eta_e \in R^N \tag{5.3a}$$

$$E w_a(t) = 0, \qquad E w_a(t) w_a^T(\tau) = W_a \delta(t-\tau) \tag{5.3b}$$

$$V \overset{\Delta}{=} y_{MS} = \lim_{t \to \infty} E \|y\|_Q^2 \tag{5.3c}$$

where only the noisy part of the control forces $u_a = u + w_a$ is considered in this section. *When* N is small enough for closed-loop control calculations, we will *not* ignore the effects of u in model reduction decisions. However, we now presume that N is very large in (5.3a) and u cannot yet be computed.

Our immediate objective is to ascertain the contribution of each mode of the system in the overall cost value V. We presume at this point to be dealing with a system of very high order whose control inputs $u(t)$ are not yet known. Yet to

ignore the source of excitation *altogether* would be a mistake since the *final* judgment of the quality of the model is *in the presence of actuator activity*. Until more is known about $u(t)$, (after control design considerations) we assume that $u = u_w(t)$ is a white noise of random disturbances being propagated through the actuators due to electronic noise in the electrical or magnetic amplifier devices, etc. The consideration of the control and its effect in the model reduction process will be postponed to the next section. To proceed we now need the following definitions.

Definition: *Let x_i be any subset of n_i state variables of the linear system*

$$\dot{x} = Ax + Dw \ , \ Ew(t) = 0 \ , \ Ew(t) \, w^T(\tau) = W \delta(t-\tau)$$

$$y = Cx$$

$$x^T = (\ldots \ x_i^T \ \ldots) \ , \ x_i \in R^{n_i} \ , \ x \in R^{n_x} \ , \ n_x = \sum_{i=1}^{n} n_i \tag{5.4}$$

$$V \overset{\Delta}{=} \lim_{t \to \infty} E \, Y \ , \ Y \overset{\Delta}{=} y^T Q y$$

Here x_i will be called the ith *"component" of the system and the "component cost" associated with component x_i is defined by*

$$V_i \overset{\Delta}{=} \frac{1}{2} \lim_{t \to \infty} E \frac{\partial Y}{\partial x_i} x_i \ , \ \frac{\partial Y}{\partial x_i} \overset{\Delta}{=} (\frac{\partial Y}{\partial x_{i_1}}, \ \ldots, \ \frac{\partial Y}{\partial x_{i n_i}}) \tag{5.5}$$

It is easy to verify that the total cost value V is the sum of all component costs

$$V = \sum_{i=1}^{n} V_i \tag{5.6}$$

and that the component costs may be computed by

$$V_i = tr[C^T Q C X]_{ii} \ , \ 0 = X A^T + A X + D W D^T \tag{5.7}$$

where $[C^T Q C X]_{ii}$ denotes the $n_i \times n_i$ matrix partition of $C^T Q C X$. The above analysis (5.6)-(5.7) of a linear system is called component cost analysis (CCA) [1]. The "components" of a system might be defined from physical or mathematical considerations. From physical considerations x_i might represent any physical component of the system such as the states associated with:

(a) A substructure of the flexible spacecraft (an antenna, a solar panel, a rigid body, etc.)

(b) An electrical or electromechanical element in the system (actuators, sensors, amplifiers, filters, etc.)

From mathematical considerations x_i might represent any mathematical component of the state in any transformed (nonphysical) coordinates. One such example which is common is to define the "components" to be "modes" of the systems. In this case the "component costs" (5.7) are called "modal costs" [1], [36], [37]. We choose to

161

now examine the system using such modal cost analysis (MCA).

Theorem [30]

For the system

$$\ddot{n}_i + 2\zeta_i\omega_i\dot{n}_i + \omega_i^2 n_i = 0 \ , \quad \{n_i(0), \dot{n}_i(0)\} \quad \text{specified, } i = 1, \ldots, N$$

$$y = \sum_{i=1}^{N} (\rho_i n_i + r_i \dot{n}_i)$$

(5.8)

the cost function

$$V \overset{\Delta}{=} \int_0^\infty y^T Q y dt = \sum_{i=1}^{N} V_i$$

(5.9)

decomposes into the modal costs V_i *given by*

$$V_i \overset{\Delta}{=} \frac{1}{2} \frac{\partial V}{\partial x_i(0)} x_i(0) = \frac{1}{4\zeta_i\omega_i} [\|p_i\|_Q^2 + \omega_i^2 \|r_i\|_Q^2] [n_i^2(0) + \frac{\dot{n}_i^2(0)}{\omega_i^2}]$$

$$x_i^T = (n_i, \dot{n}_i)$$

(5.10)

in the limit as $\zeta_i\omega_i \to 0$.

Theorem [30]

For the system

$$\ddot{n}_i + 2\zeta_i\omega_i \dot{n}_i + \omega_i^2 n_i = b_i u_w^T + d_i^T w \ , \quad w \sim N(0, W), \quad u_w \sim N(0, U)$$

$$y = \sum_{i=1}^{N} (p_i n_i + r_i \dot{n}_i)$$

(5.11)

where u_w *and* w *are zero mean uncorrelated white noises with intensities* U *and* W, *the cost function*

$$V \overset{\Delta}{=} \lim_{t\to\infty} E\{y^T Q y\} = \sum_{i=1}^{N} V_i$$

(5.12)

decomposes into the modal costs V_i *given by*

$$V_i \overset{\Delta}{=} \lim_{t\to\infty} \frac{1}{2} E \{\frac{\partial Y}{\partial x_i} x_i\} = \frac{1}{4\zeta_i\omega_i} [\|p_i\|_Q^2 + \omega_i^2 \|r_i\|][\|b_i\|_U^2 + \|d_i\|_W^2] \frac{1}{\omega_i^2}$$

(5.13)

$$Y \overset{\Delta}{=} y^T Q y$$

(5.13)

The proof of the first theorem may be found in [7] and the proof of the second may be found in [8]. The value of (5.13) is that both disturbance and control points of

excitation are considered in the subsequent model reduction decisions. Of course, the *real* purpose for including $b_i^T u_w$ in (5.11) is to anticipate some sort of excitation through the actuators *prior* to the actual design of the control law.

According to modal cost (5.13) the importance of a mode is determined basically by the product of three properties of the mode,

$$V_i = \text{(time constant) (observability)(disturbability + controllability)} \quad (5.14)$$

where mode i is: unobservable in position if and only if $\|p_i\| = 0$, unobservable in rate outputs if and only if $\|r_i\| = 0$, undisturbable from W if and only if $\|d_i\| = 0$, and uncontrollable from u_w if and only if $\|b_i\| = 0$. The expressions (5.10) and (5.13) are general modal costs for matrix second-order systems which have no gyroscopic terms.

5.3 Component Cost Analysis as a Spacecraft Control Design Algorithm

The results are now combined to form a design algorithm for flexible spacecraft control. Each step in the algorithm is discussed and motivated in some detail.

A1. The system under consideration has the form (2.1) with $G' = 0$ and (2.6) holds.

A2. Rate sensors are collocated with the m actuators. An actuator applies a force between two points in the structure, and a sensor measures the time rate of change of the resulting rectilinear displacement. Alternatively, an actuator applies a torque between two points in the structure, and a sensor measures the time rate of change of the resulting angular displacement.

A3. A number of the m actuators equal to the number of rigid body modes are located so that the rigid body modes are controllable.

A4. There are n_r inertially-referenced position sensors located so that rigid modes are observable.

A5. The number of elastic modes calculated for the structure is N.

A6. The largest Liapunov equation of the form (5.7) which can be solved reasonably accurately on the available off-line computer has dimension $2N_L \times 2N_L$.

A7. The largest Riccati equation of the types (4.13), (4.14) which can be solved reasonably accurately on the available off-line computer has dimension $N_R \times N_R$.

A8. The largest controller (4.1) which can be accommodated in the *on-line* computer has dimension N_C, where $N_C \leq N_R \leq 2N_L \leq 2N$.

A9. The highest bandwidth of the available actuators is ω_{BW}.

A10. The parameters considered uncertain are given by $p^T = (\zeta_1, \ldots, \zeta_N | \omega_1^2, \ldots, \omega_N^2 | B_{e1}, \ldots, B_{eN})$.

A11. We have in mind the performance measure

$$V = \lim_{t \to \infty} E\{\alpha y^T Q y + \beta \dot{y}^T Q \dot{y} + \rho u^T R_0 u + \sum_{i=1}^{\nu} \sigma_i^2 (\frac{\partial y}{\partial p_i}^T Q \frac{\partial y}{\partial p_i} + \rho \frac{\partial u}{\partial p_i}^T R_0 \frac{\partial u}{\partial p_i})\} \quad (5.15)$$

where for $\nu = 2N_e + N_e m$, $N_e \overset{\Delta}{=} \frac{1}{2} N_R - n_r$

To illustrate the design procedure we use the simple example

$$\ddot{n}_r = B_r u + D_r w \; , \; n_r \varepsilon R^1$$

$$\ddot{n}_e + 2\zeta\omega n_e + \omega^2 n_e = B_e u + D_e w \; , \; n_e \varepsilon R^4 \qquad (5.16)$$

$$y = P_r n_r + P_e n_e \; , \; z_p = M_{pr} n_r + v_p \; , \; z_r = M_{re} \dot{n}_e + v_r$$

where

$$\zeta = 0.005 \; , \; \omega = \text{diag}\,[1,2,5,10], \; M_{pr} = 10, \; B_r = 1, \; D_r = 10, \; P_r = 1, \quad Q = 100$$

$$\beta = 1 \; , \; E u(t) u^T(\tau) = U\delta(t-\tau) \; , \; U = 1, \; E w(t) w^T(\tau) = W\delta(t-\tau), \; W = 100$$

$$E v_p(t) v_p^T(\tau) = V_p \delta(t-\tau) \; .$$

$$V_p = 10, \; E v_r(t) v_r^T(\tau) = V_r \delta(t-\tau) \; , \; V_r = 0.1, \; P_e = (0.1, \; 1.0, \; 0.01, \; 1.0)$$

$$B_e^T = (0.1, \; 0.01, \; 1.0, \; 0.1)$$

$$D_e^T = (0.01, \; 0.1, \; 0.01, \; 0.001)$$

and we take, for illustrative purposes only,

$$N = 4, \; n_r = 1, \; m = 1, \; N_L = 3, \; N_R = 6, \; N_c = 2$$

The measurements z_p and z_r respectively represent position of the rigid body and a rate measurement. It may be readily verified that all the assumptions (A1–A11) are satisfied.

5.4 The CCA Design Algorithm

Step I: The Preliminary Model Reduction:

Set $\beta = \rho = \sigma_i = 0$ in (5.15) and use MCA (5.13) to reduce the number of vehicle modes from $(N + n_r)$ to $(N_L + n_r')$, where n_r' is the number of rigid body modes surviving the MCA truncation.

Purpose of STEP I: Reduce the number of modes to a tractable number, *but do so with knowledge of $y^T Q y$, the primary control objective.*

Example of STEP I: For (5.16), using (5.13) we have

$$V(n_r) = \infty \; , \; V(n_1) = 1.00, \; V(n_2) = 625.00, \; V(n_3) = 40.40, \; V(n_4) = 0.50 \qquad (5.17)$$

Hence, by the modal cost rule for truncation (5.2), mode 4 is truncated and the retained modes, listed in order of their modal cost (their predicted importance in the problem), are $(n_r, \; n_2, \; n_3, \; n_1)$. The reduced model is

$$\ddot{n}_r = B_r u + D_r w \qquad (5.18a)$$

$$\ddot{n}_e' + 2\zeta\omega' n_e' + \omega'^2 n_e' = B_e' u + D_e' w \qquad (5.18b)$$

$$y = P_r n_r + P'_e n'_e \ , \ z_p = M_{pr} n_r + v_p \ , \ z_r = M'_{re} \dot{n}'_e + v_r \tag{5.18b}$$
<div align="right">cont'd.</div>

where

$$\omega' = \text{diag} [2, 5, 1] \ , \ v_e'^T = (0.10, 0.01, 0.01)$$

$$B_e'^T = (0.01, 1.00, 0.10) \ , \ P'_e = (1.00, 0.01, 0.10)$$

STEP II. Rate Feedback Design:

Set $u = u_0 + u_r$ where

$$u_r = -G_r z_r \ , \ G_r = (B_e'^T B_e')^{-1} B_e'^T (P_e'^T Q P'_e \beta - 2\zeta\omega') B_e' (B_e'^T B_e')^{-1} \tag{5.19}$$

where β is chosen large enough so that $P_e'^T Q P'_e \beta - 2\zeta\omega' > 0$.

Purpose of STEP II: It follows from theorem 6 in [30] that the control (5.19) is the control which is both the optimal measurement z_r feedback control *and* the optimal state feedback control for

$$V = \lim_{t \to \infty} E\{\dot{n}_e'^T [2\zeta\omega' + B_e' G_r B_e'^T] \dot{n}'_e + u_r^T G_r^{-1} u_r\} \tag{5.20}$$

subject to (5.18b). Furthermore, such a control increases the relative stability of all controllable modes and, of course, does not move others. Hence, the system is stable in the presence "of almost all" modal data uncertainties. However, this promise is only valid for those modes within the actuator sensor bandwidths. The main purpose of STEP II is to increase the damping of those modes that MCA has identified as critical to the cost function, and to do this for a *larger* number of modes than the subsequent outer control loop u_0 can be optimized for. This allows a control spillover "cushion" in the sense that the control spillover from u_0 will have to push those residual poles (truncated in the u_0 design but *present* in the u_r design of STEP II) further to the right to destabilize them. Now, in order to be sure that STEP II has provided "spillover protection" for the *same* modes for which such protection will be needed later, it is important that the design of u_r and u_0 be "coordinated" to the extent that they are both concerned with the regulation of the output vector y. The rate feedback design minimizes rates, so choosing u_r to minimize $\dot{y}$ is the rational thing to do. Hence, we may interpret STEP II in the spirit of (5.15) by setting $\alpha = \sigma_i = 0$ with $u \to u_r$. To match this objective as closely as possible with (5.20), we set

$$\rho R_0 = G_r^{-1} \ , \ \beta P_e'^T Q P'_e \approx 2\zeta\omega' + B_e' G_r B_e'^T \tag{5.21}$$

and find the G_r which comes closest (in a least squares sense) to satisfying the second equation in (5.21). The result is (5.19).

Example of STEP II: From (5.18), (5.19)

$$G_r = 7.82 \tag{5.22}$$

The system (5.18) is now described by

$$\ddot{n}_r + B_r G_r B_e'^T \dot{n}'_e = B_r u_0 + v_r w \tag{5.23a}$$

<div align="right">165</div>

$$\ddot{n}_e' + [2\zeta\omega' + B_e'G_rB_e'^T]\,\dot{n}_e' + \omega'^2n_e' = B_e'u_0 + \mathcal{D}_e'w \qquad (5.23b)$$

$$y = P_rn_r + P_e'n_e' \;,\; z_p = M_{pr}n_r + v_p \;,\; z_r = M_{re}'\dot{n}_e' + v_r$$

STEP III: <u>Second Stage of Model Reduction</u>:

Put (5.23b) in the state form

$$\dot{x} = A_0x + B_0u_0 + D_0w \qquad (5.24)$$

$$y = C_0x$$

$$z = M_0x + v \qquad z^T = (z_p^T \,,\; z_r^T)$$

where the $2N_L$ components of x are n_{e_i}' , $\dot{n}_{e_i}'$ $i = 1, \ldots, N_L$ arranged in any order. Compute

$$V_i = [C^TQC_0X_0]_{ii} \;,\; 0 = X_0A_0^T + A_0X_0 + D_0WD_0^T \qquad (5.25)$$

and delete from (5.23b) those modes with the smaller component costs defined by

$$V(n_{e_j}'\,,\; \dot{n}_{e_j}') \overset{\Delta}{=} V(n_{e_j}') + V(\dot{n}_{e_j}') \qquad (5.26)$$

where $V(n_{e_j}')$ and $V(\dot{n}_{e_j}')$ are computed from (5.25). The number of equations *retained* in (5.23b) is $(\frac{1}{2}N_R - n_r^j)$.

Purpose of STEP III: STEP III must reduce the model (5.23) to "Riccati-solvable" dimension N_R to prepare for design of the control u_0.

Example of STEP III: From (5.23b)-(5.26) we have

$$V(n_{e_1}'\,,\; \dot{n}_{e_1}') = 0.60 \;,\; V(n_{e_2}'\,,\; \dot{n}_{e_2}) = 609.20 \;,\; V(n_{e_3}\,,\; \dot{n}_{e_3}') = -0.02 \qquad (5.27)$$

indicating that the equation for $n_{e_3}'(t)$ is to be truncated from (5.23b). The model now is put into the form

$$\dot{x} = Ax + Bu_0 + Dw$$

$$y = Cx \qquad (5.28)$$

$$z = Mx + v$$

where $x^T = (n_r^T, n_{e_2}'^T, n_{e_1}'^T, \dot{n}_r^T, \dot{n}_{e_2}'^T, \dot{n}_{e_1}'^T)$.

STEP IV: <u>Design of the Outer Loop u_0</u>:

Set $\sigma_i = 0 = \beta$, $\rho R_0 = G_r^{-1}$ in (5.15) to get the optimal controller

$$u_o = G\hat{x} \ , \ \dot{\hat{x}} = A\hat{x} + Bu_o + F(z - M\hat{x})$$

$$G = -G_r B^T K \ , \ 0 = KA + A^T K - KBG_r B^T K + C^T QC\alpha \tag{5.29}$$

$$F = XM^T V^{-1} \ , \ 0 = XA^T + AX - XM^T V^{-1} MX + DWD^T$$

Purpose of STEP IV: The value of $R = G_r^{-1}$ has been established earlier. Now the optimal controller for (5.28) has been computed in (5.29), assuming certain parameters, $\sigma_i = 0$. Those modes of the structure that are observable in y are also observable in $\dot{y}$. It is in this sense that the rate feedback controller of STEP II (which focused on the $\dot{y}^T Q \dot{y}$ term) is "coordinated".

Example of STEP IV: The essential data from (5.29) is

$$G = (-3.16E\text{-}01, \ -4.41E\text{-}02, \ -5.77E\text{-}01, \ -8.16E\text{-}01, \ -4.41E\text{-}03, \ 2.62E\text{-}01)$$

$$C = (1.00E\text{+}00, \ 1.00E\text{+}00, \ 1.00E\text{-}01, \ 0, \ 0, \ 0) \ , \quad \alpha = 7.82 \ E\text{-}03^*$$

$$M = \begin{bmatrix} 1.00E\text{+}01 & 0 & 0 & 0 & 0 & 0 \\ 0 & 0 & 0 & 0 & 1.00E\text{-}02 & 1.00E\text{-}01 \end{bmatrix}$$

$$A = \begin{bmatrix} 0 & 0 & 0 & 1 & 0 & 0 \\ 0 & 0 & 0 & 0 & 1 & 0 \\ 0 & 0 & 0 & 0 & 0 & 1 \\ 0 & 0 & 0 & 0 & -7.82E\text{-}02 & -7.82E\text{-}01 \\ 0 & -4 & 0 & 0 & -2.08E\text{-}02 & -7.82E\text{-}03 \\ 0 & 0 & -1 & 0 & -7.82E\text{-}03 & -8.82E\text{-}02 \end{bmatrix}$$

$$D = \begin{bmatrix} 0 & 0 & 0 \\ 0 & 0 & 0 \\ 0 & 0 & 0 \\ 1 & 1.0E\text{+}01 & -7.82E\text{+}00 \\ 1.0E\text{-}02 & 1.0E\text{-}01 & -7.82E\text{-}02 \\ 1.0E\text{-}01 & 1.0E\text{-}02 & -7.82E\text{-}01 \end{bmatrix} , \ B = \begin{bmatrix} 0 \\ 0 \\ 0 \\ 1.00E\text{+}00 \\ 1.00E\text{-}02 \\ 1.00E\text{-}01 \end{bmatrix} , \ F = \begin{bmatrix} 2.51E\text{+}00 & 6.35E\text{-}02 \\ 2.51E\text{-}02 & 6.30E\text{-}04 \\ 2.60E\text{-}03 & 6.78E\text{-}05 \\ 3.16E\text{+}01 & 1.62E\text{+}00 \\ 3.12E\text{-}01 & 1.66E\text{-}02 \\ 3.23E\text{-}02 & 3.36E\text{-}01 \end{bmatrix}$$

*Multiplying (5.15) by $1/\alpha$ yields a parameter ρ/α to be selected to achieve an acceptable control effort. The best value of α is therefore determined from Fig. 1 as that choice which corresponds to the lowest point on the dotted curve of Fig. 1. This point is found numerically, first picking an α then truncating the controller to the desired order N_c, and repeating this process for a new α. Thus, the above value of α was found _after_ several passes through STEP V.

167

STEP V: Controller Reduction:

The optimal system of STEP IV is

$$\dot{x} = \begin{pmatrix} \dot{x} \\ \dot{\hat{x}} \end{pmatrix} = \begin{bmatrix} A \cdot & BG \\ FM & A+BG-FM \end{bmatrix} \begin{pmatrix} x \\ \hat{x} \end{pmatrix} + \begin{bmatrix} D & 0 \\ 0 & F \end{bmatrix} \begin{pmatrix} w \\ v \end{pmatrix} = Ax + Dw$$

$$(5.30)$$

$$y = \begin{pmatrix} y \\ u \end{pmatrix} = \begin{bmatrix} C & 0 \\ 0 & G \end{bmatrix} \begin{pmatrix} x \\ \hat{x} \end{pmatrix} = Cx$$

which is now to be evaluated by criterion (5.15). First we show the simpler case of known parameters $(\sigma_i = 0)$.

STEP V-A: Controller Reduction With Certain Parameters $(\sigma_i = 0)$:

Delete from the controller

$$\dot{\hat{x}} = [A+BG-FM]\hat{x} + Fz , \quad \hat{x} \in R^{N_R}$$

$$(5.31)$$

$$u_0 = G\hat{x}$$

those states $(\hat{n}_i, \dot{\hat{n}}_i)$ with the smallest costs $V(\hat{n}_i, \dot{\hat{n}}_i) = V(\hat{n}_i) + V(\dot{\hat{n}}_i)$ defined by

$$V_i = [C^T Q C X]_{jj} , \quad 0 = X A^T + A X + D W D^T , \quad Q = \text{block diag } [Q, G_r^{-1}]. \quad (5.32)$$

for $j = i + N_R$, $i = 1, \ldots, N_R$ where $V_i = V(\hat{n}_i)$ and $V_{i+1} = V(\dot{\hat{n}}_i)$ if $\hat{x}$ has the form $\hat{x}^T = (\ldots \hat{n}_i, \dot{\hat{n}}_i, \ldots)$. This yields the reduced controller

$$\dot{\hat{x}}_R = A_R \hat{x}_R + F_R z , \quad u_0 = G_R \hat{x}_R , \quad \hat{x}_R \in R^{N_C}$$

$$(5.33)$$

where A_R is obtained by deleting the indicated rows and columns of $[A+BG-FM]$, F_R is obtained by deleting the same rows of F, and G_R is obtained by deleting the same columns of G.

Purpose of STEP V-A: Reduce the order of the controller (5.31) to the order N_C acceptable by on-line software limitations.

Example of STEP V-A: The calculation (5.32) reveals that the *cost-ordered* components of the controller are

$$\hat{x}^T = (\hat{n}_r, \dot{\hat{n}}_r, \hat{n}_{e_2}, \dot{\hat{n}}_{e_2}, \hat{n}_{e_1}, \dot{\hat{n}}_{e_1})$$

$$(5.34)$$

Hence, if only 4 components of the controller are to be retained they would be

$$\hat{x}_R^T = (\hat{n}_r, \dot{\hat{n}}_r, \hat{n}_{e_2}, \dot{\hat{n}}_{e_2})$$

$$(5.35)$$

and if only 2 components of the controller are to be retained, they would be

168

$$\hat{x}_R^T = (\hat{n}_r, \hat{\dot{n}}_r) \tag{5.36}$$

The corresponding reduced controller dynamics are deduced from (5.32) in the manner described above.

STEP V-B: Controller Reduction With Uncertain Parameters ($\sigma_i > 0$)

Delete from the controller (5.31) those states $\hat{x}_i$ with the smallest component costs $V_i = V(\hat{x}_i, \hat{x}_{i_p})$ computed by

$$V_i = \sum_{k=0}^{\nu} [C_\delta Q_\delta C_\delta X_\delta]_{jj} , \quad 0 = X_\delta A_\delta^T + A_\delta X_\delta + D_\delta W D_\delta^T \tag{5.37}$$

for $j = (i + N_R + 2N_R k)$, $i = 1, \ldots, N_R$, where

$$A_\delta = \begin{bmatrix} A & 0 \\ A_p & \tilde{A} \end{bmatrix}, \quad D_\delta = \begin{bmatrix} D \\ D_p \end{bmatrix}, \quad C_\delta = \begin{bmatrix} C & 0 \\ C_p & \tilde{C} \end{bmatrix} \tag{5.38}$$

$$Q_\delta = \text{block diag } [Q, \sigma_1^2 Q, \ldots, \sigma_\nu^2 Q]$$

and where Q is defined by (5.32)

Purpose of STEP V-B: The component costs (5.37) represent the sum

$$V_i = V(\hat{x}_i) + \sum_{k=1}^{\nu} V((\hat{x}_i)_{pk}) \tag{5.39}$$

where the total cost is given by (5.15) with $\beta = 0$. By use of (5.38) and (5.30) the total cost may be written

$$V = \text{tr } [C_\delta Q_\delta C_\delta X_\delta] = \sum_{i=1}^{N_R} V(\hat{x}_i, \hat{x}_{ip}) + \sum_{i=1}^{N_R} V(x_i, x_{ip}), \quad x_{ip} \overset{\Delta}{=} \frac{\partial x_i}{\partial p} \tag{5.40}$$

where V_i in (5.37) picks out the first terms in (5.40) due to $\hat{x}_i$. The remaining terms in (5.40) are due to the states x_i and their sensitivities, which are not needed for this design but may be computed from the remaining terms in (5.37). The particular range of indices in the V_i computation of (7.58) is due to the choice of coordinates represented by (5.38). Of course, any other choice of coordinates may be chosen with an attendant change in the range of indices jj in (5.37) to identify those variables of the augmented state vector X representing controller dynamics and their sensitivites, $\hat{x}_i$ and $\hat{x}_{ip}$. STEP V-B allows sensitivity considerations to influence the controller reduction, whereas STEP V-A assumes the parameters are known a priori. There is an additional computational burden in STEP V-B and for this step assumption A8 must be changed to

$$N_c \leq 2N_R \leq 2 N_L \leq 2N$$

due to the fact that (5.37) decomposes into (ν+1) Liapunov equations *each* of which

is $2N_R \times 2N_R$ [35].

Example of STEP V-B: Assume uncertain frequencies ω_1, ω_2. Hence

$$p^T = (\omega_1, \omega_2), \quad \bar{p}^T = (1, 2)$$

$$\sigma_1^2 = E(\omega_1 - \bar{\omega}_1)^2 = \sigma_0^2 = 100$$

$$\sigma_2^2 = E(\omega_2 - \bar{\omega}_2)^2 = i\sigma_0^2 = 2(100) = 200$$

Carrying out the computations (5.37) we find that the controller states arranged in their cost order are

$$\hat{x}^T = (\hat{n}_{e1}, \dot{\hat{n}}_{e1}, \hat{n}_r, \dot{\hat{n}}_r, \hat{n}_{e2}, \dot{\hat{n}}_{e2}) \tag{5.41}$$

Hence if only a fourth-order controller is desired we would choose

$$\hat{x}_R^T = (\hat{n}_{e1}, \dot{\hat{n}}_{e1}, \hat{n}_{r1}, \dot{\hat{n}}_r) \tag{5.42}$$

If only a second-order controller is desired we would choose

$$\hat{x}_R^T = (\hat{n}_{e1}, \dot{\hat{n}}_{e1}) \tag{5.43}$$

Controller (5.43) would lead to instability since the rigid body mode has been truncated. By comparing (5.34), (5.35) and (5.36), respectively, with (5.41), (5.42) and (5.43), the influence of parameter sensitivity on the reduced controller design can clearly be seen. For example, (5.34) indicates that $(\hat{n}_{e2}, \dot{\hat{n}}_{e2})$ are more important than $(\hat{n}_{e1}, \dot{\hat{n}}_{e1})$ in the nominal optimal controller (5.31), whereas (5.41) indicates that, from parameter sensitivity consideration, $(\hat{n}_{e1}, \dot{\hat{n}}_{e1})$ is more important.

6.0 CONCLUSIONS

We have outlined in some detail many of the critical problems associated with the control of highly damped flexible structures. The practical problems include:

- High performance
- Assembly in space, configuration changes
- On-line controller software design
- Lack of test data

Underlying all of these practical problems is the central problem of modeling errors. To justify the expense of a space structure, the performance requirements will necessarily be very severe. On the other hand, the absence of economical tests precludes the availability of reliable data before flight. Thus, *a greater burden of responsibility is placed upon analytical methods* in the design *without*

the benefit of test data for a system nearly *unstable without control.* This is the triple jeopardy faced by all flexible space structure designs.

Some precise statements have been verified concerning the performance of such structures in the presence of controllers based upon erroneous models. The modeling errors can always be classified into four categories: (1) parameter errors, (2) model order errors, (3) disturbance errors and (4) neglected nonlinearities. Finally, a design algorithm is offered which has these properties:

1. Provides damping for a larger number of modes than the optimal attitude controller controls. This rate measurement feedback design, with collocated rate sensors and actuators, provides control spillover protection for the truncated controller

2. Coordinates the rate feedback design with the attitude control design by use of a similar cost function

3. Provides model reduction and controller reduction decisions which are systematically connected to the mathematical statement of the control objectives and the disturbance models

There are many possible versions of the CCA design algorithm. Some versions would require more computation with some attendant improvement in performance. For example, other choices of coordinates besides "modal" coordinates may provide better reduced models in Section 5. However, in the interest of clarity the procedures have been explained with some economy of detail.

Flexible space structure control is indeed a fitting challenge to the best of available control and estimation theories. And, conversely, out of such challenging examples come pointed needs for new theory.

REFERENCES

1. Skelton, R.E., and Yousuff, A., "Component Cost Analysis of Large Scale Systems," Control and Dynamic Systems, Vol. 18, Academic Press, 1982.

2. Johnson, C.R., "On an Approach to Distributed System Adaptive Control as Applied to Regulation of a Flexible AMCD," Paper presented at the Int. Workshop on Applications of Adaptive Control, Yale University, New Haven, Ct., August 1979.

3. Ljung, L., Söderström, T., and Gustavsson, I., "Counterexamples to General Convergence of a Commonly Used Recursive Identification Method," IEEE Trans. Auto. Control, Vol. AC-20, No. 5, October 1975, pp. 643-652.

4. Astrom, K.J., and Eykhoff, P., "System Identification: A Survey," Automatica, Vol. 7, No. 2, March 1971, pp. 123-162.

5. Akaike, H., "A New Look at the Statistical Model Identification," IEEE Trans. Auto. Control, Vol. AC-19, No. 6, December 1974, pp. 716-723.

6. Akaike, H., "Information Theory and an Extension of the Maximum Likelihood Principle," Paper presented at the IEEE Second International Symposium on Information Theory, Armenia, USSR, September 1971.

7. Kashyap, R.L., "A Bayesian Comparison of Different Classes of Dynamic Models Using Empirical Data," IEEE Trans. Auto. Control, Vol. AC-22, No. 5, October 1977, pp. 715-727.

8. Kashyap, R.L., "Inconsistency of the AIC Rule for Estimating the Order of Auto-regressive Models," IEEE Trans. Auto. Control, Vol. AC-25, No. 5, October 1980. pp. 996-998.

9. Schwarz, G., "Estimating the Dimension of a Model," The Annals of Statistics, Vol. 6, No. 2, 1978.

10. Pilkington, W.C., "Vehicle Motions as Inferred from Radio-Signal-Strength Records," External Publication No. 551, Jet Propulsion Laboratory, Pasadena, CA, September 1958.

11. "A Collection of Technical Papers." AIAA/NASA Conference on Advanced Technology for Future Space Systems, AIAA, N.Y., 1979.

12. Nissim, E., "Flutter Suppression and Gust Alleviation Using Active Controls," NASA TN D-8212, 1976. Also see J. Guidance and Control, Vol. 2, No. 5, September-October 1979, pp. 395-401.

13. Nordell, W.J., "Active Systems for Blast-Resistant Structures," Technical Report R-611, Naval Civil Engineering Laboratory, Post Hueneme, CA, February 1969.

14. Balas, M.J., "Some Trends in Large Space Structure Control Theory: Fondest Hopes, Wildest Dreams," IEEE Trans. Auto. Control, Vol. AC-27, No. 3, June 1982, pp. 522-535.

15. Zienkiewicz, O., The Finite Element Method in Engineering Science, McGraw-Hill, NY, 1971.

16. Oden, J.T., and Reddy, J., An Introduction to the Mathematical Theory of Finite Elements, Wiley, NY, 1976.

17. Likins, P.W., "Finite Element Appendage Equations, for Hybrid Coordinate Dynamic Analysis," NASA CR-123213, 1979.

18. Skelton, R.E., and Likins, P.W., "Techniques of Modeling and Model Error Compensation in Linear Regulator Problems," Control and Dynamic Systems, Vol. 14, edited by C.T. Leondes, Academic Press, 1978, pp. 1-101.

19. Mehra, R.K., and Lainiotis, D.G., System Identification: Advances and Case Studies, Academic Press, 1976.

20. Eykhoff, P., System Identification, Parameter and State Estimation, Wiley, 1974.

21. Johnson, C.R., "Approaches to Adaptive Digital Control Focusing on the Second Order Modal Descriptions of Large, Flexible Spacecraft Dynamics," Proceedings of the Second VPI&SU/AIAA Symposium on Dynamics and Control of Large Flexible Spacecraft, Blacksburg, Va., June 1979, pp. 301-316. Also see IEEE Trans. Auto. Control, Vol. AC-25, No. 4, August 1980, pp. 697-702.

22. Balas, M.J., "Feedback Control of Flexible Systems," IEEE Trans. Auto. Control, Vol. AC-23, No. 4, 1978, pp. 673-679.

23. Sesak, J.R., "Control of LSS Via Singular Perturbation Optimal Control," AIAA Paper No. 78-1690, September 1978.

24. Sesak, J.R., Likins, P.W., and Coradetti, T., "Flexible Spacecraft Control by Model Error Sensitivity Suppression," Proceedings of the Second VPI&SU/AIAA Symposium on Dynamics and Control of Large Flexible Spacecraft, Blacksburg, Va., June 1979, pp. 349-368.

25. Skelton, R.E., "Adaptive Orthogonal Filters for Compensation of Model Errors in Matrix-Second-Order Systems," J. Guidance and Control, Vol. 4, No. 2, March-April 1981, pp. 214-221.

26. Skelton, R.E., and Likins, P.W., "Orthogonal Filters for Model Error Compensation in the Control of Nonrigid Spacecraft," J. Guidance and Control, Vol. 1, No. 1, January-February 1978, pp. 41-49.

27. Potter, J.E., and Ginter, S.D., "A New Concept in Adaptive Structural Control," Proceedings of the Second VPI&SU/AIAA Symposium on Dynamics and Control of Large Flexible Spacecraft, Blacksburg, Va., June 1979, pp. 331-348.

28. Johnson, C.D., "State Variable Design Methods May Produce Unstable Feedback Controllers." Int. J. Control, Vol. 29, No. 4, April 1979, pp. 607-620.

29. Green, C., and Stein, G., "Inherent Damping, Solvability Conditions and Solutions for Structural Vibration Control," Proceedings of the 18th IEEE Conference on Decision and Control, Fort Lauderdale, Fla., December 1979, pp. 230-232.

30. Skelton, R.E., "Control Design of Flexible Spacecraft," Theory and Applications of Optimal Control in Aerospace Systems, AGARDograph No. AG-251, edited by P. Kant, July 1981, Chapter 8, pp. 1-27.

31. Skelton, R.E., and Yousuff, A., "A Solar Optical Telescope Controller Design by Component Cost Analysis," paper presented at IFAC Symposium on the Control of Distributed Parameter Systems, International Federation on Automatic Control, Toulouse, France, June 1982.

32. Kwarkernaak, H., and Sivan, R., Linear Optimal Control Systems, Wiley, NY, 1972.

33. Skelton, R.E., "Cost Decomposition of Linear Systems With Application to Model Reduction," International J. Control, Vol. 32, No. 6, 1980, pp. 1031-1055.

34. Skelton, R.E., "A Control Design Algorithm for Flexible Structures," Proceedings of the 19th IEEE Conference on Decision and Control and Symposium on Adaptive Processes, Vol. 2, December 1980, pp. 1232-1234.

35. Skelton, R.E., and Yedavalli, R.K., "Modal Cost Analysis of Flexible Space Structures With Uncertain Modal Data," Proceedings of the 19th IEEE Conference on Decision and Control and Symposium on Adaptive Processes, Vol. 2, December 1980, pp. 792-794.

36. Skelton, R.E., and P.C. Hughes, "Modal Cost Analysis for Linear Matrix Second Order Systems," J. Dynamic Systems, Measurement and Control, Vol. 102, September 1980.

37. Skelton, R.E., Hughes, P.C., "Flexible Space Structure Model Reduction by Modal Cost Analysis," Proceedings of the Second VPI&SU/AIAA Symposium on Dynamics and Control of Large Flexible Spacecraft, Blacksburg, Va., June 1979, pp. 641-660.

174
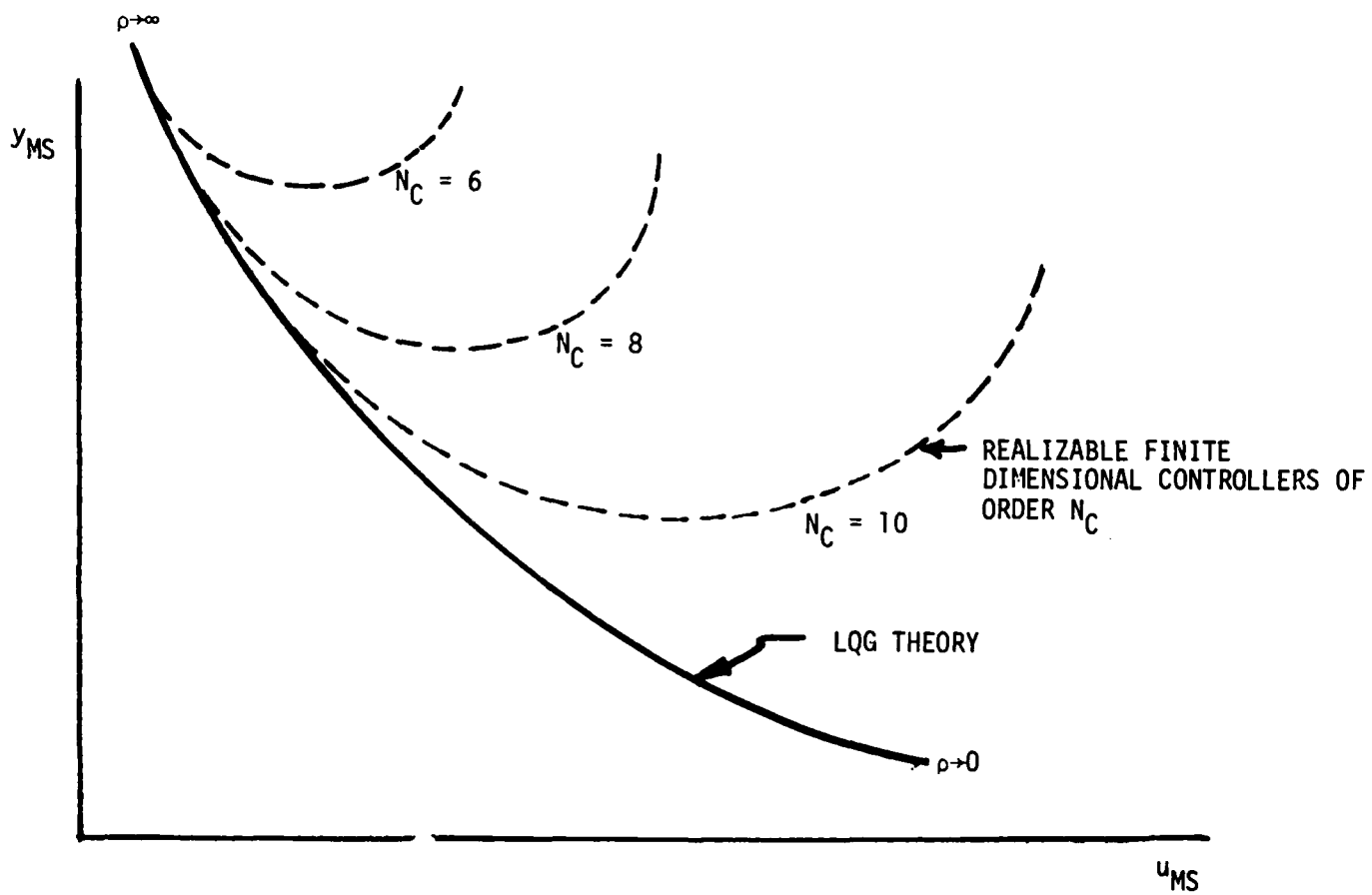
Figure 1. Performance versus control effort to minimize $V = y_{MS} + \rho\, u_{MS}$.

OPTIMAL LARGE-ANGLE MANEUVERS
WITH VIBRATION SUPPRESSION

James D. Turner and Hon M. Chun
The Charles Stark Draper Laboratory
Cambridge, Massachusetts

John L. Junkins
Virginia Polytechnic Institute
and State University
Blacksburg, Virginia

1.0 INTRODUCTION

Many proposed large spacecraft have missions which embody two challenging requirements:

(1) Rapid reorientation maneuvers ("slews")

(2) Rapid vibration arrest and fine pointing upon completion of the slew

The objective of this discussion is to overview some methods and applications which determine optimal maneuver controls. Aside from the usual modeling issues for large space structures, the large-angle maneuver problem is complicated by the inherent nonlinearity (i.e., three-dimensional rotational maneuvers are nonlinear even for a rigid spacecraft). Of course, additional nonlinear effects arise when even small deflections are considered due to kinematic effects such as rotational stiffening. Thus, we have the dual curse of nonlinearity and high dimensionality.

One can approach optimal maneuvers in a fashion analogous to trajectory design for launch vehicles. A nominal open-loop maneuver could be determined *a priori*; realtime feedback controls would then determine small perturbations to the open-loop controls to account for modeling imperfections and external disturbances. For many vehicles and missions, it may prove satisfactory to determine open-loop maneuvers which suppress vibration and simply forego feedback controls until the terminal finepointing phase after completion of each slew. Of course the terminal vibration suppression and fine-pointing problem is naturally suited to feedback control. In this paper, we emphasize determination of the optimal open-loop nonlinear maneuvers (slews). The slew controls are determined in such a fashion that vibration of selected modes is penalized en route and arrested upon arrival at the target state. Some attention is also given to large, slow, linear maneuvers for which the associated slew controls can be cast in feedback form.

We initially summarize the main aspects of optimal control theory which are implicit in the remaining developments. We then discuss the essential ideas involved in a class of methods ("continuation" or "homotopy" methods) which we have found most useful in solving the resulting two-point boundary value problems. Several low-dimensioned, nonlinear maneuvers of multiple rigid-body configurations using optimal momentum transfer are discussed. Several linear and nonlinear flexible-body maneuvers are then presented and include distributed controls, vibration suppression/arrest, and computational issues. Finally, we summarize the status of our present work and the key problem areas in which future research appears most urgent.

2.0 NECESSARY CONDITIONS FOR OPTIMAL MANEUVERS

We will consider here only finite dimensional systems which can be satisfactorily modeled by a system of generally nonlinear ordinary differential equations of the form

$$\dot{\underline{x}} = \underline{f}\,(t,\,\underline{x},\,\underline{u}) \qquad\qquad (2.1)$$

where $\underline{x}$ is the $n \times 1$ state vector, $\underline{u}$ is the $m \times 1$ control vector, and $\underline{f}$ is an $n \times 1$ vector of generally nonlinear functions of all arguments. Suppose, for the present discussion, that we are concerned only with the fixed-end point problem for which the boundary conditions

178

$$\underline{x}~(t_o) = \underline{x}_o \qquad \underline{x}~(t_f) = \underline{x}_f \tag{2.2}$$

are fully specified. The more general circumstance in which some boundary conditions are free or are constrained to lie on a terminal manifold is considered in references 1-6; essentially, some of the 2n conditions (2.2) are replaced by appropriate transversality conditions. The number of boundary conditions will remain 2n. Suppose we seek an optimal control vector $\underline{u}(t)$ initiating at $\underline{x}_o$ and terminating at $\underline{x}_f$, subject to the requirement that a performance functional of the form

$$J = \int_{t_o}^{t_f} F(t, \underline{x}, \underline{u})dt \tag{2.3}$$

is minimized. For the present discussion, we restrict $\underline{u}(t)$ to be continuous with two continuous derivatives. The necessary conditions (Pontryagin's principle form) involve the Hamiltonian functional

$$H = F + \underline{\lambda}^T \underline{f} \tag{2.4}$$

where $\underline{\lambda}$ is an $n \times 1$ co-state vector of Lagrange multipliers satisfying the adjoint differential equation

$$\underline{\dot{\lambda}} = -\left\{\frac{\partial H}{\partial \underline{x}}\right\}^T \tag{2.5}$$

and the optimal control is determined at each instant by requiring $H(t,\underline{x},\underline{\lambda},\underline{u})$ to be minimized with respect to admissible $\underline{u}(t)$; for twice differentiable $\underline{f}, \underline{u}$, this requirement yields the conditions

$$\frac{\partial H}{\partial \underline{u}} = \underline{0}, \frac{\partial^2 H}{\partial \underline{u}^2} \text{ positive definite} \tag{2.6}$$

The conditions (2.6) can usually be solved for $\underline{u}(t)$ to determine the optimal control in the functional form

$$\underline{u} = \underline{g}~(t,\underline{\lambda},\underline{x}) \tag{2.7}$$

Finally, substitution of (2.7) into (2.1) and (2.5) allows us to eliminate $\underline{u}$ and obtain the 2nth order system

$$\underline{\dot{x}} = \underline{F}(t,\underline{x},\underline{\lambda}) \qquad \underline{x}(t_o) = \underline{x}_o \qquad \underline{x}(t_f) = \underline{x}_f$$

$$\underline{\dot{\lambda}} = \underline{G}(t,\underline{x},\underline{\lambda}) \tag{2.8}$$

The above formulation is summarized in figure 1.

Since the 2n boundary conditions are split, we have a two-point boundary value problem (TPBVP). These differential equations (2.8) are generally nonlinear, often exhibit "stiff" character, and generally resist solution except by iterative numerical methods. Indeed, a substantial fraction of the optimization literature ("direct" methods) have been motivated by the numerical difficulties one often encounters in a frontal attack upon equations (2.8). In essence, most of the direct methods are iterative function space gradient methods which "directly" adjust $\underline{u}(t)$ and iteratively solve equations (2.1) to minimize (2.3) and satisfy terminal boundary conditions. Numerical experience suggests that the direct methods efficiency degrades rapidly as the problem dimension increases, especially if one does not possess "good" starting estimates for $\underline{u}(t)$; so the issue of which algorithm to apply remains open. The recent progress of references 1-6 suggests that improved "indirect" algorithms based upon continuation method iterative solutions of equations (2.8) are indeed feasible; the methods discussed herein are of this type. The main recent progress is associated with greatly decreased reliance upon "sufficiently good starting estimates" implicit in the continuation family of algorithms. The essential ideas are indicated in the following section.

3.0 CONTINUATION METHODS FOR SOLUTION OF TWO-POINT BOUNDARY VALUE PROBLEMS

The basic approach is to embed the problem you wish to solve into a one parameter (α) family containing two prominent members:

> For $\alpha = 0$, the family reduces continuously to a problem whose solution is available
>
> For $\alpha = 1$, the family reduces continuously to the problem whose solution is sought

By sweeping α, one can generate a sequence of neighboring problems (e.g., for $0 = \alpha_1 < \alpha_2 < \alpha_3 < , \ldots < \alpha_N = 1$); by solving each (α_k) problem in sequence, we determine "stepping stone" solutions which provide, by extrapolation, starting iteratives for the next (α_{k+1}) problem. In principle, arbitrarily close starting iteratives can be determined. Except for certain singular events (e.g., bifurcation points), this approach can very nearly guarantee convergence. Within this approach, there exists a variety of ways to construct the family (homotopy chain). The manner in which the homotopy family is constructed has definite impact upon the ensuing algorithms. We have made productive use of three continuation methods which we now summarize.

3.1 Continuation Method 1. Differential Equation Embedding

The nonlinear system (2.8) is written in the form shown in equation (3.1). This form is quite natural for many weakly nonlinear problems; of course, $\alpha = 1$ is the true physical value, and $\alpha = 0$ results in a linear problem. Provided the linear boundary value problem can be solved (which is not a foregone conclusion, especially for high degree-of-freedom systems which possess a wide eigenvalue spectrum, i.e., the system is large and stiff), then sweeping α in principle generates a family of neighboring problems which can be iterated for $\underline{\lambda}_o(\alpha)$ to satisfy the final boundary condition $\underline{x}(t_f) = \underline{x}_f$. Each Newton iteration for $\underline{\lambda}_o(\alpha)$ can be initiated with an estimate based upon extrapolating the neighboring α solutions. This method is used to solve for optimal maneuvers for several cases in the developments below.

180

The nonlinear state and co-state differential equations (2.8) are rearranged and the continuation parameter (α) introduced so that

$$\dot{\underline{x}} = A_{11}\,\underline{x} + A_{12}\underline{\lambda} + \alpha \ \{\text{nonlinear terms}\}$$

$$\tag{3.1}$$

$$\dot{\underline{\lambda}} = A_{21}\,\underline{x} + A_{22}\underline{\lambda} + \alpha \ \{\text{nonlinear terms}\}$$

For $\alpha = 0$ $\longrightarrow$ linear problem

For $\alpha = 1$ $\longrightarrow$ problem of interest

Sweep α to generate a family of neighboring dynamical systems; for each α, iterate $\underline{\lambda}_o(\alpha)$ using Newton's method to satisfy the terminal boundary conditions using neighboring α solutions for $\underline{\lambda}_o(\alpha)$ to start each iteration.

With reference to equations (3.2) through (3.6), we consider the Method 2, fixed-point algorithm continuation method of reference 7. This method is called a "fixed point algorithm" since it has the property that $\underline{\lambda}_o = \underline{C}$ is the solution of the homotopy family at $\alpha = 0$ for any arbitrary specified $\underline{C}$. This algorithm is most useful if one wishes to use an approximate initial guess $\underline{C}$ for $\underline{\lambda}_o$ which is too far from the solution to permit reliable convergence using Newton's method.

Method 3 (boundary condition embedding) constructs a homotopy family of boundary conditions for those problems which have the property:

> The general nonlinear problem degenerates continuously to a linear problem for certain choices on the specified state boundary conditions. As an example, three-dimensional rigid-body maneuvers are nonlinear, but the single-axis maneuver special cases are linear.

By sweeping α, the specified initial and final boundary conditions are varied from the easily solved problem at $\alpha = 0$ to the problem of interest at $\alpha = 1$.

3.2 Continuation Methods 2 and 3

Method 2. Fixed-Point Algorithm:

An algebraic root solving illustration is:

$$\underline{F}(\underline{x}) = \underline{0} \tag{3.2}$$

Initial guess: $\underline{x} \cong \underline{c}$

Construct the homotopy family

$$\underline{H}\,[\underline{z}(\alpha),\alpha] = \underline{F}\,[\underline{z}(\alpha)] - (1 - \alpha)\,\underline{F}\,(\underline{c}) = \underline{0} \tag{3.3}$$

Note the properties:

$$\underline{H}\left[\underline{z}(0),0\right] = \underline{0} \tag{3.4}$$

If we take $\underline{z}(0) = \underline{c}$ arbitrary "fixed point" and

$$\underline{H}\left[\underline{z}(1),1\right] \equiv \underline{F}\left[\underline{z}(1)\right] = \underline{0} \tag{3.5}$$

thus $\underline{z}(1) \equiv \underline{x}$ by comparison of equations (3.2) and (3.5).

Method 3. Boundary Condition Embedding:

When the TPBVP at hand can be easily solved if the <u>specified</u> boundary conditions are given a special set of values, then we can construct the homotopy family of boundary conditions:

$$
\begin{bmatrix}
\text{CONTINUATION} \\
\text{VECTOR OF} \\
\text{SPECIFIED} \\
\text{B.C.}
\end{bmatrix}
= \alpha
\begin{bmatrix}
\text{FINAL DESIRED} \\
\text{VECTOR OF} \\
\text{SPECIFIED} \\
\text{B.C.}
\end{bmatrix}
+ (1 - \alpha)
\begin{bmatrix}
\text{SPECIAL SET OF} \\
\text{SPECIFIED B.C.,} \\
\text{...FOR WHICH THE} \\
\text{TPBVP CAN BE} \\
\text{SOLVED}
\end{bmatrix}
\tag{3.6}
$$

These considerations are addressed to the important issue of decreasing the amount of prior information required to start an iterative solution of equations (2.8). For high-dimensional problems with high sensitivity to $\underline{\lambda}_0$, these methods are most important; it may prove impractical to extract a solution via the classical "shooting technique." A separate and fairly well-developed subject matter concerns the calculation of the successive numerical solutions (i.e., for each α). The most popular method is Newton's root solving method in conjunction with Runge-Kutta integrations; $\underline{\lambda}_0$ is adjusted based upon linearizing the n boundary condition residuals dependence upon $\underline{\lambda}_0$ about the previous iteration.

Another popular class of procedures is the weighted residual methods. In this approach, each state and co-state variable is expanded with undetermined coefficients times a finite set of specified functions of time (typically, a set of orthogonal polynomials). The coefficients of the series are adjusted by solving a linear system of equations obtained from substituting the expansions into the equations of motion, linearizing, and evaluating these linear equations at a sufficient number of times along the previous trial trajectory. This class of procedures seems particularly well-suited to stiff differential equations for which the traditional (e.g., Runge-Kutta) numerical methods prove unstable; however, the large linear algebraic systems encountered are a deterrent to many degree-of-freedom applications.

We mention a third approach, the quasi-linearization method of Miele (the method of particular solutions), as developed in references 5, 6, and 8. This approach forms successive iterations by: (i) linearizing the departure motion differential equations along the previous trial solution of equations (2.8); (ii) determining a set of n coefficients to linearly combine n trial integrations of these linear equations to produce a new departure motion which satisfies the boundary conditions; and (iii) adding the departure motion to the previous iteration to produce the next

trial solution. The major disadvantage of this approach is the necessity to store each trial trajectory; for many state variables, this storage penalty becomes excessive.

All of the above methods are developed in detail in reference 4 and compared using a common set of example problems. Here we note that all of these have been used successfully (refs. 4, 6) to calculate optimal nonlinear spacecraft maneuvers; if the trial trajectories of equations (2.8) can be integrated accurately using Runge-Kutta methods, then we find the classical Newton iterations used (if necessary) in conjunction with a continuation method (to provide accurate starting iterations) to be preferred. However, for very stiff differential equations, one must resort to other methods such as those discussed above, or indeed, abandon the indirect approach altogether. It is apparent, however, that a large fraction of the optimal nonlinear maneuver problems of practical interest can be solved by the indirect methods illustrated herein and documented in the references.

4.0 OPTIMAL LARGE-ANGLE MANEUVERS OF MULTIPLE REACTION WHEEL SPACECRAFT

With reference to figure 2, we consider the dynamics of a generally asymmetric vehicle B having three identical rotors aligned with the principal axes. The vehicle is maneuvered via internal motor torques $[u_1(t), u_2(t), u_3(t)]$ applied to the wheels, $[-u_1(t), -u_2(t), -u_3(t)]$ applied to assumed rigid body B, and external torques $[L_1(t), L_2(t), L_3(t)]$ from unspecified actuators. The equations of motion are equations (4.1) - (4.3).

Kinematics:

$$\dot{\beta}_0 = (-\omega_1\beta_1 - \omega_2\beta_2 - \omega_3\beta_3)/2$$

$$\dot{\beta}_1 = (\omega_1\beta_0 - \omega_2\beta_3 + \omega_3\beta_2)/2$$

$$\dot{\beta}_2 = (\omega_1\beta_3 + \omega_2\beta_3 + \omega_3\beta_1)/2 \tag{4.1}$$

$$\dot{\beta}_3 = (-\omega_1\beta_2 + \omega_2\beta_1 + \omega_3\beta_0)/2$$

Spacecraft Dynamics:

$$\dot{\omega}_1 = -\frac{1}{I_1 - J}(I_3 - I_2)\omega_2\omega_3 + h_3\omega_2 - h_2\omega_3 + \frac{L_1 - u_1}{I_1 - J}$$

$$\dot{\omega}_2 = -\frac{1}{I_2 - J}(I_1 - I_3)\omega_1\omega_3 + h_1\omega_3 - h_3\omega_1 + \frac{L_2 - u_2}{I_2 - J} \tag{4.2}$$

$$\dot{\omega}_3 = -\frac{1}{I_3 - J}(I_2 - I_1)\omega_1\omega_2 + h_2\omega_1 - h_1\omega_2 + \frac{L_2 - u_3}{I_3 - J}$$

Wheel Dynamics:

$$\dot{h}_i = -J\dot{\omega}_i + u_i \qquad i = 1,2,3 \tag{4.3}$$

4.1 Optimal Maneuver Necessary Conditions for the Four–Body Configuration

Performance Indices:

$$J_1 = \frac{1}{2} \int_0^{t_f} \left[W_1\left(L_1^2 + L_2^2 + L_3^2\right) + W_2\left(u_1^2 + u_2^2 + u_3^2\right) \right] dt = \int_0^{t_f} F_1 \, dt \tag{4.4}$$

$$J_2 = \frac{1}{2} \int_0^{t_f} \left[W_1'\left(\dot{L}_1^2 + \dot{L}_2^2 + \dot{L}_3^2\right) + W_2'\left(\dot{u}_1^2 + \dot{u}_2^2 + \dot{u}_3^2\right) \right] dt = \int_0^{t_f} F_2 \, dt \tag{4.5}$$

$$J_3 = \frac{1}{2} \int_0^{t_f} \left[W_1''\left(\ddot{L}_1^2 + \ddot{L}_2^2 + \ddot{L}_3^2\right) + W_2''\left(\ddot{u}_1^2 + \ddot{u}_2^2 + \ddot{u}_3^2\right) \right] dt = \int_0^{t_f} F_3 \, dt \tag{4.6}$$

$$J_4 = \sum_{i=1}^{3} J_i = \int_0^{t_f} F_4 \, dt \tag{4.7}$$

Hamiltonian:

$$H = \underline{\gamma}^T \underline{\dot{\beta}} + \underline{\lambda}^T \underline{\dot{\omega}} + \underline{\alpha}^T \underline{\dot{h}} + F_1 \tag{4.8}$$

where the γ_i and λ_i are Euler parameter and angular velocity co-states, and the α_i are wheel relative momenta co-states.

Pontryagin Necessary Conditions:

$$\text{Minimize } H \text{ with respect to } u_i(t) \quad \left\{ \begin{array}{ll} \dfrac{\partial H}{\partial L_i} = 0 & 0 = 1,2,3 \\[4mm] \dfrac{\partial H}{\partial u_i} = 0 & i = 1,2,3 \end{array} \right\} \text{ for } J_1 \text{ of equation (4.4)} \tag{4.9}$$

184

$$\text{Co-state differential equations} \begin{cases} \dfrac{d\gamma_i}{dt} = -\dfrac{\partial H}{\partial \beta_i} & i = 0,1,2,3 \qquad (4.10) \\[2ex] \dfrac{d\lambda_i}{dt} = -\dfrac{\partial H}{\partial \omega_i} & i = 1,2,3 \qquad (4.11) \\[2ex] \dfrac{d\alpha_i}{dt} = -\dfrac{\partial H}{\partial h_i} & i = 1,2,3 \qquad (4.12) \end{cases}$$

(+ boundary conditions)

Notice we have a once redundant ten-element state vector

$$\underline{x} = \left[\underbrace{\beta_0 \ \beta_1 \ \beta_2 \ \beta_3}_{\underline{\beta}^T} \Big| \underbrace{\omega_1 \ \omega_2 \ \omega_3}_{\underline{\omega}^T} \Big| \underbrace{h_1 \ h_2 \ h_3}_{\underline{h}^T} \right]^T \qquad (4.13)$$

where

$\underline{\beta}$ is the Euler parameter vector which describes the inertial orientation of B

$\underline{\omega}$ is the inertial angular velocity of B

$\underline{h}$ is the momentum of the reaction wheels relative to B ($\underline{h} = 0$, for locked wheels)

The Euler parameters satisfy the constraint

$$\underline{\beta}^T \underline{\beta} = 1 \qquad (4.14)$$

Their use makes the formulation universal, as opposed to the transcendental differential equations with a singularity which one obtains for any choice of Euler angles. However, one often requires a transformation from Euler angles to Euler parameters; for the 1-2-3 set of Euler angles $(\theta_1, \theta_2, \theta_3)$, the transformation is

$$\beta_0 = c(\theta 1/2) \ c(\theta 2/2) \ c(\theta 3/2) - s(\theta 1/2) \ s(\theta 2/2) \ s(\theta 3/2)$$

$$\beta_1 = s(\theta 1/2) \ c(\theta 2/1) \ c(\theta 3/2) + c(\theta 1/2) \ s(\theta 2/2) \ s(\theta 3/2)$$

$$(4.15)$$

$$\beta_2 = c(\theta 1/2) \ s(\theta 2/2) \ c(\theta 3/2) - s(\theta 1/2) \ c(\theta 2/2) \ s(\theta 3/2)$$

$$\beta_3 = c(\theta 1/2) \ c(\theta 2/2) \ s(\theta 3/2) + s(\theta 1/2) \ s(\theta 2/2) \ c(\theta 3/2)$$

$$c(\ ) \equiv \cos (\ ), \quad s(\ ) \equiv \sin (\ )$$

185

These results and similar developments for all twelve classical Euler angle sets are given in reference 4.

We must now consider the necessary conditions [in addition to satisfying equations (4.1) - (4.3)] for optimal maneuvers of the configuration of figure 2. First, one must define how to measure optimality. Equations (4.4) - (4.7) define four integral measures of optimality (from refs. 4, 5, 6). The first of these can be interpreted as a positive measure of the control effort, while the remaining three penalize control derivative variations. As one might expect, the derivative penalties lead to smoother optimal torques with lower frequency content; such controls are attractive when generalized to flexible vehicles because they tend to excite only lower modes (which are usually better modeled).

Notice the ten co-state equations couple together with the ten state equations [equations (4.1) - (4.3)] to yield a 20th-order system. Typically, the ten initial co-states must be determined iteratively to satisfy ten constraints at the final time.

In order to discuss solution techniques, it is useful to consider particular maneuvers. Four cases are now discussed. Table 1 summarizes some macroscopic information concerning the four cases. Case 1 is the simplest; the solution of this particular case is treated in detail in reference 2. Since the wheels are locked, the system becomes a single rigid body with seven state variables $\underline{x}^T = [\beta_0 \ \beta_1 \ \beta_2 \ \beta_3 \ \omega_1 \ \omega_2 \ \omega_3]$. The reader can readily verify that any set of "pure spin" boundary conditions causes all of the gyroscopic nonlinearities of equations (4.1), 4.2) and (4.10), (4.11) to vanish and results in a linear system which is readily solved analytically; reference 2 gives the details. Thus, "boundary condition embedding" *is motivated as an attractive way to solve the TPBVP by continuation.*

4.2 Four Maneuver Cases

For this case, table 2 gives the corresponding Euler angle boundary conditions and equation (4.16) gives the boundary condition embedding (homotopy chain) family of boundary conditions:
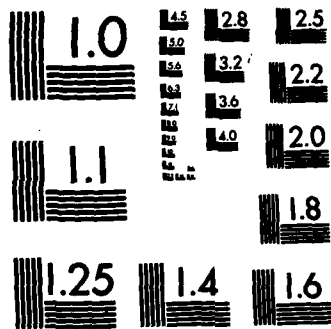
MICROCOPY RESOLUTION TEST CHART

NATIONAL BUREAU OF STANDARDS-1963-A

$$
\begin{bmatrix}
\theta_{10}\,(\alpha) \\
\theta_{20}\,(\alpha) \\
\theta_{30}\,(\alpha) \\
\omega_{10}\,(\alpha) \\
\omega_{20}\,(\alpha) \\
\omega_{30}\,(\alpha) \\
\text{---} \\
\theta_{1f}\,(\alpha) \\
\theta_{2f}\,(\alpha) \\
\theta_{3f}\,(\alpha) \\
\omega_{1f}\,(\alpha) \\
\omega_{2f}\,(\alpha) \\
\omega_{3f}\,(\alpha)
\end{bmatrix}
= \alpha
\begin{bmatrix}
0 \\
0 \\
0 \\
0.01 \\
0.005 \\
0.001 \\
\text{---} \\
5\pi/2 \\
\pi/3 \\
\pi/4 \\
0 \\
0 \\
0
\end{bmatrix}
+ (1 - \alpha)
\begin{bmatrix}
0 \\
0 \\
0 \\
0.01 \\
0 \\
0 \\
\text{---} \\
5\pi/2 \\
0 \\
0 \\
0 \\
0 \\
0
\end{bmatrix}
\qquad (4.16)
$$

We found $\{\alpha_1, \alpha_2, \ldots, \alpha_6\} = \{0, 0.0001, 0.25, 0.5, 0.75, 1\}$ resulted in reliable convergence for large variations in boundary conditions.

We note in passing that the $\alpha = 0$ case is a pure spin single-axis rotation about the $\hat{\underline{b}}_1$ axis; this case can be solved analytically (ref. 2). We performed other continuations corresponding to rotations about $\hat{\underline{b}}_2$ and $\hat{\underline{b}}_3$ and obtained the same final solution. In this case, it was found that introducing the α-sequence $\{\alpha_1 \ldots \alpha_6\} = \{0, 0.001, 0.25, 0.50, 0.75, 1\}$ and using Newton's method to iterate the initial co-states $\{\lambda_1(t_0)\ \lambda_2(t_0)\ \lambda_3(t_0)\ \gamma_0(t_0)\ \gamma_1(t_0)\ \gamma_2(t_0)\ \gamma_3(t_0)\} \equiv \underline{\Lambda}_o^T$ converged efficiently. Specifically, the iteration for $\underline{\Lambda}_o(\alpha_i)$ was initiated using the following starting procedure:

For $\alpha_2 = 0.001$, $\underline{\Lambda}_o(\alpha_2) = \underline{\Lambda}_o(\alpha_1)$, calculated from analytic solution

$\alpha_3 = 0.25$, $\underline{\Lambda}_o(\alpha_3)$ extrapolated linearly from the <u>converged</u> $\underline{\Lambda}_o(\alpha_2)\ \underline{\Lambda}_o(\alpha_1)$

α_4, α_5, α_6, $\underline{\Lambda}_o(\alpha_i)$ extrapolated quadratically from the <u>converged</u>

$\underline{\Lambda}_o(\alpha_{i-1})$, $\underline{\Lambda}_o(\alpha_{i-2})$, and $\underline{\Lambda}_o(\alpha_{i-3})$

As is evident from table 3, the convergence tolerance was held loose (10^{-2} maximum relative error of final boundary conditions) until the final ($\alpha_6 = 1$) continuation. This iteration process proved rather efficient as can be judged by the small number of Newton iterations. The history of state and control variables on the converged optimal maneuver is graphed in figure 3. Thus the final maneuver, which does not resemble a single-axis maneuver, is easily obtained via a continuation process initiated with the single-axis special case.

187

We now consider Case 2 (table 1). For this case, only the wheel along $\hat{\underline{b}}_2$ is free to rotate. The initial state is a "flat spin"; the body rotates uniformly about $\hat{\underline{b}}_3$ (the largest axis of inertia); it is desired to transfer all angular momentum to the wheel via a judicious motor torque $u(t)$. This problem has received considerable attention historically (e.g., refs. 9, 10) for the constant torque ($u(t)$ = constant) and constant relative momentum transfer ($h(t)$ = constant) case. In figure 4 (the right half of the figure), we display the constant torque ($u(t)$ = 0.005 N·m) maneuver published by Barba and Aubrun (ref. 9). The general features of the maneuver are the following:

(i) The maneuver is nonlinear; a separatrix occurs around 1000 sec prior to which the body $\hat{\underline{b}}_3$ axis cones about the inertially fixed momentum vector and after which the wheel axis ($\hat{\underline{b}}_2$) cones about the fixed momentum vector

(ii) Without damping or another torque mechanism, the momentum transfer maneuver cannot be perfectly realized; i.e., the body cones at a nonzero final mutation angle θ between $\hat{\underline{b}}_2$ and the inertially fixed angular momentum vector

We address the issue as to whether a nonconstant torque would significantly improve this flat-spin recovery maneuver. As is evident in the left half of figure 4, the optimal maneuver is qualitatively similar to the Barba/Aubrun maneuver, but the final mutation angle is decreased by 50 percent. The optimal torque history fluctuates ±10 percent about 0.05 N·m during the first 1000 seconds as is evident in figure 4.

The flat-spin recovery, while interesting, *does not represent a very general class of maneuvers*, since only one final rest orientation is stable (and it cannot be reached exactly without bringing other control or energy dissipation elements into action). Cases 3 and 4 are provided to demonstrate maneuvers which bring a generally rotating body to a state of rest in a general final orientation. These maneuvers also demonstrate the practicality of calculating highly nonlinear maneuvers with up to six control variables and of solving up to a 20th-order system of simultaneous nonlinear equations.

Case 3 is a generalized optimal momentum transfer using all three wheels simultaneously. In essence, the objective is to transfer all of the angular momentum into the three wheels and leave the body at a prescribed inertial pointing. Figure 5 shows the state and control variable history. Notice, since this is an internal torque maneuver, the total angular momentum is fixed; therefore, the final wheel speeds can be calculated from the initially calculated angular momentum.

Case 4 is a maneuver involving both internal and external torques. The criterion

$$J = \frac{1}{2} \int_{t_o}^{t_f} \left[u_1^2 + u_2^2 + u_3^2 \right] dt$$

$$+ \frac{1}{2} \int_{t_o}^{t_f} \left[L_1^2 + L_2^2 + L_3^2 \right] dt$$

is minimized. The terminal boundary conditions require that the body be at rest and all wheel speeds be reduced to zero. Thus this maneuver has the simultaneous objective of dumping the system momentum. As is evident in figure 6, the maneuver is quite smooth and the terminal boundary conditions are satisfied. Cases 3 and 4 contrast sharply with Case 2; the nutational motion associated with a one-wheel configuration is not evident due to (i) the lower wheel speeds, and (ii) the ability to generate optimal torques in any desired direction.

The foregoing results clearly suggest that we can, at least for a wide spectrum of problems, routinely determine optimal nonlinear maneuvers for spacecraft having a moderate number of degrees of freedom. Of course, nonlinearity is only one complicating issue for large flexible spacecraft; to what extent can we generalize these applications for vehicles where flexibility is a paramount concern? Specifically, can we apply similar methods to maneuver flexible vehicles, penalizing vibratory motion en route and arresting certain modes upon arrival? As is evident in the following developments, we have made some significant progress toward answering these questions in the affirmative.

5.0 SLEWING MANEUVERS FOR FLEXIBLE SPACECRAFT

The optimal control problem for maneuvering a vehicle of the shape shown in figure 7 is complicated by the presence of the attached flexible appendages. Mathematically, the presence of flexibility in the plant description increases the number of degrees of freedom required to model the motion of the vehicle (refs. 1, 3, 4, and 11). As a result, in order to successfully maneuver the vehicle, the control designer must have an accurate plant description which accounts for both rigid and flexible effects. In addition, when high angular rates are achieved during the maneuvers, great care must be exercised in modelling the vehicle and formulating systematic algorithms for solving the resulting nonlinear optimal control problems. However, the issues of model truncation and control spillover effects are not dealt with in this paper.

Section 6 develops an open-loop optimal control strategy for linear large-angle single-axis maneuver of a flexible spacecraft possessing a distributed control system. Section 7 presents a closed-loop formulation for maneuvering flexible vehicles. Section 8 develops a differential equation embedding continuation method for solving nonlinear open-loop formulations of the flexible spacecraft equations of motion. Example maneuvers are given in section 9.

6.0 LINEAR LARGE-ANGLE MANEUVERS OF FLEXIBLE SPACECRAFT USING DISTRIBUTED CONTROL

6.1 Equations of Motion

The linear time-invariant form of the equation of motion for the vehicle depicted in figure 7 is given by (see refs. 4 and 11)

$$M\ddot{\underline{\xi}} + K\underline{\xi} = P\underline{u} \tag{6.1}$$

where

$$\underline{\xi} = \begin{Bmatrix} \theta \\ \underline{\eta} \end{Bmatrix} \qquad M = \begin{bmatrix} \hat{I} & M_{-\theta\eta}^T \\ \underline{M}_{\theta\eta} & \underline{M}_{\eta\eta} \end{bmatrix} \qquad K = \begin{bmatrix} 0 & \underline{0}^T \\ 0 & K_{\eta\eta} \end{bmatrix}$$

$$P = \begin{bmatrix} 1 & 4\underline{r}^T \\ \underline{0} & F \end{bmatrix} \qquad \underline{u} = [u_1 \underline{u}_2]^T \qquad \underline{r} = [1, 1, \ldots, 1]^T$$
$$(N_{ac} \times 1)$$

$$[F]_{ij} = 4 \left. \frac{d}{dx}(\phi_i) \right|_{x = x_j - r} \qquad i = 1, \ldots, n \qquad j = 1, \ldots, N_{ac}$$

where n is the number of flexible modes in the model, N_{ac} is the number of appendage controls, x_j denotes the point of application of the jth appendage control, θ is the rigid-body angle, $\underline{\eta}$ is the vector of modal amplitudes, u_1 is the rigid-body torque, $\underline{u}_2$ is the vector of appendage control torques, r is the radius of the rigid hub, the integral definitions of $M_{\theta n}$, $M_{\eta\eta}$, and $K_{\eta\eta}$ are given in references 4 and 11, M is positive definite, and K is positive semidefinite. In equation (6.1) it has been assumed that quadratic terms in the modal amplitudes, amplitude rates, and angular velocity are vanishingly small and thus deleted.

For the optimal control problem, equation (6.1) is transformed to modal space and cast in the first-order form given by

$$\underline{\dot{s}} = A\underline{s} + B\underline{u} \tag{6.2}$$

where

$$A = \begin{bmatrix} 0 & I \\ -\Delta & 0 \end{bmatrix} \qquad B = \begin{bmatrix} 0 \\ E^T P \end{bmatrix} \qquad \underline{s} = \begin{Bmatrix} E\underline{\xi} \\ E\underline{\dot{\xi}} \end{Bmatrix}$$

$$E^T M E = I \qquad E^T K E = \Delta \qquad \Delta = \text{diag}(0, \lambda_1, \lambda_2, \ldots, \lambda_n)$$

where E is the normalized eigenvector matrix for M and K, and Δ is the diagonal matrix containing the eigenvalues of M and K.

190

6.2 Optimal Control Formulation

We seek an optimal solution of equation (6.2) which first satisfies the prescribed terminal boundary conditions given by

$$\underline{\xi}_0 = \left[\theta(t_o) \; \underline{\eta}^T(t_o)\right]^T \qquad \underline{\dot{\xi}}_0 = \left[\dot{\theta}(t_o) \; \underline{\dot{\eta}}^T(t_o)\right]^T \tag{6.3}$$

$$\underline{\xi}_f = \left[\theta(t_f) \; \underline{\eta}^T(t_f)\right]^T \qquad \underline{\dot{\xi}}_f = \left[\dot{\theta}(t_f) \; \underline{\dot{\eta}}^T(t_f)\right]^T \tag{6.4}$$

and second, minimizes the performance index given by

$$J = \frac{1}{2} \int_{t_o}^{t_f} \left[\underline{u}^T \, W_{uu} \, \underline{u} + \underline{s}^T \, W_{ss} \underline{s}\right] dt \tag{6.5}$$

The selection of the performance index of equation (6.5) is arbitrary although made for convenience. The elements of the state weighting matrix W_{ss} are selected to make the state penalty term in J proportional to the kinetic and potential energy of the vehicle. Since it is desirable to suppress the elastic deformations and deformation rates at the end of the slew, we also impose the constraint $\underline{\eta}(t_f) = \underline{\dot{\eta}}(t_f) = \underline{0}$ in equation (6.4).

The control weight matrix is chosen to be diagonal with smaller weighting on the rigid-body control torque than on the appendage control torque. This is because the elastic appendage controllers are meant to serve as vibration suppressors while the rigid hub controller is meant to execute most of the slewing maneuver. The penalty on the rigid-body angle is also chosen to be small because the structure is required to undergo a large-angle rotation. The rigid-body angle penalty is not set to zero since this choice leads to numerical problems in computing the state transition matrix. However, by adjusting the rigid-body angle penalty to be two to three orders of magnitude smaller than the penalties on the modal amplitudes, amplitude rates, and angular rates, the potential numerical problems can be overcome.

Using Pontryagin's principle (ref. 4), the necessary conditions defining the optimal maneuver are given by equations (6.6), (6.7), and (6.8):

State:

$$\underline{\dot{s}} = A\underline{s} - BW_{uu}^{-1}B^T\underline{\lambda} \tag{6.6}$$

Co-state:

$$\underline{\dot{\lambda}} = -W_{ss}\underline{s} - A^T\underline{\lambda} \tag{6.7}$$

Control:

$$\underline{u} = -W_{uu}^{-1}B^T\underline{\lambda} \tag{6.8}$$

The solution for equations (6.6) and (6.7) is given by

$$\left\{ \begin{array}{c} \underline{s}(t_f) \\ \underline{\lambda}(t_f) \end{array} \right\} = e^{\Omega(t_f - t_o)} \left\{ \begin{array}{c} \underline{s}(t_o) \\ \underline{\lambda}(t_o) \end{array} \right\} \qquad \Omega = \left[\begin{array}{cc} A & -BW_{uu}^{-1}B^T \\ -W_{ss} & -A^T \end{array} \right] \qquad (6.9)$$

where $e^{\Omega(t_f - t_o)}$ is the exponential matrix. Since $\underline{s}(t_o)$ and $\underline{s}(t_f)$ are known and $\underline{\lambda}(t_o)$ and $\underline{\lambda}(t_f)$ are unknown in equation (6.9), we need to solve for $\underline{\lambda}(t_o)$ to obtain the complete solution. Upon setting $\phi = e^{\Omega(t_f - t_o)}$ the partitioned matrix solution for $\underline{s}(t_f)$ is given by

$$\underline{s}(t_f) = \phi_{ss}\underline{s}(t_o) + \phi_{s\lambda}\underline{\lambda}(t_o) \qquad (6.10)$$

Solving equation (6.10) for the initial co-states yields

$$\underline{\lambda}(t_o) = [\phi_{s\lambda}]^{-1}\{\underline{s}(t_f) - \phi_{ss}\underline{s}(t_o)\} \qquad (6.11)$$

The optimal control time histories follow upon integrating equations (6.6) and (6.7) subject to $\underline{s}(t_o)$ given by equation (6.3) and $\underline{\lambda}(t_o)$ given by equation (6.11). Example maneuvers are given in section 9.

7.0 LINEAR LARGE-ANGLE MANEUVERS OF FLEXIBLE SPACECRAFT USING FEEDBACK CONTROL

7.1 Equations of Motion

The equations of motion given by equations (6.1) and (6.2) are used for the plant description of the feedback control problem of this section.

7.2 Optimal Control Formulation

The optimal feedback control for slewing a flexible spacecraft differs fundamentally from the open-loop problem of section 6.2 in two ways. First, the instantaneous values for the state influence the applied control. Second, the boundary conditions for the maneuver are specified initially and are free at the final time.

Breakwell (ref. 12) has recently presented two approaches for feedback control of a flexible spacecraft. First, he presented a constant feedback gain approach. Second, he developed a time-to-go formulation with time varying gains. The performance index he selected is of the form

$$J = \frac{1}{2} \underline{s}_f^T S\underline{s}_f + \int_0^{t_f} \left[\underline{s}^T Q\underline{s} + \underline{u}^T R\underline{u} \right] dt \qquad (7.1)$$

192

where S is the terminal state weighting matrix, Q is the state weighting matrix, and R is the control weighting matrix. Breakwell (ref. 13) has also developed a distributed transfer function approach for the feedback control problem; however, his distributed transfer function approach is not presented in this paper. Breakwell's constant gain solution is given by equation (7.2) and his time varying solution is given by (7.3):

$$t_f = \infty: \quad \underline{u} = -R^{-1}B^T P_\infty \underline{s} \tag{7.2}$$

$$t_f \ll \infty: \quad \underline{u} = R^{-1}B^T \left[S_f^{-1} \, \phi_{22}(\tau) - \phi_{12}(\tau) \right]^{-1} \left[\phi_{11}(\tau) - S_f^{-1} \, \phi_{21}(\tau) \right] \underline{s}(t) \tag{7.3}$$

where P_∞ is the solution to the algebraic matrix Riccati equation and τ is the time to go. Example maneuvers are given in section 9.

8.0 NONLINEAR LARGE-ANGLE MANEUVERS OF FLEXIBLE SPACECRAFT USING DISTRIBUTED CONTROL

8.1 Equations of Motion

When high angular rates are achieved during slewing maneuvers, the equation of motion given by equation (6.1) must be modified in two ways. First, quadratic terms in the angular velocity are retained in the equation of motion. Second, an arc length correction is added to the kinetic and potential energy integrals in order to properly account for second-order effects in the mass and stiffness distributions. As a result, the nonlinear equation of motion given by equation (8.1) accounts for the so-called centrifugal stiffening effect of the elastic appendages:

$$M\ddot{\underline{\xi}} + K\underline{\xi} = P \, \underline{u} \tag{8.1}$$

where

$$\xi = \left\{ \begin{matrix} \theta \\ \underline{\eta} \end{matrix} \right\} \qquad M = \begin{bmatrix} \hat{I} & \underline{M}_{\theta\eta}^T \\ \underline{M}_{\theta\eta} & \underline{M}_{\eta\eta} \end{bmatrix} \qquad K = \begin{bmatrix} 0 & 0 \\ 0 & (K_{\eta\eta} + \dot{\theta}^2 M^*) \end{bmatrix}$$

$$P = \begin{bmatrix} 1 & 4\underline{r}^T \\ \underline{0} & F \end{bmatrix} \qquad \underline{r} = \left\{ \begin{matrix} 1 \\ \vdots \\ 1 \end{matrix} \right\} (N_{ac}x1) \qquad \underline{u} = \left\{ \begin{matrix} u_1 \\ \underline{u}_2 \end{matrix} \right\}$$

The integral definitions of $\underline{M}_{\theta\eta}$, $M_{\eta\eta}$, M^*, and $K_{\eta\eta}$ can be found in references 4 and 11.

Equation (8.1) is transformed into modal space and cast in the first-order form for the optimal control problem using the coordinate transformation defined in equation (6.2):

$$\dot{\underline{s}} = A(\underline{s},\alpha)\underline{s} + B \underline{u} \tag{8.2}$$

where

$$A(\underline{s},\alpha) = \begin{bmatrix} 0 & I \\ \\ A_{21}(\underline{s},\alpha) & 0 \end{bmatrix} \qquad A_{21}(\underline{s},\alpha) = -\Delta - \alpha\left(\underline{e}^T\underline{s}_2\right)^2 L$$

$$L = E^T \begin{bmatrix} 0 & \underline{0}^T \\ \\ \underline{0} & M^* \end{bmatrix} E \qquad \underline{e} = E^T \left\{ \begin{array}{c} 1 \\ \\ 0 \end{array} \right\} \qquad \underline{s} = \left\{ \begin{array}{c} E\underline{\xi} \\ \\ E\dot{\underline{\xi}} \end{array} \right\}$$

and α is the continuation parameter which has been introduced to aid in the solution of the nonlinear problem.

8.2 Optimal Control Formulation

We seek an optimal solution of equation (8.2) which satisfies the prescribed terminal boundary conditions given in equations (8.3) and (8.4) and minimizes the performance index of equation (8.5).

$$\underline{\xi}_0 = \left[\theta(t_o) \ \underline{n}^T(t_o) \right]^T \qquad \dot{\underline{\xi}}_0 = \left[\dot{\theta}(t_o) \ \dot{\underline{n}}(t_o) \right]^T \tag{8.3}$$

$$\underline{\xi}_f = \left[\theta(t_f) \ \underline{n}^T(t_f) \right]^T \qquad \dot{\underline{\xi}}_f = \left[\dot{\theta}(t_f) \ \dot{\underline{n}}(t_f) \right]^T \tag{8.4}$$

$$J = \frac{1}{2} \int_{t_o}^{t_f} \left[\underline{u}^T W_{uu}\underline{u} + \underline{s}^T W_{ss}\underline{s} \right] dt \tag{8.5}$$

As part of the prescribed terminal boundary conditions in equation (8.4) we also impose the constraint that $\underline{n}(t_f) = \dot{\underline{n}}(t_f) = \underline{0}$.

Since equation (8.2) is nonlinear, a closed-form solution for the initial co-states is not possible. However, the artificially introduced continuation parameter in equation (8.2) can be varied from 0 to 1 in a manner which embeds the nonlinear problem in a family of problems which includes the linear problem of section 6 (i.e. $\alpha = 0$) as a special case. Thus the solution for $\alpha = 0$ can be used to establish a sequence of problems which converges to the nonlinear problem of interest (namely, when $\alpha = 1$).

194

The necessary conditions defining the nonlinear optimal solution are given by equations (8.6), (8.7), and (8.8).

State:

$$\dot{\underline{s}} = A(\underline{s},\alpha)\underline{s} - BW_{uu}^{-1}B^T\underline{\lambda} \qquad (8.6)$$

Co-state:

$$\dot{\underline{\lambda}} = -W_{ss}\underline{s} - C(\underline{s},\alpha)\underline{\lambda} \qquad (8.7)$$

where

$$C(\underline{s},\alpha) = \begin{bmatrix} 0 & A_{21}^T(\underline{s},\alpha) \\ I & -2\alpha(\underline{e}^T\underline{s}_2)\underline{e}\underline{s}_1^T L^T \end{bmatrix}$$

Control:

$$\underline{u} = -W_{uu}^{-1}B^T\underline{\lambda} \qquad (8.8)$$

The partial derivatives of equations (8.6) and (8.7) required in the nonlinear state transition matrix are given in references 4 and 11.

8.3 The Continuation Method Using Differential Equation Embedding

For the solution of the nonlinear optimal control problem, we introduce the sequence of continuation parameters $\{0 = \alpha_o < a_1 < \ldots \alpha_p = 1\}$, where p is either preset or determined during the solution process. The operator equation defining the optimal control solution is given by

$$\underline{F}\left(\underline{s}(t_o),\underline{\lambda}_i(t_o),\alpha_i\right) = \begin{Bmatrix} \dot{\underline{s}} - A(\underline{s},\alpha_i)\underline{s} + BW_{uu}^{-1}B^T\underline{\lambda} \\ \dot{\underline{\lambda}} + W_{ss}\underline{s} + C(\underline{s},\alpha_i)\underline{\lambda} \\ \underline{s}_{f(desired)} - \underline{s}\left(\underline{s}(t_o),\underline{\lambda}_i(t_o),\alpha_i\right) \end{Bmatrix} = \begin{Bmatrix} \underline{0} \\ \underline{0} \\ \underline{0} \end{Bmatrix} \qquad (8.9)$$

The continuation method of this section seeks the solution $\underline{\lambda}_{i+1}(t_o)$ of equation (8.10) using extrapolated estimates of $\underline{\lambda}_{i+1}$ based on back α-values.

$$\underline{F}\left(\underline{s}(t_o),\underline{\lambda}_{i+1}(t_o),\alpha_{i+1}\right) = \underline{0} \qquad (8.10)$$

The procedure is an iterative method since $\underline{F}$ is nonlinear; however, we have found that only two to four intermediate α-values are typically required to solve the

195

nonlinear problems of this section. In the nonlinear examples of section 9 the iterative solution for each α-value required at most two or three iterations to converge.

The differential correction strategy is to seek the correction vector $\underline{\Delta\lambda}$ subject to the terminal constraint given by

$$\underline{s}_{f(\text{desired})} - \underline{s}(\hat{\underline{\lambda}}_o + \underline{\Delta\lambda}, \ t_f) = \underline{0} \qquad \hat{\underline{\lambda}}_o = \hat{\underline{\lambda}}(t_o) \qquad (8.11)$$

for a specific α-value. Upon linearizing equation (8.11) we obtain equation (8.12), where $\hat{s}$ denotes the numerically integrated solution of equation (8.6) using the approximate initial co-state $\hat{\underline{\lambda}}_o$

$$\underline{s}_{f(\text{desired})} - \hat{\underline{s}} - \left[\frac{\partial \underline{s}^T}{\partial \underline{\lambda}_o} \bigg|_{t_f} \right]^T \underline{\Delta\lambda} = 0 \qquad (8.12)$$

The equation defining the solution for $\underline{\Delta\lambda}$ is then given by

$$\left[\frac{\partial \underline{s}^T}{\partial \underline{\lambda}_o} \bigg|_{t_f} \right]^T \underline{\Delta\lambda} = \underline{\Delta s}_f, \qquad \underline{\Delta s}_f = \underline{s}_{f(\text{desired})} - \hat{\underline{s}} \qquad (8.13)$$

The solution for $\underline{\Delta\lambda}$ in equation (8.13) is easily obtained using Gaussian elimination.

For each α-value in equation (8.10), equation (8.13) is iteratively solved until the norm of $\underline{\Delta s}_f$ is less than some small value, that is $||\underline{\Delta s}_f|| < \epsilon$. Then α is incrementally increased, and the solution for the intermediate α-value is obtained from equation (8.13). The process continues until $\alpha = 1$ and the non-linear problem of interest has been solved. The numerical algorithm is summarized in figure 8.

9.0 EXAMPLE MANEUVERS

Table 4 summarizes the boundary conditions for the example maneuvers of this section. The structural parameters for the model used in Cases 1, 2, 3, 6, and 7 are given in references 4 and 11, and those for Cases 4 and 5 are shown in reference 12.

Cases 1 and 2 (figs. 9 and 10) demonstrate that by adding additional controls on the structure the system performance can be improved. In this particular case, the first mode peak amplitude is decreased by 9 percent and the rigid-body peak control torque is decreased by 4 percent.

196

Case 3 (fig. 11) presents a ten-mode case using distributed control and demonstrates that all ten modal amplitudes and amplitude rates (not shown) have satisfied the prescribed boundary conditions.

Case 4 (fig. 12) presents the constant feedback gain solution of reference 12 and indicates at least for the one-mode case that the vehicle's controlled performance is not unreasonable.

Case 5 (fig. 13) presents the time-varying feedback gain solution of reference 12. We see that the boundary conditions are satisfied and that for large S_f the control time history is very similar to the open-loop solution.

Case 6 (fig. 14) presents a somewhat counter-intuitive spin-reversal maneuver where the vehicle backs up before moving forward. It can be shown (refs. 4 and 11) that the spin-reversal phenomenon is the result of fixing either the maneuver time or the final maneuver angle.

Case 7 (fig. 15) presents a stressing spin-reversal maneuver where the peak modal amplitudes for the nonlinear maneuver differ from the linear solution by about 17 percent to 41 percent. In particular, the first mode had small amplitudes while the higher modes had larger amplitudes when compared with the linear solution. The shape of the modal amplitude responses is also slightly different from the linear solution.

REFERENCES

1. Turner, J. D., "Optimal Continuous Torque Attitude Maneuvers for Flexible Space-craft," Ph. D. Dissertation, Virginia Polytechnic Institute and State University, Blacksburg, Va., 1980.

2. Junkins, J. L., and Turner, J. D., "Optimal Continuous Torque Attitude Maneuvers," Journal of Guidance and Control, Vol. 3, No. 3, May-June 1980, pp. 210-217.

3. Turner, J. D., and Junkins, J. L., "Optimal Large-Angle Single-Axis Rotational Maneuvers of Flexible Spacecraft," AIAA Journal of Guidance and Control, Vol. 3, No. 6, November-December 1980, pp. 578-585.

4. Junkins, J. L., and Turner, J. D., Optimal Spacecraft Rotational Maneuvers, Elsevier Scientific Publishing Company, Amsterdam, The Netherlands. (In Press).

5. Vadali, S. R., and Junkins, J. L., "Spacecraft Large-Angle Maneuvers With Optimal Momentum Transfer," paper presented at AIAA/AAS Astrodynamics Conference, August 1982, San Diego, Calif.

6. Vadali, S. R., "Optimal Momentum Transfer Maneuvers of Multiple Reaction Wheel Spacecraft," Ph. D. Dissertation, Virginia Polytechnic Institute and State University, Blacksburg, Va., January 1983.

7. Kane, T. R., Dynamics, Holt, Rinehart, and Winston, Inc., New York, 1968, pp. 204-207.

8. Miele, A., and Iyer, R. R., "General Technique for Solving Nonlinear, Two-Point Boundary-Value Problems Via ̇e Method of Particular Solutions," J. of Optimization Theory and Applications, Vol. 5, No. 5, 1970, pp. 382-399.

9. Barba, P. M., and Aubrun, J. N., "Satellite Attitude Acquisition by Momentum Transfer," American Astronautical Society Paper No. AAS 75-043, presented to the AAS/AIAA Astrodynamics Conference, Nassau, Bahamas, July 1975.

10. Gebman, J. R., and Mingori, D. L., "Perturbation Solution for the Flat Spin Recovery of a Dual-Spin Spacecraft," AIAA Journal, Vol. 14, July 1976, pp. 859-867.

11. Chun, H. M., "Optimal Distributed Control of a Flexible Spacecraft During a Large-Scale Rotational Maneuver," SM Thesis, MIT, Cambridge, Massachusetts, 1982.

12. Breakwell, J. A., "Optimal Feedback Slewing of Flexible Spacecraft," Journal of Guidance and Control, Vol. 4, No. 5, September-October 1981, pp. 472-479.

13. Breakwell, J. A., "Optimal Feedback Maneuvering of Flexible Spacecraft," Paper No. 79-157, presented to AAS/AIAA Astrodynamics Specialist Conference, Provincetown, Mass., June 1979.

TABLE 1. – FOUR LARGE-ANGLE MANEUVERS OF THE VEHICLE IN FIGURE 2

CASE	DESCRIPTION	PERFORMANCE INDEX	SYSTEM PARAMETERS	INITIAL CONDITIONS	DESIRED FINAL CONDITIONS	CONTINUATION METHOD	NUMERICAL METHOD TO SOLVE ODEs
1	GENERAL MANEUVER OF A SINGLE RIGID BODY STATE: $\underline{\theta},\underline{\omega}$ CONTROL: $\underline{L}$	$\int_{t_0}^{t_f}(L_1^2+L_2^2+L_3^2)dt$	$\begin{bmatrix}I_1\\I_2\\I_3\end{bmatrix}=\begin{bmatrix}86.215\\85.07\\113.565\end{bmatrix}kg\ m^2$ WHEELS LOCKED	$\begin{bmatrix}\theta_1(t_0)\\\theta_2(t_0)\\\theta_3(t_0)\end{bmatrix}=\begin{bmatrix}0\\0\\0\end{bmatrix}$ $\underline{\omega}(t_0)=\begin{bmatrix}.01\ r/s\\.005\\.001\end{bmatrix}$ $t_0=0\ S$	$\begin{bmatrix}\theta_1(t_f)\\\theta_2(t_f)\\\theta_3(t_f)\end{bmatrix}=\begin{bmatrix}5\pi/2\\\pi/3\\\pi/4\end{bmatrix}$ $\underline{\omega}(t_f)=\underline{0}$ $t_f=100\ S$	BOUNDARY CONDITION IMBEDDING	NEWTON DIFFERENTIAL CORRECTIONS OF SUCCESSIVE RUNGE-KUTTA SOLUTIONS ALSO SOLVED USING WEIGHTED RESIDUAL METHOD (REF. 5) "METHOD OF PARTICULAR SOLUTIONS" (REFS. 5 AND 6)
2	OPTIMAL "FLAT SPIN RECOVERY" USING ONLY THE PITCH WHEEL STATE: $\underline{\omega}$, h_2 CONTROL: u_2	$\int_{t_0}^{t_f}u_2^2\,dt$ $+\ \underline{\omega}^T(t_f)\underline{\omega}(t_f)$ $+\ [h_2(t_f)-H]^2$	SAME AS ABOVE EXCEPT "2" WHEEL IS NOT LOCKED: $J_2=J\ .05\ kg\ m^2$ $H=I_3\,\omega_3(t_0)$ $=20\ NMS$	$\underline{\omega}(t_0)=\begin{bmatrix}0\\0\\.176\ r/s\end{bmatrix}$ $h_2(t_0)=0$ $t_0=0\ S$	$\underline{\omega}(t_f)=\underline{0}$ $h_2(t_f)=H$ $t_f=4000\ S$ IMPOSED TRANSVERSATILITY CONDITIONS: $\underline{\lambda}(t_f)=\underline{0}$ $\sigma(t_f)=0$	FIXED POINT ALGORITHM	NEWTON DIFFERENTIAL CORRECTIONS OF SUCCESSIVE RUNGE-KUTTA SOLUTIONS ALSO SOLVED USING "METHODS OF PARTICULAR SOLUTIONS" (REFS. 5 AND 6)
3	OPTIMAL INTERNAL TORQUE MANEUVER USING 3 WHEELS STATE: $\underline{\beta},\underline{\omega},\underline{h}$ CONTROL: $\underline{u}$	$\int_0^{t_f}(u_1^2+u_2^2+u_3^2)\,dt$	$\begin{bmatrix}I_1\\I_2\\I_3\end{bmatrix}=\begin{bmatrix}86.215\\85.07\\113.565\end{bmatrix}kg\ m^2$ $J_1=J=.05\ kg\ m^2$ $\underline{H}=$ INITIAL ANG. MOM.	$\underline{\beta}(t_0)=\begin{bmatrix}.642780\\.442275\\.442275\\.442275\end{bmatrix}$ $\underline{\omega}(t_0)=\begin{bmatrix}.01\ r/s\\.005\\.001\end{bmatrix}$ $\underline{h}(t_0)=\begin{bmatrix}0\\0\\0\end{bmatrix}$	$\underline{\beta}(t_f)=\begin{bmatrix}1\\0\\0\\0\end{bmatrix}$ $\underline{\omega}(t_f)=\underline{0}$ $\underline{h}(t_f)=\underline{H}$	—	MIELE'S "METHOD OF PARTICULAR SOLUTIONS", QUASILINEARIZATION METHOD, AS DEVELOPED IN REFS 5 AND 6
4	OPTIMAL INTERNAL/EXTERNAL TORQUE MANEUVER STATE: $\underline{\beta},\underline{\omega},\underline{h}$ CONTROL: $\underline{u},\underline{L}$	$\int_{t_0}^{t_f}(L_1^2+L_2^2+L_3^2)\,dt$ $+\int_{t_0}^{t_f}(u_1^2+u_2^2+u_3^2)\,dt$	$\begin{bmatrix}I_1\\I_2\\I_3\end{bmatrix}=\begin{bmatrix}10\\8.33333\\9.16666\end{bmatrix}\times10^5\ kg\ m^2$ $J_1=J=5\ kg\ m^2$	$\underline{\beta}(t_0)=\begin{bmatrix}1\\0\\0\\0\end{bmatrix}$ $\underline{\omega}(t_0)=\begin{bmatrix}.01\ r/s\\.005\\.001\end{bmatrix}$ $\underline{h}(t_f)=\begin{bmatrix}5\ NMS\\2\\3\end{bmatrix}$	$\underline{\beta}(t_f)=\begin{bmatrix}.43047\\.70106\\.09230\\.56098\end{bmatrix}$ $\underline{\omega}(t_f)=\underline{0}$ $\underline{h}(t_f)=\underline{0}$	—	MIELE'S "METHOD OF PARTICULAR SOLUTIONS", QUASILINEARIZATION METHOD, AS DEVELOPED IN REFS 5 AND 6

199

TABLE 2.— RIGID BODY MANEUVER (CASE 1)

$$(I_1, I_2, I_3) = (1, 0.833333, 0.916667) \times 10^6 \text{ kg m}^2$$

	INITIAL STATE ($t_0 = 0$ s)	DESIRED FINAL STATE ($t_f = 100$ s)
1-2-3 Euler Angles	$\theta_1(t_0) = \theta_{10} = 0$	$\theta_1(t_f) = \theta_{1f} = 5\pi/2$
	$\theta_2(t_0) = \theta_{20} = 0$	$\theta_2(t_f) = \theta_{2f} = \pi/3$
	$\theta_3(t_0) = \theta_{30} = 0$	$\theta_3(t_f) = \theta_{3f} = \pi/4$
Orthogonal Ang. Vel. Components	$\omega_1(t_0) = \omega_{10} = 0.01$ r/s	$\omega_1(t_f) = \omega_{1f} = 0$
	$\omega_2(t_0) = \omega_{20} = 0.005$	$\omega_2(t_f) = \omega_{2f} = 0$
	$\omega_3(t_0) = \omega_{30} = 0.001$	$\omega_3(t_f) = \omega_{3f} = 0$

TABLE 3.— BOUNDARY CONDITION CONTINUATION FOR CASE 1
[From ref. 4]

	$\alpha_n \rightarrow$	0	0.001	0.25	0.50	0.75	1.00
	Tolerance[a] $\rightarrow$	...	10^{-2}	10^{-2}	10^{-2}	10^{-2}	10^{-5}
	No. of iterations $\rightarrow$	...	1	4	8	6	4
Initial state	$\theta_1(t_0)$	0	0	0	0	0	0
	$\theta_2(t_0)$	0	0	0	0	0	0
	$\theta_3(t_0)$	0	0	0	0	0	0
	$\omega_1(t_0)$	0.01 rad/s	0.0100	0.0100	0.0100	0.0100	0.01
	$\omega_2(t_0)$	0	0.00005	0.00125	0.00250	0.00375	0.005
	$\omega_3(t_0)$	0	0.00001	0.00025	0.00050	0.00075	0.001
Final state	$\theta_1(t_f)$	$5\pi/2$	$5\pi/2$	$5\pi/2$	$5\pi/2$	$5\pi/2$	7.85397 ($= 5\pi/2$)
	$\theta_2(t_f)$	0	0.01048	0.260829	0.52249	0.78471	1.04731 ($= \pi/3$)
	$\theta_3(t_f)$	0	0.07857	0.19620	0.39248	0.58909	0.78546 ($= \pi/4$)
	$\omega_1(t_f)$	0	0	0	0	0	0
	$\omega_2(t_f)$	0	0	0	0	0	0
	$\omega_3(t_f)$	0	0	0	0	0	0
Converged co-state ($\times 10^9$)	$\lambda_1(t_0)$	-4.3124	-4.31237	-4.22029	-4.01835	-3.81454	-3.64945
	$\lambda_2(t_0)$	0	-0.01576	-0.37601	-0.67991	-0.91423	-1.10589
	$\lambda_3(t_0)$	0	-0.03034	-0.73721	-1.34988	-1.80119	-2.13870
	$\gamma_0(t_0)$	0	0	0	0	0	0
	$\gamma_1(t_0)$	-0.17649	-0.17649	-0.17685	-0.17546	-0.17082	-0.16634
	$\gamma_2(t_0)$	0	-0.00063	-0.01501	-0.02674	-0.03496	-0.04117
	$\gamma_3(t_0)$	0	-0.00039	-0.01101	-0.02672	-0.04411	-0.05838

[a] Maximum relative error in ω's (normalized by 0.001)

TABLE 4.— DESCRIPTION OF TEST CASE MANEUVERS

Case No.	Qualitative Description	No. of modes n	θ_0, rad	$\dot\theta_0$ rad/s	θ_f, rad	$\dot\theta_f$, rad/s	No. of Controls N_{cc}	W_{uu}	W_{ss}
1	Rest-to-Rest Manuever t_f= 60 sec	2	0	0	π	0	1	I	$10^{-3}\tilde{I}$**
2	Rest-to-Rest Manuever t_f = 60 sec	2	0	0	π	0	5	$\tilde{I}$*	$10^{-3}\tilde{I}$
3	Rest-to-Rest Manuever t_f = 5 sec	10	0	0	$\pi/18$	0	5	$\tilde{I}$	$10^{-6}\tilde{I}$
4	Rest-to-Rest Manuever t_f = 5 sec	1	0	0	$\pi/18$	0	1	I	I
5	Rest-to-Rest Manuever Time Varying Feedback t_f = 5 sec	1	0	0	$\pi/18$	0	1	I	I
6	Spin-Up Maneuver t_f = 60 sec	3	0	0	2π	0.5	5	$\tilde{I}$	$10^{-3}\tilde{I}$
7	Nonlinear Spin Reversal t_f = 60 sec	3	0	-0.5	2π	0.5	5	$\tilde{I}$	$10^{-3}\tilde{I}$

* $\tilde{I}$ = diag(10^{-3}, 1, ..., 1)   ($N_c \times N_c$)

** $\tilde{I}$ = diag(10^{-2}, 1, ..., 1)   ($2(n+1) \times 2(n+1)$)

PHYSICAL PROBLEM	PONTRYAGIN'S PRINCIPLE	TWO-POINT-BOUNDARY VALUE-PROBLEM (TPBVP)
SYSTEM STATE ODE'S	HAMILTONIAN	FIND $\underline{\lambda}_0$ SO THAT THE
$\dot{\underline{x}} = \underline{f}(t,\underline{x},\underline{u})$	$H = \mathcal{J} + \underline{\lambda}^T \underline{f}$	SOLUTIONS OF
FIND OPTIMAL CONTROL $\underline{u}(t)$	CO-STATE EQUATIONS	STATE $\quad \dot{\underline{x}} = \underline{F}(t,\underline{x},\underline{\lambda})$
TO MINIMIZE	$\dot{\underline{\lambda}} = -\left\{\dfrac{\partial H}{\partial \underline{x}}\right\}^T$	CO-STATE $\dot{\underline{\lambda}} = \underline{G}(t,\underline{x},\underline{\lambda})$
$J = \phi(\underline{x}_f) + \int_{t_o}^{t_f} \mathcal{J}(t,\underline{x},\underline{u})dt$	MINIMIZE H w.r.t.	INITIATING AT
SUBJECT TO (FOR EXAMPLE)	ADMISSIBLE $\underline{u}(t)$ AT	$\underline{x}(t_0) = \underline{x}_0$
THE BOUNDARY CONDITIONS	EACH INSTANT - THIS	$\underline{\lambda}(t_0) = \underline{\lambda}_0$
	YIELDS	
$\underline{x}(t_f) = \underline{x}_0$		TERMINATE AT
$\underline{x}(t_f) = \underline{x}_f$	$\underline{u}(t) = \left\{\begin{matrix}\text{OPTIMAL}\\\text{CONTROL}\end{matrix}\right\} = \underline{g}(t,\underline{x},\underline{\lambda})$	$\underline{x}(t_f) = \underline{x}_f$

Figure 1.- The optimal maneuver necessary conditions and the associated TPBVP.

ASYMMETRIC MAIN BODY B

Wheel Momenta: $h_i = J \Omega_i;$
$\qquad\qquad\qquad i = 1,2,3$

B's Angular Velocity: $(\omega_1,\omega_2,\omega_3)$

Euler Parameters orienting B: $(\beta_0,\beta_1,\beta_2,\beta_3)$

Internal (Motor) Torques: (u_1,u_2,u_3)

External Torques: (L_1,L_2,L_3)
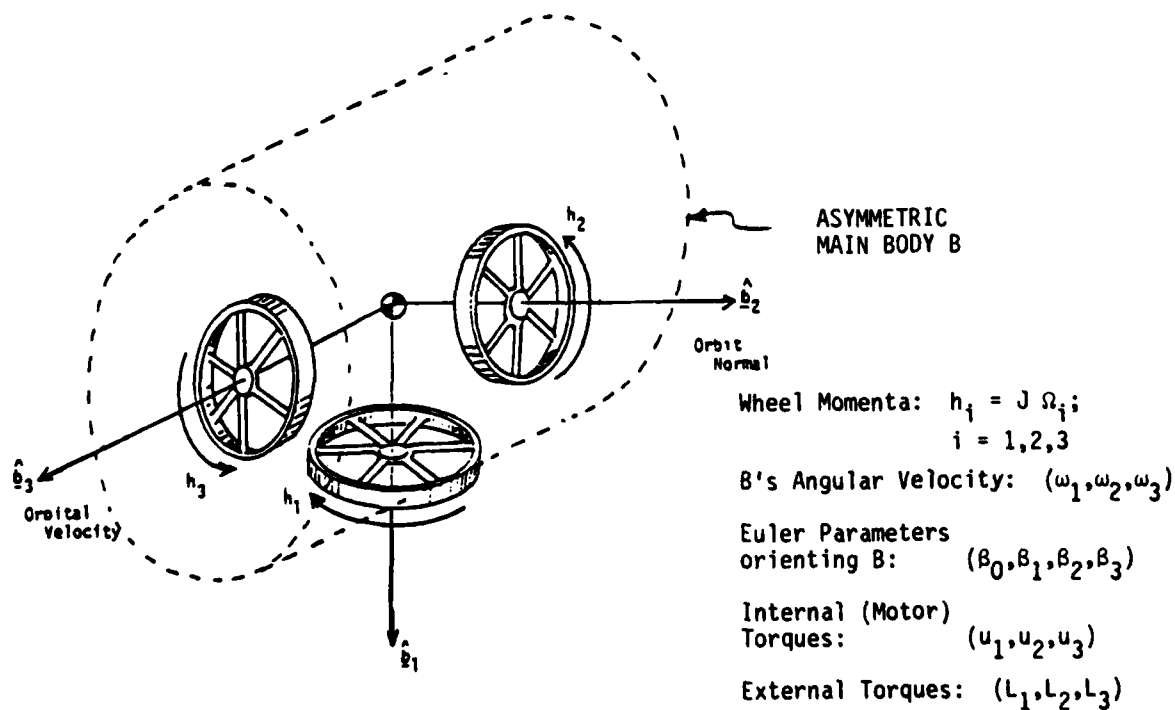
Figure 2.- Dynamics of a four-body configuration with internal and external torques.

$$J = \frac{1}{2} \int_0^{100} \left(u_1^2 + u_2^2 + u_3^2 \right) dt \cong 3.6 \times 10^8$$
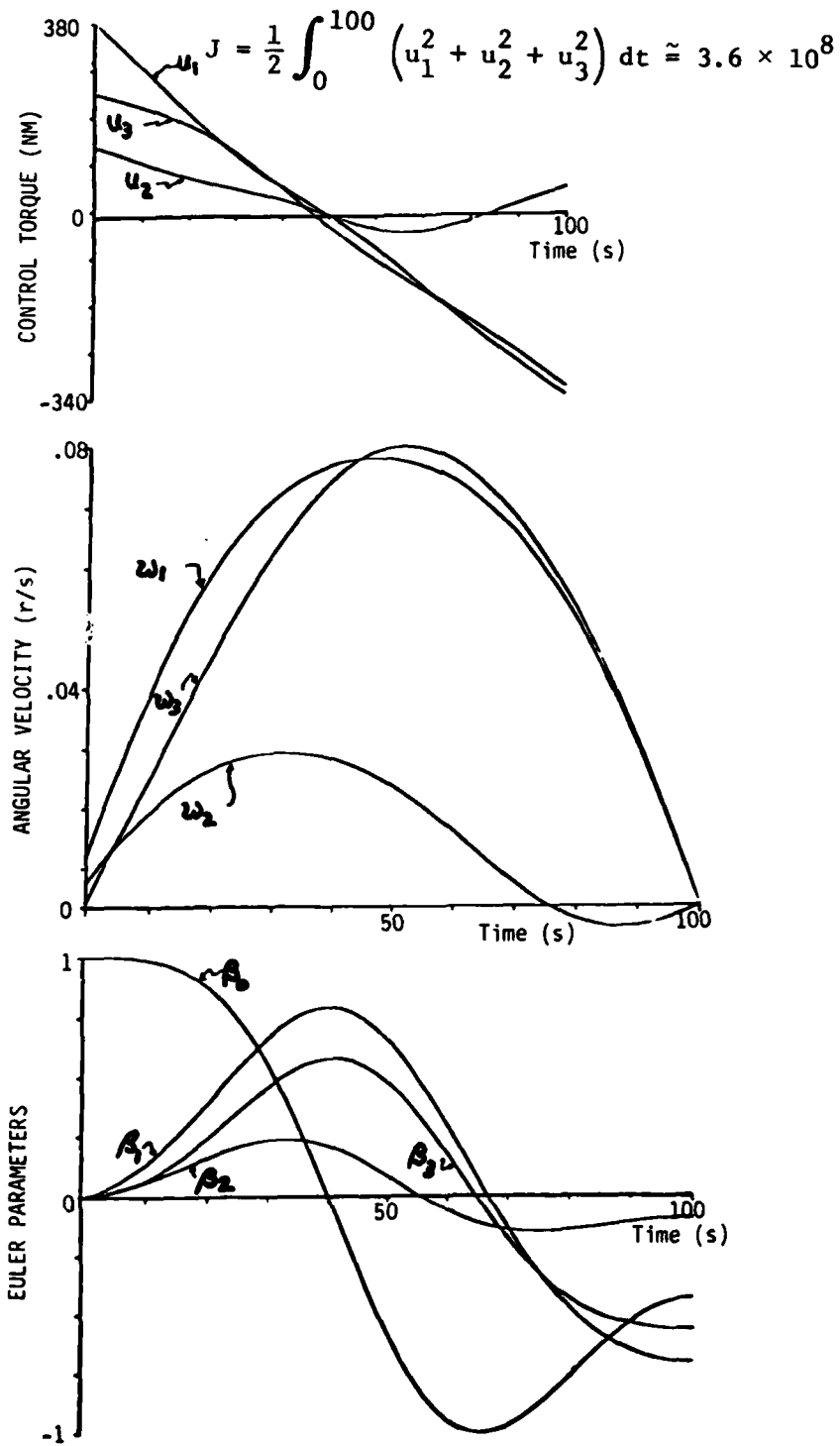
Figure 3.– Three-axis de-tumble case 1.

Optimal maneuver of Vadali & Junkins [ref. 5]   Maneuver of Barba & Aubrun [ref. 9]
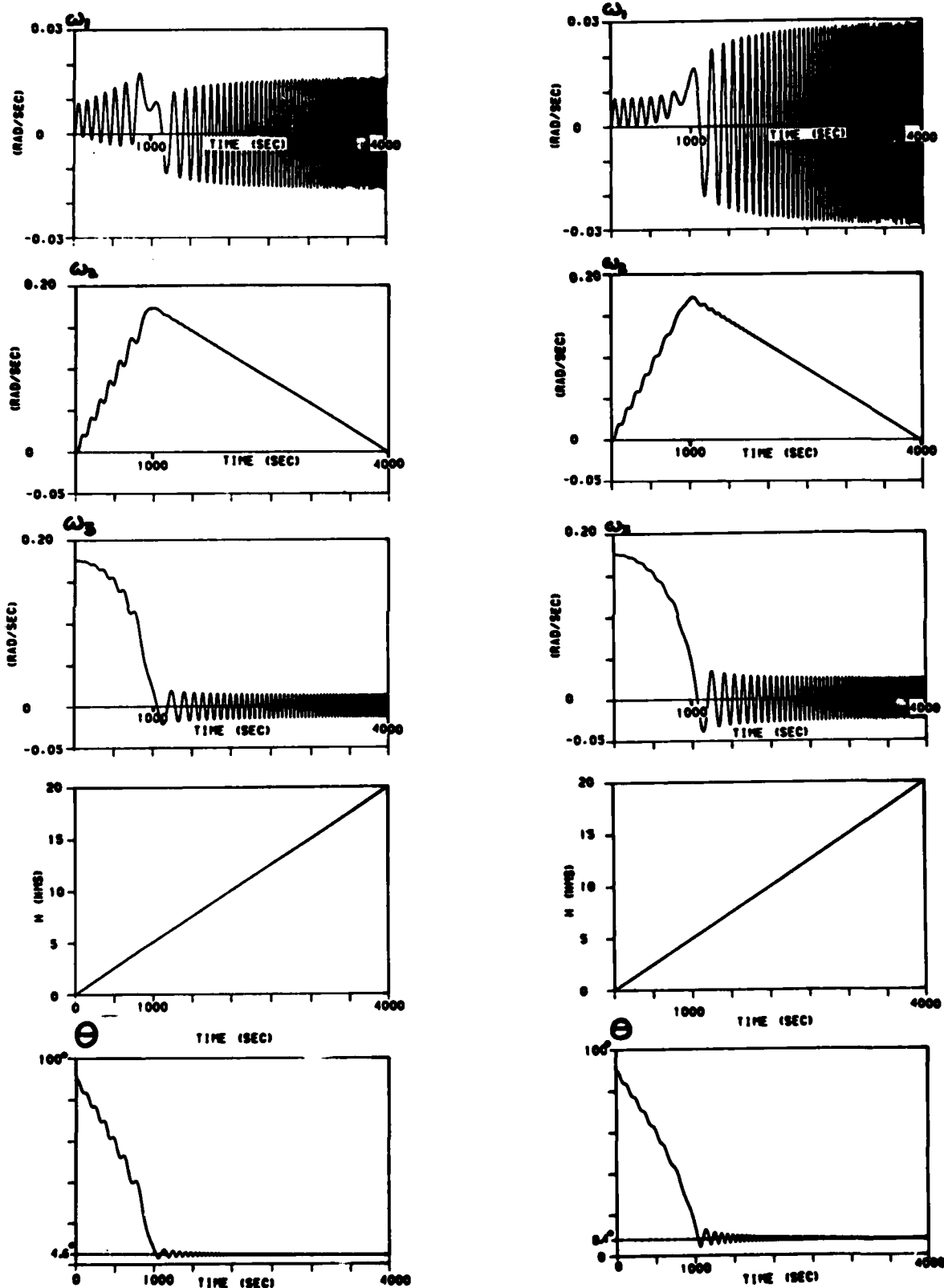
Figure 4.- A comparison of two flat-spin recovery maneuvers.
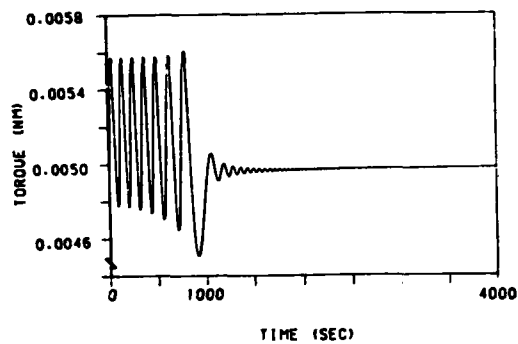
Constant torque

$u(t) = 0.005$ NM

Figure 4.- Concluded.
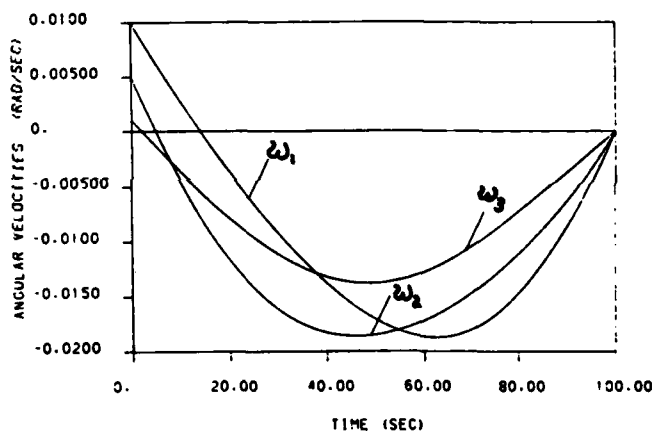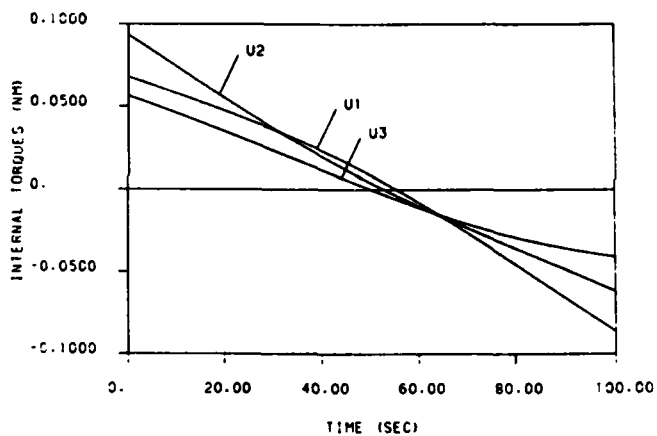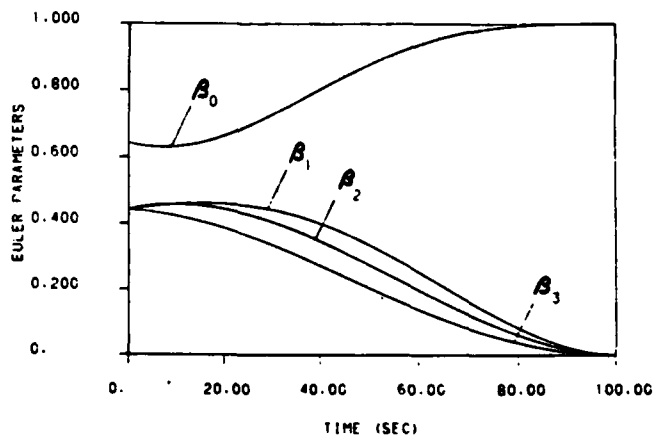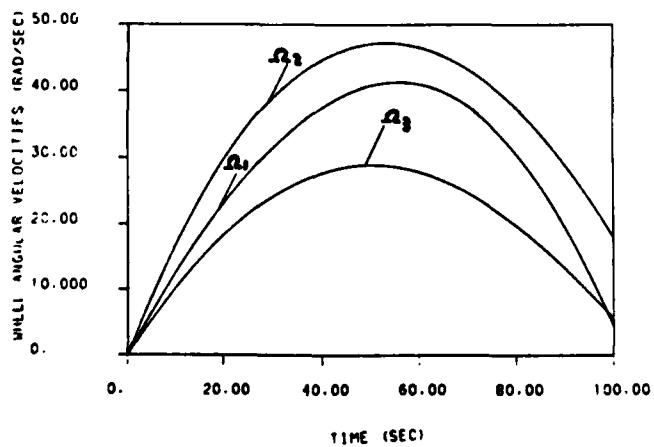
Figure 5.- Optimal internal torque momentum transfer maneuver.

CONTROL TORQUE HISTORY
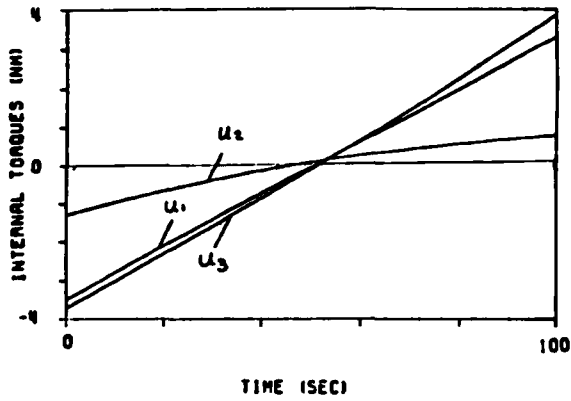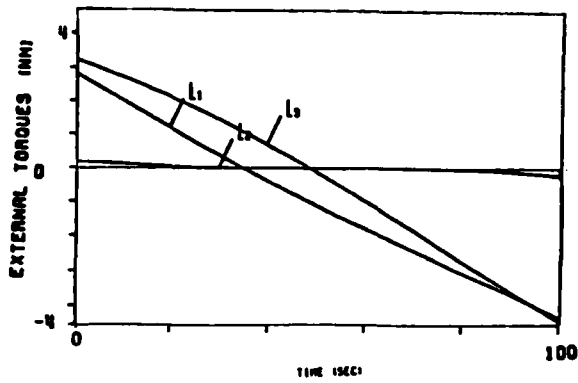
STATE VARIABLE HISTORY
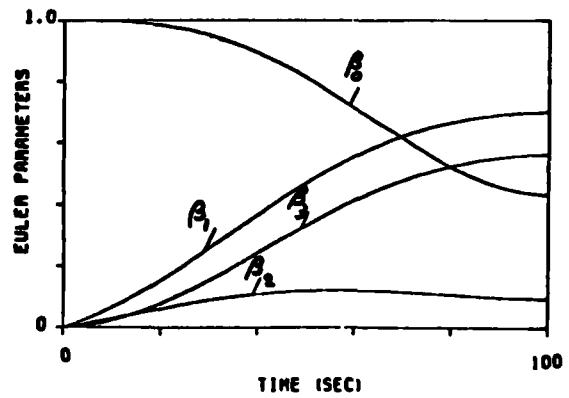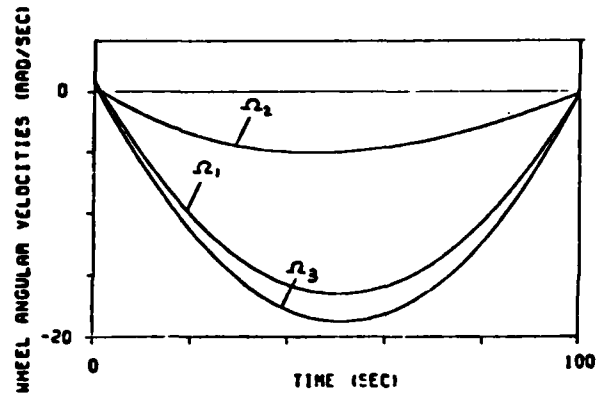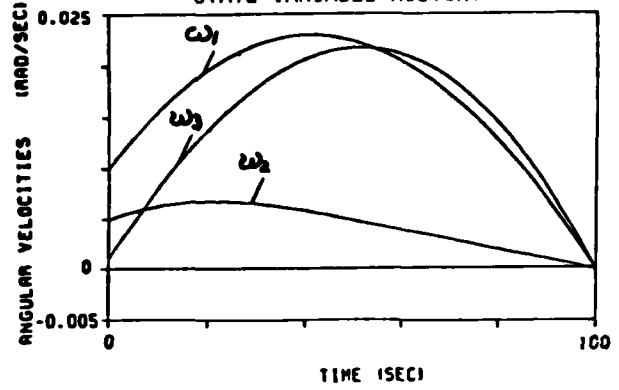
Figure 6.- Optimal internal/external torque maneuver.
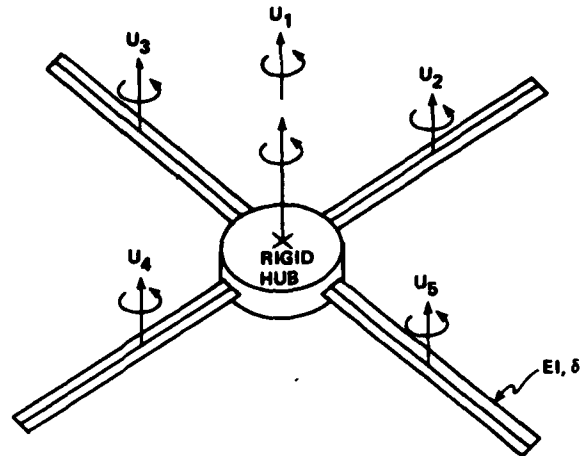
Figure 7.- Modal structure.
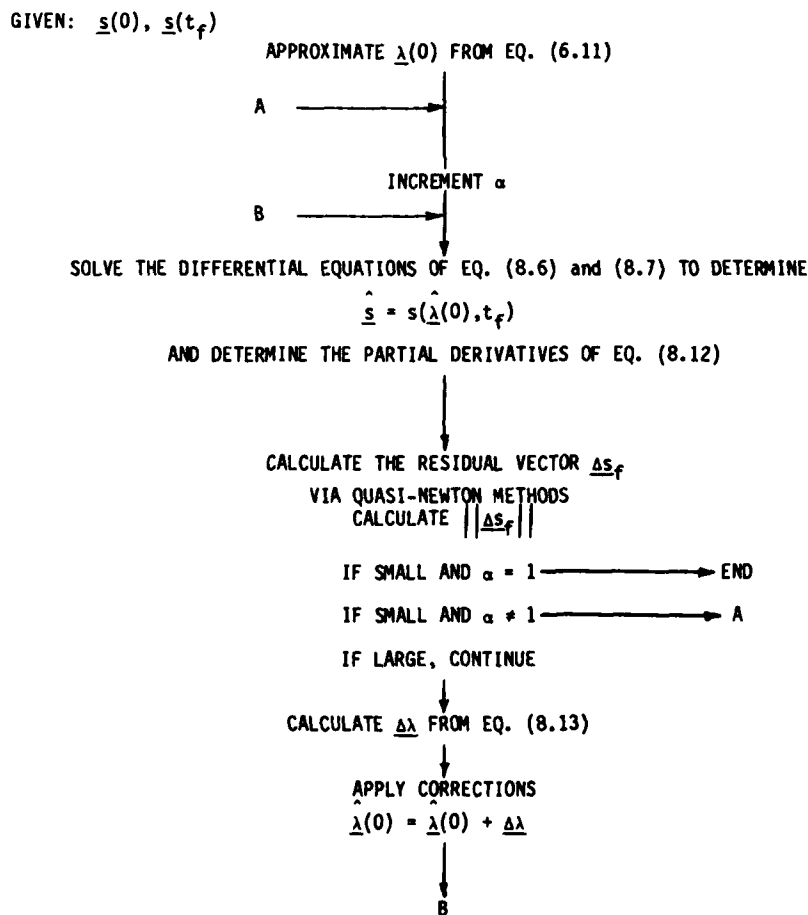
Figure 8.- Differential correction algorithm for the differential embedding method.
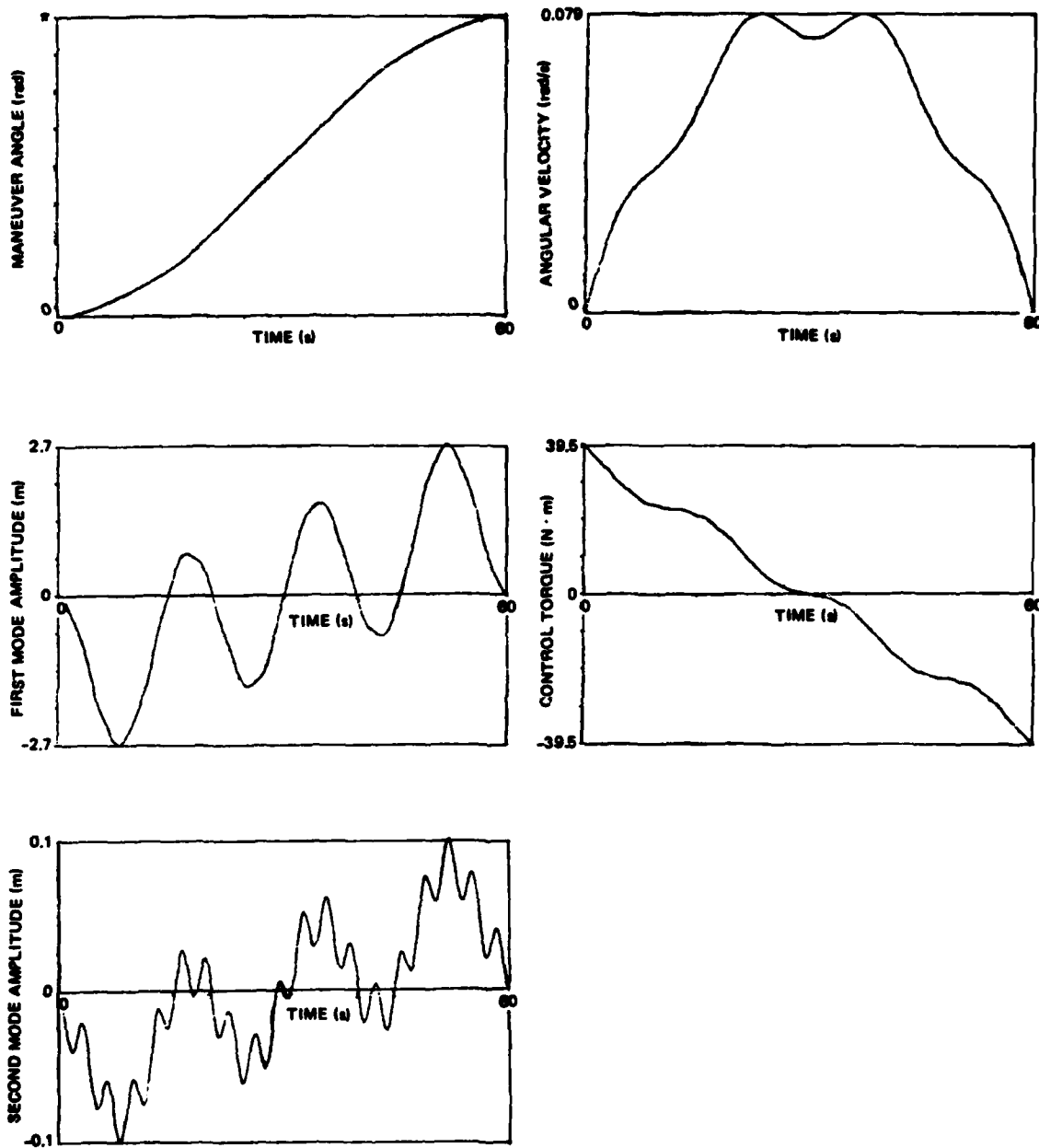
Figure 9.- Case 1, 2-mode case, rest-to-rest maneuver, 1 control.
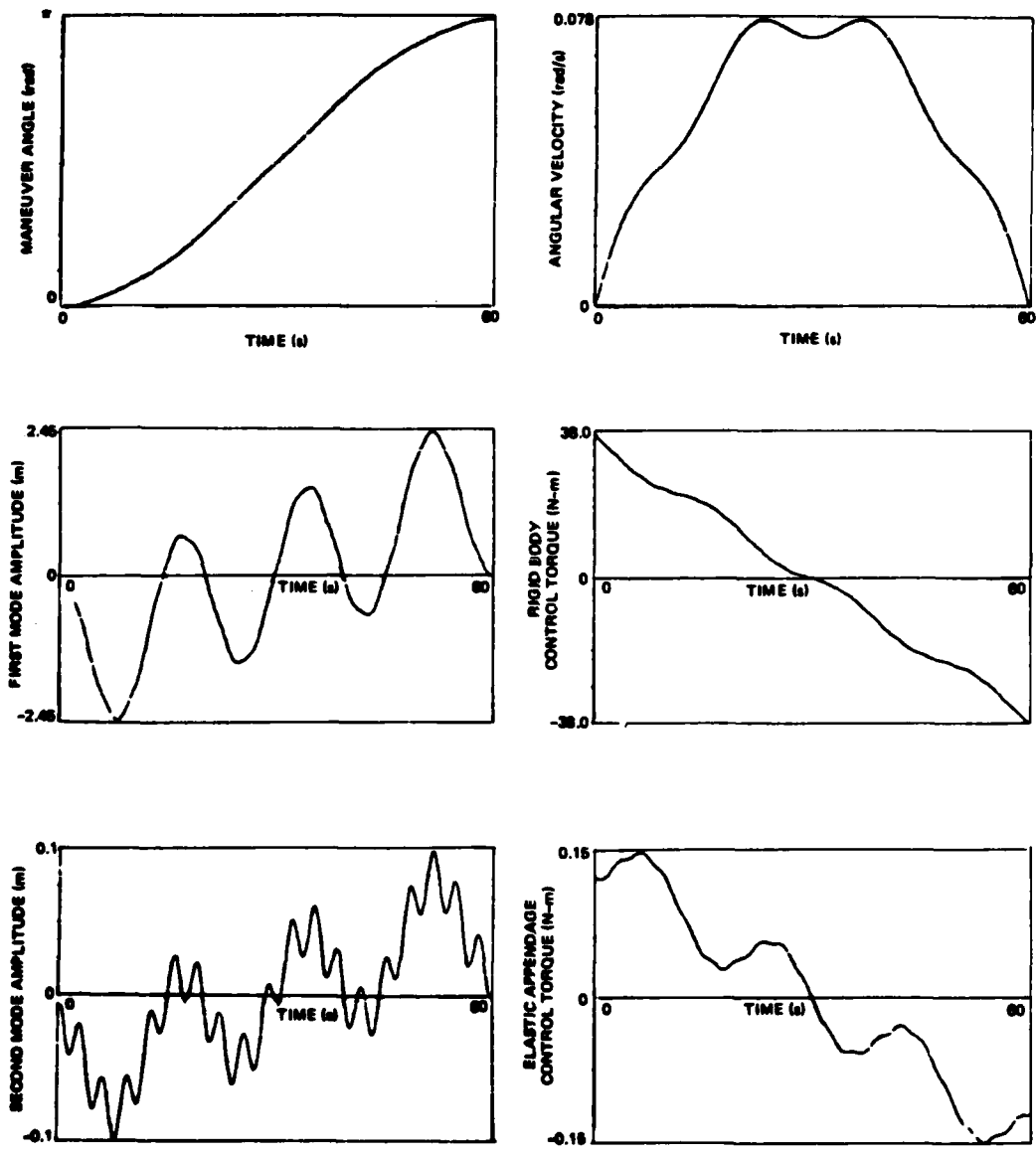
Figure 10.- Case 2, 2-mode case, rest-to-rest maneuver, 5 controls.
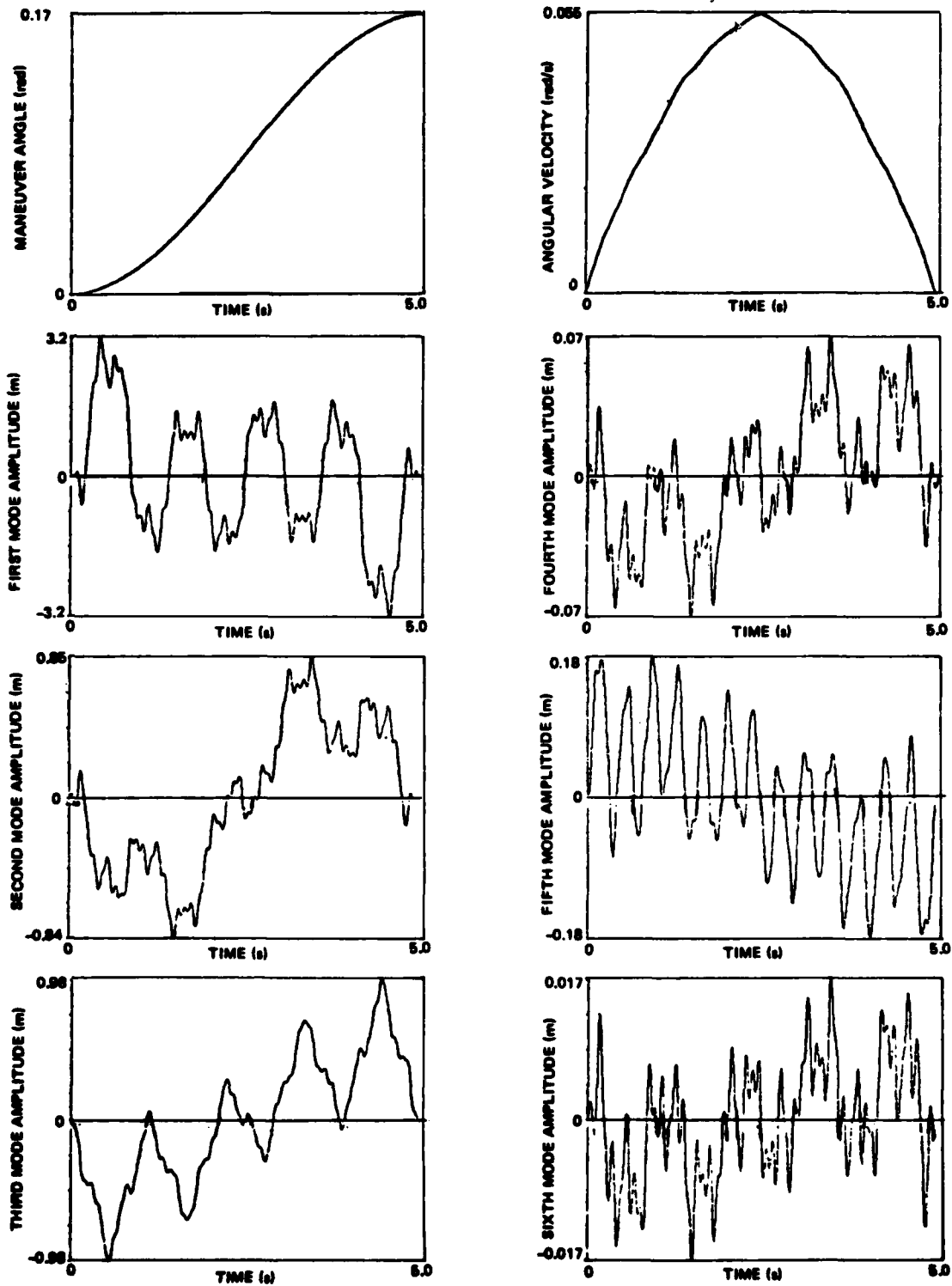
Figure 11.- Case 3, 10-mode case, rest-to-rest maneuver, 5 controls.
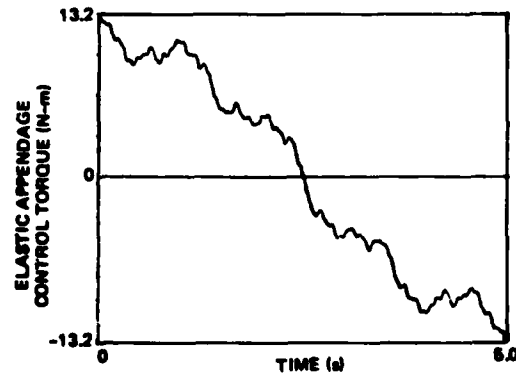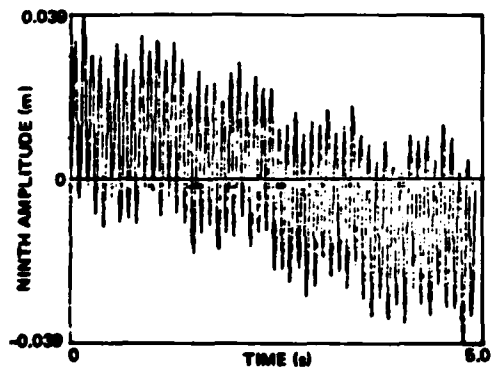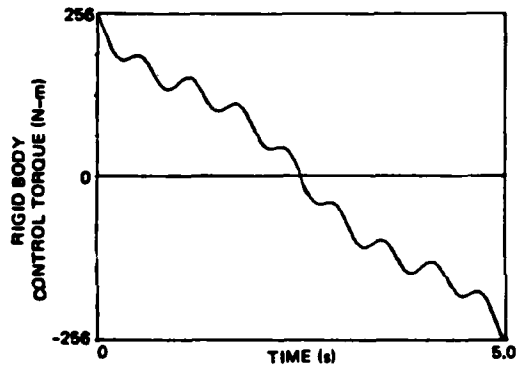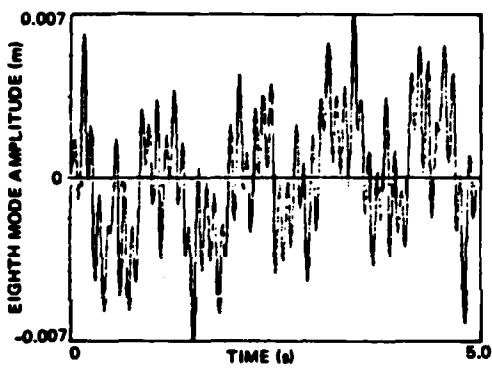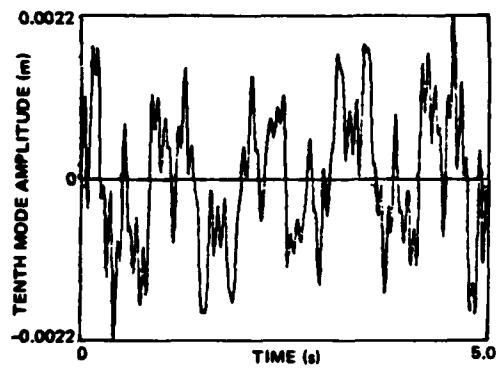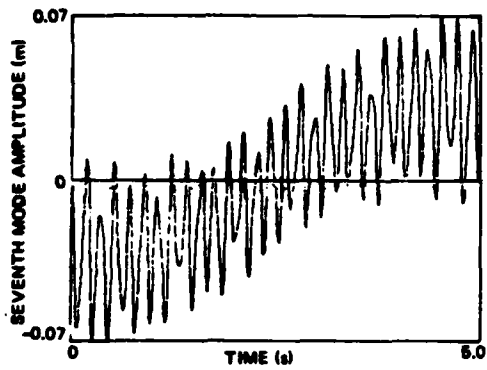
Figure 11.- Concluded.
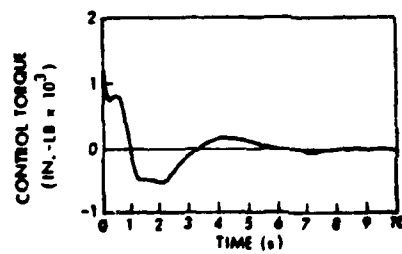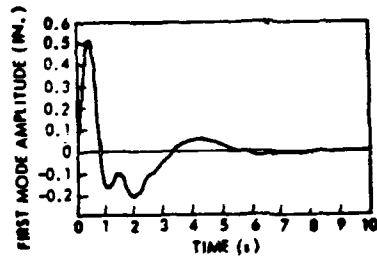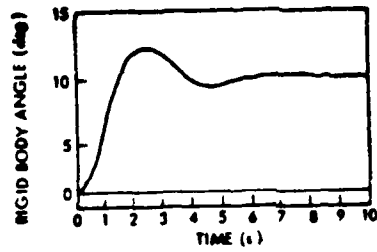
Figure 12.- Case 4, 1-mode case, rest-to-rest maneuver, steady-state feedback.

212
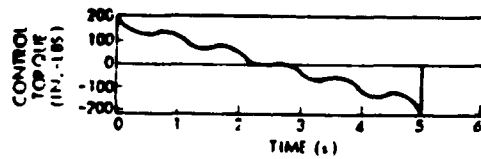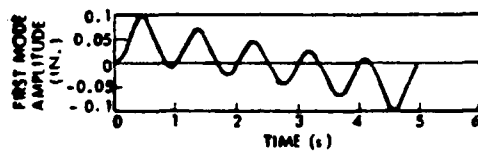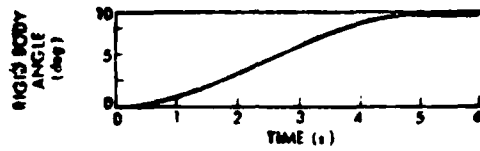
Figure 13.- Case 5, 1-mode case, rest-to-rest maneuver, steady-state feedback.
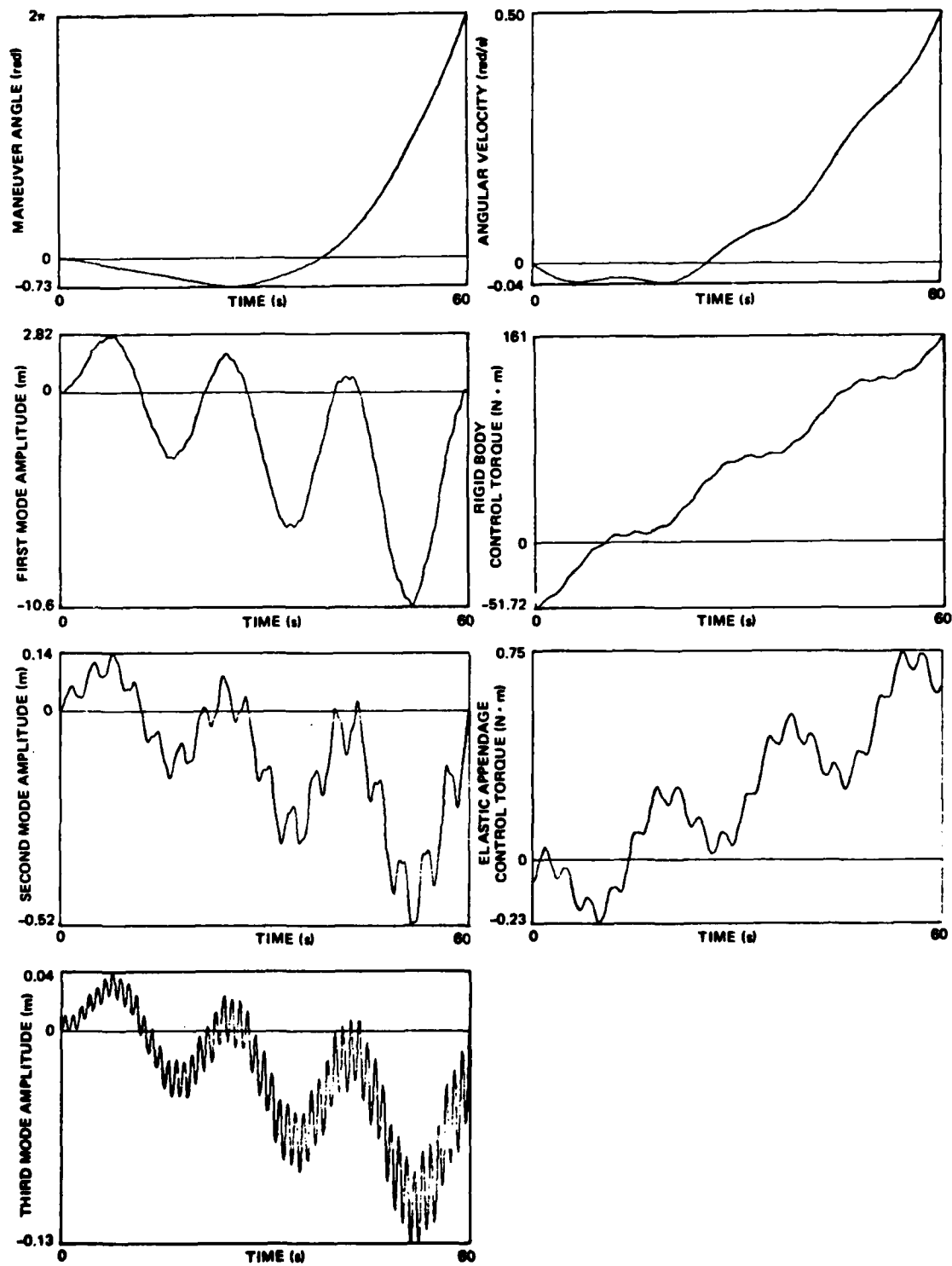
Figure 14.- Case 6, 3-mode, linear spin-up maneuver, 5 controls.
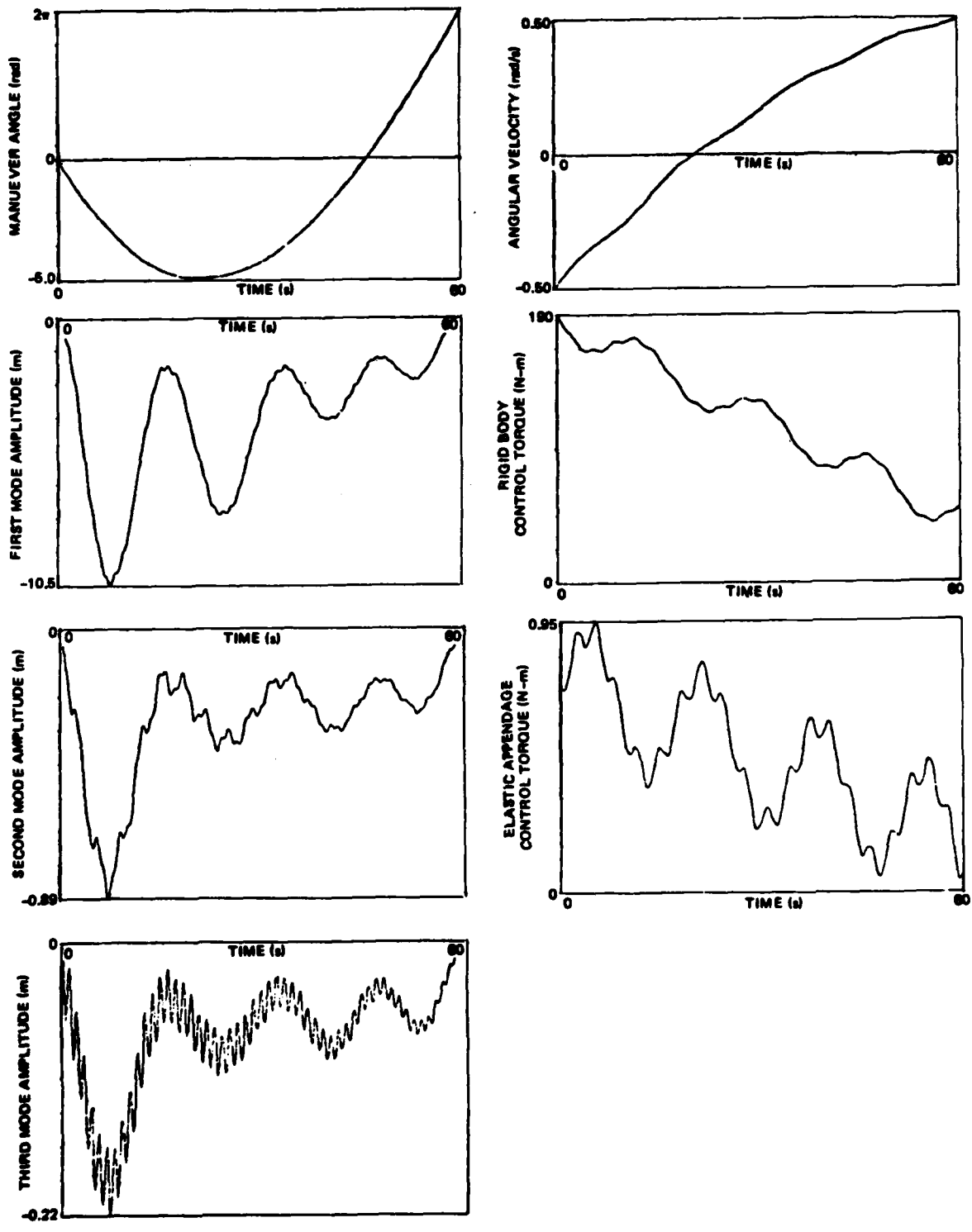
Figure 15.- Case 7, 3 modes, nonlinear spin-reversal maneuver, 5 controls.

1. Report No. NASA CP-2258	2. Government Accession No. AD-A214 579	3. Recipient's Catalog No.
4. Title and Subtitle MODELING, ANALYSIS, AND OPTIMIZATION ISSUES FOR LARGE SPACE STRUCTURES		5. Report Date February 1983
		6. Performing Organization Code 506-53-53-08
7. Author(s) Larry D. Pinson, Anthony K. Amos, and V. B. Venkayya, compilers		8. Performing Organization Report No. L-15564
		10. Work Unit No.
9. Performing Organization Name and Address NASA Langley Research Center Hampton, Virginia 23665		
		11. Contract or Grant No.
		13. Type of Report and Period Covered
12. Sponsoring Agency Name and Address National Aeronautics and Space Administration Washington, D.C. 20546 Air Force Office of Scientific Research Bolling Air Force Base Washington, D.C. Air Force Wright Aeronautical Laboratories Wright Patterson Air Force Base, Ohio		Conference Publication
		14. Sponsoring Agency Code

15. Supplementary Notes

Larry D. Pinson: NASA Langley Research Center, Hampton, Virginia
Anthony K. Amos: Air Force Office of Scientific Research, Bolling Air Force Base, Washington, D.C.
V. B. Venkayya: Air Force Wright Aeronautical Laboratories, Wright Patterson Air Force Base, Ohio

16. Abstract

This document contains the proceedings of the Air Force/NASA Workshop on Modeling, Analysis, and Optimization Issues for Large Space Structures held in Williamsburg, Virginia, May 13-14, 1982. The workshop was jointly sponsored by NASA Langley Research Center, the Air Force Office of Scientific Research, and the Air Force Wright Aeronautical Laboratories. The theme of the workshop was modeling, analysis, and optimization of large space structures, including structure-control interaction. Speakers were drawn primarily from industry, with participation from universities and government. The workshop was organized into three sessions: mathematical modeling, analysis methodology, and optimization for controllability. Results of the workshop were discussed in a final session. Summaries of each session were presented by session technical secretaries, and general discussion followed.

17. Key Words (Suggested by Author(s)) Structure-control interaction Large space structures Thermal analysis Structural modeling	18. Distribution Statement Unclassified - Unlimited Subject Category 15

19. Security Classif. (of this report) Unclassified	20. Security Classif. (of this page) Unclassified	21. No. of Pages 230	22. Price A11